

DISCOVERY, OPTIMIZATION, AND CHARACTERIZATION OF NOVEL
SUBTYPE-SELECTIVE MUSCARINIC ACETYLCHOLINE RECEPTOR
M4 AND M5 POSITIVE ALLOSTERIC MODULATORS

By

Thomas Miller Bridges

Dissertation

Submitted to the Faculty of the
Graduate School of Vanderbilt University
in partial fulfillment of the requirements
for the degree of

DOCTOR OF PHILOSOPHY

in

Pharmacology

December, 2010

Nashville, Tennessee

Approved:

Professor Craig Lindsley

Professor Vsevolod Gurevich

Professor Jeffrey Conn

Professor Aaron Bowman

To my parents Vicki and Allen Bridges

ACKNOWLEDGEMENTS

Many individuals and organizations have provided indispensable help and support to myself and to the work described herein, and I wish to specifically name and thank a number of them. My undergraduate biology professor, Jennifer Busch, who first introduced me to Vanderbilt and to the biomedical research field, has been a great friend and source of advice throughout my graduate career. Without her invitation to pursue an internship at Vanderbilt, I would not have moved to Nashville and ultimately entered this program. Likewise, Jackie Corbin and Sharron Francis allowed me to work as a summer research intern in their laboratory alongside Dr. Busch, for which I'm very grateful. I also want to thank Martin Egli and his lab for granting me a research assistant position during the time I was applying to this program. The IGP staff and the Vanderbilt department of Pharmacology as a whole have been an invaluable and integral part of my education and graduate training as well. I thank all of the professors and the administration of the department, in particular Joey Barnett, who have taught or helped me throughout the past four years. Furthermore, none of this research would have been possible without generous funding from the VICB, NIH, NIMH, and the Alzheimer's Association.

My advisor Craig Lindsley deserves the greatest degree of gratitude and recognition for his help, consideration, and leadership during my training. I'm forever indebted to him for first allowing me to rotate and later join his lab at a time when he was new to Vanderbilt and the lab was just beginning. Virtually all of my research, publications, and other accomplishments during this degree program can be attributed

largely to Craig for providing me with endless opportunities and encouragement. Craig is one of the most intelligent, hard-working, and successful scientists I've known and I cannot thank him enough for all of his help and support throughout my time in his lab. Likewise, I would like to thank and acknowledge all past and present members of the Lindsley lab, and Phil Kennedy in particular, as well as the larger VPDD group for all of their help and for creating a friendly and all-round outstanding research environment.

Jeff Conn has been a fantastic co-mentor who has provided crucial advice, support, and encouragement throughout my graduate career. Jeff is also a wonderful role model and thoughtful leader whom I deeply respect. I thank him and all of his lab members for their never-ending help and instruction during my research. Similarly, I'm grateful for the help and insight I've received from all of my committee. Seva Gurevich and Aaron Bowman have been extremely kind and supportive to me, and I'm grateful for their participation and guidance as part of my committee. I also thank Larry Marnett for his help throughout my training and for allowing me to participate in the ITTD. Dave Weaver and his lab members have contributed greatly to this research in numerous ways and have provided me with crucial training and help throughout this work as well.

I would like to thank my friends and family for their continual support throughout the course of my degree. My parents, Vicki and Al, have always provided me with everything I've needed or asked and have been a vital source of assurance and financial help. My sister, Sydney, has also been a great friend and resource during this time. I thank all of my extended family including my grandparents as well for their assistance and encouragement. Last, I would like to thank my classmate Kelsey Duggan for her friendship and support during my pursuit of this degree.

TABLE OF CONTENTS

	Page
DEDICATION	ii
ACKNOWLEDGEMENTS	iii
LIST OF TABLES	viii
LIST OF FIGURES	x
LIST OF ABBREVIATIONS	xvii
Chapter	
I. INTRODUCTION	1
Muscarinic acetylcholine receptors.....	1
Acetylcholine biosynthesis and receptors	1
Structure and signaling of mAChR subtypes.....	4
Localization of mAChR subtypes	6
Genetic deletion of mAChR subtypes.....	8
Therapeutic potential of mAChRs as drug targets	15
Allosteric modulation of mAChRs	24
Introduction to allosteric modulation of GPCRs	24
Characterization of allosteric modulators of GPCRs.....	29
Discovery of early allosteric modulators of mAChRs.....	31
Notes on figure, table, and compound numbering/nomenclature	33
II: MATERIALS AND METHODS	34
Medicinal chemistry	34
General synthetic methods, instrumentation, and work-flow	34
M ₄ PAM syntheses.....	37
M ₅ PAM syntheses.....	46
M ₁ PAM syntheses.....	53
M ₁ allosteric agonist syntheses	61
M ₁ agonist TBPB analog syntheses	63
M ₁ antagonist syntheses.....	66
Jet-milling/scale-up.....	68
<i>In vitro</i> pharmacology	68

Cell lines and cell culture.....	68
Calcium mobilization assays.....	69
Radioligand binding assays.....	71
Ancillary/off-target screening assays.....	76
<i>In vivo</i> pharmacology	76
Amphetamine-induced hyperlocomotion behavioral rat studies	77
Roto-rod behavioral rat studies.....	78
Pharmacokinetic/PBL rat studies.....	79
III: DISCOVERY, OPTIMIZATION, AND CHARACTERIZATION OF NOVEL SUBTYPE-SELECTIVE M ₄ POSITIVE ALLOSTERIC MODULATORS	83
Discovery of M ₄ PAM VU010010	83
Optimization of M ₄ PAM VU010010 to obtain VU0152099 and VU0152100	85
<i>In vitro</i> characterization of M ₄ PAMs VU0152099 and VU0152100	91
<i>In vivo</i> pharmacokinetics of M ₄ PAMs VU0152099 and VU0152100.....	98
<i>In vivo</i> behavioral studies with M ₄ PAMs VU0152099 and VU0152100.....	100
Optimization of M ₄ PAMs VU0152099 and VU0152100.....	102
<i>In vivo</i> behavioral studies with 3 rd -generation optimized M ₄ PAMs.....	114
Species-specific differences in 3 rd -generation M ₄ PAM potencies.....	115
Potential for dual M ₄ PAM / H ₃ antagonist anti-psychotic activity.....	116
Summary	118
IV: DISCOVERY, OPTIMIZATION, AND CHARACTERIZATION OF NOVEL SUBTYPE-SELECTIVE M ₅ POSITIVE ALLOSTERIC MODULATORS	119
Discovery of M ₁ /M ₃ /M ₅ PAM VU0119498	119
Optimization of VU0119498 to obtain M ₅ PAM VU0238429	123
<i>In vitro</i> characterization of M ₅ PAM VU0238429	141
<i>In vivo</i> rat pharmacokinetics of M ₅ PAM VU0238429	146
Optimization of M ₅ PAM VU0238429.....	147
Ancillary pharmacology and physiochemical optimization of M ₅ PAMs	177
<i>In vitro</i> characterization of M ₅ PAMs at rat M ₅ receptor.....	193
Summary	195
V: DISCOVERY, OPTIMIZATION, AND CHARACTERIZATION OF NOVEL SUBTYPE-SELECTIVE M ₁ LIGANDS	197
M ₁ PAMs derived from VU0119498.....	197
M ₁ PAMs VU0028767 and VU0090157	206
M ₁ PAM BQCA and analogs.....	208
M ₁ PAMs derived from MLPCN probe project.....	214
M ₁ agonist VU0357017 and analogs	225

M ₁ agonist TBPB and analogs	235
M ₁ antagonist VU0255035 analogs	242
Summary	249
VI: SUMMARY AND FUTURE DIRECTIONS	251
M ₄ PAMs based on VU010010	252
M ₅ PAMs based on VU0238429	257
REFERENCES	265

LIST OF TABLES

Chapter III

Table	Page
1 M ₄ PAM potency and ACh CRC fold-shift SAR for VU010010 analogs based on scaffold 7.....	89
2 Ancillary pharmacology activity of M ₄ PAMs VU0152099 and VU0152100 in singlepoint (10 μ M) competition binding assays across a large panel of off-targets ...	96
3 Pharmacokinetic parameters calculated for M ₄ PAMs VU0152099 and VU0152100 from a rat PK/PBL study.....	100
4 M ₄ PAM SAR for select analogs from alkylamine library 9a-s and ether library 13a-s chosen based on an initial singlepoint triage screen.....	106
5 M ₄ PAM SAR for select compounds from second library iteration analogs 17-21.....	112

Chapter IV

Table	Page
1 Structures for compounds 21-112 and associated PAM activity data from initial single concentration (30 μ M) potentiator screen against M ₁ and M ₅	125
2 Potency SAR at M ₁ and M ₅ for 18 compounds selected from an initial singlepoint screen	139
3 Structures and VU numbers for 13 VU01109498 analogs chosen for a M ₃ PAM singlepoint screen based on their inactivity at M ₁ and M ₅	141
4 M ₁ and M ₅ potency SAR for biaryl/heterobiaryl and phenethyl analogs of VU0238429	151
5 Structures of western ether analog library based on M ₅ PAM VU0365114.....	173
6 Ancillary/off-target binding screening results for five M ₅ PAM leads.....	178
7 Ancillary/off-target binding screening results for physiochemically-optimized M ₅ PAMs VU0414747 and VU0415478	191

Chapter V

Table	Page
1 SAR of fluorine-bearing analogs of lead compound VU0365137.....	203
2 SAR for 3-position biaryl/heterobiaryl analogs based on VU0402606.....	220
3 SAR for fluorinated analogs based on VU04010 lead.....	221
4 M ₁ and D ₂ potency/efficacy SAR for TBPB analogs synthesized according to Figure 30.....	237
5 SAR for fluorine-substituted TBPB analogs.....	241
6 M ₁ -M ₅ SAR for active M ₁ antagonist analogs 5.....	245
7 Summary of functional and binding mAChR subtype-selectivity for M ₁ antagonist (compound 5b).....	247

LIST OF FIGURES

Chapter I

Figure	Page
1 Generalized diagram of cholinergic biosynthesis, packaging, degradation, and reuptake.....	2
2 Diagram of six main central cholinergic neuron projection pathways in the rat brain	3
3 Abbreviated diagram of the putative roles of M ₄ and M ₅ in the central mesolimbic DA pathway brain.....	12
4 Proposed signaling relationships between M ₁ , APP processing, tau NFTs, and cognition, within the context of Alzheimer’s disease.....	20
5 Generalized cartoon model of mAChR allosteric modulation depicting putative allosteric sites in relation to the orthosteric binding site.....	26
6 Allosteric ternary receptor complex model describing interaction between two ligands and a receptor	28
7 Example of a ‘double-add’ assay format designed to identify PAMs by functional fluorometric Ca ²⁺ mobilization readout	29
8 Example of generic PAM CRC in the presence of a fixed submaximal concentration of orthosteric agonist to determine PAM potency (A) and agonist CRC in the absence and presence of increasing fixed concentrations of PAM to determine fold-shift (B)	30
9 Structures of examples of early allosteric mAChR modulators.....	32

Chapter II

Figure	Page
1 Generalized work-flow utilizing iterative synthesis and testing of parallel analog libraries aimed at optimizing a given property or characteristic of the lead structure/scaffold.....	36

Chapter III

Figure	Page
1 Structures of Eli Lilly hM ₄ PAM LY2033298 and Vanderbilt rM ₄ PAM VU010010.....	84
2 Chemical optimization of VU010010.....	86
3 Singlepoint screen of M ₄ PAM VU010010 analogs based on scaffold 7 bearing eastern amide side chain substitutions.....	88
4 Structures, potency CRCs, and ACh CRC fold-shifts for M ₄ PAM leads.....	90
5 GIRK-mediated thallium flux M ₄ PAM assays with lead compounds VU0152099 and VU0152100.....	92
6 [³ H]-NMS competition binding experiments with M ₄ PAMs VU0152099 and VU0152100 at rM ₄ cell membranes.....	93
7 mAChR subtype-selectivity profiles for M ₄ PAMs VU0152099 and VU0152100 determined by ACh CRC fold-shift.....	95
8 Functional GPCR off-target activity screening for M ₄ PAMs VU0152099 and VU0152100.....	97
9 <i>In vivo</i> rat pharmacokinetic/PBL studies with M ₄ PAMs VU0152099 and VU0152100.....	99
10 Reversal of amphetamine-induced hyperlocomotion and absence of sedation <i>in vivo</i> by M ₄ PAMs VU0152099 and VU0152100.....	101
11 Structures of first- and second-generation M ₄ PAMs based on optimization of the dimethylamino-thienopyridine amide scaffold.....	103
12 Synthesis of M ₄ PAM analog libraries 9a-s and 13a-s.....	104
13 CRCs and ACh fold-shift for analog 13k in rat M ₄ cells by Ca ²⁺ mobilization assay.....	108
14 Synthesis of M ₄ PAM analog libraries.....	110
15 Singlepoint (10 μM) M ₄ PAM screen of analog sets 17-21.....	110
16 M ₄ PAM characterization of analog 21n in rat M ₄ /G _{q15} -CHO cells by functional Ca ²⁺ mobilization assay.....	113

17	Effects of compounds 13k, 18h, 21n, and 21o in human M ₄ /G _{q15/16} -expressing cells by functional Ca ²⁺ mobilization assay.....	116
18	Alignment of M ₄ PAM lead compounds 21n with refined histamine H ₃ receptor antagonist pharmacophore	117

Chapter IV

Figure		Page
1	Compounds identified by M ₁ PAM HTS chosen for <i>in vitro</i> characterization.....	119
2	<i>In vitro</i> characterization of VU0119498	120
3	Resynthesis and retesting of HTS hit VU0119498.....	122
4	Synthesis and singlepoint screening of initial matrix library of VU0119498 analogs	124
5	Singlepoint screen of at M ₃ of a subset of VU0119498 analogs chosen based on inactivity at M ₁ and M ₅	140
6	mAChR subtype-selectivity of compound 42 (VU0238429) displaying high M ₅ PAM selectivity	142
7	mAChR subtype-selectivity of compound 56 displaying pan-mAChR PAM activity.....	142
8	Compound 42 (VU0238429) requires ACh to activate M ₅ and causes a robust increase in ACh potency at M ₅	144
9	Competition binding experiments with VU0238429 and compound VU0119498 ...	145
10	Rat pharmacokinetic PBL study of VU0238429 and calculated PK parameters.....	146
11	Initial optimization strategy for M ₅ PAM VU0238429	148
12	Synthesis and M ₁ /M ₅ singlepoint screening of biaryl/heterobiaryl and phenethyl analogs VU0238429.....	149
13	M ₁ , M ₃ , and M ₅ subtype-selectivity and ACh CRC fold-shift of compound 6a (VU0365114) and 6d (VU0365117).....	153
14	Strategy for second round of M ₅ PAM analog library iterations	154

15	Structures, mAChR subtype-selectivity profile, and ACh CRC fold-shift for VU0400265, the first M ₅ -selective PAM	155
16	M ₁ /M ₅ singlepoint screening of substituted indole and oxindole analogs.....	156
17	Synthesis of oxindole M ₅ PAM analogs VU0402733, VU0402734, and VU0402735	158
18	Structures and CRCs for M ₅ PAM analogs bearing 3-position ketone replacements	159
19	M ₁ , M ₃ , and M ₅ subtype-selectivity profile for VU0402734, the gem di-fluoro analog of M ₅ PAM VU0238429	160
20	Optimization strategy for third round of M ₅ PAM library iterations.....	162
21	Structure and M ₅ PAM activity of piperonyl analog VU0366628	162
22	Structures and CRCs for ortho-fluorinated M ₅ PAMs based on VU0365114 lead structure.....	163
23	Subtype-selectivity profiles for VU0400266 and VU0400267	165
24	Structures and M ₅ CRCs for 2x2 matrix library of phenoxybenzyl gen-difluoro analogs	167
25	M ₁ , M ₃ , and M ₅ CRCs for VU0403751 and VU0403753	168
26	ACh CRC fold-shift effect of gem-difluoro lead analogs VU0403751 and VU0403753.....	169
27	M ₅ CRCs for tricyclic analogs VU0403897 and VU0403898.....	170
28	Synthetic scheme for generation of a diverse set of M ₅ PAM analogs based on VU0365114 bearing western ethers.....	172
29	M ₅ singlepoint screening of western ether analogs.....	174
30	Basic-amine containing western ether analogs that partially inhibited an ACh ~EC ₂₀ response in M ₅ PAM screen shown in Figure 29, suggesting potential M ₅ NAM or antagonism	175
31	Synthesis and M ₅ CRC for 5-methoxy analog VU0366627	177
32	Synthesis of four southern heterobiaryl ether analogs based on VU0400265	182

33	Structures, lipophilicities, and M ₅ potency/efficacy for four heterobiaryl ether M ₅ PAMs	183
34	M ₅ ACh CRC foldshift assay with analog VU0414747	184
35	Synthesis and SAR for southern heterobiaryl amine-containing M ₅ PAM analogs ..	185
36	M ₅ ACh CRC fold-shift assay with analog VU0415478	187
37	Synthesis and M ₅ potency/efficacy of VU0415486, the 3-pyridyl congener of VU0238429	188
38	Structures and M ₅ potency/efficacy of acidic and basic moieties in the distal southern region of the M ₅ PAM scaffold	189
39	M ₅ ACh inhibition CRCs for VU0414750, a potential M ₅ NAM	190
40	Rat M ₅ ACh CRC fold-shift assay with early lead compound VU0238429	194

Chapter V

Figure		Page
1	Initial optimization strategy for VU0119498 aimed at discovering modifications that engender increased M ₁ PAM activity and subtype-selectivity	198
2	Synthesis of initial biaryl/heterobiaryl library based on VU0119498	199
3	Singlepoint (10 μM) M ₁ /M ₅ screen of initial 12-member biaryl/heterobiaryl and Phenethyl analog library based on VU0119498	200
4	Structure and PAM activity of VU0365137	201
5	Subtype-selectivity of M ₁ PAMs VU0366368 and VU0366369	204
6	Structure and M ₁ PAM CRC for VU03663657	206
7	SAR summary for M ₁ PAM HTS hits VU0029767 and VU0090157	207
8	Singlepoint (10 μM) M ₁ PAM screen of VU0090157 analogs bearing diverse northern substitutions	207
9	Structures of VU0090157 analogs generated to explore SAR at the northern headpiece	208

10	Synthesis and screening of BQCA and BQCA analogs at rat M ₁	210
11	CRCs of BQCA and three analogs at rM ₁ by Ca ²⁺ mobilization assay	211
12	Structure and M ₅ CRCs for BQCA-based analogs VU0400268 and VU0400269	214
13	Structure of two M ₁ PAM hits identified by 30 μM singlepoint screen of approximately 200 re-ordered putative PAMs identified from a functional M ₁ antagonist HTS campaign.....	216
14	M ₁ CRCs of PAM hits VU0108370 and VU0165202	216
15	Initial optimization strategy for M ₁ PAM hit VU0108370.....	217
16	Synthesis of M ₁ PAM hit VU0108370 used to generate southern benzyl-derivatized library	217
17	Structures and M ₁ PAM CRCs of southern benzyl analogs based on the VU0108370 / VU0165202 scaffold identified from a larger singlepoint triage assay	218
18	Structures and M ₁ PAM CRCs of <i>meta</i> -substituted southern benzyl analogs based on the VU108370 / VU0165202 scaffold	219
19	Structure and ACh CRC fold-shifts for M ₁ PAM leads VU0405652 and VU0405645.....	222
20	M ₃ and M ₅ subtype-selectivity CRCs for original M ₁ PAM HTS hits and select intermediate lead analogs.....	223
21	mAChR subtype-selectivity for probe compound VU0405652.....	224
22	Singlepoint (10 μM) screen of large panel of compounds from the VU HTS collection identified from a VU0108370-based structure similarity virtual screen...	225
23	Structure and subtype-selectivity profiles of novel M ₁ agonist HTS hits.....	227
24	M ₁ agonist SAR revealed by initial matrix library and singleton syntheses.....	228
25	mAChR subtype-selectivity profiles of M ₁ agonist leads VU0184670 and VU0357017	229
26	M ₂ -M ₅ functional antagonism profiles of M ₁ agonist leads VU0184670 and VU0357017 as well as parent hits VU0177548 and VU0207811	230

27	[³ H]-NMS competition binding CRCs with parent M ₁ agonist leads VU0184670 and VU0357017 as well as parent hits VU0177548 and VU0207811	231
28	CRCs of M ₁ agonist leads VU0184670 and VU0357017 as well as parent hits VU0177548 and VU0207811	232
29	Structure and mAChR subtype-selectivity of M ₁ agonist TBPB.....	235
30	First round of synthesis of TBPB analogs	236
31	mAChR subtype-selectivity profile for TBPB analog 1b.....	237
32	Synthesis of fluorine-substituted TBPB analogs	239
33	Synthesis of additional fluorinated TBPB analogs	240
34	M ₁ -M ₅ CRCs for M ₁ antagonist compound 1	243
35	Synthesis of M ₁ antagonist compound 1 analogs	244
36	M ₁ -M ₅ CRCs for lead compound 5b.....	246
37	Additional SAR exploration around the M ₁ antagonist scaffold resulting in inactive analogs.....	248

Chapter VI

Figure		Page
1	Optimization progression summary for M ₄ PAMs based on a substituted thienopyridine scaffold	253
2	Abbreviated SAR summary for M ₅ PAM optimization based on early lead VU0238429.....	258
3	Overview of key lead compounds identified during M ₅ PAM optimization project.....	260

LIST OF ABBREVIATIONS

°C	Degrees celsius
[³ H]-NMS	[³ H]- <i>N</i> -methylscopolamine
α	Cooperativity factor
AC	Adenylyl cyclase
Acetyl-CoA	acetyl-coenzyme A
ACh	Acetylcholine
AChE	Acetylcholinesterase
AChEI	Acetylcholinesterase inhibitor
AD	Alzheimer's disease
A β	Amyloid- β
APP	Amyloid precursor protein
ATCM	Allosteric ternary complex model
AUC	Area under the curve
β	Efficacy modulation factor
BBB	Blood-brain barrier
BQCA	Benzyl quinolone carboxylic acid
BuChE	Butyrylcholinesterase
CAA	Cerebral amyloid angiopathy
cAMP	Cyclic adenosine monophosphate
CAR	Conditioned avoidance responding
CCh	Carbachol
cGMP	Cyclic guanosine monophosphate
CBF	Cerebral blood flow
ChAT	Choline acetyltransferase

CHO-K1	Chinese hamster ovary-K1
CNS	Central nervous system
CPP	Conditioned place preference
CRC	Concentration-response curve
CSF	Cerebrospinal fluid
D ₁	Dopamine D ₁ receptor
D ₂	Dopamine D ₂ receptor
DA	Dopamine
DMPK	Drug metabolism and pharmacokinetic
DMSO	Dimethyl sulfoxide
DOS	Diversity-oriented synthesis
EDTA	Ethylenediamine tetra-acetic acid
ELSD	Evaporative light scattering device
EPSC	Excitatory post-synaptic current
ERK	Extracellular signal regulated kinase
GABA	γ -amino-butyric acid
GABA _A	γ -amino-butyric acid receptor A
GlyT1	Glycine type-1 transporter
GIRK	G-protein coupled inward-rectifying K ⁺ channel
GPCR	G-protein coupled receptor
GRK	G-protein coupled receptor kinase
GTP γ S	Guanosine trisphosphate- γ S
HPLC	High-performance liquid chromatography
HTS	High-throughput screening
Hz	coupling constant
IHC	Immunohistochemistry
IP	Immunoprecipitation

I.P.	Intraperitoneal
IP ₃	Inositol trisphosphate
$K_{A/a}/K_{B/b}/K_{D/d}$	Equilibrium dissociation constant
$K_{I/i}$	Equilibrium dissociation constant from competition binding
KO	Knockout
LCMS	Liquid chromatography mass spectrometry
logP	Log partition coefficient
LTP	Long-term potentiation
M ₁ -M ₅	Muscarinic acetylcholine receptor subtypes 1-5
mAChR	Muscarinic acetylcholine receptor
MAPK	Mitrogen-activated protein kinase
MCH	Melanin-concentrating hormone
mGluR	Metabotropic glutamate receptor
MHz	Megahertz
MLSCN	Molecular libraries screening center network
MLPCN	Molecular libraries probe center network
mPFC	Medial pre-frontal cortical/cortex
NAc	Nucleus accumbens
nAChR	Nicotinic acetylcholine receptor
NAM	Negative allosteric modulator
NDMC	<i>N</i> -desmethyl clozapine
NFT	Neurofibrillary tangle
NMDA	<i>N</i> -methyl-D-aspartic acid
NMDAR	<i>N</i> -methyl-D-aspartic acid receptor
NMR	Nuclear magnetic resonance
NO	Nitric oxide
PAM	Positive allosteric modulator

PBL	Plasma-brain levels
PCP	Phencyclidine
PEG	Polyethylene glycol
PET	Positron emission tomography
P-gp	P-glycoprotein
PI3K	Phosphatidyl inositol-3 kinase
PK	Pharmacokinetic
PKA	Protein kinase A
PKG	Protein kinase G
PLA	Phospholipase A
PLC	Phospholipase C
PLD	Phospholipase D
PNS	Peripheral nervous system
PPI	Prepulse-inhibition
ppm	Parts per million
RT-PCR	Reverse transcriptase polymerase chain reaction
SAR	Structure-activity relationship(s)
S.C.	Subcutaneous
SEM	Standard error of the mean
SNe	Substantia nigra pars compacta
TCM	Ternary complex model
TLC	Thin-layer chromatography
UV	Ultra-violet
VAcHT	Vesicular ACh transporter
VHTSC	Vanderbilt high-throughput screening center
VTA	Ventral tegmental area
WT	Wild-type

Chapter I

INTRODUCTION

Muscarinic acetylcholine receptors

Acetylcholine biosynthesis and receptors

Acetylcholine (ACh) is the only known non- amino acid or non- amino acid-derived small molecule neurotransmitter and is vitally important to a wide range of basic physiological processes and functions throughout the mammalian body¹⁻⁵. ACh is synthesized endogenously from dietary choline, which is acetylated within the cell by the enzyme choline acetyltransferase (ChAT) using acetyl-coenzyme A (acetyl-CoA) as substrate to furnish the acetyl group (**Fig. 1**)¹. Subsequent intraneuronal packaging of cytoplasmic ACh into synaptic vesicles occurs via the vesicular ACh transporter (VACHT) (**Fig. 1**)^{6,7}. Following ACh release into the synapse, the enzyme acetylcholinesterase (AChE) rapidly terminates ACh signaling by hydrolyzing the ester of ACh to produce acetate and choline, the latter of which is then subject to local neuronal reuptake by the high-affinity choline transporter (**Fig. 1**)^{8,9}. Such reuptake represents the rate-limiting step in the ACh synthetic cycle⁹. In addition to AChE, which is encoded by a single gene but occurs in multiple forms via alternative mRNA-splicing, butyrylcholinesterase (BuChE) serves as a second enzyme responsible for degradation of ACh¹⁰⁻¹². However, BuChE is mainly present in plasma and in non-neuronal tissues where it contributes to termination of ACh signaling^{11,12}.

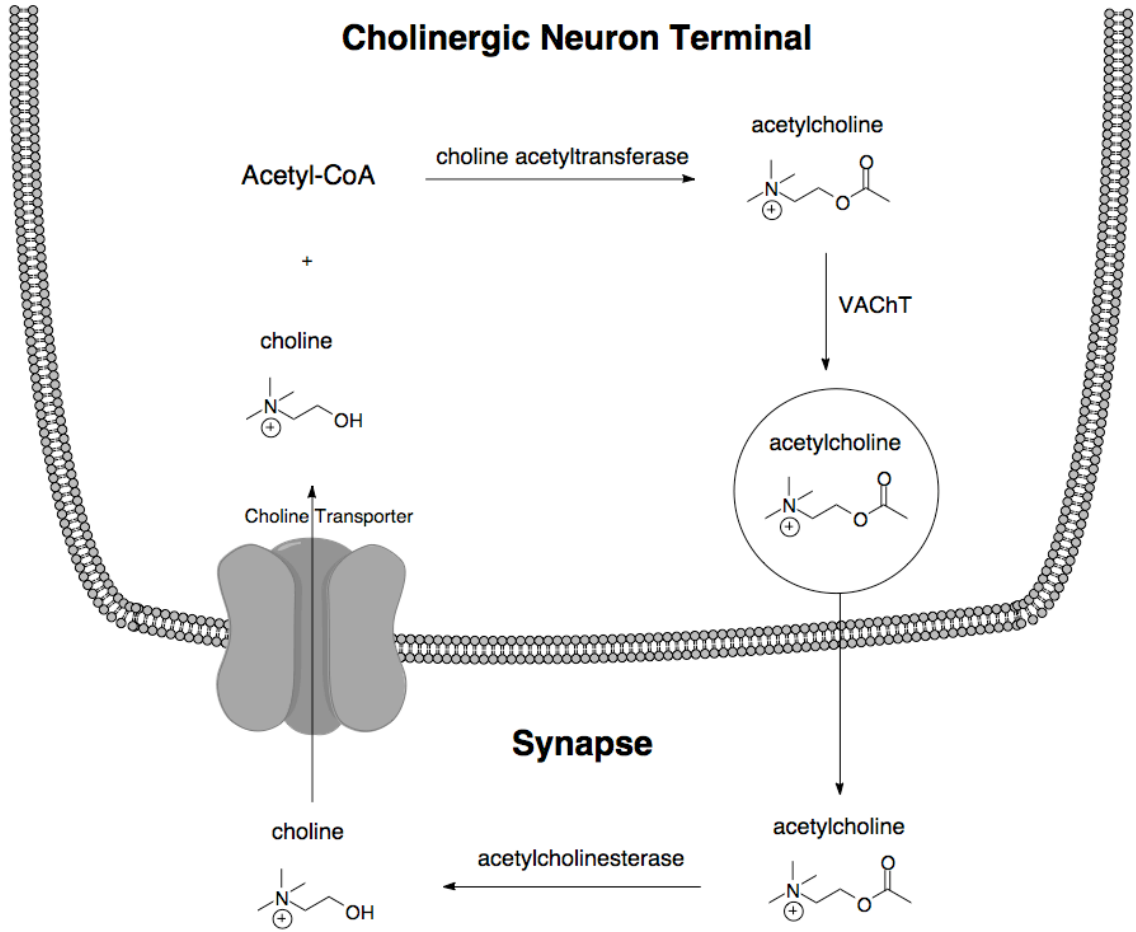


Figure 1. Generalized diagram of cholinergic biosynthesis, packaging, degradation, and reuptake.

As a neurotransmitter, ACh plays essential roles in both the central nervous system (CNS) and peripheral nervous system (PNS)^{3,13}. Within the autonomic arm of the PNS, cholinergic signaling occurs at the pre-ganglionic sympathetic and parasympathetic synapses, the post-ganglionic parasympathetic synapses, and at a subset of post-ganglionic sympathetic synapses in skin and sweat glands^{3,13}. ACh is also released at the skeletal neuromuscular junction, where it is responsible for initiation of muscle contraction^{3,13}. In the CNS, ACh is released from cholinergic neurons arising from six main brain regions (denoted as Ch. I – Ch. VI) and is responsible for a multitude of

integral brain functions and processes such as regulation of motor control, reward, sleep/wake cycles, metabolism, learning and memory, attention, and more (**Fig. 2**)^{3,13,14}.

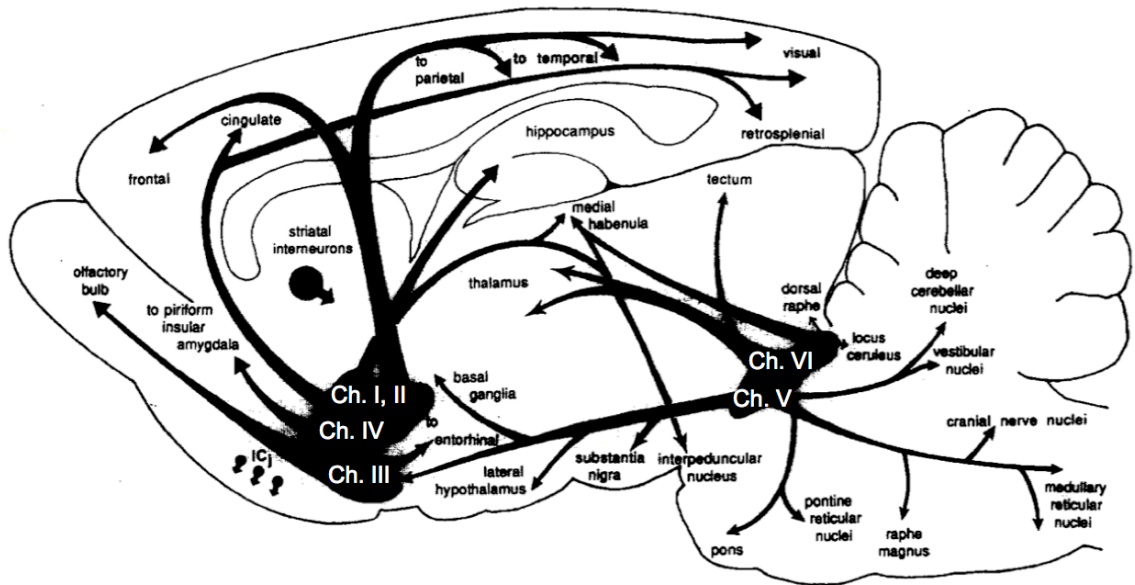


Figure 2. Diagram of six main central cholinergic neuron projection pathways in the rat brain (adapted from Woolfe 1991).

There exist two classes of ACh receptors, the ionotropic receptors activated by exogenous nicotine and the metabotropic receptors activated by exogenous muscarine, termed nicotinic acetylcholine receptors (nAChRs) and muscarinic acetylcholine receptors (mAChRs), respectively^{15,16}. These two classes can also be delineated by their sensitivity to antagonism by either tubocurarine (selective for nAChRs) or atropine (selective for mAChRs). Of the nAChRs, muscular (N_m) nAChRs mediate the actions of ACh at the skeletal neuromuscular junction while neuronal (N_n) nAChRs are present in the autonomic ganglia and CNS¹⁵. All nAChRs are pentameric ion channels comprised of various combinations of subunits (α_{1-10} , β_{1-4} , as well as the less common γ , δ , and ϵ subunits), which confer distinct structures and functions¹⁵. In general, nAChRs in the

CNS, such as those comprised of α_4 and β_2 subunits or all α_7 subunits, are present at both pre- and post-synaptic membranes where they enhance neuronal excitation by increasing Na^+ and Ca^{2+} permeability¹⁵. In contrast, mAChRs are G-protein coupled receptors (GPCRs) of which there exist five distinct subtypes (mAChR₁₋₅ or M₁-M₅), each encoded by a separate intron-less gene (CHRM1-5)^{2,5,16}. These mAChR subtypes are expressed differentially in both central and peripheral tissues, where they mediate the metabotropic signaling of ACh.

Structure and signaling of mAChR subtypes

Following cloning of the rat and human mAChR genes, a large body of research has focused on elucidating the molecular structure and function of these receptors. mAChRs are Type I (or Class A) rhodopsin-like GPCRs ranging in size from 460 (M₁) to 590 (M₃) amino acids and sharing a high degree of homology among their respective orthosteric ACh-binding sites^{2,5,16-18}. M₁, M₃, and M₅ exhibit higher structural homology to each other than to M₂ and M₄, which themselves share highest homology to each other^{2,5}. Correspondingly, the pre- versus post- synaptic localization patterns and associated downstream signaling pathways are generally similar for M₁, M₃, and M₅ versus M₂ and M₄^{17,18}. The former three are often considered stimulatory or excitatory given their predominantly post-synaptic localization and coupling to the $\text{G}\alpha_q$ /phospholipase-C (PLC)/inositol triphosphate (IP₃)/ Ca^{2+} pathway, while the latter two are typically regarded as inhibitory with predominantly pre-synaptic localizations as autoreceptors or heteroreceptors with coupling to the $\text{G}\alpha_i$ /adenylyl cyclase (AC)/cyclic adenosine monophosphate (cAMP)/protein kinase A (PKA) effector system^{17,18}.

It is important to note that many of the intracellular effects of mAChR activation are also mediated by $G\beta\gamma$, such as the $G\beta\gamma$ -induced opening of inward rectifying K^+ channels (GIRKs) in the case of M_2 and M_4 or $G\beta\gamma$ -mediated phosphatidyl inositol-3 kinase (PI3K)/Src signaling in the case of M_1 ^{17,19-24}. Furthermore, mAChRs have been found to activate many other downstream effectors including the phospholipases PLA and PLD, and all mAChRs have been shown to activate mitogen-activated protein kinase (MAPK)-signaling as measured by extracellular signal regulated kinase (ERK) phosphorylation^{17,25}. Like other Type I GPCRs, additional mAChR signaling occurs via β -arrestin1/2 (Arrestin2/3) binding following phosphorylation of the receptor by G-protein coupled receptor kinases (GRKs)¹⁷. In addition to their role(s) in receptor desensitization and internalization, Arrestins can also serve as protein scaffolds and signal-transduction nodes themselves²⁶. Thus, mAChR signaling within the cell can involve a broad and complex network of pathways, which are highly dependent upon the specific cell type and its protein composition.

More recently, pharmacological studies have revealed that different small molecule mAChR ligands are capable of exerting drastically different downstream signaling effects (through the same receptor subtype), presumably due to stabilization of distinct receptor structure conformations^{27,28}. Such phenomena, often referred to as ligand-induced receptor trafficking/signaling-bias, represent an important area of study for neuropharmacology, as ligands with the same mode of pharmacology (e.g. agonists) but of different chemical classes/chemotypes may cause divergent intracellular signaling through the same mAChR. This has obvious implications for use of novel (and particularly allosteric) ligands in basic neurobiological research and in therapeutic drug

discovery because different compounds targeting the same receptor may yet cause different electrophysiological, neurochemical, and behavioral effects²⁸.

Activation of mAChRs occurs via structural rearrangement and subsequent G-protein activation in response to ACh-binding to the orthosteric site deep within the transmembrane-spanning α -helical domain of the receptor²⁹. Within this site, a number of key residues form reversible non-bonding interactions with ACh²⁹. For example in the case of M₁, tyrosine-381, which is located in the 6th-transmembrane α -helix, forms a π -cation interaction with the positively charged ACh quaternary amine that is crucial to potent receptor activation by ACh³⁰. When this residue is mutated to an alanine, ACh potency at M₁ is right-shifted by several orders of magnitude³⁰. This M₁ mutant is thus particularly useful for characterization of novel M₁ activators because it can provide evidence for or against an orthosteric mode of binding³¹.

Localization of mAChR subtypes

A number of molecular biology techniques, including *in-situ* mRNA hybridization, reverse transcriptase PCR (RT-PCR), immunohistochemistry (IHC), immunoprecipitation (IP), and radioligand-binding have been used to investigate the neuroanatomical localization patterns of each mAChR³²⁻⁴⁰. Due to differences inherent among these various techniques, the fact that different investigators have used different antibody preparations (in the case of IHC/IP studies), and the observation that presence of mRNA for a given receptor in a particular tissue does not directly demonstrate equivalent functional protein levels in that tissue, has prevented widespread quantitative agreement on mAChR subtype density and localization. Nonetheless, relative distributions and

general localization of each subtype is known. At the mRNA level, transcripts for all five mAChR subtypes are found throughout the body in most tissues with detection levels ranging from high to near-baseline. At the protein level, the breadth of mAChR expression appears lower; however, there is generally good agreement between receptor mRNA levels and protein levels in most brain regions of primary interest to neurobiological research.

In the CNS, M₁ represents the predominant subtype, with high levels of expression throughout the cortex, striatum, hippocampus, and to a lesser extent the olfactory bulb and amygdala^{33,35,40}. M₁ is also present at low levels in peripheral smooth muscle³³. Similar to M₁, the M₃ subtype is found in the brain cortex, striatum, thalamus/hypothalamus, hippocampus, and olfactory bulb; though, levels of M₃ in the CNS are generally lower than those of M₁ across each shared brain region^{33,35,40,41}. Peripheral M₃ is predominately found throughout cardiovascular and gastrointestinal smooth muscles as well as in numerous glandular tissues, and to a lesser extent in the heart³³. The structurally related M₅ receptor initially proved the most difficult subtype to localize due to its extremely low levels of expression. Indeed, it has been estimated that this subtype represents less than 2% of all mAChR protein in the brain³⁸. Ultimately, M₅ has been shown to be the only mAChR present on midbrain dopaminergic cell bodies originating in the ventral tegmental area (VTA) and substantial nigra pars compacta (SNc)^{34,37}. These midbrain regions contain the highest levels of M₅ in the CNS, with cortical and hippocampal tissues containing M₅ at levels far below those of M₁ or M₃^{33,35,40}. Importantly, non-neuronal M₅ is found throughout the cerebrovascular system, including within the microvessels and epithelial cells comprising the blood-brain barrier

(BBB), and in the larger arterioles and arteries of the brain^{36,42}. The M₂ subtype is expressed largely on brainstem and basal forebrain cholinergic neurons (Ch. V-VI and Ch. IV, respectively) as well as in the thalamus, hippocampus, and striatum^{33,35,40}. M₂ is also highly expressed in cardiac tissues and to a lesser extent in peripheral smooth muscles³³. The M₄ subtype is most heavily expressed in the midbrain, striatum, and other areas of the basal ganglia, with lower levels present in the hippocampus and cortex^{32,33,35,37,40,43}. Peripherally, M₄ may be present in mainly in lung tissue³³.

Genetic deletion of mAChR subtypes

Given the high structural homology of the orthosteric ACh-binding site across the five mAChR subtypes, discovery of small molecule ligands possessing high binding and/or functional selectivity for an individual subtype has proven challenging⁴⁴. As discussed in greater detail in a subsequent section of this Chapter, a number of potent orthosteric mAChR agonists and antagonists have been discovered, which have provided utility in certain pharmacological research contexts but most have suffered from poor subtype-selectivity. Due to the longstanding paucity of selective pharmacological tools, insight into the specific functions of each mAChR at the cellular, neurocircuitry, neurochemical, and behavioral levels have relied largely on studies using mice genetically engineered to lack one or more mAChR subtype⁴⁵. These receptor knockout (KO) mice have provided insight to the role(s) of each mAChR in basic physiology, neurobiology, and within the context of various CNS disorders⁴⁵. Overall, the multitude of findings from mAChR-KO mice agree well with the predicted functions of each subtype based on their localization and known signaling.

Given the high density of M₁ in brain regions known to be important to cognitive function, such as the cortex and hippocampus, it is not surprising that M₁-KO mice exhibited deficits in multiple biochemical and behavioral studies related to learning and memory. Specifically, M₁-KO mice have been shown to exhibit cognitive deficits in behavioral tests such as the eight-arm radial maze, fear-conditioning (under conditions requiring extra-hippocampal mechanisms), and social discrimination⁴⁵⁻⁴⁷. Interestingly, no deficits were found in other tests of cognition such as the Morris water maze, a common paradigm for assessing impairments in hippocampal-dependant spatial reference memory^{45,47}. These and other related behavioral findings have contributed to the hypothesis that M₁ is not required for initial formation of memory in the hippocampus but is likely important to long-term memory consolidation and to interactions between the hippocampus and cortex⁴⁶. Electrophysiological experiments using M₁-KO mice have suggested that M₁ activation enhances *N*-methyl-D-aspartic acid receptor (NMDAR) currents in hippocampal slices⁴⁸. Likewise, in related electrophysiology experiments investigating long-term potentiation (LTP) in M₁-KO mice, selective hippocampal impairments were found compared to wild-type (WT) under certain conditions^{45,49,50}. Biochemical evidence from M₁-KO mice also supports a role for M₁ in certain learning and memory processes. For instance, activation of MAPK signaling, which is believed to be highly important to synaptic plasticity, was absent in cultured cortical cells from M₁-KO mice (versus WT) following muscarinic agonist stimulation^{51,52}. Similar results were also found in analogous experiments using hippocampal pyramidal neurons from M₁-KO mice⁵².

Taken together, these and other related findings support the notion that M₁ plays a role in learning and memory; however, it is likely that other mAChRs are also important to specific cognitive functions. Indeed, pan-mAChR antagonists such as scopolamine induce substantial cognitive deficits beyond those observed with genetic deletion of M₁ alone, and other mAChRs have been implicated in various electrophysiological and biochemical roles highly relevant to learning and memory functions^{45,53,54}. Moreover, M₁-KO mice exhibit hyperlocomotor activity, which complicates other behavioral assessments and may be related to the expression of striatal M₁ receptors in WT animals^{45,47,55}. Such hyperlocomotion is likely due to elevated striatal dopamine (DA) levels in M₁-KO mice, which were found to be approximately 2-fold greater than in WT controls⁵⁵. Lastly, WT mice given high doses of the muscarinic agonist pilocarpine will fall into seizures that most often culminate in death. This effect was completely abolished in M₁-KO mice, suggesting that M₁-mediates pilocarpine-induced seizure activity, possibly via the enhancement of NMDAR signaling⁴⁹.

Genetic deletion of M₃ in mice has suggested that this subtype plays an important role in central regulation of metabolism, which is consistent with M₃ localization in the thalamus/hypothalamus. Specifically, mice lacking M₃ are hypophagic and exhibit significantly reduced total body weight (~25% decrease versus WT), reduced fat pad mass (~50% decrease versus WT), and reduced serum levels of leptin and insulin (~5-10x decrease versus WT)^{45,56}. These effects have been hypothesized to occur due to absence of M₃ that is normally expressed on melanin-concentrating hormone (MCH)-positive neurons located in the hypothalamus⁵⁶. Given the overlapping CNS expression pattern and similar signaling properties between M₃ and M₁, it is likely that cortical and/or

hippocampal M₃ contributes to certain aspects of learning and memory. Indeed, recent behavioral studies with M₃-KO mice revealed profound deficits in contextual fear-conditioning but none in auditory cue fear-conditioning, suggesting that M₃ plays a role in hippocampal-dependent learning and memory⁵⁷. In agreement with localization data, deletion of M₃ has also been shown to substantially reduce ACh-induced smooth muscle contraction in the periphery⁵⁸⁻⁶⁰. Likewise, muscarinic agonist-induced salivation was decreased but not abolished in M₃-KO mice, suggesting that M₃ as well as other mAChRs play a role in salivary secretion⁶¹.

In the case of M₅, consistent with its highest expression in midbrain dopaminergic neurons where it is the only mAChR present, M₅-KO mice have suggested that this subtype plays an important role in mediating reward-responses through the mesolimbic DA pathway and in regulation of striatal DA levels (**Fig. 3**)^{34,37,45}. Specifically, muscarinic-agonist induced elevations in striatal DA release were reduced (~5-10x versus WT), but not abolished in M₅-KO mice brain slices, which has led to the hypothesis that lack of pre-synaptic M₅ heteroreceptors located on dopaminergic terminals innervating the striatum are responsible for this effect⁶². However, based on numerous localization studies, a virtual absence of M₅ expression in the striatum is at odds with this hypothesis, and the slices used in this particular study would not have contained the distal DA cell bodies that originate from the midbrain, where M₅ is most likely excitatory and post-synaptic^{37,62}. Additional evidence that M₅ plays a vital role in the mesolimbic DA pathway comes from microdialysis experiments with M₅-KO mice. In WT mice, electrical stimulation of hindbrain cholinergic nuclei (Ch. V and Ch. VI) leads to a prolonged and significant rise in DA levels of the nucleus accumbens (NAc), the primary

forebrain target of VTA dopaminergic projections, which was completely abolished in M_5 -KO mice⁶³. Behaviorally, M_5 -KO mice exhibit substantially reduced sensitivity to the rewarding effects of drugs such as cocaine and opiates (both of which act as strong activators of mesolimbic DA signaling)^{45,64,65}. These mice displayed large decreases in self-administration of cocaine and decreased conditioned place-preference (CPP) in response to training with cocaine or morphine place-pairing^{64,65}. Additionally, morphine-induced elevations of DA levels in the NAc and in Fos-B expression were reduced in M_5 -KO mice⁶⁴. Furthermore, withdrawal-induced anxiety behaviors were less pronounced in M_5 -KO⁶⁴. Interestingly, morphine retained its analgesic efficacy in M_5 -KO mice, suggesting that if M_5 antagonists proved useful in the treatment of opiate addiction, the pain-alleviating effects of such drugs may be retained in clinical settings⁶⁴.

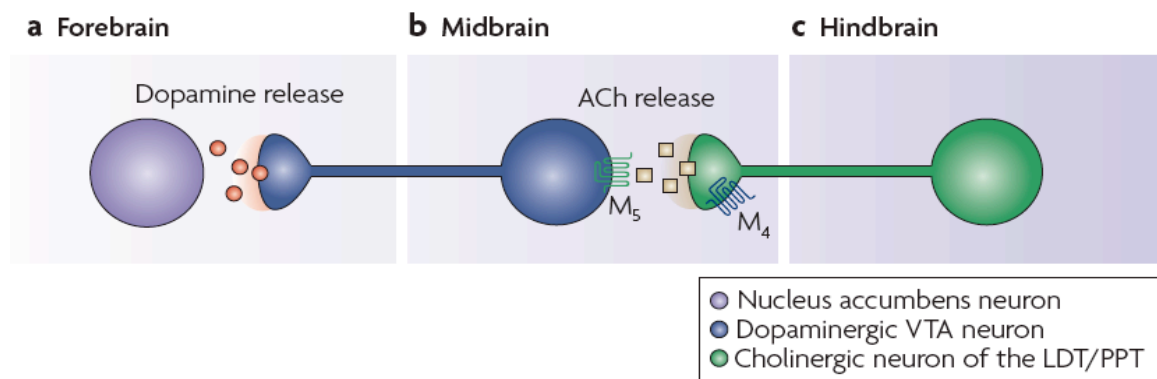


Figure 3. Abbreviated diagram of the putative roles of M_4 and M_5 in the central mesolimbic DA pathway (Wess 2007).

Taken together, this large body of data supports the hypothesis that the primary role of neuronal M_5 is in regulation of central DA signaling/pathways. Although less research has focused on nigrostriatal DA signaling, it is likely that M_5 plays a similarly important and parallel role. However, other studies with M_5 -KO mice have found subtle

deficits in cognitive function and in neuroanatomical/biochemical correlates of cognition. Specifically, atrophy of cortical pyramidal neurons from M₅-KO mice was observed along with modest behavioral deficits in spatial and non-spatial memory functions (as assessed by Y-maze and novel object recognition tests, respectively)⁶⁶. LTP at the mossy fiber-CA3 synapse of the hippocampus was also impaired in brain slices from M₅-KO mice⁶⁶. Some or all of these deficits may be indirect results of decreased cerebral blood flow (CBF) and oxygen delivery resulting from absence of M₅ in the cerebrovascular system. It is well established that decreased blood flow to the brain can disrupt cognitive functions and alter brain histology^{67,68}. In WT animals, ACh-induces a pronounced vasodilatory effect across multiple cerebrovascular structures, which is completely abolished in M₅-KO mice⁶². Furthermore, mice lacking M₅ exhibit a tonic/constitutive constriction of cerebral blood vessels that results in decreased cerebral blood flow, which may underlie the cognitive effects⁶⁶. Interestingly, ACh-induced vasodilation in peripheral vascular tissues was unaffected by genetic M₅ deletion, consistent with the hypothesis that the M₃ receptor mediates the peripheral vasodilatory effects of ACh⁶². Cholinergic neurons, particularly those originating in basal forebrain structures, provide direct innervation to cerebral blood vessels, where ACh release induces vasodilation likely via a nitric oxide (NO)/cyclic guanosine monophosphate (cGMP)/protein kinase G (PKG)-dependent mechanism⁶⁹⁻⁷². Thus, some of the cognitive symptoms of CNS disorders, including Alzheimer's disease (AD) and cerebrovascular dementia, may be related to decreased CBF resulting from loss of cholinergic nuclei of the basal forebrain and consequently decreased activation of cerebrovascular M₅^{66,67}. The potential

therapeutic relevance of these findings is discussed in more detail in a subsequent section of this Chapter.

High doses of muscarinic agonists such as oxotremorine induce tremor and hypothermia in rodents, which was completely abolished and reduced, respectively, in M₂-KO mice⁷³. Likewise, analgesic efficacy of muscarinic agonist administration was reduced in these mice, consistent with related studies that found electrophysiological deficits in spinal ganglion neurons of M₂-KO mice^{73,74}. In isolated heart atria, absence of M₂ resulted in a complete lack of carbachol-induced bradycardia, which agrees with previous localization and pharmacological studies suggesting that M₂ is the predominant mAChR mediating the parasympathetic actions of ACh in cardiac tissue⁷⁵. In the case of central M₂, mice lacking this receptor were devoid of oxotremorine-induced inhibition of ACh-release in both cortical and hippocampal brain slices, which supports the hypothesis that M₂ is mainly present as a pre-synaptic autoreceptor governing ACh release⁷⁶. *In vivo*, behavioral studies with M₂-KO mice found impairments in passive avoidance as well as elevated ACh efflux in the hippocampus⁷⁷.

Consistent with high striatal M₄ expression and principally pre-synaptic auto/heteroreceptor role(s) for M₄ in the CNS, M₄-KO mice were found to lack oxotremorine-mediated inhibition of ACh and DA release in striatal slices^{76,78}. These mice also exhibited increased basal locomotor activity, increased sensitivity to dopamine D₁ receptor (D₁) agonist-induced hyperlocomotion, and increased sensitivity to phencyclidine (PCP)-mediated disruptions in pre-pulse inhibition (PPI)^{79,80}. These results are not surprising given the purported interplay between central M₄ activation and decreased DA signaling⁸¹. Furthermore, they suggest that activation of M₄ may have

therapeutic relevance to treatment of the positive symptoms of schizophrenia, given the established role of elevated DA as a large component underlying this symptom cluster⁴⁴.

Despite these pronounced phenotypic effects of selective mAChR genetic deletion, all M₁-M₅-KO mice are devoid of overt abnormalities in general development, reproductive ability, or lifespan⁴⁵. Furthermore, compensatory up-regulation of other mAChR subtypes in these KO mice appears to be absent, as expression levels for all remaining mAChR subtypes in every individual KO mice strain are approximately equal to those of WT mice⁴⁵. Nonetheless, genetic approaches to studying mAChR function suffer from several disadvantages and caveats, such as differences in genetic background between multiple strains, unseen compensatory effects beyond the context of the cholinergic system, and the generally challenging technical aspects of mouse neurobiological research.

Therapeutic potential of mAChRs as drug targets

In light of the large body of data obtained from receptor localization and mAChR-KO mice studies, it is evident that selective activation or inhibition of signaling through one or more mAChR subtype may provide therapeutic utility for treatment of a wide range of diseases and disorders. Numerous pharmaceutical companies and research organizations have thus sought to discover and develop novel small molecule mAChR-targeted drugs⁴⁴. However, due to the difficulty in obtaining truly selective ligands for a particular subtype that arises from high orthosteric binding site structural homology across all mAChRs, few muscarinic drugs have reached the market⁴⁴. Internationally, current clinical use of approved muscarinic drugs is generally limited to antagonists for

the treatment of urinary incontinence, gastrointestinal and respiratory disorders, and in some cases Parkinson's disease. Nevertheless, great potential remains for drug discovery and development projects aimed at identifying novel subtype-selective mAChR ligands, particularly in the treatment of numerous CNS disorders based on the following hypotheses. For purposes of relevance to this thesis and in order to maintain focus on M₁, M₄, and M₅, which comprise the most important subtypes to treatment of CNS disorders, discussion of the therapeutic potential of selective M₂- or M₃- targeting is limited in the sections below.

One of the most well-known therapeutic potentials of selective M₁ activation is in the treatment of Alzheimer's disease, the most common cause of dementia, which is characterized by the two pathophysiological hallmarks of amyloid plaques comprised of amyloid- β (A β) and neurofibrillary tangles (NFTs) comprised of hyperphosphorylated tau^{44,82}. In general, progressive neurodegeneration with increased oxidative stress, inflammation, and decreased cerebral blood flow accompany these two hallmarks⁸². As is the situation for many CNS disorders, obtaining a clear and comprehensive understanding of the cause, progression, and complex molecular characteristics of AD has proven challenging, but will likely be vital to development of newer, more effective therapies. With the exception of the NMDA receptor antagonist Memantine, the only drugs currently approved for treatment of AD are AChE inhibitors (AChEIs), such as Donepezil and Rivastigmine, which are only moderately efficacious in addressing cognitive symptoms and cause numerous side effects^{83,84}. The rationale for this AChE inhibition approach stems from a longstanding cholinergic hypothesis of AD^{83,84}.

Degeneration of basal forebrain cholinergic neurons was observed as an early event in AD, and it is now believed that this contributes to the impairments in cognitive function⁸⁵⁻⁸⁷. Furthermore, numerous links between decreased ACh, A β deposition, and tau NFTs, have been found⁸⁸⁻⁹¹. This may provide a connection between the historic cholinergic hypothesis and more recent hypotheses that center on A β or tau as the primary factor in AD. Although a wide group of potential therapeutic strategies continue to emerge, many focus solely on reducing A β via inhibition of β -secretase, inhibition of γ -secretase, immunization to promote A β clearance, or prevention of A β aggregation⁹². However, cholinergic treatments directly targeting muscarinic receptors such as M₁ have also been explored preclinical and clinically as a means to overcome the limitations of AChE inhibitors. Although no M₁ agonists have reached the market, many have provided preclinical evidence supporting the M₁ receptor as a putative molecular target for AD⁴⁴.

In the cortex and hippocampus, M₁ is believed to mediate the post-synaptic actions of ACh released from basal forebrain neurons such as the nucleus basalis of Meynert (Ch. IV) and the diagonal band of Broca (Ch. II)^{41,53,93}. Early and selective loss of these cholinergic neurons is a frequent feature of AD, and the degree of this degeneration correlates well with degree of dementia^{94,95}. In light of this, lesioning of these neurons by molecular neurotoxins such as 192 IgG-saporin has been used in rats as a model for AD, which has been found to recapitulate many aspects of the disease⁹⁶. Depending on specifics of the behavior test parameters, such as toxin dose and corresponding degree of lesioning, impairments in the learning of an attention task were observed in this model; however, performance defects in the Morris water maze were

only moderate, consistent with the results from studies using M₁-KO mice in this behavioral paradigm⁹⁶. In agreement with *in vitro* experiments demonstrating that activation of M₁ or M₃ (but not M₂ or M₄) in recombinant cells drives amyloid precursor protein (APP) processing towards the non-amyloidogenic pathway, basal forebrain cholinergic lesioning has been shown to increase cortical APP expression and amyloidogenic processing⁹⁷⁻⁹⁹. Interestingly, these effects can be partially reversed by treatment of lesioned animals with a muscarinic agonist, further implicating the connection between the muscarinic system and APP regulation⁹⁹. However, whether the observed non-amyloidogenic APP processing (i.e. reduction in A β secretion) *in vivo* is mediated by M₁ or M₃ and what downstream signaling pathways underlie this regulation remains to be determined, as the absence of subtype-selective ligands has hampered such investigation.

Many M₁ agonists have been evaluated in human AD trials, such as talsaclidine, sabcomeline, and xanomeline¹⁰⁰. Although some of these compounds displayed efficacy in reducing behavioral symptoms or in decreasing A β levels in the cerebrospinal fluid (CSF), all such candidates to date have failed in development largely due to side effects arising from lack of subtype-selectivity, such as those mediated by peripheral M₂ and M₃ activation⁴⁴. Efficacy of mAChR agonists in tests of cognitive function in AD trials was absent or moderate; however, it is not known whether this was due to lack of selectivity for M₁, poor CNS penetration or other drug metabolism and pharmacokinetic (DMPK) factors, dose-limitations from peripheral side effects, or if M₁ is simply not a clinically valid target for AD (or perhaps some combination of these possibilities)⁴⁴.

In cortical and hippocampal samples obtained post-mortem from human AD patients, the protein levels of M₁ generally remain unaltered; however, M₂ levels are significantly reduced^{101,102}. This is likely due to the pre-synaptic localization of M₂ on basal forebrain cholinergic neurons, which would be expected to reflect decreased M₂ levels as degeneration occurs. This decrease in M₂ is also found in basal forebrain cholinergic lesioned animals⁹⁶. Given the pre-synaptic role of M₂ in regulating ACh release from these nuclei, selective targeting of this mAChR by small molecule antagonists has been considered in pharmaceutical development for AD⁴⁴. *In vivo* antagonism of M₂ has been shown to increase ACh release; although, this approach suffers from potential drawbacks associated with the likely diminished M₂ receptor protein levels in already-diagnosed AD patients as well as the serious cardiovascular liabilities inherent to M₂ antagonism^{44,102}. The fact that post-synaptic M₁ levels in the cortex remain approximately the same throughout AD suggests that selective activation of this subtype may be a more optimal approach if truly selective drugs were available. These findings and related considerations based on links between M₁, cognition, APP processing, and tau phosphorylation have been used to construct proposals that integrate putative signaling relationships in AD (**Fig. 4**)⁴⁴.

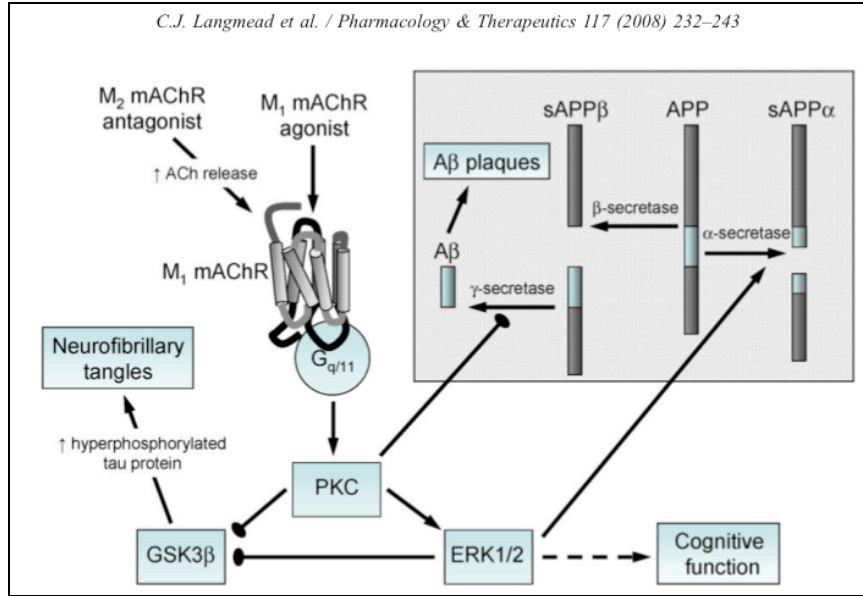


Figure 4. Proposed signaling relationships between M₁, APP processing, tau NFTs, and cognition, within the context of Alzheimer’s disease. (Adapted from Langmead *et al.* 2008)

However, decreased functional activity of M₁ in brain tissue from AD patients may still limit the utility of this strategy, which may have contributed to the failure of muscarinic agonists in clinical trials for AD. Interestingly, decreases in high affinity agonist binding, agonist-stimulated PLC activity, agonist-stimulated guanosine trisphosphate-γS (GTPγS)-binding, and GTPase activity provide evidence that G-protein coupling downstream of M₁ is disrupted in AD^{101,103}. The reason for this uncoupling is not known, nor is it established that restoration of G-protein signaling downstream of M₁ could be achieved via receptor agonism or potentiation by allosteric modulators known to increase G-protein coupling efficiency in recombinant systems.

In addition to AD, M₁ activation may prove useful in the treatment of schizophrenia⁴⁴. Although a thorough discussion of the current understanding of the underlying mechanisms responsible for producing each of the positive, negative, and cognitive symptom clusters observed in schizophrenic patients lies beyond this scope of

this Chapter, it is generally believed that hyperactivity of the forebrain DA signaling contributes heavily to the positive symptom cluster¹⁰⁴. This belief arose from numerous lines of evidence, including the observation that chronic administration of dopaminergic drugs of abuse such as cocaine and amphetamine can lead to emergence of positive symptom-like behaviors in non-schizophrenic individuals as well as the fact that most currently used antipsychotic drugs with positive symptom efficacy possess high-affinity DA receptor antagonist properties¹⁰⁴. In light of the high expression of M₁ and M₄ in the striatum, the pronounced elevation in forebrain DA levels as well as the pro-psychotic phenotype (i.e. increased locomotion and increased sensitivity to dopamine agonists in behavioral models of psychosis) observed in mice lacking these receptors, it is possible that drugs targeting central M₁ and/or M₄ may prove efficacious in the alleviation of the positive symptoms of schizophrenia.

Interestingly, administration of NMDAR antagonists such as PCP can recapitulate all symptom clusters of schizophrenia in normal individuals and can also exacerbate symptoms in previously stable psychotic patients¹⁰⁵⁻¹⁰⁷. Correspondingly, enhancement of NMDAR signaling by increasing the synaptic concentration of its co-agonist glycine via inhibition of the central glycine type-1 transporter (GlyT1) has exhibited broad and robust efficacy in numerous preclinical models of psychosis^{108,109}. These and other related findings have led to a NMDA hypofunction hypothesis of schizophrenia¹⁰⁶. Given the importance of M₁ to certain aspects of learning and memory, including potentiation of NMDAR signaling, it is possible that M₁ activation may also prove efficacious in treatment of the cognitive symptom cluster. Although less established, M₄ activation may affect certain cognitive aspects of schizophrenia as well, given its

hippocampal expression and putative autoreceptor-mediated regulation of ACh release in multiple brain regions.

Perhaps the strongest evidence that M₁ and/or M₄ activation represents a viable treatment strategy for schizophrenia comes from clinical trials with the M₁/M₄-preferring orthosteric agonist xanomeline. Although lacking adequate subtype-selectivity and ultimately failing to successfully emerge from clinical development due to M₂/M₃-mediated dose-limiting peripheral side effects and DMPK-related issues, this compound proved effective in reducing a broad range of psychotic-like behavioral disturbances in a large phase III AD trial¹⁰⁰. A subsequent phase II trial performed to directly explore the utility of xanomeline in treatment of schizophrenia revealed improvements in measures of cognitive function and in some positive symptoms, and a multitude of preclinical animal studies found similarly promising results¹¹⁰. However, it has remained a longstanding question as to what degree activation of M₁ and M₄ has contributed to these anti-psychotic effects of xanomeline.

Given the relationships between M₁- and M₄-mediated regulation of striatal DA signaling and motor function, antagonism of M₁ and/or M₄ has been proposed as an attractive therapeutic strategy for treatment of various motor-related disorders such as Parkinson's disease and dystonia^{44,81}. Orthosteric anticholinergic drugs, such as procylidine and trihexyphenidyl, are presently used in the clinical management of such disorders; however, they suffer from poor-subtype selectivity and carry numerous side effects. Because M₁ activation is likely to be more important to cognitive function than M₄ activation in general, and because midbrain autoreceptor M₄ expression on cholinergic neurons projecting to the SNc and VTA (where it is believed to regulate ACh

release and thus subsequent excitation of dopaminergic projection neurons) renders M₄ antagonism particularly suited to reduction of forebrain DA levels, it has been suggested that selective M₄ antagonists would prove superior to M₁ antagonists in the treatment of motor dysfunction^{44,111}. However, to date no highly selective M₄ antagonists have passed through clinical development.

In the case of M₅, selective antagonism could be hypothesized to provide efficacy in treating the positive symptoms of schizophrenia due to its associated but opposite relationship to M₄ in regulation of mesolimbic DA release (**Fig. 3**). Whereas activation of M₄ in the VTA would purportedly cause decreased DA release in the NAc, antagonism of M₅ would be required to exert the same effect, and vice-versa for increasing NAc DA levels, due to the putative post-synaptic excitatory role of M₅ compared to the pre-synaptic inhibitory role of M₄, in the VTA. Similarly, given the importance of activation of the mesolimbic DA pathway to the rewarding and addictive properties of many illicit drugs such as cocaine and opiates, similar pharmacological approaches may be useful in the treatment of drug addiction^{44,111}. This represents perhaps the most well recognized therapeutic hypothesis for selective M₅ antagonism and lies in close agreement with studies using M₅-KO mice in models of drug addiction and reward. However, given the role of M₅ in mediating ACh-induced cerebrovasodilation and the various neuroanatomical and behavioral cognitive defects observed in M₅-KO mice, antagonism of M₅ for treatment of drug addiction may carry cerebrovascular and/or cognitive side effects.

Conversely, selective M₅ activation using a non-CNS penetrant drug would presumably produce the sole result of cerebrovasodilation, without impacting cholinergic

or dopaminergic neuronal activity and thereby avoiding unwanted side effects and recreational abuse potential. This possibility presents M₅ as a virtually ideal target for treatment of cerebrovascular disorders such as cerebrovascular dementia and prevention and/or treatment of ischemic stroke. If M₅ activation is found to regulate APP processing toward the non-amyloidogenic pathway in a manner analogous to that of M₁ or M₃, which would be predicted based on the close relationship between M₁, M₃, and M₅ intracellular signaling profiles, selective M₅ agonists may also prove useful for treating cerebral amyloid angiopathy (CAA). Furthermore, given that impaired cerebral blood flow and associated decreased cholinergic tone at cerebrovascular structures due to loss of cholinergic basal forebrain neurons has been observed in AD, it is possible that M₅ agonism alone or in combination with agonism of M₁ could address multiple aspects of AD pathology and thereby provide greater therapeutic benefit. However, no subtype-selective or even –preferring agonists or antagonists for the M₅ receptor have been reported, and therefore discovery of such ligands will clearly be necessary in order to pharmacological test these various therapeutic hypotheses.

Allosteric modulation of GPCRs

Introduction to allosteric modulation of GPCRs

Small molecules that bind to cell-surface receptors at sites topographically distinct from the orthosteric binding site and thereby modulate receptor activity were discovered long ago for ligand-gated ion channels such as the γ -amino-butyric acid (GABA) receptor A (GABA_A)¹¹². Numerous drugs of the benzodiazepine class bind to such allosteric

(“other”) sites on GABA_A, where they potentiate receptor activation in response to binding by orthosteric agonist (e.g. GABA)¹¹³. More recently, a number of small molecule chemotypes have been found to bind to allosteric sites on various GPCRs, such as the Class C metabotropic glutamate receptors (mGluRs) as well as numerous members of GPCR Class A including mAChRs (**Fig. 5**) and various chemokine receptors^{112,114}. Relatively fewer allosteric ligands have been identified for Class B GPCRs, which could be related to their lower abundance compared to Class A GPCRs¹¹⁵. These allosteric ligands may exhibit positive or negative modulatory effects on the target receptor, wherein the affinity and/or efficacy of the orthosteric probe (often the endogenous agonist) may be increased or decreased, termed positive allosteric modulation (PAM) and negative allosteric modulation (NAM), respectively¹¹⁵. Such modulation is fully dependent upon the presence of an orthosteric ligand; however, some series of allosteric modulators may also exhibit intrinsic receptor activity on their own in the absence of orthosteric ligand, which is typically observed at higher concentrations¹¹⁶. Alternatively, an allosteric modulator may bind to a receptor but exhibit a pharmacologically neutral/silent effect, wherein the binding affinity and functional efficacy of the orthosteric ligand remains unchanged^{114,116}. Increasingly, evidence for probe-dependent allosteric modulation has demonstrated that a given PAM or NAM may cause dramatically different modulatory effects on the same receptor, depending on what orthosteric ligand is present¹¹⁵.

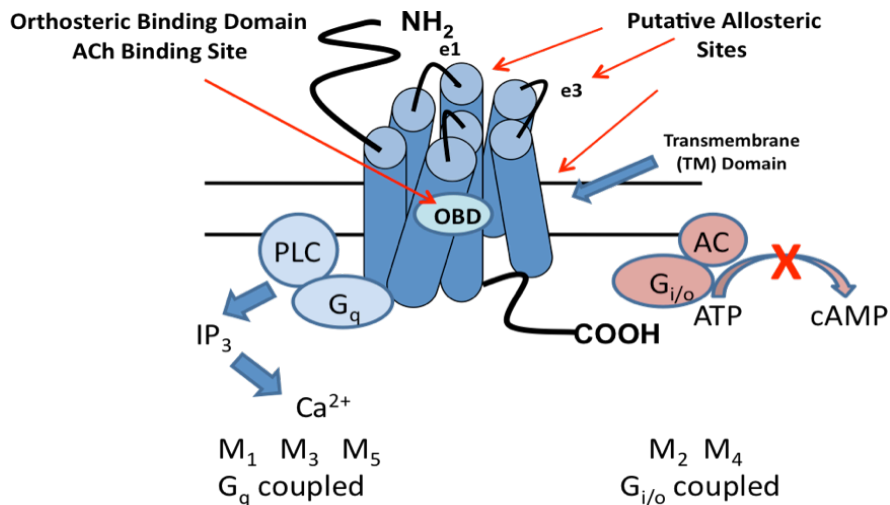


Figure 5. Generalized cartoon model of mAChR allosteric modulation depicting putative allosteric sites in relation to the orthosteric binding site.

Because receptor structure is often less conserved at allosteric binding sites across a given receptor subfamily (e.g. mAChRs), allosteric modulators often represent a means to achieve increased subtype-selectivity within a particular GPCR subfamily. However, given the possibility for probe-dependence, evidence is mounting that some purportedly highly-selective allosteric modulators only exhibit functional selectivity in the presence of a particular orthosteric agonist while actually binding to multiple subtypes of the target receptor subfamily with neutral modulation. In the presence of a different orthosteric probe, positive or negative modulatory effects at the other receptor subtypes may emerge, which underlines the importance of exploring functional selectivity with multiple orthosteric ligands. Nonetheless, allosteric modulators provide a number of possible therapeutic advantages over traditional orthosteric ligands beyond their often-superior selectivity for a given receptor¹¹⁵. Allosteric modulators provide a more subtle and physiologically-relevant approach to increasing or decreasing target activity because receptor activation will still only occur in the presence of the endogenous agonist that

remains under normal regulation^{115,116}. This may confer greater therapeutic tolerability and benefit for different CNS disorders. Furthermore, allosteric modulation may in some cases avoid receptor desensitization and/or down-regulation that often occurs following chronic administration of a traditional agonist^{115,116}. Target/mechanism-mediated side effects that could arise from accidental overdose may also be avoided with allosteric modulator drugs because they confer a ‘ceiling-effect’ where maximal receptor occupancy does not directly translate to a maximal effect of receptor activation that would normally result from a high dose of an orthosteric drug¹¹⁵.

Beyond the positive or negative modulation of a GPCR via an allosteric site, direct activation of the receptor in the absence of orthosteric ligand may also occur via allosteric ligand binding¹¹⁵. However, such allosteric agonists may also exhibit distinct subtype-selectivity via binding or functional propensities, positive or negative cooperativity with certain orthosteric ligands, and other pharmacological properties similar to those of PAMs or NAMs. Furthermore, different allosteric chemotypes may appear to be pure PAMs, NAMs, or agonists when a single receptor activation readout is used (e.g. mobilization of intracellular Ca^{2+}) but in reality possess various degrees of potency and efficacy for modulation of multiple downstream signaling cascades through the same receptor¹¹⁷. Such phenomena represent an additional layer of complexity in the study and use of allosteric modulators, which underlines the importance of thorough pharmacological characterization of a given compound prior to initiation of *in vivo* studies so that results may be properly interpreted.

Within the context of receptor theory, a variety of mathematical models have been presented to describe the relationships between allosteric modulator, orthosteric ligand,

and receptor. These range in complexity from the simpler four-point allosteric ternary complex model (ATCM, **Fig. 6**) to intricate multidimensional sixteen-point models^{114,115}. The former is based on the original ternary complex model (TCM) used to describe interactions between a ligand, receptor, and G-protein but is used here to describe interactions between two ligands and a receptor. In this model, each ligand is assigned an equilibrium dissociation constant (K_a and K_b) as well as a cooperativity factor (α) that denotes the mutual effect of the two ligands' on each other's affinity for the receptor. The value of α for two ligands can be determined empirically by measuring the affinity of one ligand (e.g. an orthosteric agonist) in the absence and presence of a saturating concentration of the second ligand (e.g. allosteric modulator) and then dividing the latter affinity by the former. Thus, values for α that are > 1.0 reflect positive cooperativity and those < 1.0 reflect negative cooperativity. An $\alpha = 1.0$ describes a cooperatively neutral relationship. Furthermore, efficacy modulation can be included in the ATCM by addition of the β variable, to reflect the positive or negative effect of one ligand (e.g. PAM) on another's efficacy (e.g. orthosteric agonist) (**Fig. 6**).

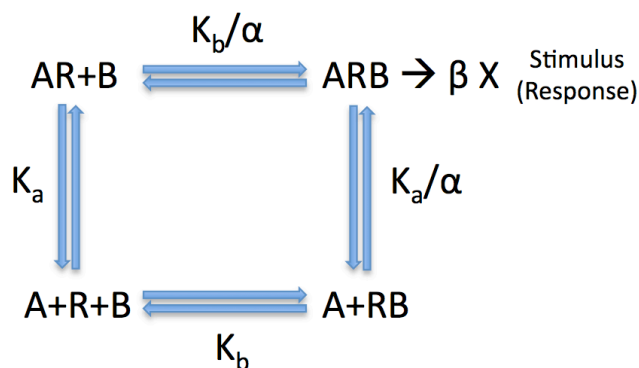


Figure 6. Allosteric ternary receptor complex model describing interaction between two ligands (e.g. allosteric modulator and orthosteric agonist) and a receptor. K_a and K_b reflect equilibrium dissociation constants (i.e. affinity values) for two ligands A and B that both bind simultaneously to receptor R. Binding cooperativity between A and B is denoted by α . Modulation of efficacy is denoted by β .

Characterization of allosteric modulators of GPCRs

A variety of functional and binding assays are often used to identify and characterize allosteric modulators. In the case of cell-based functional high-throughput screening (HTS) campaigns aimed at discovering novel allosteric modulators, which often utilize recombinant stably-transfected receptor expression systems with a straightforward readout for receptor activation such as fluorometric determination of intracellular Ca^{2+} mobilization, ‘double-add’ or ‘triple-add’ assay formats are most often employed¹¹⁶. For example, under a double-add format (**Fig. 7**), test compound is added to the cells at a fixed concentration after baseline has been established (i.e. first add). After a 2-5 minute equilibration period, a submaximal (e.g. $\sim\text{EC}_{20}$) concentration of agonist is added (i.e. second add). If the test compound is a PAM, it will enhance or potentiate the response to the submaximal agonist concentration (**Fig. 7**). Similar formats can be used to identify NAMs or antagonists by searching for compounds that decrease receptor activation in response to a near maximal (e.g. $\sim\text{EC}_{80}$) concentration of agonist.

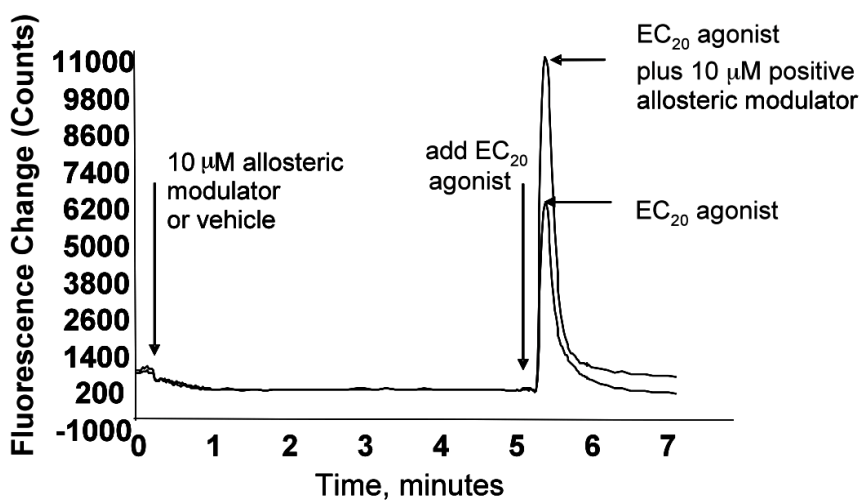


Figure 7. Example of a ‘double-add’ assay format designed to identify PAMs by functional fluorometric Ca^{2+} mobilization readout.

Once hits from such HTS have been identified, similar functional counter-screening and secondary screening is often performed using a test compound CRC assay format in the presence of a fixed submaximal concentration of orthosteric agonist (**Fig. 8a**). This allows determination of PAM (or NAM) potency values. Related functional assays using CRCs of orthosteric agonist in the absence and presence of increasing fixed concentrations of test compound can be used to assess a modulator's maximum efficacy in terms of 'fold-shift' of the agonist EC₅₀ induced by the test compound (**Fig 8b**). Together, these two basic assays can be used to characterize allosteric modulators' functional effects, which are typically used as the primary parameters in SAR descriptions and for driving potency/efficacy optimization efforts.

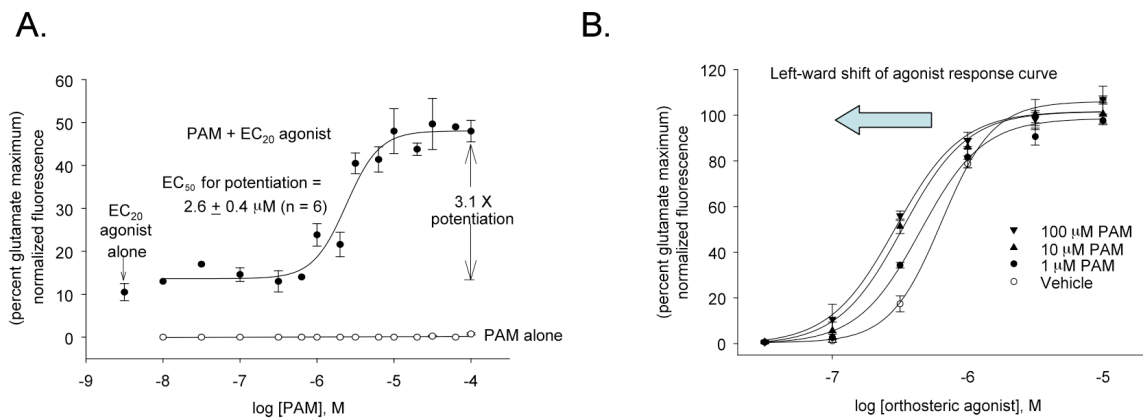


Figure 8. Example of generic PAM CRC in the presence of a fixed submaximal concentration of orthosteric agonist to determine PAM potency (A) and agonist CRC in the absence and presence of increasing fixed concentrations of PAM to determine fold-shift (B).

Radioligand binding experiments are useful for assessing the location and mechanism(s) of modulation for a given allosteric ligand. For instance, competition-binding under equilibrium conditions using a fixed low concentration of orthosteric antagonist radioligand in the presence of a CRC of an unlabelled allosteric modulator can

suggest or confirm that a novel compound binds to a site other than the orthosteric site if no inhibition is observed (i.e. allosteric). However, when a test compound causes binding inhibition, further experiments in the form of kinetic binding assays are often required to determine if such inhibition is via direct orthosteric competition with the radioligand or via a negative cooperativity effect (e.g. $1.0 > \alpha > 0$) through an allosteric site. Similar competition binding experiments utilizing CRCs of an orthosteric agonist in the absence and presence of fixed concentration(s) of allosteric modulator can be used to assess the latter's effect on the former's affinity and thereby calculate cooperativity (α)¹¹⁴. Together, these various functional and binding assays comprise the most common methods for characterizing novel allosteric modulators and have been used throughout many of the mAChR ligand optimization projects described in subsequent Chapters of this thesis (Chapters III-V).

Discovery of early allosteric modulators of mAChRs

A number of small molecules emerged early on providing proof of concept for allosteric mAChR modulation (**Fig. 9**). These included gallamine, brucine, thiochromine, and other related compounds, which were found to exhibit positive or negative cooperativity with an orthosteric probe at one or more mAChR in functional and/or binding assays^{118,119}. However, most of these ligands possessed poor potency, physiochemical properties, and DMPK liabilities that precluded their widespread use as mAChR research tools. Similarly, one of the first putative mAChR allosteric agonists, AC-42 (**Fig. 9**), exhibited highly M₁-selective functional activity but was found to exhibit little to no binding subtype-selectivity and displayed competition with multiple

orthosteric ligands^{119,120}. Interestingly, this compound was equipotent and efficacious in assays with the Y381A mutant M₁ receptor, which has been used along with evidence from other experiments to argue that AC-42 interacts with either an ectopic site near or overlapping with the orthosteric ACh site or to multiple sites at M₁^{117,121}. A second example of an early M₁ allosteric agonist is *N*-desmethylclozapine (NDMC, **Fig 9**), the primary circulating human metabolite of the commonly used antipsychotic drug clozapine³¹. Although NDMC is not completely selective for M₁, strong evidence that it binds to an allosteric site completely distinct from the orthosteric ACh site has been obtained from pharmacological experiments and receptor-mutagenesis studies³¹.

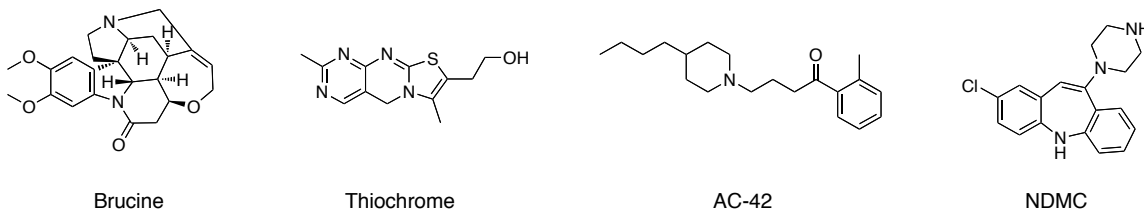


Figure 9. Structures of examples of early allosteric mAChR modulators.

Despite these discoveries and until recently, no highly subtype-selective mAChR allosteric ligands possessing the necessary drug-like pharmacological properties for universal and *in vivo* use had been reported. For instance, the AC-42 scaffold (now represented by its newer analog 77-LH-28-1) has been shown to possess a wide range of problematic off-target activities, NDMC exhibits similarly broad polypharmacology, and the early PAMs/NAMs do not represent tractable chemical optimization leads^{120,122}. However, contemporary high-throughput screening technology utilizing functional cell-based assays has led to a re-emergence of novel allosteric mAChR modulator discovery

projects. Subsequent Chapters of this thesis present and discuss our own efforts at identifying, optimizing, and characterizing novel subtype-selective ligands for M₄, M₅, and M₁ with the aim of obtaining useful drug-like tools suitable for the *in vitro* and *in vivo* study of mAChR neurobiology.

Notes on figure, table, and compound numbering/nomenclature

Throughout the remaining Chapters, all figure and table numbering is specific to each Chapter. Put differently, each Chapter's figure and table numbering begins with "1". Similarly, compound numbering formats and nomenclature are specific to each Chapter and in some cases each section of a given Chapter. Arbitrary numbering and letter codes (e.g. Compound 5 or **(5)**, analog 9a or **(9a)**) are used interchangeably throughout each Chapter. These are often used in place of full VU registration codes (e.g. VU0119498) in order to increase the ease of readability and to reduce space. Furthermore, for Materials and Methods Chapter II, compound numbering/nomenclature essentially mirrors that found in the associated Chapters III-V.

Chapter II

MATERIALS AND METHODS

Medicinal Chemistry

General synthetic methods, instrumentation, and workflow

In general, small scale (20-100 mg) reactions were carried out in parallel to generate compound libraries ranging from approximately 4-100 members in size. A small percentage of the total compounds synthesized across all projects were generated as singletons (i.e. individual isolated syntheses and not part of a library). Standard chemistry techniques were used for all reactions, and traditional thin-layer chromatography (TLC) and liquid chromatography mass spectrometry (LCMS) was used for analytical reaction monitoring. The following general purification methods were utilized depending on the particular chemical/compound and the amount of material: classical normal-phase glass-column silica gel chromatography, mass-directed reverse-phase high-performance liquid chromatography (HPLC), ultraviolet (UV)-directed reverse-phase HPLC, and standard recrystallization/filtration. Only high-quality HPLC grade solvents were used for purifications, and purity was defined as a sample containing approximately >98% of desired product by at least two independent analytical methods (e.g. evaporative light scattering device [ELSD], UV).

Microwave-assisted reactions were conducted using a Biotage Initiator-60. All nuclear magnetic resonance (NMR) spectra were recorded on a 400 megahertz (MHz) Bruker AMX NMR. ¹H chemical shifts are reported in δ values in parts per million

(ppm) downfield from TMS as the internal standard in dimethyl sulfoxide (DMSO). Data are reported as follows: chemical shift, multiplicity (s = singlet, d = doublet, t = triplet, q = quartet, br = broad, m = multiplet), coupling constant (Hz), and integration. ¹³C chemical shifts are reported in δ values in ppm with the DMSO carbon peak set to 39.5 ppm. Low resolution mass spectra were obtained on an Agilent 1200 LCMS with electrospray ionization. High resolution mass spectra were recorded on a Waters QToF-API-US plus Acquity system with electrospray ionization. Analytical thin layer chromatography was performed on 250 μ m silica gel 60 F₂₅₄ plates. Analytical HPLC was performed on an Agilent 1200 analytical LCMS with UV detection at 214 nm and 254 nm along with ELSD detection. Preparative purification of library compounds was performed on a custom Agilent 1200 preparative LCMS with collection triggered by mass detection.

For purposes of compound tracking and organization, all final compounds were transferred to 4 mL barcoded vials and diluted to a final concentration of 10 (or in some cases 50) mM in DMSO. Each new compound and each new batch of a previously synthesized compound was registered into a central computer database system, which assigned a unique VU identification number. A new synthetic batch of a given compound is designated by a corresponding number following a “—“ at the end of the VU identification number (e.g. batch one of VU0238429 is registered as VU0238429-1, batch two as VU0238429-2, etc...). At the present time of writing, the commercially available ChemChart program was used as the compound registration database software.

Following purification, dilution, and registration, compounds were characterized and assayed for pharmacological activity using the methods described in the associated

pharmacology section of this Chapter. In general, optimization projects utilized an iterative parallel library work-flow, wherein a certain region of a chemical scaffold was derivatized while the remainder of the scaffold was held constant for each analog of a given library. After pharmacological evaluation, SAR data from a given present library was used to design/plan the subsequent library such that the optimization proceeds in a cyclic and progressive manner toward improvement of a given property or characteristic of the scaffold (e.g. potency, efficacy, subtype-selectivity, off-target activity, cLogP, etc.). One implementation of this paradigm that was routinely utilized is presented in **Figure 1**. For most projects, an initial HTS using a functional cell-based assay was performed with either the Molecular Libraries Screening Center Network (MLSCN)/Molecular Libraries Probe Center Network (MLPCN) or the Vanderbilt HTS center (VHTSC) compound collections to identify hits. In other projects, lead compounds were identified via cheminformatics or via public disclosures (e.g. conferences, scientific literature, patent literature, etc...).

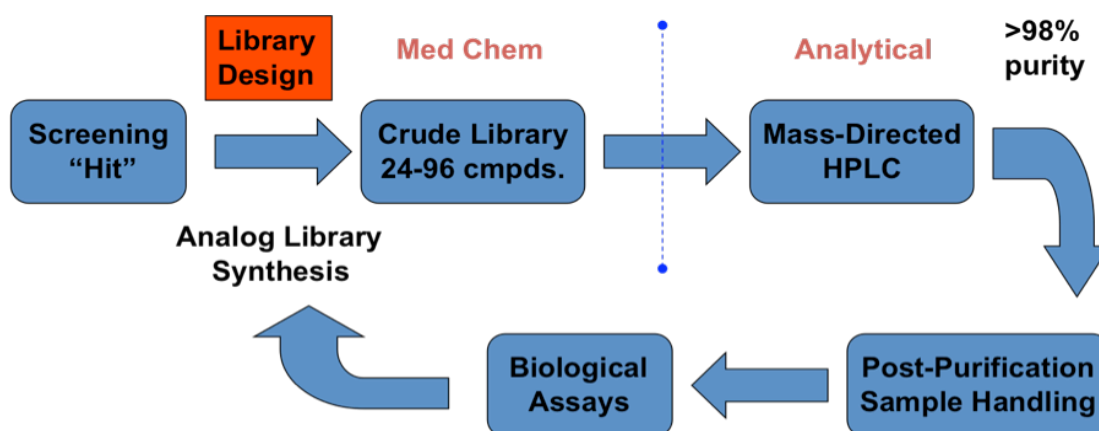


Figure 1. Generalized work-flow utilizing iterative synthesis and testing of parallel analog libraries aimed at optimizing a given property or characteristic of the lead structure/scaffold.

The complete details of each compound's full synthetic and purification procedure are too expansive for inclusion in this Chapter, and therefore such are presented only for select key and representative compounds/libraries from the various mAChR small molecule discovery/optimization projects described in this thesis. In general, the procedure for a specific type of reaction (e.g. amide-couplings, *N*- or *O*-alkylations, Suzuki-couplings, etc...) that is described for a given compound/library is applicable to other related compounds/libraries of a project that were made using the same reaction. Therefore, redundant procedures and procedures for non-key compounds/libraries have been excluded for sake of brevity and simplicity. For compounds/libraries whose procedures are not explicitly described, the conditions for their synthesis are presented in abbreviated form in the figures and text of Chapters III-V and in more detail in the associated referenced publications. Furthermore, to aid in clarity and organization, the order in which the syntheses are presented in this Chapter generally reflects the order in which the associated text and figures of Chapters III-V discuss the compounds/libraries. For some compounds whose synthesis is described under an general library procedure, only analytical characterization data is presented. Compound numbering in this Chapter is the same as that which is used in the associated text/figures of Chapters III-V.

M₄ PAM syntheses

Initial eastern amide analog library general procedure. Each of thirty-one glass vials containing 3 mL of CH₂Cl₂ were loaded with *N,N*-diisopropylethylamine (0.3 mL, 1.70 mmol), 3-amino-4,6-dimethylthioenol[2,3-*b*]-pyridine-2-carboxylic acid (50

mg, 0.225 mmol, SPECS AM-807/25050004), 1-hydroxybenzotriazole hydrate (30.4 mg, 0.225 mmol, 1.0 equivalents), polystyrene-bound *N*-cyclohexylcarbodiimide (317 mg, 0.450 mmol, 1.42 mmol/g, 2.0 equivalents), and one of thirty-one amines (0.225 mmol, 1.0 equivalents). The reactions were stirred for 48 hours at room temperature. Next, macroporous triethylammonium methylpolystyrene carbonate (145 mg, 0.225 mmol, 3.11 mmol/g, 2.0 equivalents) was added, and the reactions were stirred for an additional 3 hours at room temperature. Then, the reactions were filtered and concentrated on a heat-air block to afford 84-99% pure products. Those <99% pure were purified by mass-directed HPLC.

VU0152099. To a stirred solution of 3-amino-4,6-dimethylthioenol[2,3-*b*]-pyridine-2-carboxylic acid (3.0 g, 13.51 mmol [Chembridge cat.# 4003557]) in CH₂Cl₂ (90 mL) was added *N,N*-diisopropylethylamine (10 mL, 56.66 mmol), 1-hydroxybenzotriazole hydrate (1.83 g, 13.51 mmol, 1.0 equivalents), 4-methoxybenzylamine (2.04 g, 14.86 mmol, 1.1 equivalents), and *N*-(3-dimethylaminopropyl)-*N'*-ethyl-carbodiimide hydrochloride (5.18 g, 27.02 mmol, 2.0 equivalents) at 25 °C under room atmosphere. After 48 hours, macroporous triethylammonium methylpolystyrene carbonate (4.4 g, 13.51 mmol, 3.077 mmol/g, 1.0 equivalents) was added to the solution, which was then stirred for 3 hours at 25°C under room atmosphere. Next, the solution was vacuum filtered and the filtrate was separated with citric acid (1.0 M in water) and CH₂Cl₂. The organics were dried over MgSO₄ and concentrated *in vacuo* to produce a dark yellow solid. The solid was purified by column chromatography (silica gel, fixed 1:2 EtOAc:hexanes) to afford 2.5 g (7.33 mmol, 54%) of the title compound as a bright yellow solid. Analytical LC/MS (J-Sphere80-S4, 3.0 x

50 mm, 4.0 min gradient, 5%[CH₃CN]:95%[0.1%TFA/H₂O] to 100%[CH₃CN]): 2.773 min, >99% (214 nm and ELSD), M+1 peak *m/e* 342.12; ¹H NMR (400 MHz, DMSO-d₆) δ 7.27 (d, *J* = 8.8 Hz, 2H), 6.89 (s, 1H), 6.86 (d, *J* = 8.8 Hz, 2H), 6.34 (br s, 2H), 5.80 (s, 1H), 4.53 (d, *J* = 6.0 Hz, 2H), 3.79 (s, 3H), 2.73 (s, 3H), 2.57 (s, 3H); ¹³C NMR (100 MHz, DMSO-d₆) δ 165.9, 159.3, 159.2, 147.7, 143.9, 130.7, 129.3, 123.7, 122.4, 114.4, 98.5, 55.5, 43.3, 24.5, 20.4; HRMS (Q-ToF): *m/z* calc for C₁₈H₁₉N₃O₂S [M + H]: 342.1198; found, 342.1276.

VU0152100. To a stirred solution of 3-amino-4,6-dimethylthioenol[2,3-*b*]-pyridine-2-carboxylic acid (2.50 g, 11.26 mmol [Chembridge cat.# 4003557]) in CH₂Cl₂ (90 mL) was added *N,N*-diisopropylethylamine (10 mL, 56.66 mmol), 1-hydroxybenzotriazole hydrate (1.52 g, 11.26 mmol, 1.0 equivalents), piperonylamine (1.87 g, 12.38 mmol, 1.1 equivalents), and *N*-(3-dimethylaminopropyl)-*N'*-ethylcarbodiimide hydrochloride (4.32 g, 22.52 mmol, 2 equivalents) at 25 °C under room atmosphere. After 48 hours, macroporous triethylammonium methylpolystyrene carbonate (3.66 g, 11.26 mmol, 3.077 mmol/g, 1.0 equivalents) was added to the solution, which was then stirred for 3 hours at 25 °C under room atmosphere. Next, the solution was vacuum filtered and the filtrate was separated with citric acid (1.0 M in water) and CH₂Cl₂. The organics were dried over MgSO₄ and concentrated *in vacuo* to produce a dark yellow solid. The solid was purified by column chromatography (silica gel, fixed 1:2 EtOAc:hexanes) to afford 2.0 g (5.63 mmol, 50%) of the title compound as a yellow solid. Analytical LC/MS (J-Sphere80-S4, 3.0 x 50 mm, 4.0 min gradient, 5%[CH₃CN]:95%[0.1%TFA/H₂O] to 100%[CH₃CN]): 2.740 min, >99% (214 nm and ELSD), M+1 peak *m/e* 356.10; ¹H NMR (400 MHz, DMSO-d₆) δ 8.38 (s, 1H), 7.18 (s,

1H), 6.88 (s, 1H), 6.84 (d, $J = 8.0$ Hz, 1H), 6.78 (d, $J = 8.0$ Hz, 1H), 5.98 (br s, 2H), 5.97 (s, 2H), 4.30 (d, $J = 5.2$ Hz, 2H), 2.77 (s, 3H), 2.57 (s, 3H); ^{13}C NMR (100 MHz, DMSO- d_6) δ 179.9, 164.8, 161.7, 158.0, 153.4, 147.4, 133.8, 122.4, 121.9, 120.5, 108.0, 107.9, 100.8, 92.8, 42.1, 22.4, 20.0; HRMS (Q-ToF): m/z calc for $\text{C}_{18}\text{H}_{17}\text{N}_3\text{O}_3\text{S}$ [M + H]: 356.0991; found, 356.1069.

6-amino-2-mercapto-4-methylnicotinonitrile (6). To five 20 mL microwave vials containing 2-cyanothioacetamide (0.01 mol) each was added 3-aminocrotonitrile (0.01 mol) and then EtOH (10 mL). Once dissolved, pyridine (0.05 mol) was added and the vial was capped. The reaction mixtures were heated to 160°C for 12 min. consecutively. The crude reaction mixtures were combined and concentrated to a dark red oil. To this was added MeOH (150ml) and heated to reflux, upon cooling an orange solid crashed out which was filtered and washed with ether to afford 3.47g of pure **(6)** (42%). ^1H NMR (400MHz, DMSO- d_6): δ 7.20 (br s, 2H), 5.90 (s, 1H), 2.2 (s, 3H). ^{13}C (100MHz, DMSO- d_6): δ 175.3, 155.1, 153.5, 118.0, 100.2, 98.9, 20.8. HRMS calcd for $\text{C}_7\text{H}_7\text{N}_3\text{S}$ [M + H] 166.0435; found 166.0439.

3,6-diamino-N-(4-methoxybenzyl)-4-methylthieno[2,3-*b*]pyridine-2-carboxamide (8). To a 20 mL microwave vial containing **(6)** (3.0 mmol) was added K_2CO_3 (6 mmol), and DMF (10 mL). To this solution was added solid **(7)** then capped, and heated to 160°C for 10 min. Once complete the reaction was partitioned between H_2O (100 mL) and DCM (100 mL), separated, and the aqueous layer washed 2x with DCM (100 mL). The organic layer was dried with solid MgSO_4 , filtered, and concentrated to a light brown solid. This solid was crystallized in EtOAc and Hexanes and filtered to obtain 0.8g of pure **(8)** as a light yellow solid (75%). ^1H NMR (400MHz,

DMSO-d₆): d= 8.41 (s, 1H), 7.13 (d, *J* = 8.8Hz, 2H), 6.98 (br s, 2H), 6.83 (d, *J* = 8.4 Hz, 2H), 6.12 (s, 1H), 3.89 (s, 2H), 3.72 (s, 3H), 2.22 (s, 3H). ¹³C (100MHz, DMSO-d₆): d= 167.4, 160.8, 160.1, 158.1, 151.0, 131.1, 128.3, 116.7, 113.7, 103.9, 55.0, 41.9, 32.8, 19.6. HRMS calcd for C₁₇H₁₈N₄O₂S [M + H] 343.1222; found 343.1229.

Alkylamine library (9a-s) general procedure. To a 5 mL microwave vial containing **(8)** (0.073 mmol), was added Cs₂CO₃ (0.21 mmol), KI (0.073 mmol), R¹-Cl (0.080 mmol), and DMF (3 mL). The reaction was stirred 5 min. to eliminate CO₂, capped, and heated to 160°C for 30 min. Once complete the reaction was partitioned between H₂O (5 mL), and DCM (5 mL), separated via a 12 mL IST phase separator, concentrated and purified by mass directed HPLC to furnish **9a-s** (15-80%).

Alkylether library (13a-s) general procedure. To a 5 mL microwave vial containing **(12)** (0.146 mmol), was added Cs₂CO₃ (0.438 mmol), KI (0.291 mmol), R¹-Cl (0.219 mmol), and DMF (3 mL). The reaction was stirred 5 min. to eliminate CO₂, capped, and heated to 160°C for 30 min. Once complete the reaction was partitioned between H₂O (5 mL), and DCM (5 mL), separated via a 12 mL IST phase separator, concentrated and purified by mass directed HPLC to furnish **13a-s** (15-80%).

2-mercapto-4-methyl-6-oxo-1,6-dihydropyridine-3-carbonitrile (11). To twelve 20 mL microwave vials containing 2-cyanothioacetamide (0.01 mol) each was added morpholine (0.01 mol) and then EtOH (10 mL). Once dissolved, ethylacetoacetate (0.01 mol) was added and the vial was capped. The reaction mixtures were heated to 160°C for 10 min. consecutively. The crude reaction mixtures were combined and concentrated to a dark red oil. To this was added DCM (200ml) and heated to reflux. Once cool, the solid product was filtered and washed 2x with DCM (200ml) to give 12.4g

of pale yellow **(11)** (62%). ¹H NMR (400MHz, DMSO-d₆): d= 10.40 (br s, 1H), 8.67 (br s, 1H), 5.38 (s, 1H), 1.99 (s, 3H). ¹³C (100MHz, DMSO-d₆): d= 176.3, 162.4, 151.0, 120.7, 106.8, 92.7, 20.5. HRMS calcd for C₇H₆N₂OS [M + H] 167.0277; found 167.0279.

3-amino-N-(4-methoxybenzyl)-4-methyl-6-oxo-6,7-dihydrothieno[2,3-b]pyridine-2-carboxamide (12). To a flask containing **(11)** (6.0 mmol) was added DMF (30 mL) then TEA (6.6 mmol), and cooled to 0°C with an ice bath. A solution of **(7)** (6.0 mmol) in DMF (30 mL) was slowly added to the reaction via addition funnel over 30 min. and allowed to return to r.t. overnight. The reaction was concentrated then partitioned between DCM (100 mL) and H₂O (100 mL), separated, and the aqueous layer washed 2x with DCM (100 mL). The organic layer was dried with solid MgSO₄, filtered, and concentrated to a pale yellow solid which was washed with EtOAc (3x 50 mL) to give 1.28g of pure **(12)** as a light yellow solid (62%). ¹H NMR (400MHz, DMSO-d₆): d= 8.52 (br s, 1H), 7.15 (d, *J* = 8.8 Hz, 2H), 6.84 (d, *J* = 8.8 Hz, 2H), 6.40 (s, 1H), 4.22 (d, *J* = 6.0 Hz, 2H), 3.97 (br s, 2H), 3.71 (s, 3H), 2.32 (s, 3H). ¹³C (100MHz, DMSO-d₆): d= 167.3, 158.2, 130.9, 128.7, 128.5, 115.5, 113.7, 113.6, 55.0, 42.0, 19.7. HRMS calcd for C₁₇H₁₇N₃O₃SNa [M + Na] 366.0888, found 366.0887.

Ethyl 3-amino-4-methyl-6-oxo-6,7-dihydrothieno[2,3-b]pyridine-2-carboxylate (15). To a flask containing **(11)** (26.5 mmol) was added DMF (250 mL) then TEA (29.2 mmol), and cooled to 0°C with an ice bath. A solution of **(14)** (26.5 mmol) in DMF (60 mL) was slowly added to the reaction via addition funnel over 30 min. and allowed to return to r.t. overnight. The reaction was concentrated then partitioned between DCM (250 mL) and H₂O (250 mL), separated, and the aqueous layer

washed 2x with DCM (150 mL). The organic layer was dried with solid MgSO₄, filtered, and concentrated to a pale yellow solid which purified via chromatography (1:1.5 EtOAc:Hexanes) to give 4.15g of pure **(15)** as a light yellow solid (63%). ¹H NMR (400MHz, DMSO-d₆): d= 6.42 (s, 1H), 4.12 (m, 4H), 2.34 (s, 3H), 1.18 (t, *J* = 7.2 Hz, 3H). ¹³C (100MHz, DMSO-d₆): d= 168.3, 164.8, 160.0, 154.5, 115.5, 106.8, 97.8, 59.9, 19.7, 13.9. HRMS calcd for C₁₁H₁₃N₂O₃S [M + H] 253.0647, found 253.0644.

Alkyl pyridone ethyl ester (16a-e) general procedure. To a 20 mL microwave vial containing **(15)** (0.04 mol), was added Cs₂CO₃ (0.012 mol), KI (0.008 mol), R¹-Cl (0.0044 mmol), and DMF (10 mL). The reaction was stirred 5 min. to eliminate CO₂, capped, and heated to 160°C for 30 min. Once complete the reaction was partitioned between H₂O (50 mL), and DCM (50 mL), separated, and the aqueous washed 1x with DCM (50 mL). The organic layer was dried with MgSO₄, filtered and concentrated. The resulting material was added to a 10g 60CC SCX cartridge and washed with 3 column volumes of MeOH. The product was then eluted with 2 column volumes of 2M NH₃ in MeOH to provide pure **(16a-e)** (75-95%).

Ethyl 3-amino-6-(3-(dimethylamino)propoxy)-4-methylthieno[2,3-*b*]pyridine-2-carboxylate (16a). ¹H NMR (400MHz, DMSO-d₆): d= 6.72 (s, 2H), 6.57 (s, 1H), 4.25 (m, 4H), 2.66 (s, 3H), 2.37 (t, *J* = 7.2 Hz, 2H), 2.16 (s, 6H), 1.84 (m, 2H), 1.27 (t, *J* = 6.8 Hz, 3H). ¹³C (100MHz, DMSO-d₆): d= 164.7, 163.8, 159.3, 150.3, 147.6, 119.1, 109.5, 64.5, 59.7, 55.5, 44.9, 26.3, 19.8, 14.4. HRMS calcd for C₁₆H₂₄N₃O₃S [M + H] 338.1538, found 338.1527.

Ethyl 3-amino-4-methyl-6-(2-morpholinoethoxy)thieno[2,3-*b*]pyridine-2-carboxylate (16b). ¹H NMR (400MHz, DMSO-d₆): d= 6.76 (s, 2H), 6.65 (s, 1H), 4.57

(br s, 2H), 4.24 (q, $J = 14.4, 7.2$ Hz, 2H), 3.72 (br s, 4H), 3.20 (br s, 6H), 2.70 (s, 3H), 1.27 (t, $J = 6.8$ Hz, 3H). ^{13}C (100MHz, DMSO- d_6): $\delta = 164.7, 163.1, 159.0, 150.3, 148.1, 119.6, 118.7, 115.7, 109.6, 64.3, 59.8, 55.5, 52.3, 19.9, 14.4$. HRMS calcd for $\text{C}_{17}\text{H}_{24}\text{N}_3\text{O}_4\text{S}$ [M + H] 366.1488, found 366.1476.

Ethyl 3-amino-4-methyl-6-(pyridin-2-ylmethoxy)thieno[2,3-*b*]pyridine-2-carboxylate (16c). ^1H NMR (400MHz, DMSO- d_6): $\delta = 8.55$ (d, $J = 4.4$ Hz, 1H), 7.80, (t, $J = 8.0$ Hz, 1H), 7.46 (d, $J = 8.0$ Hz, 1H), 7.33 (t, $J = 6$ Hz, 1H), 6.74 (s, 2H), 6.73 (s, 1H), 5.45 (s, 2H), 4.23 (q, $J = 14.0, 7.2$ Hz, 2H), 2.70 (s, 3H), 1.26 (t, $J = 7.2$ Hz, 3H). ^{13}C (100MHz, DMSO- d_6): $\delta = 164.7, 163.3, 159.0, 156.3, 150.2, 149.1, 148.1, 136.8, 122.9, 121.7, 119.6, 109.6, 68.1, 59.8, 19.9, 14.4$. HRMS calcd for $\text{C}_{17}\text{H}_{18}\text{N}_3\text{O}_3\text{S}$ [M + H] 344.1069, found 344.1057.

Ethyl 3-amino-4-methyl-6-(pyridin-3-ylmethoxy)thieno[2,3-*b*]pyridine-2-carboxylate (16d). ^1H NMR (400MHz, DMSO- d_6): $\delta = 8.70$ (s, 1H), 8.54 (d, $J = 4.8$ Hz, 1H), 7.89 (d, $J = 8.0$ Hz, 1H), 7.42 (t, $J = 4.8$ Hz, 1H), 6.75 (s, 2H), 6.97 (s, 1H), 5.42 (s, 2H), 4.24 (q, $J = 14.4, 7.2$ Hz, 2H), 2.69 (s, 3H), 1.28 (t, $J = 6.8$ Hz, 3H). ^{13}C (100MHz, DMSO- d_6): $\delta = 164.7, 163.3, 159.0, 150.3, 149.4, 149.1, 148.1, 136.1, 132.3, 123.5, 119.6, 109.6, 65.3, 59.8, 19.9, 14.4$. HRMS calcd for $\text{C}_{17}\text{H}_{18}\text{N}_3\text{O}_3\text{S}$ [M + H] 344.1069, found 344.1064.

Ethyl 3-amino-4-methyl-6-(pyridin-4-ylmethoxy)thieno[2,3-*b*]pyridine-2-carboxylate (16e). ^1H NMR (400MHz, DMSO- d_6): $\delta = 8.56$ (d, $J = 6.0$ Hz, 2H), 7.45 (d, $J = 6.0$ Hz, 2H), 6.77 (s, 1H), 6.75 (s, 2H), 5.45 (s, 2H), 4.24 (q, $J = 14.0, 6.8$ Hz, 2H), 2.71 (s, 3H), 1.27 (t, $J = 7.2$ Hz, 3H). ^{13}C (100MHz, DMSO- d_6): $\delta = 164.6, 163.1, 159.0,$

150.2, 149.6, 148.3, 145.9, 122.0, 109.6, 65.7, 59.8, 19.9, 14.4. HRMS calcd for $C_{17}H_{18}N_3O_3S$ [M + H] 344.1069, found 344.1057.

3-amino-*N*-(4-methoxybenzyl)-4-methyl-6-(pyridin-4-ylmethoxy)thieno[2,3-*b*]pyridine-2-carboxamide dihydrochloride (13k). 1H NMR (400MHz, DMSO- d_6): δ = 8.90 (d, J = 6.4 Hz, 2H), 8.14 (t, J = 5.6 Hz, 1H), 8.05 (d, J = 6.4 Hz, 2H), 7.22 (d, J = 8.8 Hz, 2H), 6.87 (d, J = 8.8 Hz, 2H), 6.84 (s, 1H), 5.73 (s, 2H), 4.32 (d, J = 5.6 Hz, 2H), 3.72 (s, 3H), 2.74 (s, 3H). ^{13}C (100MHz, DMSO- d_6): δ = 165.0, 162.0, 158.1, 156.9, 148.1, 147.9, 142.2, 132.0, 129.3, 128.5, 124.1, 121.0, 115.1, 113.6, 109.4, 65.3, 55.0, 41.6, 19.9. HRMS calcd for $C_{23}H_{23}N_4O_3S$ [M + H] 435.1491, found 435.1490.

3-amino-*N*-(2,3-difluorobenzyl)-4-methyl-6-(pyridin-4-ylmethoxy)thieno[2,3-*b*]pyridine-2-carboxamide dihydrochloride (21n). 1H NMR (400MHz, DMSO- d_6): δ = 8.92 (d, J = 6.8 Hz, 2H), 8.30 (t, J = 5.6 Hz, 1H), 8.09 (d, J = 6.4 Hz, 2H), 7.32 (m, 1H), 7.16 (m, 2H), 6.85 (s, 1H), 5.75 (s, 2H), 4.46 (d, J = 5.6 Hz, 2H), 2.74 (s, 3H). ^{13}C (100MHz, DMSO- d_6): δ = 165.2, 162.1, 157.8, 157.0, 150.8, 148.8, 148.3, 148.1, 146.4, 146.2, 141.4, 129.3 (d, J = 11.0 Hz), 124.5, 124.3, 120.9, 115.6 (d, J = 17.0 Hz), 109.5, 65.3, 35.7, 19.9. HRMS calcd for $C_{22}H_{19}N_4O_2F_2S$ [M + H] 441.1197, found 441.1196.

3-amino-*N*-(2,5-difluorobenzyl)-4-methyl-6-(pyridin-4-ylmethoxy)thieno[2,3-*b*]pyridine-2-carboxamide dihydrochloride (21o). 1H NMR (400MHz, DMSO- d_6): δ = 8.57 (d, J = 6.0 Hz, 2H), 8.19 (t, J = 5.6 Hz, 1H), 7.44 (d, J = 6.0 Hz, 2H), 7.24 (m, 1H), 7.10 (m, 2H), 6.77 (br s, 2H), 6.77 (s, 1H), 5.46 (s, 2H), 4.43 (d, J = 5.6 Hz, 2H), 2.72 (s, 3H). ^{13}C (100MHz, DMSO- d_6): δ = 165.3, 162.7, 159.3, 157.2, 156.9, 154.7, 149.6, 148.4, 147.9, 146.0, 128.8 (dd, J = 7.0, 17.0 Hz), 121.9, 120.6, 116.6 (dd, J = 8.0, 24.0

Hz), 115.2 (dd, $J = 5.0, 25.0$ Hz), 114.9 (dd, $J = 8.0, 24.0$ Hz), 109.6, 65.7, 35.9, 19.9. HRMS calcd for $C_{22}H_{19}N_4O_2F_2S$ [M + H] 441.1197, found 441.1194.

3-amino-*N*-tert-butyl-4-methyl-6-(2-morpholinoethoxy)thieno[2,3-*b*]pyridine-2-carboxamide dihydrochloride (18h). 1H NMR (400MHz, DMSO- d_6): δ 6.65 (s, 1H), 6.62 (s, 1H), 6.31 (br s, 3H), 4.71 (t, $J = 4.8$ Hz, 2H), 3.87 (m, 4H), 3.50 (m, 4H), 3.17 (m, 2H), 2.70 (s, 3H), 1.36 (s, 9H). ^{13}C (100MHz, DMSO- d_6): δ 165.3, 162.2, 162.1, 156.6, 147.6, 147.1, 120.9, 109.5, 62.0, 60.5, 54.7, 51.6, 51.2, 28.8, 19.9. HRMS calcd for $C_{19}H_{29}N_4O_3S$ [M + H] 393.1960, found 393.1958.

*M*₅ PAM syntheses

Initial matrix library of VU0119498 analogs. Compounds 21-112 were synthesized in parallel according to the following procedure. Isatin starting materials (0.34 mmol) were added to vials containing ACN (3 mL), K_2CO_3 (0.68 mmol, 2.0 eq), KI (0.03 mmol, 0.1 eq), and respective benzyl halides (0.85 mmol, 2.5 eq). The reactions were microwave irradiated at 160 °C for 10 min. Next, the reactions were partitioned into $CHCl_2$ and H_2O and then passed through disposable phase-separator columns (Biotage Isolute). The organics were concentrated on a heated air-drying block and then analyzed by LCMS. Purification by mass-directed Preparative HPLC afforded desired products as colored solids (20-95%) with >98% purity by ELSD and 214 nM UV analysis.

VU0119498. This HTS screening hit was resynthesized classically as a singleton prior to the library synthesis. To a vial containing ACN (25 mL) was added isatin (1.00 g, 6.80 mmol), K_2CO_3 (13.6 mmol, 2.0 eq), KI (0.68 mmol, 0.1 eq), and 4-

bromobenzylbromide (7.48 mmol, 1.1 eq). The reaction was stirred for ~24 hours at room temperature while monitored by TLC. After judging complete, the reaction was partitioned into EtOAc and H₂O, and the combined organics were dried over MgSO₄, filtered, and then concentrated *in vacuo*. The dried solid was then washed with diethyl ether (3 x 15 mL) to afford the pure 1-(4-bromobenzyl)indoline-2,3-dione title compound as a bright orange solid (1.96 g, 6.18 mmol, 91%). ¹H-NMR (400MHz, *d*₆-DMSO) δ 7.55 (m, 4H), 7.39 (d, *J* = 8.5, 2H), 7.11 (t, *J* = 7.8, 1H), 6.94 (d, *J* = 8.1, 1H), 4.88 (s, 2H). ¹³C-NMR (100MHz, *d*₆-DMSO) δ 182.91, 158.35, 150.07, 137.87, 135.01, 131.47, 129.64, 124.46, 123.33, 120.65, 117.80, 110.95, 42.27. LCMS (214 nm) 3.25 min (>98%); *m/z* 316.0 [M+H]. HRMS calcd for C₁₅H₁₀BrNO₂ [M+H] 315.9973 found 315.9974.

VU0238429. To a vial containing ACN (15 mL) was added 5-trifluoromethoxyisatin (1.00 g, 4.33 mmol), K₂CO₃ (8.66 mmol, 2.0 eq), KI (0.43 mmol, 0.1 eq), and 4-methoxybenzyl chloride (4.76 mmol, 1.1 eq). The reaction was stirred for ~24 hours at room temperature while monitoring by TLC. After judging complete, the reaction was partitioned into EtOAc and H₂O, and the combined organics were dried over MgSO₄, filtered, and then concentrated *in vacuo* to afford the pure 1-(4-methoxybenzyl)-5-(trifluoromethoxy)indoline-2,3-dione title compound as an orange solid (1.50 g, 4.26 mmol, 98%). ¹H-NMR (400MHz, *d*₆-DMSO) δ 7.60 (m, 2H), 7.36 (d, *J* = 8.7, 2H), 7.04 (m, 1H), 6.89 (m, 2H), 4.84 (s, 2H), 3.71 (s, 3H). ¹³C-NMR (100MHz, *d*₆-DMSO) δ 181.99, 158.73, 158.33, 149.00, 143.83, 130.35, 128.88, 126.94, 121.32, 118.79, 117.66, 114.02, 112.36, 55.05, 42.45. LCMS (214 nm) 3.37 min (>98%); *m/z* 352.1 [M+H]. HRMS calcd for C₁₇H₁₂F₃NO₄ [M+H] 352.0797 found 352.0795.

VU0238441. To a vial containing ACN (3 mL) was added 7-chloroisatin (150 mg, 0.826 mmol), K₂CO₃ (1.652 mmol, 2.0 eq), KI (0.083 mmol, 0.1 eq), and 4-trifluoromethylbenzyl bromide (0.909 mmol, 1.1 eq). The reaction was stirred for ~24 hours at room temperature while monitoring by TLC. After judging complete, the reaction was partitioned into EtOAc and H₂O, and the combined organics were dried over MgSO₄, filtered, and then concentrated *in vacuo* to afford the pure 7-chloro-1-(4-(trifluoromethyl)benzyl)indoline-2,3-dione title compound as an orange solid (267 mg, 0.786 mmol, 95%). ¹H-NMR (400MHz, *d*₆-DMSO) δ 7.64 (m, 4H), 7.15 (m, 3H), 5.28 (s, 2H). ¹³C-NMR (100MHz, *d*₆-DMSO) δ 181.56, 159.37, 145.27, 142.25, 139.26, 127.01, 125.30, 124.80, 123.51, 121.40, 115.58, 44.28. LCMS (214 nm) 3.46 min (>98%); *m/z* 340.0 [M+H]. HRMS calcd for C₁₆H₉ClF₃NO₂ [M+H] 340.0352 found 340.0353.

General procedure for Suzuki-coupling libraries. Glass vials containing 1-2 mL anhydrous THF were charged with starting material bearing a -bromo or -chloro substituted aryl/heteroaryl ring, a substituted boronic acid (1.2 equivalents), aqueous 1M Cs₂CO₃ solution (2.0 equivalents), and tetrakis(PPh₃)Pd(0) catalyst (0.1-0.2 equivalents). The vials were flushed with argon and then subjected to microwave irradiation for 5-20 min at 120 °C. Once complete, the reactions were passed through disposable celite (Isolute HM-N) columns (rinsing 2-3x column volume with DCM). The filtered organics were then concentrated *in-vacuo* or on a heated-air drying block to provide the crude products, which were analyzed by LCMS and then purified by HPLC.

VU0400265. To a flask containing acetonitrile (20 mL) was added 5-trifluoromethoxyisatin (750 mg, 3.245 mmol), potassium carbonate (897 mg, 6.490

mmol), 4-phenoxybenzyl bromide (897 mg, 3.407 mmol), and potassium iodide (54 mg, 0.325 mmol). The reaction was stirred overnight at room temperature and then judged complete by LCMS analysis. The solution was partitioned between CHCl_2 and H_2O , the organics were dried over MgSO_4 , and then the solution was filtered and concentrated *in vacuo* to afford the crude product. Purification by silica gel plug (1:3 EtOAc:Hexanes fixed solvent gradient) afforded the title compound as a bright red-orange sticky solid (1.340 g, 3.242 mmol, 99%); LCMS (>98%) M+H = 414.09 (1.65 min retention), ^1H NMR (>95%) (400 MHz, CDCl_3) δ = 7.52 (s, 1H), 7.36 (m, 6H), 7.15 (t, J = 7.2 Hz, 1H), 7.10 (t, J = 5.2 Hz, 2H), 6.86 (d, J = 8.8 Hz, 2H), 4.93 (s, 2H).

VU0402735. A 100 mL round bottom flask containing 5-(trifluoromethoxy)indoline-2-one (250 mg, 1.15 mmol) was vacuum purged 3x with argon, dissolved in DMF (30 mL), and cooled to 0 °C. Solid sodium hydride (82.8 mg, 3.45 mmol, 60% in mineral oil) was then added all at once and the reaction stirred until bubbling ceased. Dibromoethane (259 mg, 1.38 mmol) was added all at once and the reaction allowed to warm to room temperature overnight. Once complete the reaction was quenched with H_2O (4 mL) and concentrated *in situ*. The remaining material was partitioned between H_2O (50 mL) and DCM (50 mL) and filtered through a phase separator, and concentrated. The crude material was purified by HPLC (Gilson, ACN: H_2O w/ 0.1% TFA) obtain the pure intermediate (35 mg, 12.5% yield). LCMS [M+H]: 218.1.

This intermediate (30 mg, 0.138 mmol) was then brought up in ACN (1.5 mL) in a glass vial, to which K_2CO_3 (0.274 mmol), 4-methoxybenzyl chloride (0.166 mmol), and KI (0.014 mmol) was added. The vial was sealed and subjected to microwave irradiation

at 160 °C for 10 mins. After LCMS analysis, the reaction was judged complete and the solution was partitioned between DCM and H₂O before passage through a disposable phase separator column (Isolute). The organics were then concentrated on a heated-drying block to afford the crude product. Purification by HPLC (Gilson, ACN:H₂O w/ 0.1% TFA) provided the title compound with 98% purity (LCMS). LCMS [M+H]: 364.33

VU0402734. A 50 mL round bottom flask containing VU0238429 as starting material (50 mg, 0.142 mmol) was vacuum purged 3x with argon, dissolved in DCM (2 mL), added EtOH (100 mL) and cooled to 0 °C. Once cool added DAST (68.8 mg, 0.427 mmol) and allowed to warm to room temperature overnight. Once complete the reaction was quenched with saturated sodium bicarbonate (50 mL), H₂O (50 mL) and partitioned between DCM and filtered through a phase separator and concentrated. The crude material was purified by HPLC (Gilson, ACN:H₂O w/ 0.1% TFA) obtain the pure final product (23 mg, 43.4 % yield). LCMS [M+H]: 374.1.

VU0402733. A 100 mL round bottom flask containing VU0238429 as starting material (117 mg, 0.333 mmol) was vacuum purged 3x with argon, dissolved in THF (30 mL) and cooled to -78 °C. Once cool added 3.0 M solution of methyl magnesium bromide (0.122 mL, 0.366 mmol) over 5 min. and the reaction allowed to warm to room temperature overnight. Once complete the reaction was quenched with H₂O (50 mL), 1N HCl (50 mL) and partitioned between DCM and filtered through a phase separator and concentrated. The crude material was purified via column chromatography using EtOAc:Hexanes (1:2) to afford the pure final product (45 mg, 37 % yield). LCMS [M+H]: 368.1.

VU0414747. To a glass vial containing 3 mL DMF was added methyl 4-hydroxybenzoate (500 mg, 3.286 mmol), Cs₂CO₃ (4.929 mmol), and 2,6-difluoropyridine. The vial was then sealed and thermally heated to 130 °C for approximately 5 hr before judging complete by TLC/LCMS. The reaction was then partitioned between EtOAc and H₂O, and the organics were washed with brine, dried over MgSO₄, filtered, and then concentrated *in-vacuo*. The crude intermediate product was carried forward without purification as highly pure (>90%) clear oil (738 mg, 2.985 mmol, 91%).

To a vial containing this intermediate product (431 mg, 1.88 mmol) was added 30 mL toluene under air-free argon atmosphere and the solution was cooled to 0 °C by ice bath. Next, DIBAL (1M solution in toluene, 2.1 equivalents) was added to the vial via argon syringe slowly over approximately 5 min. The reaction was stirred and allowed to warm to room temperature by removal of the ice bath. After approximately 2 hr, the reaction was judged complete by LCMS and then quenched with excess Rochelle's salt solution while continuing to stir at room temperature for 1.5 hr. The solution was then partitioned into EtOAc and H₂O, and the organics were dried over MgSO₄, filtered, and then concentrated *in-vacuo* to afford the crude product with high (>90%) purity, which was carried forward without further purification (627 mg, 2.86 mmol, 96%).

To a glass vial containing this second intermediate product (100 mg, 0.456 mmol) was added 3 mL anhydrous DCM and then PBr₃ (0.547 mmol) under air-free argon atmosphere at 0 °C by ice bath. The reaction was stirred and allowed to warm to room temperature by removal of the ice bath. After 2 hr, the reaction was judged complete by LCMS and then quenched with aqueous saturated sodium bicarbonate solution. The

solution was then partitioned with DCM, the organics were separated and concentrated *in-vacuo* to afford the crude product. Purification by HPLC (Gilson, ACN:H₂O w/ 0.1% TFA) provided the pure intermediate (>95% by LCMS) as a clear oily solid (75 mg, 0.266 mmol, 58%).

To a glass vial containing 1.5 mL DMF was added 5-trifluoromethoxyisatin (30 mg, 0.130 mmol), K₂CO₃ (0.260 mmol), the third intermediate product (0.156 mmol), and KI (0.013 mmol). The vial was then sealed and subjected to microwave irradiation at 120 °C for 30 min. The reaction was judged complete by LCMS and then partitioned between EtOAc and H₂O. The organics were then washed with brine, dried over MgSO₄, filtered, and concentrated *in-vacuo* to afford the crude final product. Purification by HPLC (Gilson, ACN:H₂O w/ 0.1% TFA) provided the title compound with high purity (>98% by LCMS) as an orange solid (8.8 mg, 0.020 mmol, 16%).

General procedure for *O*-alkylations. To a glass vial containing 1-2 mL DMF was added a phenol-bearing starting material (25-50 mg), substituted alkyl halide (1.5 equivalents), Cs₂CO₃ (3.0 equivalents), KI (0.2 equivalents), and HMPA (4.0 equivalents). The vial was then flushed with argon and subjected to microwave irradiation at 160 °C for 15 min. The reaction was then partitioned between EtOAc and saturated aqueous sodium bicarbonate. The organics were washed with brine, dried over MgSO₄, filtered, and then concentrated *in-vacuo* or on a heated-air drying block to afford the crude products, which were purified by HPLC.

General procedure for Mitsunobu libraries. To glass vials containing 2 mL THF was added PS-PPh₃ (2.63 mmol/g, 0.334 mmol) and DIAD (0.243 mmol) under argon. The solutions were stirred for 20 min at room temperature and then a phenol-

bearing starting material (0.152 mmol) and a substituted alcohol (0.197 mmol) was added under argon. The solutions were then stirred overnight at room temperature before being partitioned into DCM and H₂O. The solutions were passed through a disposable phase-separator column (Isolute) and the resulting organics were concentrated on a heated-air drying block to afford the crude products. Purification by mass-directed HPLC provided the final products with high purity (>98% by LCMS).

M₁ PAM syntheses

VU HTS hit VU0029767. To a solution of 4-ethoxyaniline (10.0 g, 72.9 mmol) in EtOH (100 mL) was added ethyl 2-bromoacetate (14.61 g, 87.0 mmol) and sodium acetate (8.97 g, 109.0 mmol) and stirred for 48 h at room temperature. Once complete, the reaction was then partitioned into H₂O and EtOAc and the organics washed with brine and dried over MgSO₄ before concentration *in vacuo*. The crude product was purified by passage through a silica plug eluting with 5% EtOAc in hexanes to afford the intermediate product ethyl 2-(4-ethoxyphenylamino)acetate (11.7 g, 72%) as a dark brown oil. To a solution of the acetate intermediate (4.0 g, 17.93 mmol) in MeOH (50 mL) was added hydrazine (177.9 mL, 177.9 mmol) and stirred for 16 h at 65 degrees C. Once complete, the reaction was then partitioned into H₂O and EtOAc, and the organics washed with brine and dried over MgSO₄ before concentration *in vacuo*. The crude product was purified by column chromatography (silica gel) eluting with 5% MeOH in CH₂Cl₂ to afford the intermediate product 2-(4-ethoxyphenylamino)acetohydrazide (2.5 g, 67%) as a white solid. To a solution of the hydrazide intermediate (2.0 g, 9.56 mmol) in DMF (100 mL) was added 2-hydroxy-1-naphthaldehyde (1.64 g, 9.56 mmol) and stirred

for 16 h at room temperature. Once complete, the reaction was concentrated *in vacuo* and the crude product was purified by filtration with diethyl ether wash (3x250 mL) to afford title compound (3.41 g, 98%) as a yellow solid; ¹H NMR (400 MHz, DMSO-d₆) δ 9.38 (s, 1H), 8.09 (d, *J* = 4.2 Hz, 1H), 7.80 (dd, *J* = 8.8, 4.4 Hz, 2H), 7.50 (t, *J* = 7.2 Hz, 1H), 7.31 (t, *J* = 7.2 Hz, 1H), 7.12 (d, *J* = 8.8 Hz, 1H), 6.67 (d, *J* = 8.8 Hz, 2H), 6.49 (d, *J* = 8.8 Hz, 2H), 5.69 (t, *J* = 6.0 Hz, 1H), 3.80 (q, *J* = 6.8 Hz, 2H), 3.73 (d, *J* = 5.6 Hz, 1H), 3.32 (s, 2H), 1.18 (t, *J* = 6.8 Hz, 3H). ¹³C NMR (100 MHz, DMSO-d₆) δ 167.2, 157.8, 150.6, 146.3, 142.7, 132.6, 131.6, 128.9, 127.8, 123.5, 120.7, 118.8, 115.4, 113.5, 113.3, 108.4, 63.3, 47.4, 14.8.; LC-MS (214 nm) 3.09 min (>98%); *m/z* 364.2 [M+H].

VU HTS hit VU0090157. To a solution of 6-nitrobenzo[*d*][1,3]dioxole-5-carbaldehyde (195 mg, 1.0 mmol) in MeOH (100 mL) was added 2-cyanoethyl 3-oxobutanoate (186 mg, 1.2 mmol), 1-methylurea (111 mg, 1.5 mmol), and *p*-TsOH (17 mg, 0.1 mmol) and refluxed for 4 h. Once complete, the reaction was filtered and the crude product was purified by recrystallization with MeOH and H₂O to afford the intermediate product 2-cyanoethyl 1,6-dimethyl-4-(6-nitrobenzo[*d*][1,3]dioxol-5-yl)-2-oxo-1,2,3,4-tetrahydropyrimidine-5-carboxylate (283 mg, 78%) as a white crystalline solid. To a solution of the carboxylate intermediate (1.0 g, 2.57 mmol) in acetone/H₂O (6/2 mL) was added 2 M NaOH (4 mL) at 0 degrees C, and the solution was warmed to room temperature and stirred for 2 h. Once complete, the reaction was acidified with 2 N HCl and partitioned into H₂O and CH₂Cl₂ and the organics were concentrated *in vacuo*. The crude product was purified by recrystallization with MeOH and H₂O to afford the intermediate product 1,6-dimethyl-4-(6-nitrobenzo[*d*][1,3]dioxol-5-yl)-2-oxo-1,2,3,4-tetrahydropyrimidine-5-carboxylic acid (790 mg, 92%) as a white crystalline solid. To a

solution of the acid intermediate (500mg, 1.49 mmol) in DMF (12 mL) was added cyclopentanol (385 mg, 4.48 mmol), EDC (428 mg, 2.24 mmol), and polystyrene-bound DMAP (1.5 mmol/g, 5.96 mmol) and irradiated at 100 degrees C for 20 m. Once complete, the reaction was partitioned into 1N HCl in H₂O and CH₂Cl₂ and the organics were concentrated *in vacuo*. The crude product was purified by recrystallization in EtOAc and hexanes to afford the title compound (200 mg, 33%) as a brown crystalline solid. ¹H NMR (400 MHz, DMSO-d₆) δ 7.60 (s 1H), 7.58 (d, *J* = 1.6 Hz, 1H), 6.95 (s, 1H), 6.23 (s, 1H), 6.20 (s, 1H), 5.81 (d, *J* = 1.4 Hz, 1H), 4.93 (m, 1H), 3.16 (s, 3H), 2.57 (s, 3H), 1.66 (m, 1H), 1.55 (m, 1H), 1.40 (m, 4H), 1.19 (m, 1H), 1.09 (m, 1H). ¹³C NMR (100 MHz, DMSO-d₆) δ 164.5, 152.6, 152.3, 151.8, 147.0, 141.3, 135.3, 106.9, 104.8, 103.4, 100.4, 75.9, 48.5, 32.0, 29.6, 23.0, 15.9. ; LC-MS (214 nm) 3.14 min (>98%); m/z 404.2

General procedure for Suzuki-coupling libraries. Glass vials containing 1-2 mL anhydrous THF were charged with starting material bearing a -bromo or -chloro substituted aryl/heteroaryl ring, a substituted boronic acid (1.2 equivalents), aqueous 1M Cs₂CO₃ solution (2.0 equivalents), and tetrakis(PPh₃)Pd(0) catalyst (0.1-0.2 equivalents). The vials were flushed with argon and then subjected to microwave irradiation for 5-20 min at 120 °C. Once complete, the reactions were passed through disposable celite (Isolute HM-N) columns (rinsing 2-3x column volume with DCM). The filtered organics were then concentrated *in-vacuo* or on a heated-air drying block to provide the crude products, which were analyzed by LCMS and then purified by HPLC.

General procedure for BQCA library I. Each of seven glass vials containing 2 mL of DMF were loaded with ethyl 8-fluoro-4-oxo-1,4-dihydroquinoline-3-carboxylate

(25 mg, 0.106 mmol, Maybridge BTB02003EA), K₂CO₃ (30 mg, 0.212 mmol, 2.0 equivalents), KI (2 mg, 0.011 mmol, 0.1 equivalents), and one of seven benzyl bromides (0.319 mmol, 3.0 equivalents). The reactions were stirred for 24 hours at room temperature before receiving polystyrene-bound thiophenol (0.159 mmol, 1.5 equivalents) each, and then stirred for an additional 3 hours. The reactions were then judged complete by LCMS, filtered, and separated into CH₂Cl₂ and H₂O. The organics were washed with brine, dried over MgSO₄, filtered, and concentrated *in vacuo* yielding seven benzyl-substituted ethyl 8-fluoro-4-oxo-1,4-dihydroquinoline-3-carboxylates confirmed by analytical LCMS. Next, crude products (0.1 mmol) and LiOH (8 mg, 0.3 mmol, 3.0 equivalents) were dissolved in 3 mL of THF:H₂O (9:1) in glass vials. The reactions were microwave irradiated at 120 °C for 10 minutes and then separated into EtOAc and H₂O, which was acidified to pH 4 drop-wise using 1N HCl. Organics were dried over MgSO₄, filtered, and concentrated *in vacuo* yielding seven benzyl-substituted 8-fluoro-4-oxo-1,4-dihydroquinoline-3-carboxylic acids confirmed by LCMS. Purification using mass-directed HPLC afforded the seven compounds (25-85% total yield) as TFA salts with >98% purity.

General procedure for BQCA library II. Each of seven glass vials containing 2 mL of DMF were loaded with ethyl 4-oxo-1,4-dihydroquinoline-3-carboxylate (25 mg, 0.115 mmol, Ryan Scientific 6J-050), K₂CO₃ (32 mg, 0.230 mmol, 2.0 equivalents), KI (2 mg, 0.012 mmol, 0.1 equivalents), and one of seven benzyl bromides (0.345 mmol, 3.0 equivalents). The reactions were stirred for 24 hours at room temperature before receiving polystyrene-bound thiophenol (0.173 mmol, 1.5 equivalents) each, and then stirred for an additional 3 hours. The reactions were then judged complete by LCMS,

filtered, and separated into CH₂Cl₂ and H₂O. The organics were washed with brine, dried over MgSO₄, filtered, and concentrated *in vacuo* yielding seven benzyl-substituted ethyl 4-oxo-1,4-dihydroquinoline-3-carboxylates confirmed by analytical LCMS. Next, crude products (0.1 mmol) and LiOH (8 mg, 0.3 mmol, 3.0 equivalents) were dissolved in 3 mL of THF:H₂O (9:1) in glass vials. The reactions were microwave irradiated at 120 °C for 10 minutes and then separated into EtOAc and H₂O, which was acidified to pH 4 dropwise using 1N HCl. Organics were dried over MgSO₄, filtered, and concentrated *in vacuo* yielding seven benzyl-substituted 4-oxo-1,4-dihydroquinoline-3-carboxylic acids confirmed by LCMS. Purification using mass-directed HPLC afforded the seven compounds (25-85% total yield) as TFA salts with >98% purity.

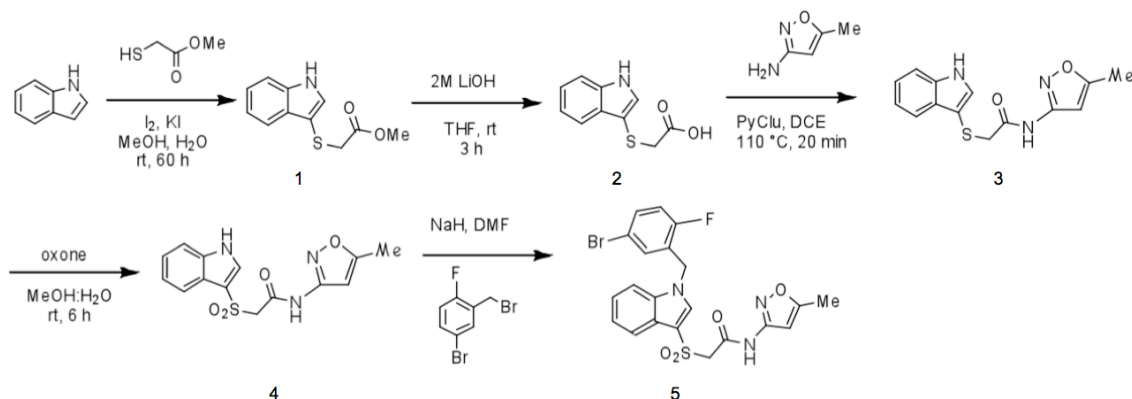
General procedure for BQCA library III. Each of seven glass vials containing 2 mL of DMF were loaded with ethyl 5,8-difluoro-4-oxo-1,4-dihydroquinoline-3-carboxylate (25 mg, 0.099 mmol, Ryan Scientific 6J-020), K₂CO₃ (27 mg, 0.198 mmol, 2.0 equivalents), KI (2 mg, 0.099 mmol, 0.1 equivalents), and one of seven benzyl bromides (0.297 mmol, 3.0 equivalents). The reactions were stirred for 24 hours at room temperature and atmosphere before receiving polystyrene-bound thiophenol (0.149 mmol, 1.5 equivalents) each, and then stirred for an additional 3 hours. The reactions were then judged complete by LCMS, filtered, and separated into CH₂Cl₂ and H₂O. The organics were washed with brine, dried over MgSO₄, and concentrated *in vacuo* yielding seven benzyl-substituted ethyl 5,8-difluoro-4-oxo-1,4-dihydroquinoline-3-carboxylates confirmed by analytical LCMS. Next, crude products (0.1 mmol) and LiOH (8 mg, 0.3 mmol, 3.0 equivalents) were dissolved in 3 mL of THF:H₂O (9:1) in glass vials. The reactions were microwave irradiated at 120 °C for 10 minutes and then separated into

EtOAc and H₂O, which was acidified to pH 4 drop-wise using 1N HCl. Organics were dried over MgSO₄ and concentrated *in vacuo* yielding seven benzyl-substituted 5,8-difluoro-4-oxo-1,4-dihydroquinoline-3-carboxylic acids confirmed by LCMS. Purification using mass-directed HPLC afforded the seven compounds (25-85% total yield) as TFA salts with >98% purity.

BQCA. To stirred solution of 200 mL DMF in a glass flask was added ethyl 4-oxo-1,4-dihydroquinoline-3-carboxylate (3.40 g, 15.66 mmol, Ryan Scientific 6J-050), K₂CO₃ (4.33 g, 31.32 mmol, 2.0 equivalents), KI (260 mg, 1.57 mmol, 0.1 equivalents), and 4-methoxybenzyl bromide (4.70 g, 23.49 mmol, 1.5 equivalents). After 48 hours of stirring at room temperature and atmosphere, the reaction was monitored by LCMS and judged complete. The reaction was then partitioned into CH₂Cl₂ and H₂O, and the organics were washed with brine, dried over MgSO₄, and concentrated *in vacuo*. Purification by diethyl ether washing (6 x 50 mL) afforded the intermediate product ethyl 1-(4-methoxybenzyl)-4-oxo-1,4-dihydroquinoline-3-carboxylate (4.99 g, 14.83 mmol, 95%) as an off-white solid at >98% purity by LCMS. To a glass vial containing ethyl 1-(4-methoxybenzyl)-4-oxo-1,4-dihydroquinoline-3-carboxylate (4.99 g, 14.83 mmol) in 90 mL THF:H₂O (5:1) was added LiOH (1.07 g, 44.49 mmol, 3.0 equivalents). The reaction was microwave irradiated at 120 °C for 10 minutes and then partitioned into CH₂Cl₂ and H₂O. The solution was re-acidified to pH 5 drop-wise using 2N HCl. The organics were dried over MgSO₄, filtered, concentrated *in vacuo*, and analyzed by LCMS. The crude product was purified by diethyl ether washing (6 x 50 mL) and additional H₂O wash (1 x 100 mL) to afford the intermediate product 1-(4-methoxybenzyl)-4-oxo-1,4-dihydroquinoline-3-carboxylic acid (3.20 g, 10.35 mmol, 70%) as an off-white crystalline

solid at >98% purity by LCMS. To a stirred solution of 1-(4-methoxybenzyl)-4-oxo-1,4-dihydroquinoline-3-carboxylic acid (1.89 g, 6.11 mmol) in 25 mL DMF in a glass flask at 0 °C was added NaH (143 mg, 5.99 mmol, 0.98 equivalents). The reaction was allowed to warm to room temperature and stirred for 1 hour before concentration *in vacuo*. The crude product was washed with diethyl ether (3 x 30 mL) to afford the title compound (1.80 g, 5.44 mmol, 89%) as a white solid at >98% purity by LCMS. ¹H NMR (400 MHz, D₂O): δ = 9.07 (s, 1H), 8.25 (d, *J* = 8.0 Hz, 1H), 7.53 (t, *J* = 8.4 Hz, 1H), 7.45 (d, *J* = 8.4 Hz, 1H), 7.39 (t, *J* = 8.0 Hz, 1H), 7.11 (d, *J* = 8.8 Hz, 2H), 6.79 (d, *J* = 8.8 Hz, 2H), 5.35 (s, 2H), 3.67 (s, 3H). ¹³C NMR (100 MHz, D₂O, externally referenced to DMSO-*d*₆): δ = 176.3, 172.2, 158.0, 147.4, 138.5, 132.3, 127.5, 127.2, 126.9, 125.5, 124.5, 117.5, 116.9, 113.8, 55.8, 54.7. HRMS calcd for C₁₈H₁₄NO₄Na₂ [M + 2Na] 354.0718, found 354.0716.

MLPCN M₁ PAM probe VU0405652.



To a solution of indole (3.00 g, 25.6mmol) and methyl thioglycolate (2.40 mL, 25.6 mmol) in methanol:water (80 mL : 20 mL) was added iodine (6.50 g, 25.6 mmol) and potassium iodide (4.25 g, 25.6 mmol). The reaction mixture was stirred at ambient temperature for 60 hours. Methanol was removed *in vacuo* and the aqueous layer diluted

with a saturated solution of sodium bicarbonate and extracted with ethyl acetate. The organic layer was dried over magnesium sulfate, evaporated *in vacuo* and the resulting residue was purified on a silica gel column (0-100% ethyl acetate:hexanes over 33 min) to afford compound **1** as an oil (LCMS >98%). Compound **1** was dissolved in a mixture of tetrahydrofuran (20 mL) and 2.0M aqueous LiOH (15 mL), then stirred vigorously at ambient temperature for 30 minutes. Tetrahydrofuran was removed *in vacuo*, the aqueous layer neutralized with 1.2 N HCl and extracted with CH₂Cl₂. The organic layer was dried over magnesium sulfate and removed *in vacuo* to produce an oily residue. Upon diluting the residue in dichloromethane a reddish-brown solid formed which was filtered and dried to yield compound **2** (2.00 grams, 9.65 mmol, 38% yield over 2 steps, LCMS >98%).

Compound **2** (650 mg, 3.14 mmol), 3-amino-5-methyl-isoxazole (616 mg, 6.28 mmol), PyClu (2.00 g, 6.28 mmol), and DIEA (1.36 mL, 7.85 mmol) were added to dichloroethane (25 mL) and microwave irradiated at 110 °C for 20 minutes. After cooling, the solvent was removed *in vacuo* and the remaining residue purified on a silica gel column (0-70% ethyl acetate:hexanes over 33 min) to yield compound **3** (642 mg, 2.23 mmol, 71% yield, LCMS >98%). Compound **3** (502 mg, 1.77 mmol) was dissolved in 25 mL (9:1, methanol:water) and oxone (10.0 g, 17.7 mmol) was added. Stirring at ambient temperature continued overnight. Water (20 mL) was added and the mixture extracted with ethyl acetate (3x20 mL). The organics were combined, dried over magnesium sulfate, and concentrated *in vacuo* to give an oily residue which was purified on silica gel (0-50% ethyl acetate:hexanes over 19 min) to yield compound **4** (500 mg, 1.57 mmol, 88% yield, LCMS >98%).

In a 5 mL microwave vial, compound **4** (55.0 mg, 0.174 mmol) was dissolved in DMF (3 mL) and cooled to 0 °C. Sodium hydride (60% by weight, 14.0 mg, 0.348 mmol) was then added in one portion and the reaction mixture vigorously stirred at 0 °C for 15 minutes. 4-bromo-2-bromomethyl-1-flouro-benzene (51.0 mg, 0.191 mmol) was added in one portion and the reaction mixture was stirred while being allowed to warm to ambient temperature over 3 hours. The reaction mixture was quenched with water (2 mL) and the solution was extracted with ethyl acetate (3x4 mL). The combined organics were dried over magnesium sulfate, concentrated *in vacuo* to give an oily residue which was purified on silica gel (0-70% ethyl acetate:hexanes over 19 min) to yield the final product (compound **5**, 45 mg, 0.088 mmol, 51% yield). LCMS >98% 214 nm, $R_T = 1.34$ min, $m/z = 506$ ($[^{79}\text{Br}]m+1$), 508 ($[^{81}\text{Br}]m+1$). $^1\text{H NMR}$ (400 MHz, DMSO_D6) 11.27 (s, 1H), 8.23 (s, 1H), 7.82 (d, $J = 8.0$ Hz, 1H), 7.63 (d, $J = 8.0$ Hz, 1H), 7.56-7.58 (m, 1H), 7.47 (dd, $J = 2.4$ Hz, 6.4 Hz, 1H), 7.35-7.23 (m, 3H), 6.54 (s, 1H), 5.62 (s, 2H), 4.43 (s, 2H), 2.37 (s, 3H), HRMS found: 506.0184; calculated for $\text{C}_{21}\text{H}_{17}\text{BrFN}_3\text{O}_4\text{S}$: 506.0185.

M₁ allosteric agonist syntheses

VU0184670. To a solution of benzoyl chloride (87.7 mg, 0.624 mmol) in dichloromethane (2 mL) was added *N*-boc-ethylenediamine (100.0 mg, 0.624 mmol) and PS-DIEA (2 eq, 356.6 mg). The reaction was agitated overnight at room temperature, after which the reaction mixture was filtered to remove polymer-supported resin. The filtrate was then concentrated and dissolved in 1mL of dichloromethane, to which was added 1mL of trifluoroacetic acid (1:1 DCM:TFA) and stirred at room temperature for 30 min. Following deprotection, the reaction mixture was again concentrated to dryness,

after which the product was dissolved in dimethylformamide (2mL). To this solution was added 1-carbethoxy-4-piperidone (106.8 mg, 0.624 mmol) and MP-BH(OAc)₃ (2.5 eq, 645 mg). The reaction mixture was then agitated overnight at room temperature, after which the resin was filtered off. Aqueous workup of the reaction mixture using brine and ethyl acetate, followed by filtration of the organic layer using an Isolute Phase Separator and sample concentration yielded ethyl 4-(2-(2-methylbenzamido)ethylamino)piperidine-1-carboxylate as a pale yellow oil. The product was then dissolved in 1 mL of DMSO and purified by mass-directed preparative HPLC to afford ethyl 4-(2-(2-methylbenzamido)ethylamino)piperidine-1-carboxylate -2,2,2-trifluoroacetate as a clear oil (64.5 mg, 23.9 %); ¹H-NMR (400 MHz, *d6* - DMSO) δ 7.9-7.8 (m, 1H), 7.52-7.42 (m, 5H), 6.73 (br s, 1H), 4.16-4.11 (q, *J* = 7.07 Hz, 1H), 3.56-3.50 (m, 4H), 2.92-2.90 (m, 6H), 2.29 (s, 1H), 1.38-1.32 (m, 7H); ¹³C-NMR (100 MHz, *d6* - CDCl₃): δ 166.95, 154.84, 134.20, 131.82, 128.65, 127.78, 61.24, 54.36, 43.60, 42.03, 36.30, 14.95; HRMS (*m/z*): [M+H] calcd. for C₁₇H₂₆N₃O₃, 320.1974; found, 320.1966.

VU0357017. To a solution of *o*-toluoyl chloride (96.5 mg, 0.624 mmol) in dichloromethane (2 mL) was added *N*-*boc*-ethylenediamine (100.0 mg, 0.624 mmol) and PS-DIEA (2 eq, 356.6 mg). The reaction was agitated overnight at room temperature, after which the reaction mixture was filtered to remove polymer-supported resin. The filtrate was then concentrated and dissolved in 1mL of dichloromethane, to which was added 1mL of trifluoroacetic acid (1:1 DCM:TFA) and stirred at room temperature for 30 min. Following deprotection, the reaction mixture was again concentrated to dryness, after which the product was dissolved in dimethylformamide (2mL). To this solution was added 1-carbethoxy-4-piperidone (106.8 mg, 0.624 mmol) and MP-BH(OAc)₃ (2.5 eq,

645 mg). The reaction mixture was then agitated overnight at room temperature, after which the resin was filtered off. Aqueous workup of the reaction mixture using brine and ethyl acetate, followed by filtration of the organic layer using an Isolute Phase Separator and sample concentration yielded ethyl 4-(2-(2-methylbenzamido)ethylamino)piperidine-1-carboxylate as a pale yellow oil. The product was then dissolved in 1 mL of DMSO and purified by mass-directed preparative HPLC to afford ethyl 4-(2-(2-methylbenzamido)ethylamino)piperidine-1-carboxylate -2,2,2-trifluoroacetate as a clear oil (102.9 mg, 36.9 %); $^1\text{H-NMR}$ (400 MHz, d_6 - CDCl_3) δ 7.37-7.18 (m, 7H), 6.30 (br s, 1H), 4.15-4.10 (q, $J = 7.07$ Hz, 1H), 3.54-3.50 (q, $J = 5.74$ Hz, 4H), 2.91-2.86 (m, 6H), 2.35 (s, 1H), 1.27-1.20 (m, 7H); $^{13}\text{C-NMR}$ (100 MHz, d_6 - DMSO) δ 130.96, 129.99, 127.76, 125.83, 61.23, 54.32, 43.38, 42.01, 28.07, 20.01, 14.94; HRMS (m/z): [M+H] calcd. for $\text{C}_{18}\text{H}_{28}\text{N}_3\text{O}_3$, 334.2131; found, 334.2130.

M₁ agonist TBPB analog syntheses

Reductive Amination with commercial piperidinones. Each of twenty-four glass reaction vials containing 3 mL of CH_2Cl_2 were loaded with MP-B(OAc)₃H (142 mg, 0.345 mmol, 2.42 mmol/g, 3.0 equivalents) and 4-(2-keto-1-benzoimidazoliny)piperidine (25 mg, 0.115 mmol, 1.0 equivalents). Then, one of 24 *N*-functionalized piperidinones (0.115 mmol, 1.0 equivalents) with either an alkyl or carbamate moiety was added to each reaction tube. The reactions were stirred overnight at room temperature. The next day, the solutions were filtered and washed with CH_2Cl_2 (3 x 3 mL), then dried before purification by mass-directed preparative HPLC.

General Procedures for Library Synthesis (Scheme 1): Synthesis of *N*-benzyl piperidinones. Each of sixty-four glass reaction vials containing 3 mL of CH₂Cl₂ and 0.1 mL of MeOH were loaded with piperidone hydrochloride (25 mg, 0.185 mmol, 1.0 equivalents) and K₂CO₃ (51 mg, 0.370 mmol, 2.0 equivalents). Then, one of sixty-four functionalized benzyl bromides (0.185 mmol, 1.0 equivalents) was added to each reaction tube. The reactions were stirred overnight at room temperature, partitioned between CH₂Cl₂ and H₂O, and the organics were concentrated on a heat-air block. Purification by preparative LCMS was performed to afford *N*-benzyl piperidinones products for subsequent reductive amination.

Reductive Aminations. Each of sixty-four glass reaction vials containing 3 mL of CH₂Cl₂ were loaded with MP-B(OAc)₃H (142 mg, 0.345 mmol, 2.42 mmol/g, 3.0 equivalents) and 4-(2-keto-1-benzoimidazoliny)piperidine (25 mg, 0.115 mmol, 1.0 equivalents) or 5-chloro-1-(4-piperidinyl)-2-benzimidazolone (29 mg, 0.115 mmol, 1.0 equivalents). Then, one of sixty-four tertiary amine hydrates (0.115 mmol, 1.0 equivalents) from the previous alkylation reactions was added to each vial, and the reactions were stirred overnight at room temperature. The next day, the solutions were filtered and washed with CH₂Cl₂ (3 x 3 mL), then dried before purification by mass-directed preparative HPLC.

TBPB. To a stirred solution of 4-piperidone monohydrate HCl (2.00 grams, 13.02 mmol) in dimethylformamide (100 mL) was added 2-methylbenzyl bromide (2.44 grams, 13.02 mmol) and K₂CO₃ (3.60 grams, 26.04 mmol, 2.0 equivalents) at room temperature. The reaction was then monitored by analytical LCMS, and once judged complete, the reaction was separated with water and EtOAc. The organics were next

washed with a saturated solution of NaCl and dried over MgSO₄ before being concentrated *in vacuo* to afford 2.59 grams (90%) of the hydrate form of 1-(2-methylbenzyl)piperidin-4-one as a colorless oil. Analytical LCMS (J-Sphere80-C18, 3.0 x 50.0 mm, 4.1 min gradient, 5%[0.05% TFA/CH₃CN]:95%[0.05% TFA/H₂O]:1.64 min, >99% (214 nm, 254 nm and ELSD) M+1 peak *m/e* 204.1; ¹H NMR (400 MHz, DMSO-d₆) d 7.28 (m, 1H), 7.16 (m, 3H), 3.53 (s, 2H), 2.67 (t, *J* = 6.4 Hz, 4H), 2.36 (s, 3H), 2.32 (t, *J* = 6.4 Hz, 4H). ¹³C NMR (100 MHz, DMSO-d₆) d 137.0, 136.4, 130.1, 129.3, 127.0, 125.4, 58.7, 52.4, 40.6, 18.8; HRMS calc'd for C₁₃H₂₀NO₂[M+H]; 222.1494 found 222.1488.

This intermediate 1-(2-methylbenzyl)piperidin-4-one (2.00 grams, 9.04 mmol) product was then brought up in a stirred solution of CH₂Cl₂ (100 mL) to which 4-(2-keto-1-benzimidazoliny)piperidine (2.16 grams, 9.95 mmol, 1.1 equivalents) was added at room temperature. Then, MP-triacetoxyborohydride (13.57 grams, 27.132 mmol [2.0 mmol/gram loading], 3.0 equivalents) was added and the reaction was monitored by analytical LCMS. Once judged complete, the reaction was filtered and the filtrate was purified by mass-directed preparative HPLC to afford 2.92 grams (80%) of title compound as a pure white solid. Analytical LCMS (J-Sphere80-C18, 3.0 x 50.0 mm, 4.1 min gradient, 5%[0.05% TFA/CH₃CN]:95%[0.05% TFA/H₂O]:2.34 min, >99% (214 nm, 254 nm and ELSD) M+1 peak *m/e* 405.2; ¹H NMR (400 MHz, DMSO-d₆) d 7.26 (d, *J* = 4.0 Hz, 1H), 7.18 (m, 3H), 6.96 (m, 4H), 4.22 (m, 1H), 4.09 (m, 1H), 3.37 (m, 2H), 3.18 (s, 1H), 3.05 (m, 1H), 2.96 (br d, *J* = 7.6 Hz, 2H), 2.81 (br d, *J* = 11.2 Hz, 2H), 2.67 (t, *J* = 6.0 Hz, 1H), 2.57 (br t, *J* = 11.2 Hz, 1H), 2.28 (m, 6H), 1.93 (br t, *J* = 10.8 Hz, 2H), 1.64 (m, 2H), 1.41 (m, 2H). ¹³C NMR (100 MHz, DMSO-d₆) d 153.6, 136.9, 130.1,

129.4, 129.2, 129.1, 128.3, 127.0, 125.5, 120.3, 108.8, 61.4, 60.2, 52.4, 49.9, 48.5, 45.8, 40.7, 29.2, 27.9, 18.8; HRMS calc'd for C₂₅H₃₃N₄O[M+H]; 405.2654 found 405.2654 .

TBPB analog 1b (ethyl carbamate derivative). To a stirred solution of 4-(2-keto-1-benzimidazolynyl)piperidine (50 mg, 0.230 mmol) in CHCl₂ (3 mL) was added ethyl 4-oxo-1-piperidinecarboxylate (43.3 mg, 0.253 mmol, 1.1 equivalents) and MP-B(OAc)₃H (285 mg, 0.691 mmol, 2.42 mmol/g, 3.0 equivalents). The reaction was then monitored by analytical LCMS, and once judged complete, the reaction was filtered and concentrated. Purification by mass-directed preparative HPLC afforded 32.50 mg (38%) of title compound as a beige-white solid. Analytical LC/MS (J-Sphere80-C18, 3.0 x 50.0 mm, 4.1 min gradient, 5%[0.05% TFA/CH₃CN]:95%[0.05% TFA/H₂O]:2.05 min, >99% (214 nm, 254 nm and ELSD) M+1 peak *m/e* 373.2; ¹H NMR (400 MHz, DMSO-d₆) δ 10.94 (s, 1H), 9.97 (br s, 1H), 7.31 (d, *J* = 4.4 Hz, 1H), 7.00 (m, 3H), 4.57 (m, 1H), 4.12 (br d, *J* = 11.6 Hz, 2H), 4.04 (q, *J* = 7.2 Hz, 2H), 3.59 (br d, *J* = 11.2 Hz, 2H), 3.47 (m, 1H), 3.24 (m, 2H), 2.82 (m, 2H), 2.66 (m, 2H), 2.05 (m, 2H), 1.94 (br d, *J* = 12.4 Hz, 2H), 1.59 (m, 2H), 1.19 (t, *J* = 6.8 Hz, 3H). ¹³C NMR (100 MHz, DMSO-d₆) δ 154.4, 153.6, 128.7, 128.4, 120.9, 120.3, 109.1, 108.6, 62.5, 60.9, 48.1, 46.6, 42.1, 25.8, 14.5; HRMS calc'd for C₂₀H₂₉N₄O₃[M+H]; 373.2240 found 373.2235.

M₁ antagonist syntheses

General parallel analog library synthesis. To a solution of 3-(benzo[*c*][1,2,5]thiadiazole-4-sulfonamido)-propanoic acid (50 mg, 0.17 mmol) and DIPEA (46 mL, 0.34 mmol) in DCM (2 mL) in a 4-mL vial was added polymer-supported DCC (283 mg, 0.34 mmol, 1.2 mmol/g), HOBT (27 mg, 0.2 mmol) and one of

24 amines (HNR_1R_2) and rotated at room temperature for 20 h. Then, MP-carbonate (151 mg, 0.5 mmol, 3.3 mmol/g) was added to scavenge excess acid and the HOBT. The reactions were filtered into 13 x 100 mm test tubes, and the resin washed (3 x 5 mL) with DCM. The combined organic layers were dried down on a nitrogen evaporator and the compounds purified to >98% by preparative LCMS on an Agilent 1200 Prep mass-directed LCMS purification system.

VU0255035 (compound 5b). To a solution of 3-(benzo[*c*][1,2,5]thiadiazole-4-sulfonamido)-propanoic acid (2.00 g, 6.94 mmol) and DIPEA (2.43 mL, 13.9 mmol) in DMF (10 mL) was added EDC (1.55 g, 8.33 mmol), HOBT (937 mg, 6.94 mmol) and 1-(4-pyridyl)piperazine (1.36 g, 8.33 mmol) and stirred at room temperature for 20 h. The reaction was diluted with water (80 mL) and extracted with EtOAc (2 x 100 mL). The combined organic extracts were washed with water (2 x 80 mL) and brine (100 mL), dried over MgSO_4 and concentrated under vacuum. The residue was triturated with CH_2Cl_2 /hexanes (1:1, 40 mL) to afford amide VU0255035 as a light tan solid (1.45 g, 48 %): mp 159.7-160.2 °C; ^1H NMR (400 MHz, DMSO-d_6) δ 8.37 (d, $J = 9.0$ Hz, 1H), 8.20 (d, $J = 7.0$ Hz, 1H), 8.16 (d, $J = 6.0$ Hz, 2H), 7.85 (dd, $J = 9.0, 7.0$ Hz, 1H), 7.71 (br s, 1H), 6.80 (d, $J = 6.0$ Hz, 2H), 3.51-3.40 (m, 4H), 3.35-3.28 (m, 4H), 3.21-3.12 (m, 2H); ^{13}C NMR (100 MHz, DMSO-d_6) δ 169.1, 155.4, 154.7, 149.5, 149.2, 132.5, 130.9, 129.3, 126.3, 108.6, 45.6, 45.3, 44.2, 41.7, 41.4, 33.0; Analytical LCMS (J-Sphere80-C18, 3.0 x 50.0 mm, 4.1 min gradient, 5%[0.05% TFA/ CH_3CN]:95%[0.05% TFA/ H_2O]: 1.95 min, >99%, (214 nM, 254 nm, ELSD), m/z $[\text{M}+\text{H}] = 433.1$; HRMS calc'd for $\text{C}_{18}\text{H}_{21}\text{N}_6\text{O}_3\text{S}_2$ $[\text{M}+\text{H}]$; 433.1117 found 433.1117.

Jetmilling/scale-up

For compounds used in *in vivo* behavioral and/or pharmacokinetic (PK)/plasma-brain levels (PBL) studies, a large-scale synthesis was performed (generally 200 mg to 10 g) to provide the required amount of material. In such cases where compound solubility or other physiochemical properties imposed substantial challenges during vehicle formulation, the material was passed through a jet-milling device (Model 00 Jet-O-Mizer with a High-Yield® Collection Module from Fluid Energy Processing & Equipment Company), which afforded uniform nanoparticles with improved solubility and physical properties.

***In vitro* Pharmacology**

Cell lines and cell culture

Rat M₁ cDNA, provided by T.I. Bonner (National Institutes of Health, Bethesda, MD), was used to generate the orthosteric-site mutant rat M₁^{Y381A} using the QuikChange site-directed mutagenesis kit. All tissue culture reagents were purchased from Invitrogen Corporation, Carlsbad, CA, unless otherwise noted. Cell lines used for all WT-mAChR studies stably expressed rat M₁, human M₂ and G_{qi5}, human M₃, rat M₄ and G_{qi5}, or human M₅ in the Chinese Hamster Ovary (CHO-K1) parental background. The M₁, M₃, and M₅ cell lines were cultured in HAM's F12 medium with 10% FBS, 20 mM HEPES, and 50 µg/mL G418 (Mediatech, Inc., Herndon, VA). M₂/G_{qi5} cells were cultured in the same media with 500 µg/mL hygromycin. M₄/G_{qi5} cells were cultured in the same media 400 µg/mL G418 and 500 µg/mL hygromycin. Cells expressing the rat M₁^{Y381A}

orthosteric-site mutant receptor were cultured in the same medium, except without hygromycin. Cell lines used for experiments performed with human M₄ were generated and used by Millipore and co-expressed the promiscuous G_{α16}.

Calcium mobilization assays

All functional cell-based calcium mobilization assays were performed essentially as previously described (Marlo *et al.*, 2009; Brady *et al.*, 2008) using either an FDSS or Flexstation according to the following protocols. These protocols represent the general methods used for the M₅ PAM, M₄ PAM, and M₁ PAM projects. The M₁ allosteric agonist and TBPB projects utilized similar methods with the exception that a single-add format was used wherein test compound is added at 2X alone with no second-add of ACh. For the M₁ antagonist project, similar methods were used as described for the M₅ PAM, M₄ PAM, and M₁ PAM projects with the exception that an ACh ~EC₈₀ was used in the second-add instead of an ~EC₂₀. Likewise for M₂-M₅ antagonism screening in the M₁ allosteric agonist project, an ACh ~EC₈₀ was used in the second-add instead of an ~EC₂₀ to assess functional antagonism.

For all FDSS screens/assays, cells (10,000 cells/20 µl/well) were plated in black-walled, clear-bottomed, TC treated, 384 well plates (Greiner Bio-One, Monroe, North Carolina) in Ham's F12 medium supplemented with 10% FBS and 20 mM HEPES. The cells were grown overnight at 37 °C in the presence of 5% CO₂. The next day, the medium was removed and replaced with 20 µl of 2 µM Fluo-4AM in calcium assay buffer (Hank's Balanced Salt Solution supplemented with 20 mM HEPES and 2.5 mM Probenecid) and the cell plates incubated for 60 minutes at 37 °C. Dye solution was

removed and replaced with 20 μ l of fresh assay buffer. Test compounds were transferred from a 384-well source plate (10 mM DMSO, 30 μ l/well) to 384-well daughter plates using an ECHO acoustic plate reformatter (Labcyte) and then diluted into assay buffer to 20 μ M stock concentration (2X). Acetylcholine (Aldrich) was diluted in a 384-well plate containing submaximal (\sim EC₁₀, determined empirically) and maximal (10 μ M) stock concentrations (5X). Mobilization of intracellular calcium was measured using the Functional Drug Screening System 6000 (FDSS6000, Hamamatsu). Baseline readings were taken and then test compounds (30 μ M final, 20 μ l/well) were added using the FDSS's integrated pipettor. After 150 seconds of equilibration, acetylcholine (EC₁₀ and maximal concentrations, 10 μ l/well) was added using the FDSS's integrated pipettor. Data were obtained as max-min fluorescent ratios and then normalized to percentage of maximum ACh response and represent mean values obtained from three independent determinations (error bars represent +/- SEM) unless otherwise specified.

For Flexstation screens/assays (which were primarily used to determine compound potency, ACh fold-shift efficacy, mAChR subtype-selectivity, etc...) the methods used were essentially the same as previously described (Marlo *et al.*, 2009, Brady *et al.*, 2008) and in a format similar to that described above using the same reagents. CHO cells stably expressing rM₁, hM₃, hM₅, rM₄/G_{qi5}, or rM₂/G_{qi5} were plated in 100 mL of growth medium at 5 X 10⁴ (rM₁, hM₃, and hM₅) or 6 X 10⁴ (hM₂, and rM₄) cells per well in Costar 96-well black-walled, TC-treated, clear-bottom plates (Fisher). Cells were incubated overnight at 37 °C under 5% CO₂. The next day, medium was removed from the cells, and they were incubated with 50 mL of 2 mM Fluo-4 AM diluted in assay buffer for 1 h at 37 °C. Dye was then removed and replaced with 45 mL of fresh

assay buffer. Test compounds were diluted in assay buffer at 2X concentration and acetylcholine was diluted in assay at a 10X concentration. FLEXstation II (Molecular Devices) automated plate reader was used for assay execution and measurement of calcium flux. After establishing baseline fluorescence, test compounds (45 μ L) were added to the cells using the FLEXstation II's integrated pipettor and allowed to equilibrate for 150 seconds before addition of acetylcholine (10 μ L). Data were obtained as max-min fluorescent ratios and then normalized to percentage of maximum ACh response. For test compounds exhibiting intrinsic fluorescence (typically found only at 30 μ M final), adjustment of analysis time window for max-min values was sometimes performed in order to obtain more accurate baseline readings. Calculation of potentiation EC_{50} and fold-shift of ACh CRC was performed using the curve-fitting software GraphPad Prism (version 4.0c). Data shown represent mean values obtained from at least three independent determinations performed in duplicate or greater (error bars represent +/- SEM) unless otherwise specified.

Radioligand binding assays

M₄ PAMs (all) competition binding assays. M₄ cells were washed once with ice-cold phosphate-buffered saline, pH 7.4. Cells were then harvested with a cell scraper, resuspended in ice-cold buffer (20 mM HEPES, 100 mM NaCl, 10 mM MgCl₂, pH 7.4), and homogenized using a glass homogenizer (Dounce). The homogenate was centrifuged at 20,000g for 20 min at 4 °C. This final step was repeated twice more with homogenization between centrifugations, and the final pellets were resuspended and homogenized in ice-cold buffer in aliquots at a final protein concentration of 1-3 mg mL⁻¹

1 and stored at -80 °C until use. Protein concentrations were measured using the Bio-Rad Protein Assay Kit (Bio-Rad, Hercules, CA) with serum albumin (Pierce Chemical, Rockford, IL) as the standard. For each binding experiment, membranes were resuspended and homogenized in ice-cold buffer. Non-specific binding, calculated in the presence of 1 μ M atropine, was never greater than 10% of total binding; in both saturation and competition binding experiments, bound radioligand did not exceed 10%.

For competition binding experiments, test compounds and atropine were dissolved in 100% DMSO, diluted in assay buffer to make a 3x stock, and then added to the assay plate for a final maximum DMSO concentration of 0.3% for test compounds and 0.01% for atropine. Vehicle for each condition was DMSO-matched control made in assay buffer. For ACh competition experiments, test compound was diluted in assay buffer to make a 5x stock and then added to the assay plate for a maximum final DMSO concentration of 0.1%. Binding reactions were incubated at room temperature for 2 h on a Titer Plate Shaker (Lab-Line Instruments, Melrose, IL), and equilibrium binding was terminated by rapid filtration through Unifilter-96 GF/B filter plates presoaked for at least 2 h with 0.1% polyethylenimine (PEI, Sigma). Filter plates were washed three times with ice-cold harvesting buffer (50 mM Tris-HCl, 150 mM NaCl, pH 7.4) using a 96-well Brandel harvester (Brandel Inc., Gaithersburg, MD). Plates were then dried overnight, and 35 μ l MicroScint-20 was added to each well the following day. Radioactivity was counted using a TopCount NXT microplate scintillation and luminescence counter (PerkinElmer Life and Analytical Sciences, Downers Grove, IL).

M₅ PAM VU0238429 and M₁/M₃/M₅ PAM VU0119498 competition binding assays. Membranes were prepared from M₅-CHO cells according to the previously

described protocol. Binding reactions contained 0.09 nM [³H]-NMS (obtained commercially from Amersham), 15-20 μg of membrane protein, and test compound or atropine in a total volume of 500 μl assay buffer (100 mM NaCl, 10 mM MgCl₂, 20 mM HEPES, pH 7.4). 1 μM (final) atropine was used to determine non-specific binding. The K_D of [³H]-NMS was determined empirically to be 0.264 nM. Binding reactions were incubated for 2 hours at room temperature on a Lab-Line Titer plate shaker at setting 7 (~750 rpm). Reactions were stopped and membranes collected onto 96-well Borex microplates with GF/B filter (1 μm pore size) using a Brandel harvester and washed 3X with ice-cold harvesting buffer (50mM Tris-HCl, 0.9% NaCl, pH 7.4). Filter plates were dried overnight and counted in a PerkinElmer TopCount scintillation counter (PerkinElmer Life and Analytical Sciences). True [³H]-NMS concentration was back-calculated after counting aliquots of 5X [³H]-NMS used in the reaction. Atropine K_i determined to be 0.21 by Cheng-Prusoff equation. For all assays, radioligand depletion was kept to approximately 10% or less. Data shown represent mean values obtained from at least three independent determinations performed using three or more replicates (error bars represent +/- SEM).

ACh +/- M₅ PAM VU0238429 competition binding assays. Membranes were prepared from M₅-CHO cells according to a previously described protocol. Binding reactions contained 0.09 nM [³H]-NMS (obtained commercially from Amersham), 20 μg of membrane protein, and ACh plus vehicle or test compound in a total volume of 500 μl assay buffer (100 mM NaCl, 10 mM MgCl₂, 20 mM HEPES, pH 7.4). 1 μM (final) atropine was used to determine non-specific binding. The K_D of [³H]-NMS was determined empirically to be 0.264 nM. Binding reactions were incubated for 2 hours at

room temperature on a Lab-Line Titer plate shaker at setting 7 (~750 rpm). Reactions were stopped and membranes collected onto 96-well Borex microplates with GF/B filter (1 μ m pore size) using a Brandel harvester and washed 3X with ice-cold harvesting buffer (50mM Tris-HCl, 0.9% NaCl, pH 7.4). Filter plates were dried overnight and counted in a PerkinElmer TopCount scintillation counter (PerkinElmer Life and Analytical Sciences). True [3 H]-NMS concentration was back-calculated after counting aliquots of 5X [3 H]-NMS used in the reaction. Radioligand depletion was kept to approximately 10% or less. Data shown represent mean values obtained from at least three independent determinations performed using three or more replicates (error bars represent +/- SEM).

M₁ PAM VU HTS hits competition binding assays. Membranes were prepared from M₁-expressing CHO cells as described. Binding reactions contained 0.1 nM [3 H]-NMS, 20 μ g of membranes and compound or vehicle (0.3% DMSO, final, to define total binding) or 1 μ M atropine (to define nonspecific binding) in a total volume of 500 μ l. The K_D of [3 H]-NMS was determined empirically to be 0.21 nM. Compounds were serially diluted in DMSO and then diluted in assay buffer (100 mM NaCl, 10 mM MgCl₂, 20 mM HEPES, pH 7.4) to give a final DMSO concentration of 0.3% in the binding reaction. Binding reactions were incubated for 2 hours at room temperature on a Lab-Line Titer plate shaker at setting 7 (~750 rpm). Reactions were stopped and membranes collected onto 96-well Borex microplates with GF/B filter (1 μ m pore size) using a Brandel harvester and washed 3X with ice-cold harvesting buffer (50mM Tris-HCl, 0.9% NaCl, pH 7.4). Filter plates were dried overnight and counted in a PerkinElmer TopCount scintillation Counter (PerkinElmer Life and Analytical Sciences). For ACh affinity experiments, the K_i of an ACh competition curve was determined in the absence and

presence of fixed concentrations (3 to 30 μM , final) of test compound. Actual [^3H]-NMS concentrations were back-calculated after counting aliquots of 5X [^3H]-NMS added to the reaction. Radioligand depletion was routinely kept to approximately 5% or less.

M₁ allosteric agonist competition binding assays. Membranes were prepared from M₁, M₂, M₃, M₄, and M₅-expressing CHO cells as previously described. Binding reactions contained 0.1 nM [^3H]-NMS, 20 μg of membrane and compound or 1 μM atropine (to define nonspecific binding) in a total volume of 500 μl . Compounds were serially diluted in DMSO-matched assay buffer (100 mM NaCl, 10 mM MgCl₂, 20 mM HEPES, pH 7.4) to give a final DMSO concentration of 0.3% in the binding reaction. Binding reactions were incubated for 2 hours at room temperature on a Lab-Line Titer plate shaker at setting 7 (~750 rpm). Reactions were stopped and membranes collected onto 96-well Borex microplates with GF/B filter (1 μm pore size) using a Brandel harvester and washed 3X with ice-cold harvesting buffer (50mM Tris-HCl, 0.9% NaCl, pH 7.4). Filter plates were dried overnight and counted in a PerkinElmer TopCount scintillation counter (PerkinElmer Life and Analytical Sciences). Actual [^3H]-NMS concentrations were back-calculated after counting aliquots of 5X [^3H]-NMS added to the reaction. Radioligand depletion was routinely kept to approximately 10% or less.

Merck M₁ PAM BQCA and M₁ Antagonist VU0255035 competition binding studies. Full methods are not described due to redundancy, as details are essentially the same as described previously for M₄ PAM and M₅ PAM projects. Binding reactions used 15-25 mg of membrane protein prepared from rM₁ receptor expressing CHO cells and 0.1 nM [^3H]-NMS (GE Healthcare) in a final volume of 1 mL. Non-specific binding was determined in the presence of 1 μM atropine.

Ancillary/off-target screening assays

Millipore functional screening. Prior to conducting *in vivo* experiments with M₁ PAM BQCA, M₄ PAM VU0152099, and M₄ PAM VU0152100, the compounds were submitted to Millipore's GPCR Profiler™ Service where it was evaluated for agonist, antagonist, and allosteric potentiator activity against a panel of 16 GPCRs in a functional screening paradigm (*N*=2). Calcium mobilization assays were used to obtain full compound CRCs, and for PAM screens a standard orthosteric agonist was used for each target.

MDS Pharma/Ricerca binding screening. M₄ PAM VU0152099, M₄ PAM VU0152100 (as reported in Chapter III), numerous M₅ PAMs (as reported in Chapter IV), and M₁ allosteric agonists (as reported in Chapter V) were submitted to MDS Pharma (now Ricerca) for LeadProfile screening across a panel of 67 different GPCRs, ion channels, enzymes, transporters, and nuclear hormone receptors. Competition binding assays were performed using standard orthosteric radioligands for each target (*N*=2) with test compounds at 10 μM. Results are reported as % inhibition of radioligand binding caused by the test compound, with >50% inhibition signifying substantial activity at a given target.

***In vivo* Pharmacology**

All experiments were conducted in accordance with the National Institutes of Health regulations of animal care covered in Principles of Laboratory Animal Care (National Institutes of Health publication 85-23, revised 1985) and were approved by the

Institutional Animal Care and Use Committee. Methods for studies performed for the M₅ PAM and M₄ PAM projects are described below, all other behavioral and PK studies associated with M₁ PAM, M₁ allosteric agonist, TBPB, and M₁ antagonist projects are similar to those described below, and in cases where data from a study is discussed in the associated text/figures (i.e. in Chapter V) that is not described below, the full methodology can be found in the associated references.

Amphetamine-induced hyperlocomotion behavioral rat studies

All behavioral studies were conducted using male Sprague-Dawley rats (Harlan Sprague-Dawley, Inc.; Indianapolis, IN) weighing 270 to 300 grams. Subjects were housed in pairs in a large colony room under a 12-h light/dark cycle (lights on at 6:00 a.m.) with food and water provided *ad libitum*. Test sessions were performed between 6:00 a.m. and 6:00 p.m. Dose groups consisted of 8-16 rats per dose group. All doses of VU0152099 and VU0152100 refer to the salt form and were injected in a 1.0 mL/kg volume. Each compound was dissolved in 10% Tween 80 and double deionized water with the pH adjusted to approximately 7.0 using 1N NaOH.

Studies were conducted using a SmartFrame Open Field System (Kinder Scientific., San Diego, CA) equipped with 32 horizontal (x- and y-axes) infrared photobeams located 1 cm above the floor of the chamber. Changes in ambulation or locomotor activity were measured as the number of total photobeam breaks as expressed in 5 min intervals and were recorded with a Pentium I computer equipped with the Motor monitor system software (Kinder Scientific).

Rats were placed in the open field chambers for a 30 min habituation interval (data not shown), followed by a pretreatment with vehicle or a 56.6 mg/kg dose of either VU0152099 or VU0152100 (I.P.) for an additional 30 min. Next, all rats received an injection of 1 mg/kg (subcutaneous [S.C.]) of amphetamine and locomotor activity was measured for an additional 60 min. Data were analyzed by a one-way ANOVA with comparison with the vehicle+amphetamine control group using Dunnett's test. Calculations were performed using JMP v5.1.2 (SAS Institute Inc., Cary, NC) statistical software.

Roto-rod behavioral rat studies

The effects of VU0152100 on motor performance were evaluated using a Rotorod (Columbus Instruments, Columbus, OH). All rats were given an initial training trial of 120 s, followed by 2 additional training trials of 85s approximately 10 min apart, using a rotarod (7.5cm in diameter) rotating at a constant speed of 20 revolutions/minute. After initial training trials, a baseline trial of 85s was conducted, and any rats that did reach the 85s criteria were excluded from the study. Rats were then pretreated for 30 minutes *i.p.* with vehicle or dose of VU0152100, specifically 30, 56.6 or 100 mg/kg, and then the time each animal remained on the rotorod was recorded; animals not falling off the rotorod were given a maximum score of 85s. Data were analyzed by a one-way ANOVA, with comparison to the vehicle control group using Dunnett's test. Calculations were performed using JMP v5.1.2 (SAS Institute Inc., Cary, NC) statistical software.

Pharmacokinetic/PBL rat studies

M₄ PAMs. Male Sprague-Dawley rats (Harlan Sprague-Dawley, Inc.; Indianapolis, IN) weighing 225-250g, were fasted overnight prior to dosing. Compounds were dissolved 10% Tween 80 and double deionized water with the pH adjusted to approximately 7.0 using 1N NaOH at a concentration of 56.6 mg/mL and sonicated until a uniform homogenous solution was obtained. The dose was administered ip at 56.6 mg/kg per compound. Three animals were used for each time point. The rat blood and brain were collected at 0.5, 1, 2 and 4h. Animals were euthanized, decapitated and the brains removed and frozen on dry ice. Trunk blood was collected in ethylenediamine tetra-acetic acid (EDTA) Vacutainer tubes and plasma was separated by centrifugation and stored at -80 °C until analysis.

For the brain sample preparation, frozen whole rat brains were weighed (1.5 to 1.8g) and placed in 3 mL of ice-cold solution of acetonitrile and methanol (1:1, volume) with a synthetic internal standard (50 ng/mL) and homogenized using a Sonic Dismembrator Model 100 (Fischer Scientific) at maximal speed for 2 min. Next, a 1ml aliquot of each homogenate was placed into 1.5 mL centrifuge tubes and centrifuged at 16,000 rpm for 5 min. Finally 100 µL of supernatant was injected into LC-MS-MS.

Plasma samples (100µl) were combined with 200µl of ice-cold solution of the internal standard (100ng/mL) in acetonitrile with 0.1% formic acid. After vortexing for one minute, the mixture was centrifuged at 16,000 rpm for 5 min in a bench-top Spectrafuge 16M Microcentrifuge (Labnet, Woodbridge, NJ). Again, 100 µL of the supernatant was injected into LC-MS-MS.

For the LCMS Analysis, the LC separation was carried out on a Phenomenex Luna ODS, 5 micron, 2.1 mm x 5 cm column (Torrance, CA) at a flow rate of 0.3 mL/min. The gradient started with 80% solvent A (0.1% Formic acid in water) and 20% solvent B (0.1% Formic acid in CH₃CN), held for 1 min and increasing to 100% B in 4 min and held for 1 min. Mass spectrometry was carried out using a ThermoFinnigan TSQ Quantum ultra (Thermo Scientific, Waltham, MA) mass spectrometer in positive ion mode. The software Xcalibur version 2.0 was used to control the instrument and collect data. The ESI source was fitted with a stainless steel capillary (100µm i.d.). Nitrogen was used as both the sheath gas and the auxiliary gas. The ion transfer tube temperature was 300°C. The spray voltage, tube lens voltage, pressure of sheath gas and auxiliary gas were optimized to achieve maximal response using the test compounds mixing with the mobile phase A (50%) and B (50%) at a flow rate of 0.3 mL/min. Collision-induced dissociation (CID) was performed on the test compounds and internal standards under 1.0 mTorr of argon. Selected reaction monitoring (SRM) was carried out using the transitions from, m/z 356 to 205 @ 30 eV for VU0152099, m/z 342 to 205 @ 27 eV for VU0152100, and m/z 310 to 223 @ 25 eV for our internal standard.

The calibration curves were constructed by spiking known amounts of test compounds in blank brain homogenates and plasma. The samples went through the same extraction steps as described above. A linear response was achieved from 50ng/mL to 100ug/mL in both matrices. Compound exposure following administration was determined by calculating AUC (0-∞) using the trapezoidal method.

M₅ PAMs. VU0238429 was formulated as a 10% Tween 80 micro-suspension in sterile water at the concentration of 5 mg/mL and administered intraperitoneally to male

Sprague-Dawley rats weighing 225 to 250 g (Harlan Sprague-Dawley, Inc., Indianapolis, IN) at the dose of 10 mg/kg. The rat blood and brain were collected at 0.5, 1, 3, and 6 h. Animals were euthanized and decapitated, and the brains were removed, thoroughly washed in cold phosphate buffered saline and immediately frozen on dry ice. Trunk blood was collected in EDTA Vacutainer tubes, and plasma was separated by centrifugation and stored at -80 °C until analysis. Three animals were used for each time point. On the day of analysis, frozen whole-rat brains were weighed and homogenized in 1:3 (w/w) volumes of ice-cold phosphate buffered saline (pH 7.4). The sample extraction of plasma (100µl) and brain homogenate (250 µl) was performed by a method based on protein precipitation, using three volumes of cold acetonitrile containing 0.1% formic acid and an internal standard (VU-178) having final concentration of 50 ng/mL. Extracts were vortex mixed for 5 min. followed by centrifugation at 14000 rpm for 10 min.

The supernatants of plasma and brain homogenate extracts were analyzed by means of HPLC/MS/MS, using a ThermoFinnigan TSQ Quantum Ultra (Thermo Fisher Scientific, Waltham, MA) mass spectrometer in positive ion mode. The chromatographic separation was achieved on an Acquity UPLC BEH C18 column (1.7µm; 2.1x50mm) at a flow rate of 0.8 mL/min. The gradient program was used with the mobile phase, combining solvent A (95: 5: 0.1% formic acid in water: acetonitrile) and solvent B (95: 5: acetonitrile: 0.1% formic acid in water) as follows: 20% B (0.5 min), 20–95% B (0.5 min), 95% B (1 min), 95–20% B (0.2 min), 20% B (2.8 min). The column temperature was set at 50 °C. The software Xcalibur version 2.0 was used to control the instrument and collect data. The electrospray ionization source was fitted with a stainless steel capillary (100 µm i.d.). Nitrogen was used as both the sheath gas and the auxiliary

gas. The ion transfer tube temperature was 300 °C. The spray voltage, tube lens voltage, and pressure of sheath gas and auxiliary gas were optimized to achieve maximal response using the test compounds mixing with the mobile phase A (50%) and B (50%) at a flow rate of 0.8 mL/min. Collision-induced dissociation was performed on compound VU0238429 and internal standard under 1.0 mTorr of argon. Selected reaction monitoring was carried out using the transitions from m/z 352 to 121 for VU0238429, and m/z 310 to 223 for VU-178 (internal standard). The calibration curves were constructed and linear response was obtained in the range of 10- 2000 ng/mL by spiking known amounts of VU0238429 in blank brain homogenates and plasma. Brain concentrations were corrected for dilution in PBS and for residual blood volume using 15 μ l/g as the vascular space (Brown et al., 1986). The final PK parameters were calculated by non-compartmental analysis using WinNonlin software (version 5.1, Pharsight Inc.).

Chapter III

DISCOVERY, OPTIMIZATION, AND CHARACTERIZATION OF NOVEL SUBTYPE-SELECTIVE MACHR4 POSITIVE ALLOSTERIC MODULATORS

Discovery of M₄ PAM VU010010

As discussed in the Introduction (Chapter I), a lack of M₄-selective small molecule tools has precluded thorough investigation into the role of M₄ in basic neurobiology and in target validation for therapeutic discovery. Based on M₄ localization data and on results from studies with M₄-KO mice, selective activation of M₄ may represent an attractive strategy for treatment of various CNS disorders such as schizophrenia⁴⁴. A disclosure by Eli Lilly revealed the first potentially M₄-selective small molecule, an M₄ PAM termed LY2033298 that was reported to possess high potency ($EC_{50} < 100$ nM) and efficacy at the human receptor with no activity at any other mAChR subtype at high concentrations using cell-based functional assays (**Fig. 1**)¹²³. At the time, no data was presented for activity of LY2033298 at rat or mouse M₄, and since preclinical research typically relies on rodent studies, the utility of this compound for our own experiments depended largely on its pharmacology in rodents. Thus, we re-synthesized LY2033298 and determined its potency in the presence of an ACh ~EC₂₀ by Ca²⁺ mobilization assay in rM₄/G_{q15} cells. Importantly, this compound exhibited an approximately two-order of magnitude loss of potency at rM₄ ($EC_{50} > 1$ μM, data not shown), rendering it sub-optimal as an rM₄ research tool.

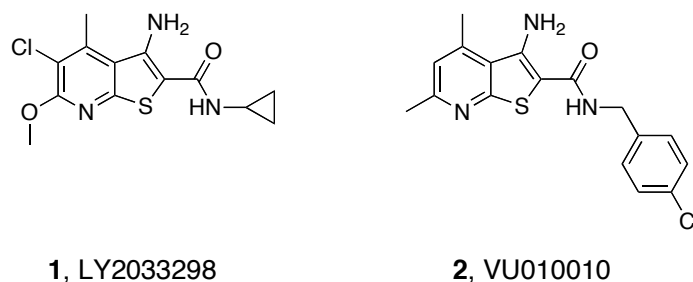


Figure 1. Structures of Eli Lilly hM₄ PAM LY2033298 (**1**) and Vanderbilt rM₄ PAM VU010010 (**2**)

Therefore, we sought to identify novel M₄ PAMs with pharmacological profiles suitable for rodent studies¹²⁴⁻¹²⁶. Rather than execute a full HTS (as was done for other mAChR PAM projects described in Chapters IV and V), we used a cheminformatic approach wherein a structure similarity search based on LY2033298 was performed on a large commercial drug-like chemical collection. This database screen provided 232 virtual hits, which were then ordered and subsequently screened for rM₄ PAM activity in a single concentration-point format using Ca²⁺ mobilization assays. Ultimately, three structurally similar hits were identified that exhibited concentration-dependent M₄ PAM activity with sub- to low-micromolar potencies (data not shown). However, these compounds suffered from poor solubility in assay buffer, resulting in incomplete CRC plateaus at higher concentrations. A limited medicinal chemical optimization of the eastern amide side chain in the form of alternative benzyl substitutions identified VU010010 (**Fig. 1**, compound **2**), which possessed relatively greater solubility, an rM₄ EC₅₀ of approximately 400 nM, and an rM₄ ACh CRC fold-shift of 47x at 30 μM.

Characterization of VU010010 in a number of *in vitro* experiments revealed that it was highly selective for M₄ and that its potentiation was mediated by enhancement of both ACh affinity and G-protein coupling efficiency (data not shown). Although this early compound represented the first potent and selective rM₄ PAM tool useful for *in*

vitro cell-based and *ex-vivo* electrophysiology experiments, it still suffered from sub-optimal physiochemical properties that precluded acceptable vehicle formulation for *in vivo* studies and likely contributed to a lack of central brain penetration in a single-dose rat PK/PBL study (data not shown). Therefore, we began a comprehensive chemical optimization project aimed at exploring structure-activity relationships (SAR) around the VU010010 scaffold in order to obtain a compound universally suitable for systemic dosing in a wide range of *in vivo* studies.

Optimization of M₄ PAM VU010010 to obtain VU0152099 and VU0152100

Optimization began with a diversity-oriented synthesis (DOS) approach to explore SAR with a variety of hypothesis-driven, structural changes to the lead compound. The rationale for this approach for the optimization of VU010010 is that SAR for allosteric ligands is often ‘flat’ or ‘shallow’, with subtle structural modifications leading to a complete loss of activity, and often only one portion of an allosteric ligand is amenable to change. Therefore, a multi-dimensional, DOS library approach provides the best opportunity to quickly identify productive SAR as opposed to a lead optimization strategy based on classical, single compound synthesis. One explanation for the lack of central activity observed with VU010010 could be the result of the poor physiochemical properties alone, or in combination with efflux through a BBB transporter such as P-glycoprotein (P-gp). The β -aminoamide motif (**Fig. 2a**) present in VU010010 represents a potential P-gp liability, which could be removed by cyclization to analogs such as compounds **4** (**Fig. 2a**). Alternatively, P-gp susceptibility could also be diminished by

electronically attenuating the basicity of the amine moieties by the incorporation of distal fluorine atoms.

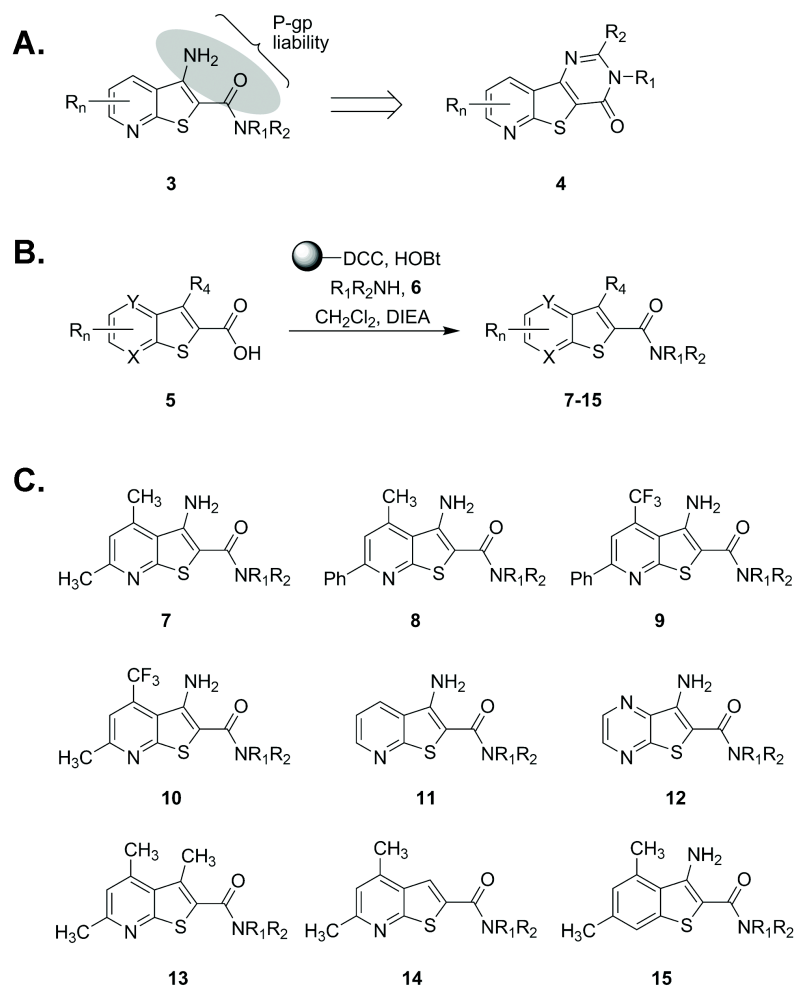


Figure 2. Chemical optimization of VU010010. Each of the ten scaffolds (**5**, **7-15**) were derivatized with diverse amide side chains in 12-24 member libraries using standard amide-coupling reaction conditions. Syntheses jointly performed with P. Kennedy.

Utilizing solution phase parallel synthesis, we synthesized small, 12- to 24-member focused libraries around each of the 10 scaffolds **5** and **7-15** (**Fig. 2b-c**), which were then purified by mass-directed preparative HPLC to analytical purity (>98%). This collection of VU010010 analogs incorporated CF₃ moieties (scaffolds **9** and **10**) to

electronically attenuate potential P-gp susceptibility, deletion of the β -amino moiety (scaffold **14**), or replacement of the β -amino moiety with an isosteric methyl group (scaffold **13**). Other scaffolds explored the deletion of substituents on the pyridine nucleus (scaffold **11**), incorporation of an additional nitrogen atom to afford a pyrimidine nucleus (scaffold **12**) or removal of the pyridine nitrogen atom in VU010010 (scaffold **15**). Finally, a library around scaffold **7** focused on maintaining the core structure of VU010010, but explored alternative amides, selected to improve physiochemical properties and lower the logP value.

As observed with positive allosteric modulators of Class C GPCRs, SAR around VU010010 was relatively flat, possibly due to a shallow binding pocket. An ACh EC₂₀ triage screen, employing a functional, fluorescence-based Ca²⁺ assay in CHO cells stably co-expressing the rat M₄ mACh receptor and the chimeric G protein, G_{qi5}, quickly eliminated all VU010010 analogs except those in library **7** (**Fig. 3**). Within library **7**, all aliphatic and non-benzyl amides were inactive, and only benzyl and heteroaryl methyl congeners of VU010010, **7a-7p**, retained M₄ PAM activity (**Table 1**). The potency of each compound was determined by pre-incubating cells with vehicle or increasing concentrations of test compound followed by the addition of an ACh EC₂₀ to yield CRCs. Subtle substitution changes on the arene ring lost activity 5-10-fold in terms of M₄ EC₅₀ and/or fold-shift of the ACh CRC (**Table 1**). For instance, analog **7d**, in which the 4-Cl moiety of VU010010 is moved to the 3-position results in a loss in potency of over 9-fold (EC₅₀ = 3.7 μ M). Similarly, the unsubstituted phenyl congener **7a** retains M₄ PAM activity (EC₅₀ = 630 nM), but the fold-shift diminishes to 8.6-fold, *versus* the 47-fold shift observed for VU010010. In general, functionalized benzyl amides and pyridyl

methyl congeners (**7f** and **7g**) were well tolerated, providing selective M₄ PAMs with EC₅₀ values ranging from 380 nM to 3.7 μM and with fold-shifts of the ACh CRC from 8.6- to 70-fold.

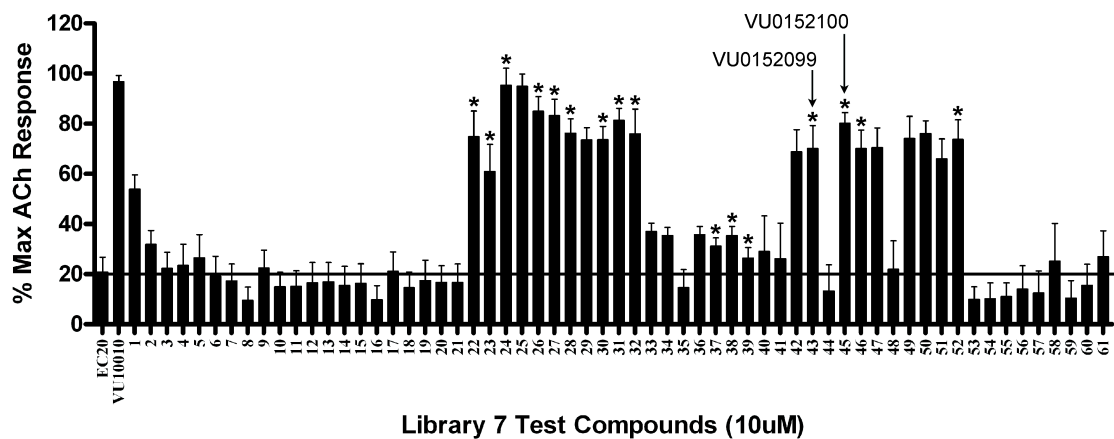
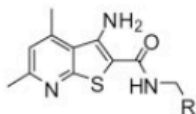


Figure 3. Singlepoint screen of M₄ PAM VU010010 analogs based on scaffold 7 bearing eastern amide side chain substitutions. Ca²⁺ mobilization was used to obtain singlepoint (10 μM) potentiation responses for each compound in the presence of an ACh ~EC₂₀ in rM₄ cells. Data represent Mean +/-SEM of at least three independent determinations. Experiments performed by A. Brady.

Table 1. M₄ PAM potency and ACh CRC fold-shift SAR for VU010010 analogs based on scaffold 7. Ca²⁺ mobilization was used to obtain CRCs of test compounds in the presence of an ACh ~EC₂₀ using rM₄ cells. Similar assays determined the fold-shift of an ACh CRC in the presence of 30 μM test compound (N.D. = not determined). Data represent Mean +/-SEM from at least three independent determinations. Experiments performed by A. Brady.



Compound	R	Rat M ₄ EC ₅₀ ^a μM	Rat M ₄ ACh -Fold Shift
7a		0.63	8.6
7b		0.83	11.8
7c		1.83	N.D.
7d		3.70	N.D.
7e		2.63	N.D.
7f		2.04	N.D.
7g		2.88	N.D.
7h		1.44	N.D.
7i		1.80	N.D.
7j		2.96	N.D.
7k		3.04	N.D.
7l		0.88	N.D.
7m		1.12	N.D.
7n		0.72	13.7
7o		0.40	29.7
7p		0.38	70.1

Two compounds were selected for further evaluation based on their ability to potentiate the M₄-mediated Ca²⁺ response to ACh. VU0152099 (**7o**), (**Fig. 4a**) and VU0152100 (**7p**), (**Fig. 4d**) retained M₄ PAM activity (EC₅₀ values of 403 ± 117 nM and 380 ± 93 nM, respectively) comparable to VU010010, and in the absence of an ACh EC₂₀, neither VU0152099 nor VU0152100 elicited a response (**Fig. 4b,e**).

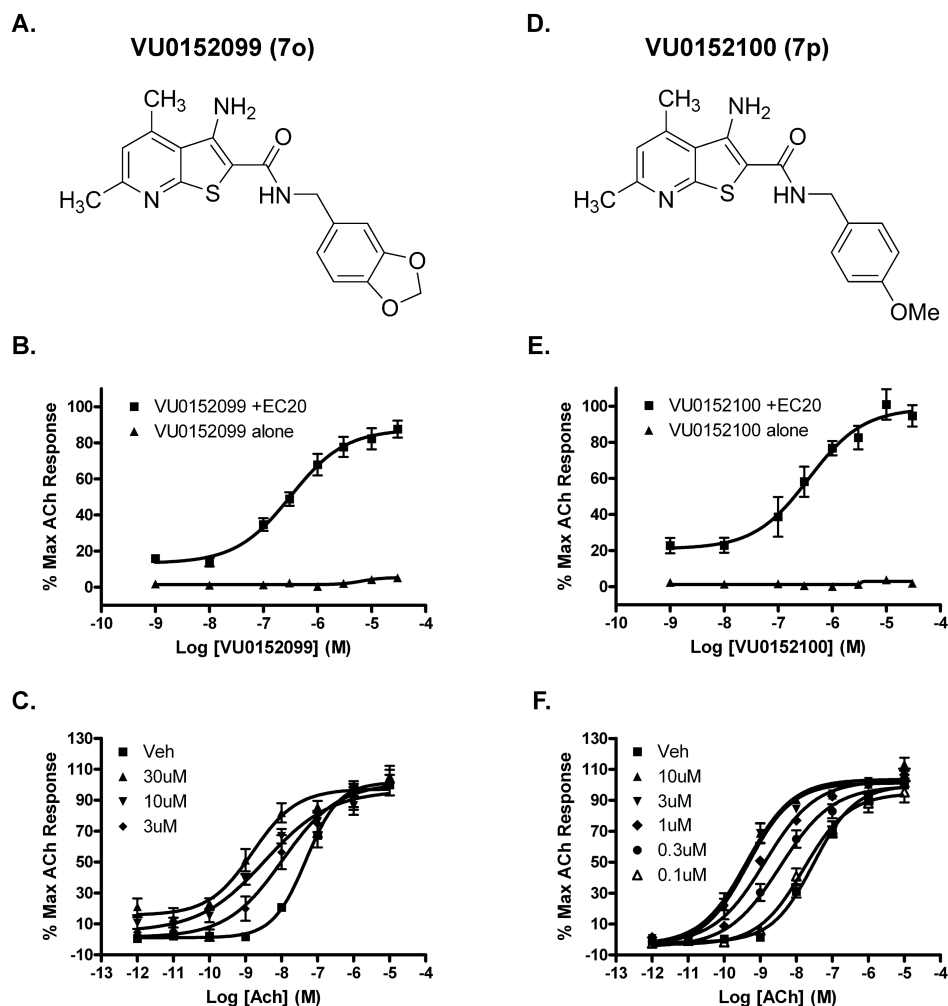


Figure 4. Structures, potency CRCs, and ACh CRC fold-shifts for M₄ PAM leads A.) VU0152099 (**7o**) and B.) VU0152100 (**7p**). Ca²⁺ mobilization was used to obtain: B., E.) CRCs of test compound in the absence and presence of an ACh ~EC₂₀, (EC₅₀ values: VU0152099 = 403 nM, VU0152100 = 380 nM) C., F.) CRCs of ACh in the absence or presence and of increasing fixed concentrations of test compound (fold-shift values: VU0152099 = 30x, VU0152100 = 70x). Data represent Mean +/-SEM from at least three independent determinations. Experiments performed by A. Brady.

We next determined the effects of maximal concentrations of each compound on the CRC of ACh. Cells were pre-incubated with a fixed concentration (0.1-30 μM) of test compound and subsequently stimulated with increasing concentrations of ACh. Both VU0152099 and VU0152100 induced a concentration-dependent left-shift of the ACh CRC with maximal shifts of 30-fold observed with 30 μM VU0152099 (**Fig. 4c**) and 70-fold observed with 10 μM VU0152100 (**Fig. 4f**).

***In vitro* characterization of M₄ PAMs VU0152099 and VU0152100**

Using Ca^{2+} mobilization to assess the functional activity of VU0152099 and VU0152100 at the M₄ receptor requires co-expression of the chimeric G protein, G_{qi5}, in order to link the G_{i/o}-coupled M₄ receptor to the PLC β /Ca²⁺ pathway. As an alternative approach to measure M₄ PAM activity, we chose to take advantage of a novel functional assay recently developed in our lab that takes advantage of the ability of endogenous G _{$\beta\gamma$} subunits of G_{i/o}-coupled GPCRs to alter the kinetics of GIRK channels to conduct the ion, thallium. For these studies, HEK293 cells stably co-expressing heteromeric GIRK1/2 channels and the human M₄ muscarinic receptor were pre-incubated with test compound and then stimulated with agonist (ACh) in the presence of thallium ion. Both VU0152099 and VU0152100 concentration-dependently potentiated the response to an EC₂₀ concentration of ACh with EC₅₀ values of $1.2 \pm 0.3 \mu\text{M}$ and $1.9 \pm 0.2 \mu\text{M}$, respectively, and increased the maximal response to ACh to approximately 130% (**Fig. 5a**). As observed in the Ca^{2+} mobilization assays described above, both VU0152099 and VU0152100 (10 μM) also enhanced the potency of ACh to induce GIRK-mediated

thallium flux, as manifest by a robust (≈ 30 -fold) left-shift of the ACh CRC from 77 ± 1.2 nM to 2.09 ± 0.3 nM and 2.35 ± 0.5 nM, respectively (**Fig. 5a**). Taken together, these *in vitro* studies suggest that VU0152099 and VU0152100 are potent positive allosteric modulators that enhance the response of the M_4 receptor to the endogenous agonist, ACh.

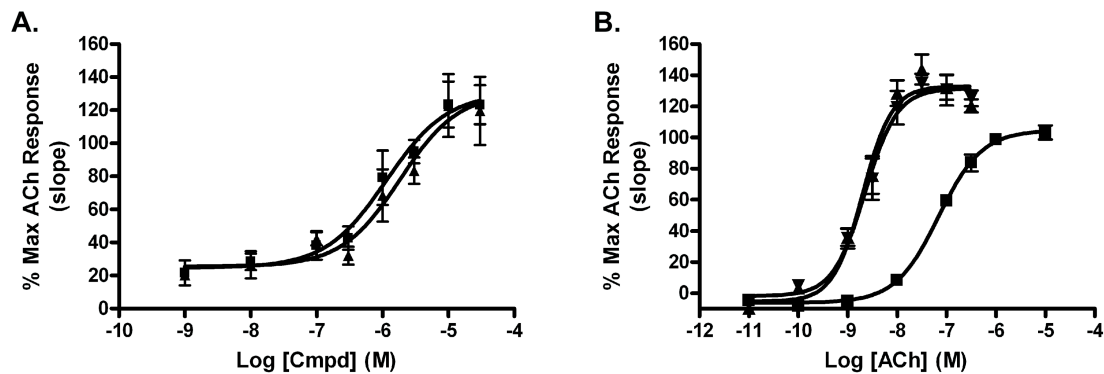


Figure 5. GIRK-mediated thallium flux M_4 PAM assays with lead compounds VU0152099 and VU0152100. A.) CRCs of test compounds in the presence of an ACh $\sim EC_{20}$ (EC_{50} values: VU0152099 = 1.2 μM , VU0152100 = 1.9 μM) and B.) CRCs of ACh in the absence and presence of a fixed 10 μM concentration of test compound (fold-shift values: VU0152099 and VU0152100 both = $\sim 30x$). Data represent Mean \pm SEM from at least three independent determinations. Experiments performed by A. Brady.

To further confirm an allosteric mechanism of action by the novel M_4 PAMs, we evaluated the effect of VU0152099 and VU0152100 on equilibrium radioligand binding studies using membranes prepared from cells expressing the r M_4 receptor. We first assessed the ability of increasing concentrations of the two M_4 PAMs to displace the orthosteric radioligand, [3H]-*N*-methylscopolamine ([3H]-NMS) (0.1 nM). Unlike the orthosteric antagonist, atropine, which potently inhibited [3H]-NMS binding ($K_i = 0.54 \pm 0.1$ nM), neither M_4 PAM displaced [3H]-NMS at concentrations up to 30 μM (**Fig. 6a**), strongly suggesting that VU0152099 and VU0152100 act at a site on the M_4 receptor that is distinct from the orthosteric binding site.

In addition, we evaluated the effect of VU0152099 and VU0152100 on the affinity of ACh for the M₄ receptor by assessing the ability of an increasing concentration of ACh to displace [³H]-NMS (0.1 nM) binding in the absence or presence of the M₄ potentiators. VU0152099 and VU0152100 were found to induce a 20-25x leftward shift in the potency of ACh to displace [³H]-NMS binding to M₄ as manifest by a reduction in the ACh K_i from 252 ± 17.9 nM (veh) to 10.4 ± 0.91 nM (VU0152099) and 12.2 ± 0.49 nM (VU0152100) (**Fig. 6a**). These data present a possible mechanism whereby these compounds could enhance receptor activation by increasing the affinity of M₄ for acetylcholine, and are in agreement with data previously determined for VU010010, where a 14 fold decrease in the ACh K_i was reported.

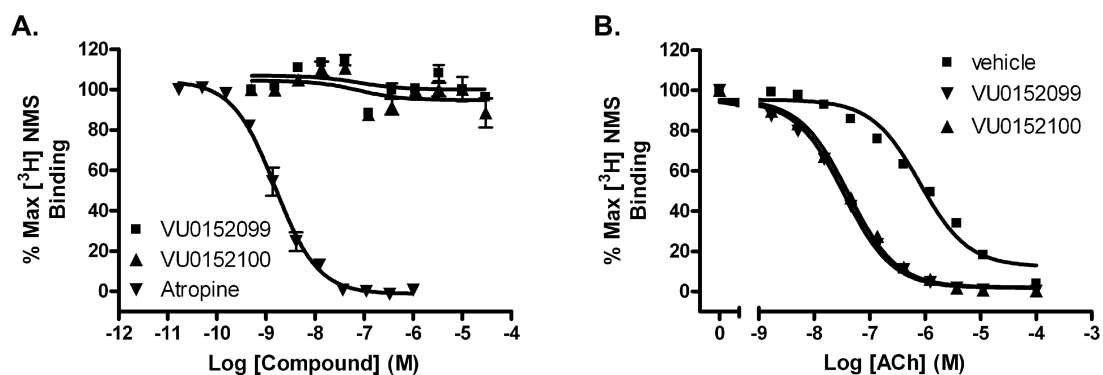


Figure 6. [³H]-NMS competition binding experiments with M₄ PAMs VU0152099 and VU0152100 at rM₄ cell membranes. A) CRCs of test compound and atropine positive control (atropine K_i = 0.54 nM). B.) CRCs of ACh in the absence (vehicle) and presence of (10 μM) test compounds (ACh K_i values: vehicle = 252 nM, VU0152099 = 10.4 nM [25x left-shift], VU0152100 = 12.2 nM [21x left-shift]). Data represent Mean +/-SEM from at least three independent determinations. Experiments performed by A. Brady.

We next evaluated VU0152099 and VU0152100 in Ca²⁺ mobilization assays for effects at all mAChR subtypes to determine whether these compounds are selective for M₄. Both VU0152099 and VU0152100 were selective for M₄ relative to M₁, M₂, M₃ and

M₅. Neither VU0152099 (**Fig. 7a**) nor VU152100 (**Fig. 7b**) had any effect on the ACh CRCs at these other mAChR subtypes at concentrations up to 30 μM. To further assess selectivity of these compounds for M₄ relative to other potential targets, the activity of VU0152099 and VU152100 also were evaluated in radioligand binding assays against a large panel of 67 discrete GPCRs, ion channels, transporters, nuclear hormone receptors, and enzymes (**Table 2**). These compounds were largely inactive at each of the targets in this panel screen. At concentrations of 10 μM, both compounds were completely inactive at most targets and induced less than 50% displacement of binding for all targets tested, with the single exception of GABA_A receptors (assessed by flunitrazepam binding), where VU0152099 displayed 51% displacement. This suggested that VU0152099 may interact with the flunitrazepam binding site with an IC₅₀ value of approximately 10 μM, which still provides high selectivity for M₄ relative to GABA_A receptors.

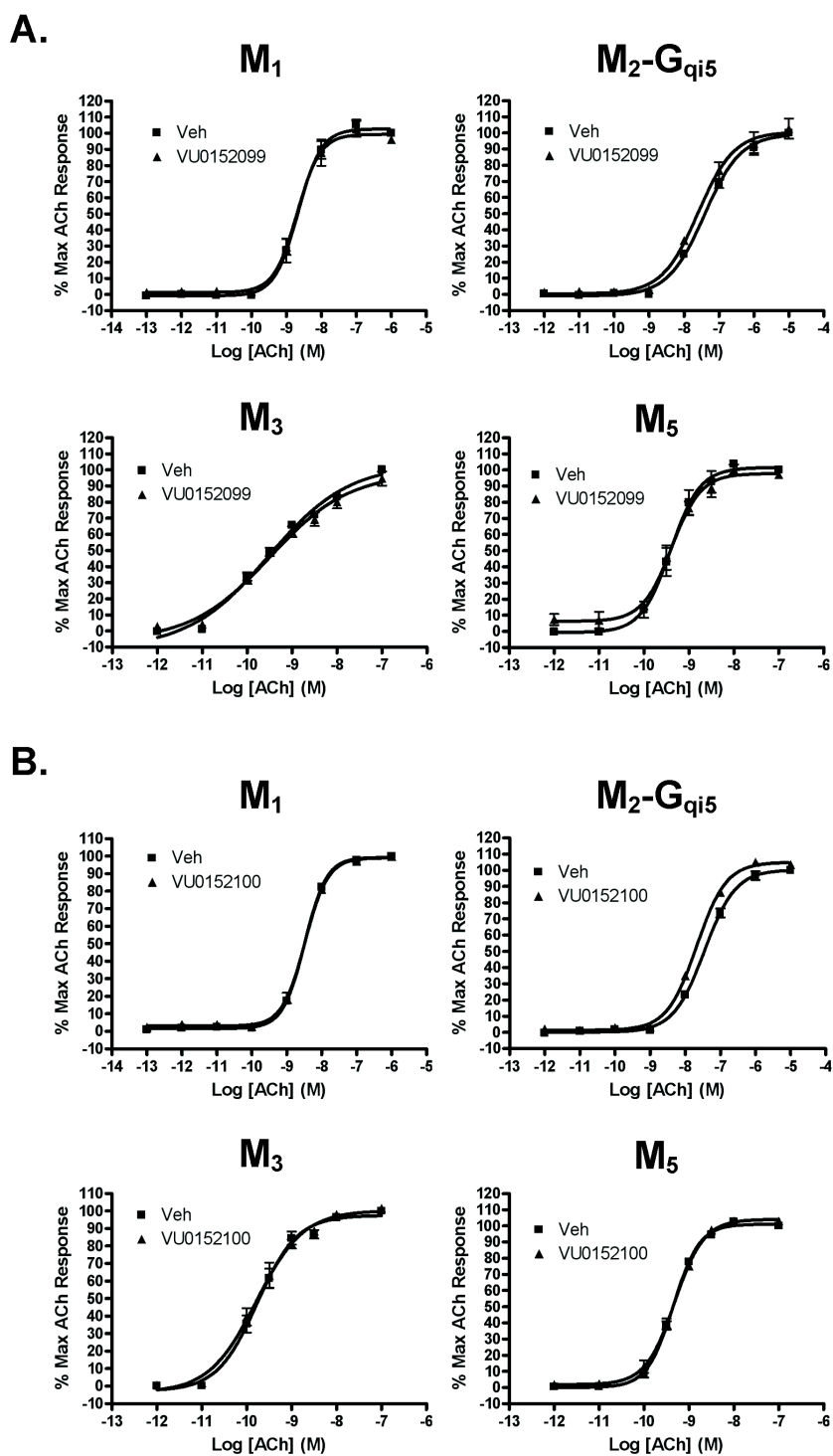


Figure 7. mAChR subtype-selectivity profiles for M_4 PAMs A.) VU0152099 and B.) VU0152100 determined by ACh CRC fold-shift. Ca^{2+} mobilization was used to obtain CRCs of ACh in the presence and absence of 30 μ M test compound using M_1 , M_2 , M_3 , and M_5 cells. Data represent Mean \pm SEM from at least three independent determinations. Experiments performed by A. Brady.

Table 2. Ancillary pharmacological activity of M₄ PAMs VU0152099 and VU0152100 in singlepoint (10 μM) competition binding assays across a large panel of off-targets. Experiments performed by MDS Pharma/Ricerca.

Target	Species	% Inhibition		Target	Species	% Inhibition	
		VU0152099	VU0152100			VU0152099	VU0152100
Adenosine A1	human	28	-1	Histamine H ₃	human	10	9
Adenosine A2	human	46	43	Imidazoline I ₂ , Central	rat	7	8
Adenosine A3	human	28	40	Interleukin IL-1	mouse	-19	-4
Adrenergic α _{1A}	rat	10	9	Leukotriene, Cysteinyl CysLT ₁	human	-4	-6
Adrenergic α _{1B}	rat	-7	-7	Melatonin MT ₁	human	15	20
Adrenergic α _{1D}	human	1	1	Muscarinic M ₁	human	-3	0
Adrenergic α _{2A}	human	7	17	Muscarinic M ₂	human	-1	-4
Adrenergic β ₁	human	17	17	Muscarinic M ₃	human	-1	-2
Adrenergic β ₂	human	30	35	Neuropeptide Y Y ₁	human	2	9
Androgen (testosterone)AR	rat	6	6	Neuropeptide Y Y ₂	human	-2	2
Bradykinin B ₁	human	13	1	Nicotinic Acetylcholine	human	6	-6
Bradykinin B ₂	human	-5	-9	Nicotinic Acetylcholine α1, Bungarotoxin	human	-10	-4
Calcium channel L-type, benzothiazepine	rat	13	7	Opiate δ (OP1, DOP)	human	2	-13
Calcium channel L-type, dihydropyridine	rat	21	17	Opiate κ (OP2, KOP)	human	5	2
Calcium channel N-type	rat	-8	-4	Opiate μ (OP3, MOP)	human	2	-2
Dopamine D ₁	human	6	7	Phorbol Ester	mouse	2	4
Dopamine D _{2S}	human	2	0	Platelet Activating Factor (PAF)	human	13	22
Dopamine D ₃	human	-1	5	Potassium Channel [K _{A,T2}]	hamster	3	6
Dopamine D _{4,2}	human	-13	-11	Potassium Channel hERG	human	5	5
Endothelin ET _A	human	-8	-8	Prostanoid EP ₄	human	15	7
Endothelin ET _B	human	2	-4	Purinergic P _{2X}	rabbit	6	-4
Epidermal Growth Factor (EGF)	human	9	-5	Purinergic P _{2Y}	rat	15	14
Estrogen ER ^α	human	-1	-1	Rolipram	rat	36	29
G protein-coupled receptor GPR103	human	-3	-4	Serotonin (5-Hydroxytryptamine) 5-HT _{1A}	human	2	2
GABA _A , Flunitrazepam, central	rat	51	43	Serotonin (5-Hydroxytryptamine) 5-HT ₃	human	-2	14
GABA _A , Muscimol, central	rat	6	9	Sigma σ ₁	human	2	6
GABA _{B1A}	human	-7	12	Sigma σ ₂	rat	-8	-3
Glucocorticoid	human	-3	8	Sodium Channel, Site 2	rat	11	20
Glutamate, Kainate	rat	3	-15	Tachykinin NK ₁	human	-15	-18
Glutamate, NMDA, Agonism	rat	17	22	Thyroid Hormone	rat	-1	0
Glutamate, NMDA, Glycine	rat	3	2	Transporter, Dopamine (DAT)	human	27	46
Glutamate, NMDA, Phencyclidine	rat	2	3	Transporter, GABA	rat	26	13
Histamine H ₁	human	14	7	Transporter, Norepinephrine (NET)	human	34	22
Histamine H ₂	human	7	10	Transporter, Serotonin (5-Hydroxytryptamine) (SERT)	human	0	4

Since VU0152099 and VU0152100 are allosteric modulators of M₄, it is possible that they have activity at similar allosteric sites on other GPCRs. If so, this would not be apparent in the radioligand binding assays of **Table 2**. The finding that these compounds are completely inactive at other mAChR subtypes makes this less likely since M₄ is more closely related to the other mAChR subtypes than to other GPCRs. However, to further evaluate the selectivity of VU0152099 for M₄ relative to other family A GPCRs, we contracted with Millipore to determine the effects of these compounds on functional responses of a panel of 15 other GPCRs to activation by their respective agonists (**Fig. 8**). For these studies, we chose family A GPCR subtypes that are among the closest relatives of mAChRs.

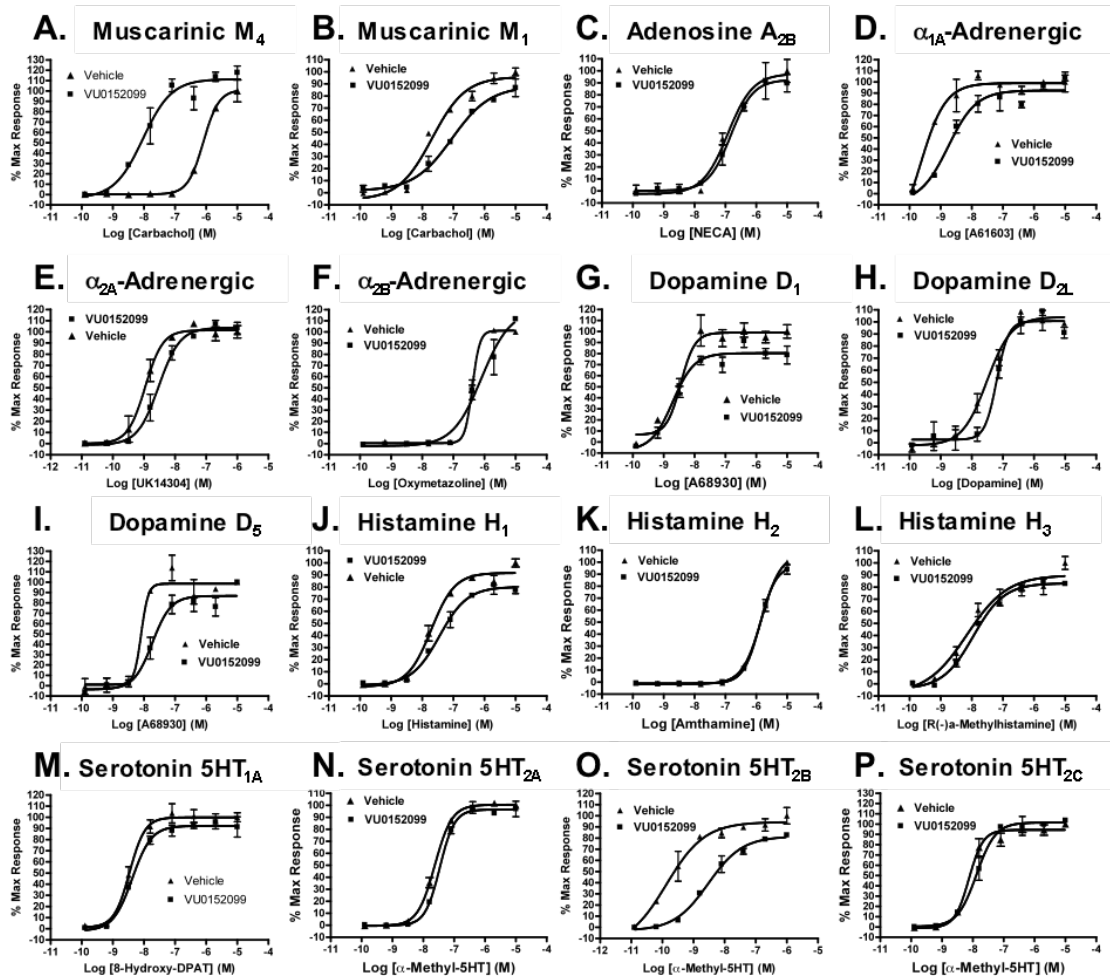


Figure 8. Functional GPCR off-target activity screening for M₄ PAMs VU0152099 and VU0152100. Ca²⁺ mobilization assays using multiple cell lines expressing each of the GPCR targets and promiscuous G protein, G_{α15/16} were used to obtain CRCs of orthosteric agonists in the absence and presence of test compound at 10 μM. VU0152099 exhibited no agonist activity at any of the targets tested, and was found to possess antagonist activity only at the 5HT_{2B} receptor (as indicated by an ≈16 fold right-shift in the agonist CRC in the presence of VU0152099). At the human M₄ mAChR, VU0152099 elicited a robust ≈80 fold left-shift in the carbachol CRC (EC₅₀s: CCh alone = 800 nM, CCh +VU0152099= 10 nM). Similar CRC curves were generated for additional GPCRs: Muscarinic M₁, Adenosine A_{2B}, α_{1A}, α_{2A}, α_{2B}-Adrenergic, Dopamine D₁, D_{2L}, D₅, Histamine H₁, H₂, H₃, and Serotonin 5HT_{1A}, 2A, 2B, 2C, with no comparable left-shift observed at any other target tested. All data represent Mean of two independent determinations. Experiments performed by Millipore GPCR Profiler Service™ service.

We first determined the effects of VU0152099 alone on each receptor and found that these compounds had no agonist activity at any receptor studied (data not shown). We then determined the effects of VU0152099 on full CRCs of agonists of each of these

receptors (**Fig. 8**). This allows unambiguous evaluation of whether the compounds possess antagonist activity (either allosteric or orthosteric) or allosteric potentiator activity at these other GPCRs. Consistent with our internal studies, VU0152099 induced a robust potentiation of ACh-induced activation of M₄, but had no potentiator activity at M₁ (**Fig. 8**). In addition, VU0152099 had no allosteric potentiator activity at any of the other GPCR subtypes tested (**Fig. 8**). The only significant activity detected for VU0152099 in this functional panel screen was weak antagonist activity at the serotonin 5HT_{2B} receptor (**Fig. 8**). Together, these data suggested that VU0152099 and VU0152100 possess clean ancillary pharmacology profiles, which would allow us to pursue the behavioral effects of selective M₄ activation *in vivo*.

***In vivo* pharmacokinetics of M₄ PAMs VU0152099 and VU0152100**

Prior to conducting *in vivo* studies with VU0152099 and VU0152100, pharmacokinetic studies were undertaken to assess brain/plasma ratios following systemic dosing of these compounds. In contrast, to the high log partition coefficient (logP) of VU010010 (4.5), both VU0152099 and VU0152100 possessed logP values of 3.7 and 3.6, respectively, a full order of magnitude less lipophilic than VU010010. As a consequence, both VU0152099 and VU0152100 displayed improved physiochemical properties and afforded homogeneous dosing solutions in multiple vehicles acceptable for *in vivo* studies. Further, we conducted *in vivo* PK/PBL studies in rats at the dose of 56.6 mg/kg (intraperitoneal [I.P.]). Both compounds exhibited substantial systemic absorption and brain penetration (**Fig. 9**). After administration, peak brain concentrations for both

compounds were in the range of 3-5 $\mu\text{g/ml}$ (Table 3). VU0152100 (Fig. 9b, Table 3) was far superior to VU0152099 (Fig. 9a, Table 3) in terms of brain penetration, as evident from area under the curve (AUC) (0- ∞) values. The AUC brain/AUC plasma ratio for VU0152099 was calculated to be 0.39 ± 0.01 , while the ratio for VU0152100 was determined to be 0.86 ± 0.08 (Table 3). The half-life of the compounds in brain was 1.25 ± 0.02 h (VU0152099) and 1.12 ± 0.01 h (VU0152100) (Table 3). Therefore, our earlier concern of P-gp susceptibility within this series was likely unwarranted, and the lack of central activity for VU010010 was most likely due solely to physicochemical properties.

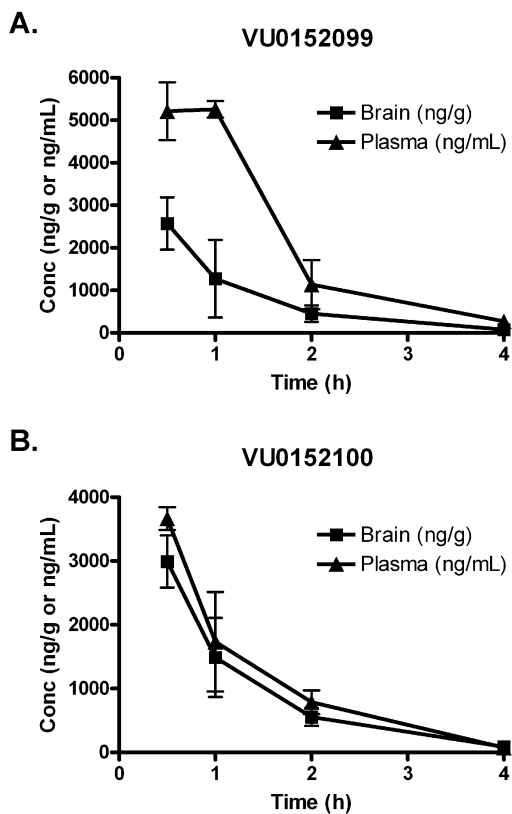


Figure 9. *In vivo* rat pharmacokinetic/PBL studies with M₄ PAMs VU0152099 and VU0152100. Concentrations were measured over time in brain and plasma following a single 56.6 mg/kg (IP) dose using male Sprague-Dawley rats ($N=3$ per compound). Experiments performed by S. Jadhav.

Table 3. Pharmacokinetic parameters calculated for M₄ PAMs VU0152099 and VU0152100 from a rat PK/PBL study using a single 56.6 mg/kg (IP) dose each compound.

PK Parameter	VU0152099	VU0152100
Mean AUC (0-∞) brain (ng · h/g)	4751.80 ± 666.17	5726.35 ± 694.68
Mean AUC(0-∞) plasma (ng · h/ml)	11928.00 ± 1472.36	6570.35 ± 235.87
AUC brain / AUC plasma	0.39 ± 0.01	0.86 ± 0.08
<i>t</i> _{1/2} plasma (h)	1.66 ± 0.39	1.62 ± 0.69
<i>t</i> _{1/2} brain (h)	1.25 ± 0.023	1.12 ± 0.01

***In vivo* behavioral studies with VU0152099 and VU0152100**

Previous studies using the M₁/M₄-preferring muscarinic agonist xanomeline produced robust effects in several preclinical models predictive of antipsychotic-like activity, including reversal of amphetamine-induced hyperlocomotion in rats, as discussed in the Introduction (Chapter I). Based on our initial PK studies suggesting that systemic administration of VU0152099 and VU0152100 provides robust brain levels of these compounds, the effects of VU0152099 and VU0152100 were evaluated in reversing amphetamine-induced hyperlocomotion using a dose of 56.6 mg/kg (I.P.) for each compound with a 30 min pretreatment interval. As shown in **Fig. 10a**, both VU0152099 and VU0152100 produced robust decreases in amphetamine-induced hyperlocomotion over the time course tested. In addition, to provide further confirmation that the M₄ PAMs have no effect on baseline levels of motor performance, which could complicate the interpretation of the amphetamine-induced hyperlocomotion data, we evaluated the effects of one of the M₄ PAMs, specifically VU0152100, after administration alone on performance in the rotorod test (**Fig. 10b**). As shown, VU0152100 had no effect on performance in the rotorod test, even when tested at a dose of 100 mg/kg, which was higher than that required to observe reversal of amphetamine-induced hyperlocomotion.

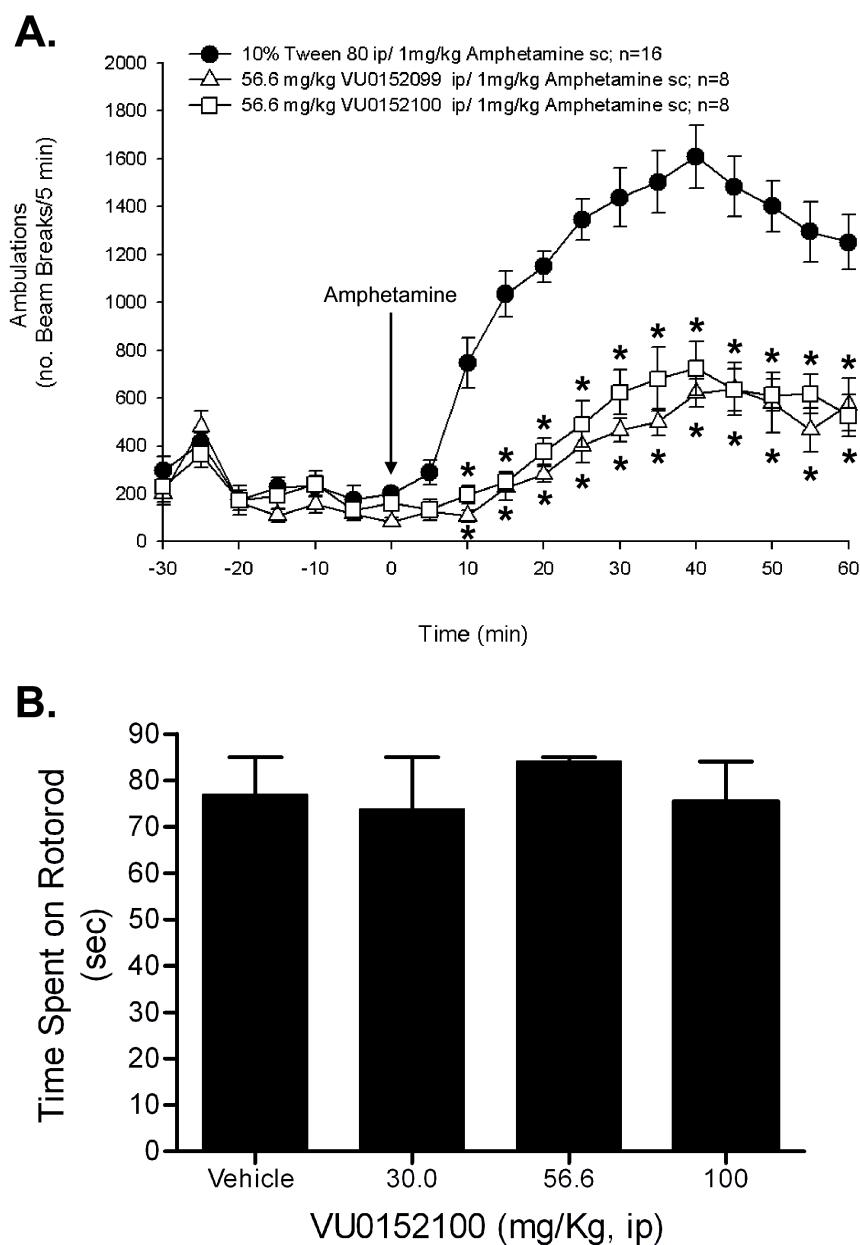


Figure 10. Reversal of amphetamine-induced hyperlocomotion and absence of sedation *in vivo* by M_4 PAMs VU0152099 and VU0152100. A.) Rats were pretreated for 30 min with vehicle or a 56.6 mg/kg dose of either VU0152099 or VU0152100 (IP). Next, all rats received an injection of 1 mg/kg (SC) of amphetamine and locomotor activity was measured for an additional 60 min. Each point represents the Mean \pm -SEM of eight-sixteen rats. *, $P < 0.05$ versus veh+amphetamine control group, Dunnett's test. B.) Lack of effect of VU0152100 on motor performance on the Rotorod. After initial training, rats were pretreated for 30 minutes (IP) with vehicle or VU0152100 (30, 56.6 or 100 mg/kg), and time each animal remained on rotorod was recorded; Each bar graph represents the Mean \pm -SEM of eight-ten rats. Experiments performed by C. Jones.

These behavioral findings represented the first published direct *in vivo* pharmacological evidence that selective M₄-modulation may be efficacious in the treatment of psychosis. Although much is known about the relationship between M₄ and regulation of central DA signaling based on M₄ localization and KO-mouse studies, which suggest that activation or positive allosteric modulation of M₄ is likely to inhibit DA-mediated motor activity, no potent, selective, and CNS penetrant M₄ activators were available to test this hypothesis in rodents, prior to our discovery of VU0152099 and VU0152100. Furthermore, these results shed important light on questions raised from clinical trials with xanomeline, the M₁/M₄-preferring orthosteric agonist that demonstrated robust anti-psychotic efficacy in multiple human trials (Chapter I)^{100,110}. Specifically, our data support the hypothesis that the mechanism(s) of action underlying xanomeline's effects were mediated at least in-part by activation of M₄. However, it is possible, perhaps even likely, that xanomeline-induced M₁ activation also contributed to the drug candidate's broad clinical efficacy across multiple symptom clusters. Nonetheless, further investigation into the neurochemistry and neurocircuitry involved in mediating the observed *in vivo* effects (**Fig. 10**) of M₄ PAMs VU0152099 and VU0152100 is required.

Optimization of M₄ PAMs VU0152099 and VU0152100

Although the novel M₄ PAMs VU0152099 and VU0152100 represented important advances over both LY2033298 and our first generation compound VU010010 and served as highly useful *in vivo* probes of selective M₄ modulation, we opted to

continue our optimization campaign in order to further improve upon these leads (**Fig. 11**). Both VU0152099 and VU0152100 possessed high potency, efficacy, and subtype-selectivity, with acceptable *in vivo* PK profiles, and were devoid of ancillary pharmacological activity; however, *in vitro* metabolic stability experiments revealed that these compounds readily underwent phase-I oxidative metabolism with <10% of parent compound remaining after 90 min incubation with rat liver microsomes (data not shown). Subsequent metabolite identification experiments indicated that hydroxylation of the pyridine ring was the major oxidative metabolite. In order to prevent this metabolic liability and further explore SAR around the lead scaffold, we employed an iterative parallel library synthesis approach for new analog generation.

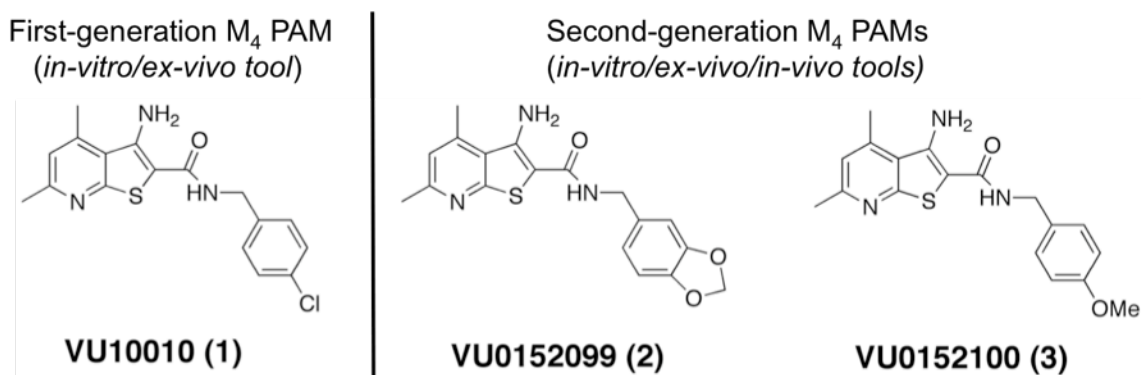


Figure 11. Structures of first- and second-generation M₄ PAMs based on optimization of the dimethylamino-thienopyridine amide scaffold. All three compounds possess approximately ~400 nM rM₄ potency with 30-70x ACh CRC fold-shift, yet suffer from poor *in vitro* metabolic stability.

Having tentatively designated the *p*-methoxybenzamide moiety of lead compound **3** as the most-favored substituent (of those screened in the initial amide side chain scan described previously) based on its functional activity at rat M₄, we first held this side chain constant while exploring alternative substituents at the 6-position to prevent formation of the hydroxy metabolite. Synthesis of initial 20-member alkylamine and 20-

member ether libraries, as shown in **Figure 12**, began with condensation between 3-aminocrotonitrile **4** and 2-cyanothioacetamide **5** to furnish the aminopyridyl core **6**. This was cyclized with *p*-chloro-*p*-methoxybenzamide **7** to give the diaminothieno[2,3-*b*]pyridine scaffold with the *p*-methoxybenzamide **8**. To produce the 20-member amine library, **8** was reacted with various alkyl chlorides to generate **9a-s**. The ether library was synthesized in a similar fashion by reacting ethylacetoacetate **10** with 2-cyanothioacetamide **5** to provide the core pyridone **11**, which was then cyclized with **7** at 0 °C then allowed to warm to r.t. overnight. Once pure, **12** was alkylated to obtain analogs **13a-s**.

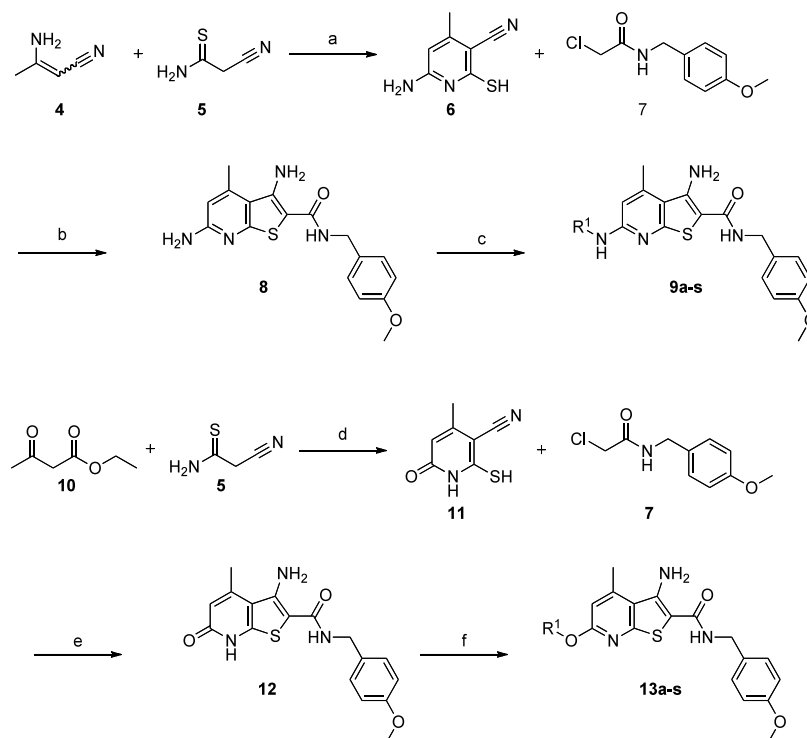
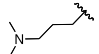
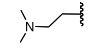
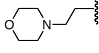
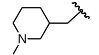
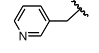
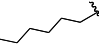
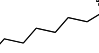

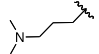
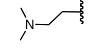
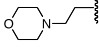
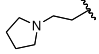
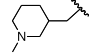
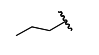

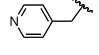
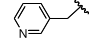
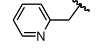
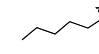


Figure 12. Synthesis of M₄ PAM analog libraries **9a-s** and **13a-s**. Reagents and conditions: a) Piperidine, EtOH, MW 160 °C, 12 min. 42%; b) K₂CO₃, MW 160 °C, 10 min., 75%; c) R₁-Cl, KI, Cs₂CO₃, DMF, MW 160 °C, 30 min. 15-80%; d) Morpholine, EtOH, MW 160 °C, 10 min. 62%; e) K₂CO₃, DMF, 0 °C->r.t., 24h 65%; f) R₁-Cl, KI, Cs₂CO₃, DMF, MW 160 °C, 30 min. 15-80%.

These libraries were first screened in a singlepoint Ca^{2+} mobilization assay using a fixed 10 μM concentration of test compound added to rat $\text{M}_4/\text{G}_{\text{qi}5}$ -cells prior to addition of a submaximal concentration ($\sim\text{EC}_{20}$) of ACh. This allowed efficient triage of analogs for further characterization. In general, alkylamine library **9a-s** showed weak efficacy with elevation of the ACh response ranging from none (inactive) to modest ($<50\%$ ACh max). However, ether library **13a-s** contained a number of robust potentiators ($\sim 60\text{-}90\%$ ACh max). The EC_{50} values for compounds selected from both libraries based on their potentiation efficacy and structural characteristics were then obtained from full CRCs in similar Ca^{2+} assays testing for potentiation of an ACh $\sim\text{EC}_{20}$ (**Table 4**).

Table 4. M₄ PAM SAR for select analogs from alkylamine library **9a-s** and ether library **13a-s** chosen based on an initial singlepoint triage screen. Ca²⁺ mobilization was used to obtain CRCs of each compound in the presence of an ACh ~EC₂₀ using rM₄ cells. Similar assays were used to obtain CRCs of ACh in the presence and absence of 30 μM of each test compound to determine fold-shift values (- denotes not determined). Data represent Means from at least three independent determinations.

<u>Compound</u>	<u>R₁</u>	<u>EC₅₀ (μM)</u>	<u>Fold-shift</u>
9a		>10	-
9b		>10	-
9c		9.1	1x
9e		>10	-
9l		>10	-
9n		>10	-
9o		>10	-
9p		>10	1x
13a		>10	1x
13b		>10	-
13c		6.5	37x
13d		8.2	25x
13e		>10	-
13f		>10	-
13g		>10	-
13k		2.0	50x
13l		2.2	9x
13m		1.8	5x
13p		>10	-

More than half of these compounds possessed EC₅₀ values over 10 μM with potentiation effects emerging only at the 10 μM and 30 μM concentrations. Among alkylamines **9a-s**, only the ethyl morpholine congener **9c** had an EC₅₀ just below 10 μM, reflecting relatively weak activity of this library. In contrast, compounds from the ether library **13a-s** possessed improved potencies. Particularly, picolyl analogs **13k**, **13l**, and **13m** each exhibited an EC₅₀ of approximately 2 μM. A concentration-response curve for **13k** in the presence of fixed ACh EC₂₀ is presented in **Figure 13a**. Analog **13k** elicited a robust potentiation of M₄ activation, elevating the submaximal ACh response to over 130% of the maximum response induced by a high concentration of ACh alone. Looking ahead to *in vivo* studies, the structure of **13k** was particularly attractive, as the presence of a basic amine would allow for an HCl salt to confer greater aqueous solubility for vehicle formulation. Based on these potency data, compounds having EC₅₀ values below 10 μM were examined for their ability to shift a full ACh CRC to the left when applied at a fixed 30 μM concentration in a similar functional Ca²⁺ assay with rM₄/G_{q15}-cells (**Table 4**). The ACh CRC fold-shift data for analog **13k** is shown in **Figure 13b**. In the case of other allosteric modulators of GPCRs, compound potency often fails to correlate tightly with fold-shift magnitude. For example, a PAM with high potency but low efficacy can exhibit next to no fold-shift effect, and conversely one with low potency but high efficacy may induce a substantial fold-shift. Hence, evaluation of fold-shift for novel potentiators having upper single-digit micromolar potencies can sometimes uncover helpful SAR that would have otherwise been missed.

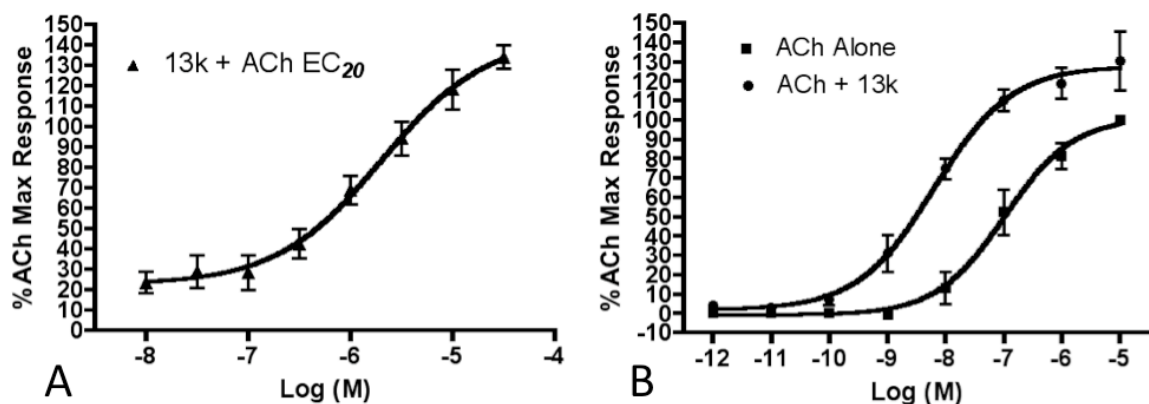


Figure 13. CRCs and ACh fold-shift for analog **13k** in rat M_4 cells by Ca^{2+} mobilization assay. A.) CRC for **13k** in the presence of an ACh $\sim EC_{20}$ ($EC_{50} = 2.0 \mu M$). B.) CRC for ACh in the presence and absence of a $30 \mu M$ concentration of **13k** (fold-shift = 50x). Data represent Mean \pm SEM from at least three independent determinations.

As shown in **Table 4**, neither morpholino compound **9c** nor ethyl compound **9p** caused a left-shift in the ACh CRC, demonstrating the compromised activity found with alkylamine modification at the 6-position of the scaffold. The same lack of effect was seen with the tertiary amine analog **13a** from the ether library. However, the ether-linked morpholino **13c** and pyrrolidine **13d** analogs demonstrated strong ACh left-shifts of 37x and 25x, respectively. Interestingly, movement of the nitrogen from the 2-position or 3-position of the picolyl ethers **13m** and **13l** to the 4-position of **13k** progressively increased the fold-shift from 5x to 9x and ultimately 50x, respectively (**Fig. 13b**).

Taken together, these data suggested ether-linked modifications to the 6-position of the scaffold were more tolerated and optimal than alkylamine-linked changes. However, despite retention of robust PAM properties in terms of ACh CRC fold-shift for **13c**, **13d**, and particularly **13k**, the potency of these analogs was moderately diminished relative to the parent compound **3** ($EC_{50} = 380 \text{ nM}$) (**Fig 13**). Furthermore, the SAR for these two libraries underlines the importance of considering both fold-shift and potency

when optimizing allosteric modulators. Although each of the three picolyl ether analogs had ~ 2 μM EC_{50} values, their left-shift effects on the ACh CRC revealed dramatic differences in maximal PAM efficacy.

For the next library iteration, we postulated that with the picolyl or ethyl morpholine ether moieties on the left-hand side of the molecule, the *p*-methoxybenzyl of the right-hand side might no longer be optimal for M_4 potency. Therefore, we opted to re-scan the amide with 18 side chain groups while holding constant each of the three picolyl ether modifications, the morpholino ether, and the dimethylpropylamine ether (**Fig. 14**). The morpholino and 4-picolyl were clear choices based on their degree of ACh CRC fold-shift, but the 2-picolyl and 3-picolyl were also included to be comprehensive. The dimethylpropylamine ether was chosen to provide for the possibility that a different amide side chain may rescue the activity of **13a** (i.e. a matrix-like approach to broaden SAR). These libraries began with the cyclization between pyridone **11** and ethyl chloroacetate **14** to produce thienopyridone ethyl ester **15**. To obtain the five alkyl ethers **16a-e**, material **15** was reacted with the five selected side chains from our previously library. These five scaffolds were saponified and immediately coupled with 18 amines to produce five alkyl ether libraries with different amide side chains **17a-p**, **18a-r**, **19a-o**, **20a-p**, **21a-o** (**Fig. 14**).

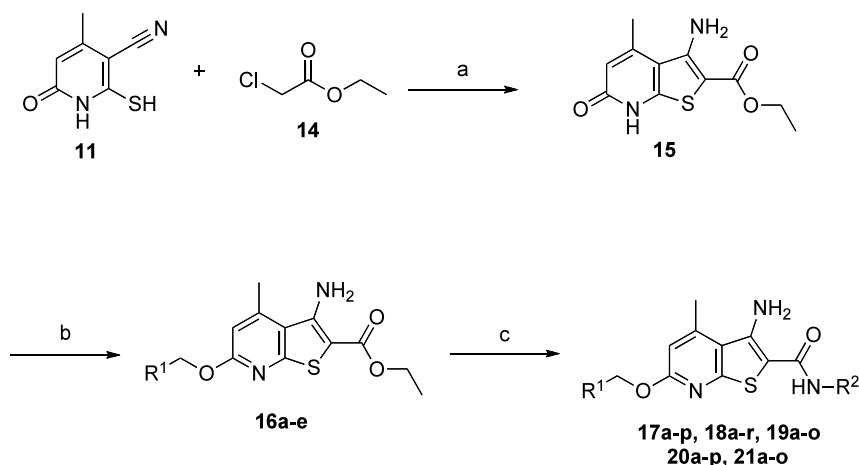


Figure 14. Synthesis of M₄ PAM analog libraries **17-21**. Reagents and conditions: a) TEA, DMF, 0 °C->r.t. 62%; b) R₁-Cl, KI, Cs₂CO₃, DMF, MW 160 °C, 30 min. 75-95%; c) 1) 3:1 1M NaOH:EtOH, MW 120 °C, 30 min. 2) R₂-NH₂, DIC, HOBt, 9:1 DMF:DIEA 20-80%.

As before, these libraries were screened first in a singlepoint 10 μM PAM assay that tested their ability to enhance the response of a submaximal (~EC₂₀) concentration of ACh in r_{M4}/G_{qi5}-cells (**Fig. 15**). PAM activity ranged from absent to robust within each of these libraries, revealing generally consistent SAR across all of the five ether-linked modifications that were held constant on the left-hand side of the structure.

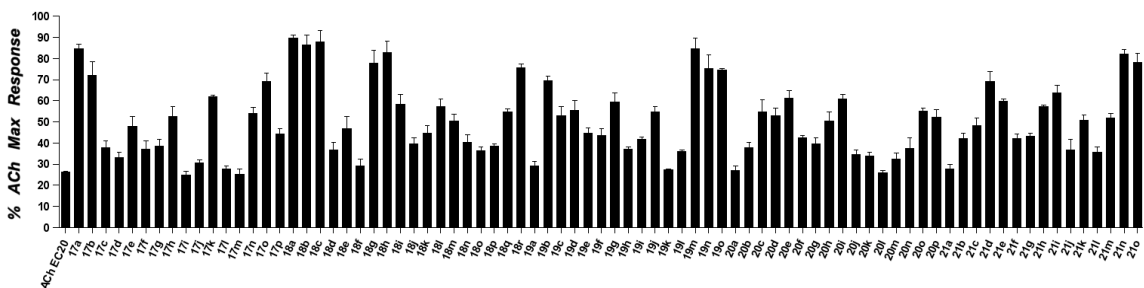
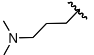
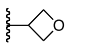
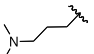
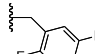
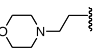
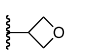
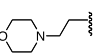
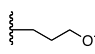
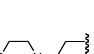
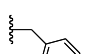
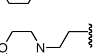
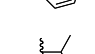
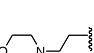
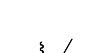
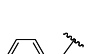
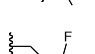
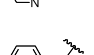
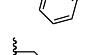
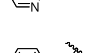
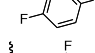
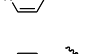
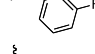


Figure 15. Singlepoint (10 μM) M₄ PAM screen of analog sets **17-21**. Ca²⁺ mobilization was used to obtain % ACh max values for each compound in the presence of an ACh ~EC₂₀. Data represent Mean +/- SEM from at least three independent determinations.

From this screen, eleven compounds were selected for CRCs and ACh fold-shift assays based on their degree of potentiation. The associated SAR data for the chosen compounds from libraries **17-21** obtained from these assays are shown in **Table 5**. All selected compounds possessed an EC₅₀ below 10 μM, except for **19n**, the di-fluorobenzyl substituted 2-picolyl analog. Similar to earlier libraries, ACh CRC fold-shift magnitude did not track closely with potency, as shown for example in the case of compound **18h**. This t-butyl substituted morpholine analog had near 9 μM potency but caused a robust 62x foldshift of the ACh CRC. Further, the two dimethylpropyl analogs **17a** and **17o** displayed approximately 3 μM potency yet induced only a moderate ACh fold-shift. Interestingly, this dimethylpropylamine moiety at R₁ conferred poor potency (EC₅₀ > 10 μM) in its parent compound **9b** that bore a *p*-methoxybenzyl group at R₂, but the amide scan library **17a-p** discovered side chains that rescued activity for this western side modification.

Table 5. M₄ PAM SAR for select compounds from second library iteration analogs **17-21**. Ca²⁺ mobilization was used to obtain CRCs of each compound in the presence of an ACh ~EC₂₀ using rM₄ cells. Similar assays were used to obtain CRCs of ACh in the presence and absence of 30 μM of each test compound to determine fold-shift values (- denotes not determined). Data represent Means from at least three independent determinations.

<u>Compound</u>	<u>R₁</u>	<u>R₂</u>	<u>EC₅₀ (μM)</u>	<u>Foldshift</u>
17a			2.58	7x
17o			2.75	14x
18a			7.42	40x
18b			6.25	67x
18c			5.81	51x
18g			7.15	36x
18h			8.73	62x
19m			5.40	28x
19n			>10	41x
21n			2.44	44x
21o			3.78	64x

In general, difluorinated benzylic substitutions at R₂ were favored, providing analogs with EC₅₀s in the 2-5 μM range at rat M₄ and with large ACh CRC fold-shift values (**Table 5**). The 4-picolyl moieties of R₁ with the 2,3-difluoro and 2,5-difluoro substitutions at R₂ of **21n** and **21o** proved most desired when seeking a balance of both potency and potentiation efficacy, consistent with previous SAR. However, the morpholines at R₁ of library **18a-r** with bare alkyl and mono-oxygenated side chains at

R₂ possessed strong fold-shift effects despite moderately weaker potency compared to **21n** and **21o**. **Figure 16** presents the CRC for elevation of an ACh ~ EC₂₀ and fold-shift effect on an ACh CRC for analog **21n**. Interestingly, this 2,3-difluorobenzyl substituted analog did not elevate the maximal response of ACh at the top of the CRC (**Fig. 16b**), which contrasts with 4-methoxybenzyl analog **13k** (**Fig. 13b**).

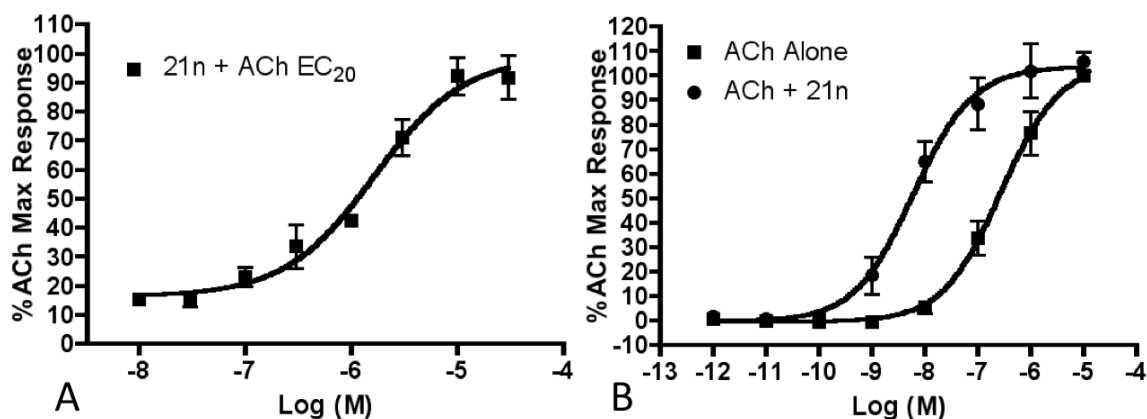


Figure 16. M₄ PAM characterization of analog **21n** in rat M₄/G_qi5-CHO cells by functional Ca²⁺ mobilization assay. A.) CRC for compound **21n** in the presence of an ACh ~EC₂₀ (EC₅₀ = 2.4 μM). B.) ACh CRC in the presence and absence of a fixed 30 μM concentration of **21n** (foldshift = 44x). Data represent Mean +/-SEM from at least three independent determinations.

Despite generation of a multi-dimensional library of analogs varying both sides of the lead molecule's scaffold, the approximately 400 nM rM4 potency of the first- and second- generation compounds **1-3** could not be maintained despite retention of robust PAM efficacy in terms of ACh CRC fold-shift (e.g. >50x). Indeed, compounds **13k**, **18b**, and **21o** each caused large left-shifts of ACh CRCs when applied at 30 μM, but were approximately an order of magnitude less potent than the earlier lead compounds. These SAR suggest the presence of a possible ~ 2 μM potency floor for this chemotype with 6-

position ether or amine modifications, as variation of the amide side chain failed to provide congeners with EC₅₀ values below this level.

We next evaluated the microsomal stability of novel analogs **13k**, **21n**, **21o**, and **18h** in both rat and human fortified liver microsomes. Replacement of the metabolically labile 6-Me group with the ether linkage did indeed improve metabolic stability for all four analogs **13k**, **21n**, **21o**, and **18h** (>90% parent remaining after 90 minutes) as compared to **1-3** (<10% parent remaining after 90 minutes). Moreover, incorporation of the basic amine moieties in these four compounds also improved solubility providing either homogeneous solutions or uniform micro-suspensions, as the HCl salts, across a panel of pharmaceutically acceptable vehicles (β -cyclodextrin, PEG400/H₂O, etc...) relative to initial lead compounds **2** (VU0152099) and **3** (VU0152100), which were only soluble in 10% Tween-80. In particular, **21n** afforded a homogeneous solution at 15 mg/mL in pH 3 saline. Thus, our optimization efforts revealed interesting and useful SAR that led to improved metabolic stability and physiochemical properties for this series of M₄ PAMs.

***In vivo* behavioral studies with 3rd-generation optimized M₄ PAMs**

Despite low micromolar potency at rat M₄, we evaluated analogs **13k**, **21n**, **21o**, and **18h** in our standard amphetamine-induced hyperlocomotion *in vivo* model. Recall, both **2** (VU0152099) and **3** (VU0152100) (EC_{50s} ~400 nM, ACh CRC fold-shifts of 30x and 70x, respectively) were efficacious in this behavioral model predictive of antipsychotic efficacy. In the event, **13k**, **21n**, **21o**, and **18h** all failed to reverse

amphetamine-induced hyperlocomotion following dosing at 56.6 mg/kg (I.P.), suggesting perhaps that the new compounds were too weak at rat M₄ (data not shown). This possibility is underlined by the fact that LY2033298 possesses similarly modest rM₄ potency and failed to achieve efficacy when dosed alone in recently disclosed *in vivo* rat behavioral studies, thereby requiring co-dosing of a muscarinic agonist (Oxotremorine) to achieve significant effects¹²⁷.

Species-specific differences in 3rd-generation M₄ PAM potencies

Primarily, our efforts were aimed at exploring SAR at rat M₄ and optimizing this series for beneficial DMPK and vehicle formulation properties suitable for *in vivo* rodent behavioral studies. While stability and physiochemical properties were improved, potency at rM₄ was diminished to a point where, most likely, *in vivo* efficacy was lost. However, rat and human mAChRs do diverge in structure (~95% amino acid sequence identity) and species-specific differences in on-target pharmacology have been noted for other mAChR PAMs. Therefore, we opted to evaluate representative compounds **13k**, **21n**, **21o**, and **18h** in analogous functional cell-based Ca²⁺ assays using cells expressing the human M₄ receptor (and promiscuous Gq_{15/16} for Ca²⁺ mobilization readout). To this end, all four compounds were submitted to Millipore and assayed in their GPCR Profiler Service™, which provided potency and ACh CRC fold-shift values with the human M₄ receptor. Remarkably, each compound possessed EC₅₀ values approximately in the 100-200 nM range at human M₄ (**Fig. 17a**), more than an order of magnitude greater potency than at the rat M₄ receptor. Each compound also elicited large left-shifts of the control

ACh CRC in human M₄ cells (**Fig. 17b**) at 30 μM, similar to their fold-shifts at rat M₄. In contrast, the prototypical M₄ PAMs **1-3**, displayed near equivalent EC₅₀s on rat and human M₄, suggesting the possibility that the basic residues in these newer analogs contact divergent residues in human M₄.

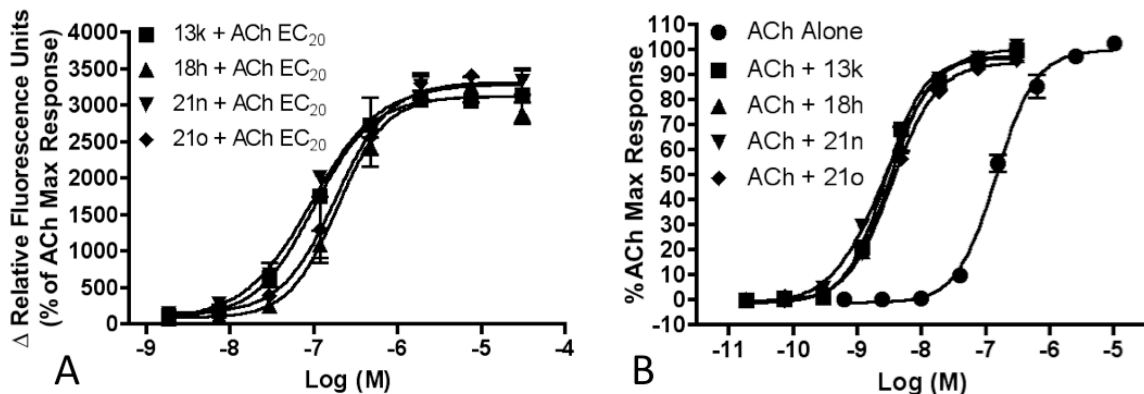


Figure 17. Effects of compounds **13k**, **18h**, **21n**, and **21o** in human M₄/G_{q15/16}-expressing cells by functional Ca²⁺ mobilization assay. A.) CRCs for potentiators in the presence of an ACh ~EC₂₀ (**13k** EC₅₀ = 100 nM, **18h** EC₅₀ = 192 nM, **21n** EC₅₀ = 95 nM, **21o** EC₅₀ = 183 nM). B.) for ACh in the presence and absence of a fixed 30 μM concentration of potentiator (**13k** foldshift = 63x, **18h** foldshift = 44x, **21n** foldshift = 60x, **21o** foldshift = 49x).

Potential for dual M₄ PAM / H₃ antagonist anti-psychotic activity

While M₁ PAMs and allosteric agonists have the potential to affect multiple symptom clusters of schizophrenia, M₄ PAMs may only prove efficacious in the treatment of positive symptoms. If so, combination therapy or possibly a monotherapy possessing poly-pharmacology may be more clinically effective for comprehensive symptom treatment in psychotic patients. For the cognitive symptom cluster specifically,

antagonism of the central histamine H₃ receptor (H₃) has been proposed as a potentially viable strategy¹²⁸⁻¹³⁰.

We observed that M₄ PAMs **13k**, **21n**, **21o**, and **18h** possessed the general features of the refined H₃ receptor antagonist pharmacophore (**Fig. 18**), and we therefore evaluated these compounds for their ability to function as H₃ antagonists (using an *in vitro* binding assay), which may provide pro-cognitive attributes *in vivo*¹²⁸. Compounds **13k**, **21o** and **18h** were found to inhibit human H₃ with IC₅₀ values of ~10 μM, while **21n** afforded an IC₅₀ value of 6.3 μM. Although weak, this result suggest that it may be possible to ‘dial in’ H₃ antagonist activity to this new series of M₄ PAMs via further optimization. Testing of this hypothesis via additional syntheses and dual M₄/H₃ screening will be required and has not yet been performed.

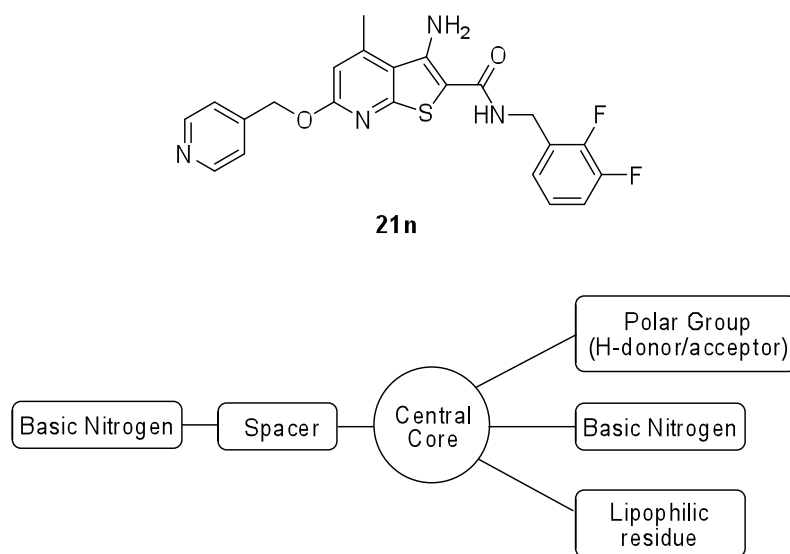


Figure 18. Alignment of M₄ PAM lead compound **21n** with the refined histamine H₃ receptor antagonist pharmacophore.

Summary

Ultimately, a lead optimization campaign around M₄ PAMs **1-3** provided novel analogs with substantially improved metabolic stability and physiochemical properties, but diminished potency at rat M₄ (EC₅₀s ~ 2 μM) while retaining comparable ACh CRC fold-shift (14x-67x) relative to early leads **1-3**. Surprisingly, we noted significant species differences within this series of M₄ PAMs, where analogs such as **21n** displayed an order of magnitude greater potency at human M₄ (EC₅₀ = 95 nM) than at the rat M₄ receptor (EC₅₀ = 2.4 μM) but with comparable ACh fold-shifts (human, 60x; rat, 44x).

To further expand the therapeutic relevance of M₄ positive allosteric modulation for the treatment of schizophrenia beyond the positive symptom cluster, we evaluated analogs against the H₃ receptor, as they align well with the refined H₃ antagonist pharmacophore model. M₄ PAM **21n** was found to provide modest inhibition of H₃ radioligand binding with an IC₅₀ of 6.3 μM, suggesting that it might be possible to discover optimized analogs with dual M₄ PAM and H₃ antagonist activity. Such compounds could be used to test the hypothesis that dual M₄/H₃ pharmacology would possess broad anti-psychotic potential across a range of preclinical behavioral studies aimed at predicting efficacy in treating different/multiple symptom clusters of schizophrenia.

Chapter IV

DISCOVERY, OPTIMIZATION, AND CHARACTERIZATION OF NOVEL SUBTYPE-SELECTIVE MACHR5 POSITIVE ALLOSTERIC MODULATORS

Discovery of M₁/M₃/M₅ PAM VU0119498

In order to identify novel M₁ PAMs, an HTS of the VHTSC compound collection (~160,000 compounds total) was performed using a fluorescence-based Ca²⁺ mobilization assay²⁷. Test compounds were added to CHO-cells stably expressing the M₁ receptor and allowed to equilibrate for approximately three minutes before addition of a submaximal (~EC₂₀) concentration of the orthosteric agonist carbachol (CCh). Compounds that potentiated the CCh response at least three standard deviations over the vehicle-control response were marked as primary hits (1,634 compounds). Secondary screening (singlepoint or CRC assays) at M₁ and counter-screening (CRC assays) at mGluR₄ identified a subset of hits (77 compounds), which exhibited concentration-dependent PAM activity at M₁ with no activity at mGluR₄.

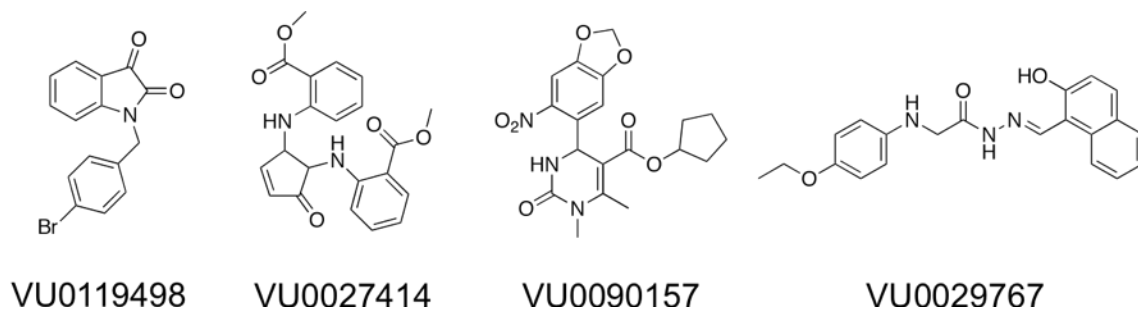


Figure 1. Compounds identified by M₁ PAM HTS chosen for *in vitro* characterization.

Four of these hits (**Fig. 1**) were chosen for further characterization, including *in vitro* mAChR subtype-selectivity assays, which identified VU0119498 as a mAChR PAM with similar potencies (~3-6 μM) and efficacies (~45-65% CCh max) in M₁, M₃, and M₅ CHO cell lines and with no PAM activity in M₂/G_{qi5} or M₄/G_{qi5} CHO cell lines, as shown in **Fig. 2**. Subsequent functional and radioligand-binding assays demonstrated that VU0119498 (30 μM) induces a 14x left-shift of an ACh CRC at M₁ by Ca²⁺ mobilization assay and does not compete with [³H]-NMS for binding to M₁ cell membranes (**Fig. 2**), similar to the other three novel mAChR PAMs evaluated from the HTS and consistent with an allosteric mode of modulation.

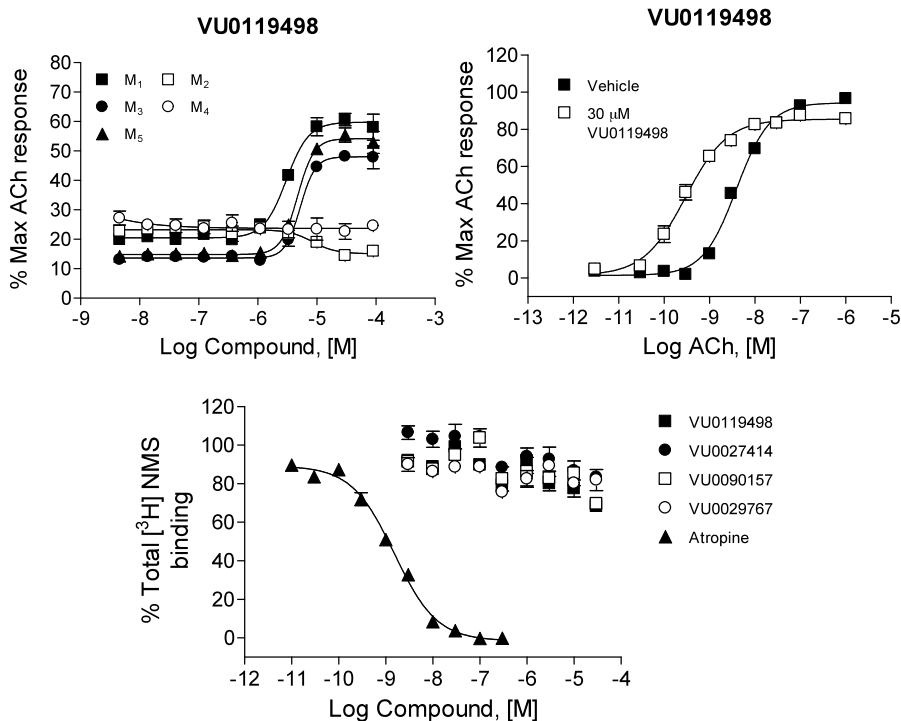


Figure 2. *In vitro* characterization of VU0119498. mAChR subtype-selectivity curves (top left panel) were obtained by Ca²⁺ mobilization assays in the presence of an $\sim\text{EC}_{20}$ of ACh at all five mAChR subtype cell lines. ACh curves in the absence and presence of VU0119498 (top right panel) were obtained by Ca²⁺ mobilization assays using M₁ cells. Competition curves (bottom panel) were obtained in the presence of 0.1 nM [³H]-NMS using membranes from M₁-expressing CHO cells. Atropine K_i = 1.08 \pm 0.09 nM. Data represent the Mean \pm S.E.M. of at least 3 independent experiments with similar results. Experiments performed by J. Marlo.

In light of the unprecedented mAChR PAM subtype-selectivity profile of VU0119498, we hypothesized that structural modification via chemical optimization of this novel compound would lead to the discovery of PAMs selective (either functionally or via binding specificity) for M₅^{131,132}. As discussed in the introduction (Chapter I), the current and longstanding lack of available small molecules with selectivity for M₅ made this an attractive endeavor with the possibility of providing a substantial contribution to the mAChR research community and thereby facilitating subsequent *ex-vivo* and/or *in vivo* M₅ neurobiology studies. To this end we executed an exploratory optimization project utilizing (Chapter I) medicinal chemistry methods. However, prior to synthesizing VU0119498 analogs, the parent compound itself was resynthesized and retested in order to confirm the validity of the structure and associated pharmacological characteristics (**Fig. 3**). *N*-alkylation of commercially available isatin with 4-bromobenzyl bromide under standard conditions provided the desired compound with high yield (**Fig. 3**), which was then tested in mAChR subtype-selectivity CRC assays by Ca²⁺ mobilization.

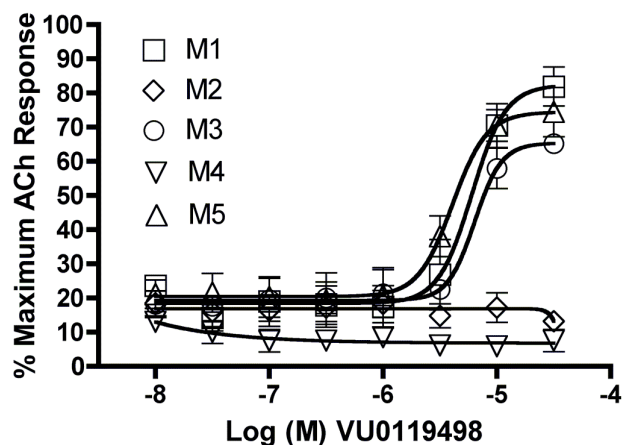
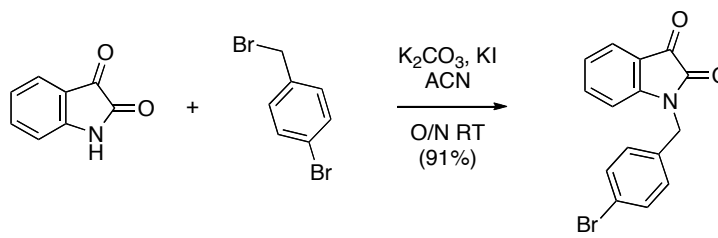
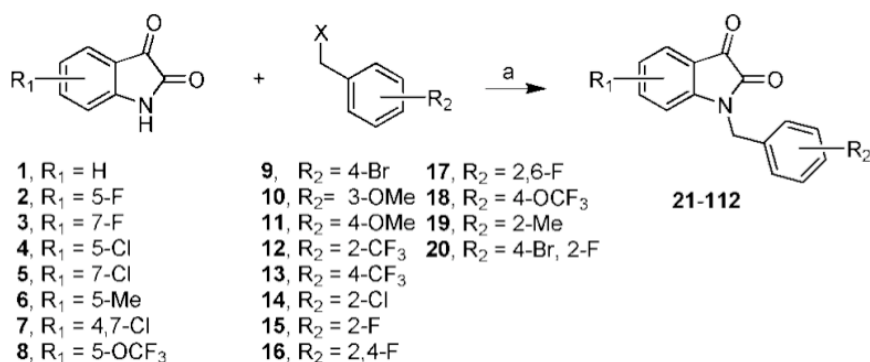


Figure 3. Resynthesis and retesting of HTS hit VU0119498. Isatin was reacted with 4-bromobenzyl bromide in the presence of K_2CO_3 , and KI, in ACN and stirred overnight at room temperature to provide desired compound (top panel). Ca^{2+} mobilization assays with M₁-M₅ cells (M₂ and M₄ co-expressed G_{q15}) were used to obtain CRCs (bottom panel) of resynthesized VU0119498 (EC₅₀ values: M₁ = 6.0 μ M 82% ACh max, M₃ = 6.4 μ M 66% ACh max, M₅ = 4.1 μ M 74% ACh max). Data represent the Mean \pm S.E.M. of at least 3 independent experiments with similar results.

This was an important step because hits from HTS campaigns can sometimes fail to retest following resynthesis due to reasons such as incorrect structure assignment from the compound vendor or in-house management system, sample or assay plate/well contamination, etc... Gratifyingly, the resynthesized batch of VU0119498 exhibited a virtually identical mAChR subtype-selectivity, potency, and efficacy profile as that of the parent batch obtained from the HTS (**Fig. 3**), which increased confidence that a subsequent optimization effort on this chemical scaffold would be worthwhile.

Optimization of VU0119498 to obtain M₅ PAM VU0238429

Given SAR findings from other medicinal chemistry projects centered on GPCR allosteric modulators that demonstrated often pronounced effects of subtle structural modifications on subtype-selectivity and other pharmacological characteristics, we chose to initially and rapidly explore SAR around VU0119498 via synthesis of a 92-member analog library in matrix format wherein each of 8 commercially available isatins was reacted with approximately 12 benzyl halides under standard microwave alkylation conditions (**Fig. 4**). Resulting analogs (compounds 21-112) were then screened in a singlepoint format at 30 μM in Ca^{2+} mobilization assays using M₅ and M₁ cells receiving a fixed submaximal ($\sim\text{EC}_{20}$) concentration of ACh (**Fig. 4**). This method was utilized to allow for efficient triage of analogs displaying high M₁ vs. M₅ or M₅ vs. M₁ preference. Interestingly, some analogs displayed robust potentiation effects at M₅ (i.e. elevation of ACh $\sim\text{EC}_{20}$ to >50-60% of maximum ACh response) with absent or weak potentiation at M₁, thus exhibiting strong preference for M₅ versus M₁ activity (**Fig. 4**).



^a Reagents and conditions: (a) K₂CO₃, KI, ACN, microwave 160°C, 10 min, 20–95%.

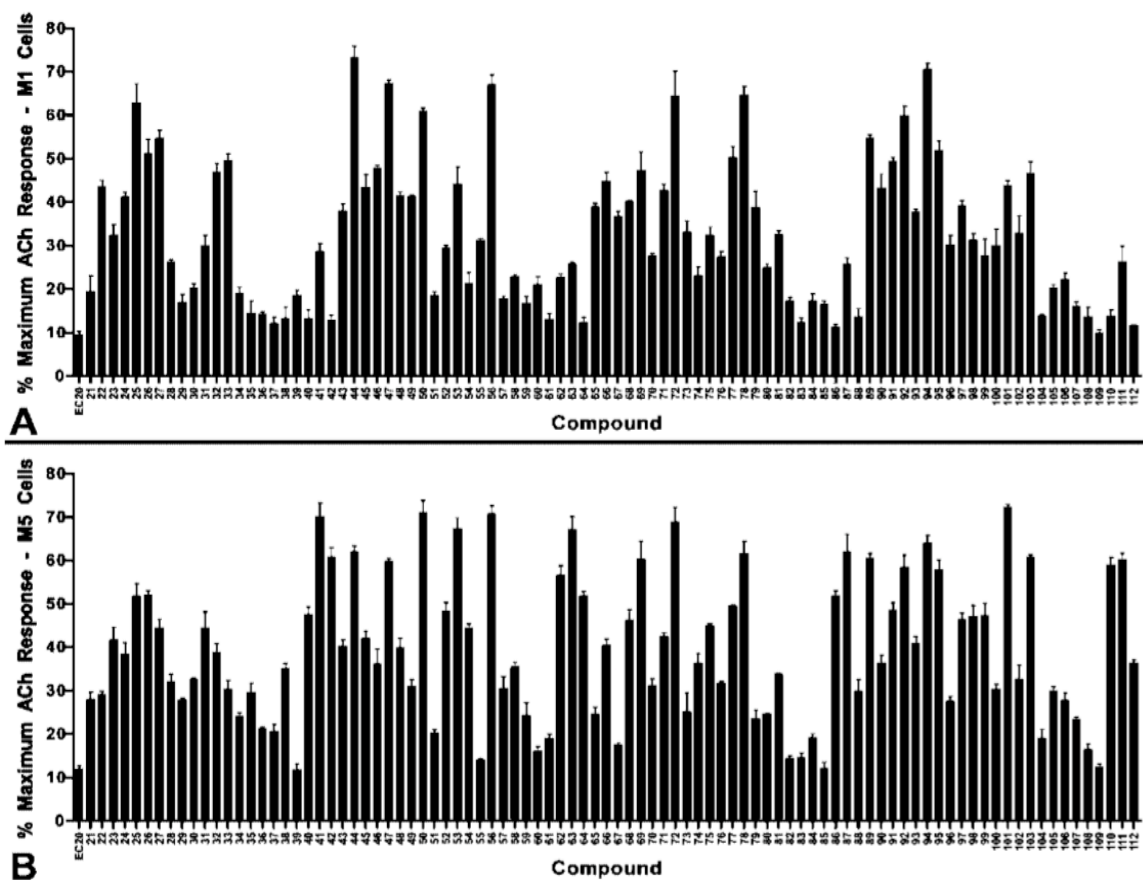
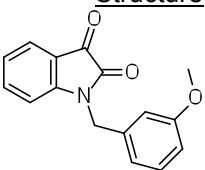
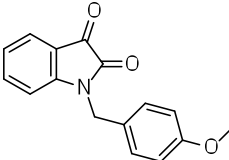
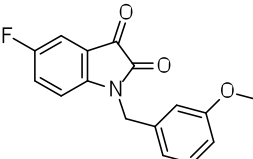
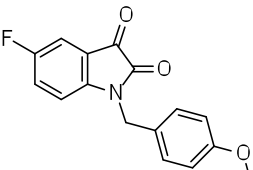
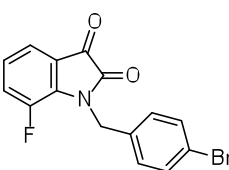
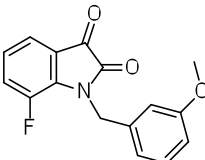
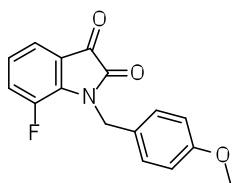


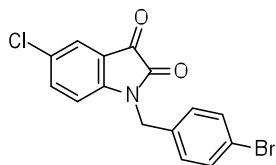
Figure 4. Synthesis and singlepoint screening of initial matrix library of VU0119498 analogs. Different substituted isatins were each *N*-alkylated with various benzyl halides under microwave conditions in the presence of K₂CO₃ and KI in ACN to generate a 92-member library (top panel). Ca²⁺ mobilization assays with M₁ and M₅ cells were used to obtain singlepoint (30 μM) potentiation responses for each analog in the presence of a submaximal (~EC₂₀) concentration of ACh (middle and bottom panels). Data represent the Mean ± S.E.M. of at least 3 independent experiments with similar results.

Table 1. Structures for compounds **21-112** and associated PAM activity data from the initial single concentration (30 μ M) potentiator screen against M_1 and M_5 . Values shown for each compound are Ca^{2+} mobilization responses as percentages of maximum ACh response. The synthetic method used to generate each compound is indicated by the following abbreviations: M, microwave; C, classical. The molecular formula for each compound is also presented. Data represent the Mean of at least 3 independent experiments with similar results.

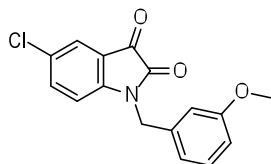
<u>Structure</u>	<u>Cmpd #</u>	<u>Synthesis</u>	<u>Formula</u>	<u>M_1 %Max</u>	<u>M_5 %Max</u>
	21	M	C ₁₆ H ₁₃ NO ₃	19.40	28.04
	22	M	C ₁₆ H ₁₃ NO ₃	43.58	29.19
	23	M	C ₁₆ H ₁₂ FNO ₃	32.32	41.61
	24	M	C ₁₆ H ₁₂ FNO ₃	41.14	38.28
	25	M	C ₁₅ H ₉ BrFNO ₂	62.67	51.69
	26	M	C ₁₆ H ₁₂ FNO ₃	51.07	51.97



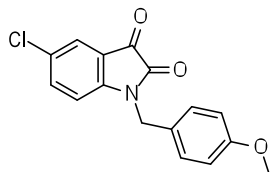
27 M C₁₆H₁₂FNO₃ 54.62 44.40



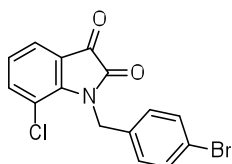
28 M C₁₅H₉BrClNO₂ 26.13 32.03



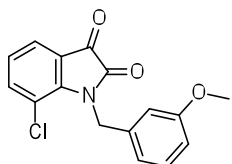
29 M C₁₆H₁₂ClNO₃ 16.94 27.87



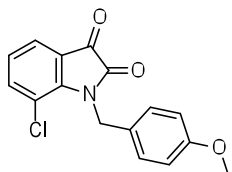
30 M C₁₆H₁₂ClNO₃ 20.31 32.61



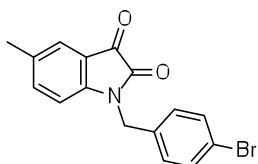
31 M C₁₅H₉BrClNO₂ 29.87 44.34



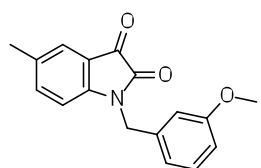
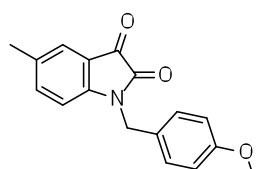
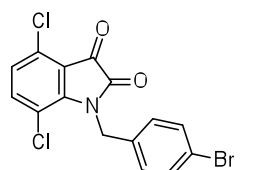
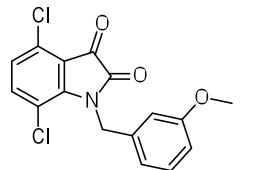
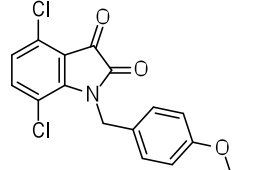
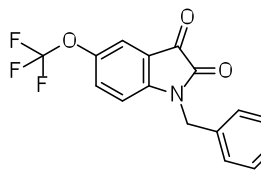
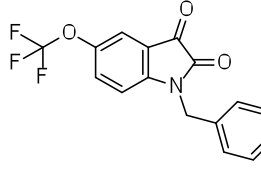
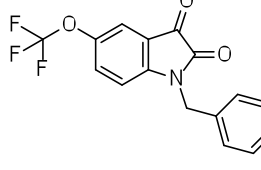
32 M C₁₆H₁₂ClNO₃ 46.88 38.74

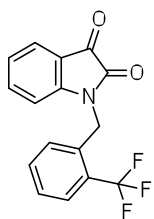


33 M C₁₆H₁₂ClNO₃ 49.44 30.32

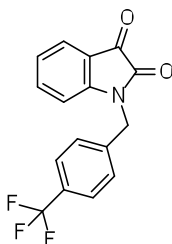


34 M C₁₆H₁₂BrNO₂ 18.98 24.06

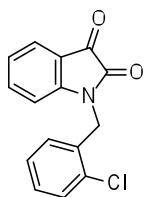
	35	M	C ₁₇ H ₁₅ NO ₃	14.49	29.57
	36	M	C ₁₇ H ₁₅ NO ₃	14.09	21.18
	37	M	C ₁₅ H ₈ BrCl ₂ NO ₂	12.08	20.67
	38	M	C ₁₆ H ₁₁ Cl ₂ NO ₃	13.26	35.11
	39	M	C ₁₆ H ₁₁ Cl ₂ NO ₃	18.60	11.73
	40	M	C ₁₆ H ₉ BrF ₃ NO ₃	13.21	47.56
	41	M	C ₁₇ H ₁₂ F ₃ NO ₄	28.55	70.08
	42	M, C	C ₁₇ H ₁₂ F ₃ NO ₄	12.69	60.73



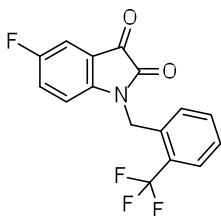
43 M C16H10F3NO2 37.89 40.23



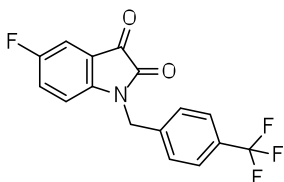
44 M C16H10F3NO2 73.26 61.99



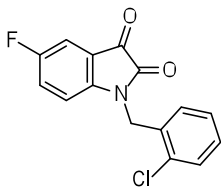
45 M C15H10ClNO2 43.42 41.96



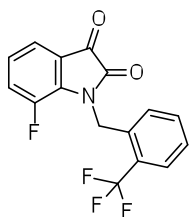
46 M C16H9F4NO2 47.78 36.15



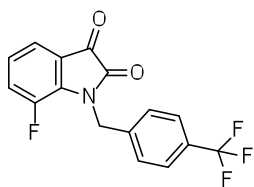
47 M C16H9F4NO2 67.30 59.76



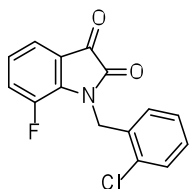
48 M C15H9ClFNO2 41.35 39.90



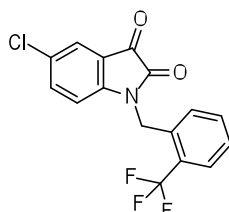
49 M C16H9F4NO2 41.26 30.92



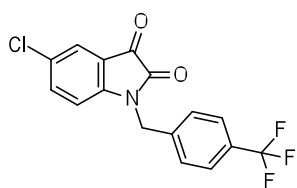
50 M C16H9F4NO2 60.86 71.10



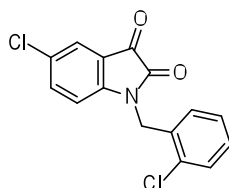
51 M C15H9ClFNO2 18.53 20.27



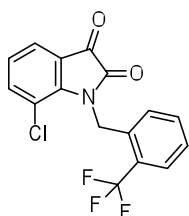
52 M C16H9ClF3NO2 29.56 48.35



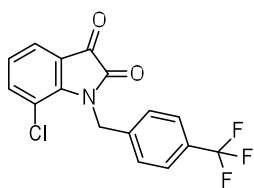
53 M C16H9ClF3NO2 44.14 67.39



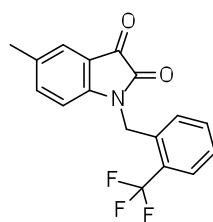
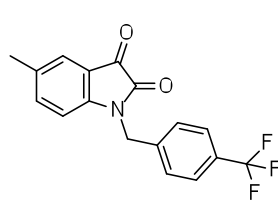
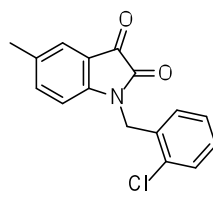
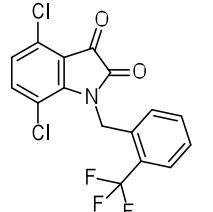
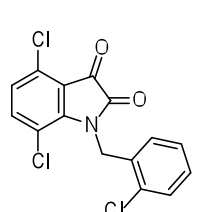
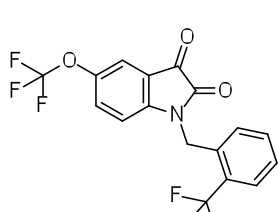
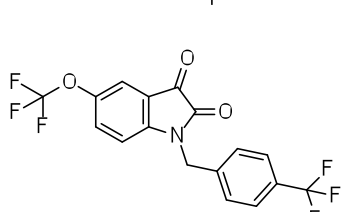
54 M C15H9Cl2NO2 21.27 44.35

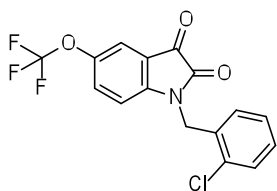


55 M C16H9ClF3NO2 31.14 13.99

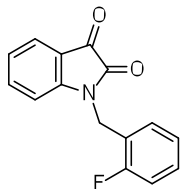


56 M,C C16H9ClF3NO2 67.04 70.76

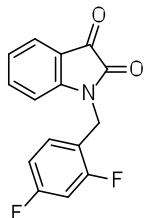
	57	M	C ₁₇ H ₁₂ F ₃ NO ₂	17.81	30.57
	58	M	C ₁₇ H ₁₂ F ₃ NO ₂	22.89	35.45
	59	M	C ₁₆ H ₁₂ ClNO ₂	16.80	24.30
	60	M	C ₁₆ H ₈ Cl ₂ F ₃ NO ₂	21.09	16.02
	61	M	C ₁₅ H ₈ Cl ₃ NO ₂	13.06	18.94
	62	M	C ₁₇ H ₉ F ₆ NO ₃	22.63	56.54
	63	M	C ₁₇ H ₉ F ₆ NO ₃	25.69	67.22



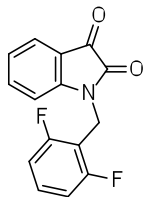
64 M C16H9ClF3NO3 12.29 51.88



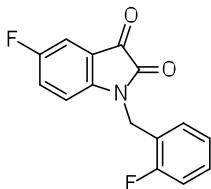
65 M C15H10FNO2 38.87 24.49



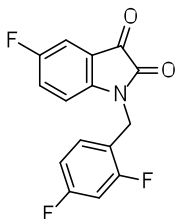
66 M C15H9F2NO2 44.84 40.38



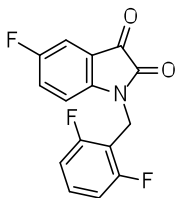
67 M C15H9F2NO2 36.65 17.44



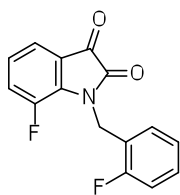
68 M C15H9F2NO2 40.11 46.18



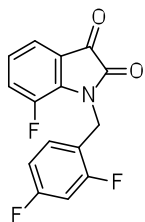
69 M C15H8F3NO2 47.31 60.32



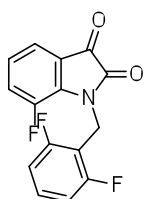
70 M C15H8F3NO2 27.59 31.11



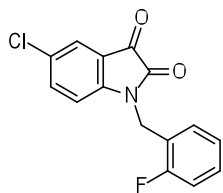
71 M C15H9F2NO2 42.71 42.40



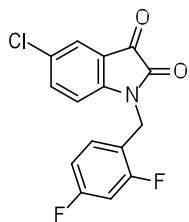
72 M C15H8F3NO2 64.42 68.93



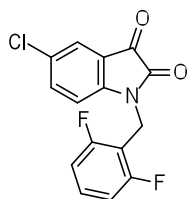
73 M C15H8F3NO2 33.10 25.10



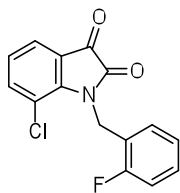
74 M C15H9ClFNO2 22.98 36.33



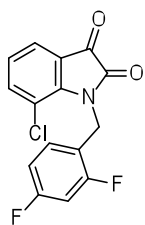
75 M C15H8ClF2NO2 32.39 44.90



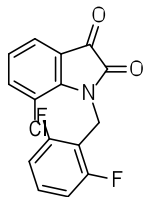
76 M C15H8ClF2NO2 27.34 31.82



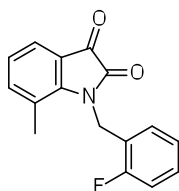
77 M C15H9ClFNO2 50.42 49.54



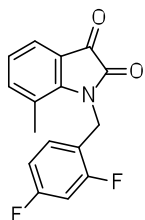
78 M C15H8ClF2NO2 64.64 61.59



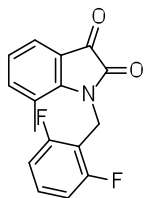
79 M C15H8ClF2NO2 38.83 23.59



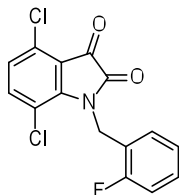
80 M C16H12FNO2 24.85 24.60



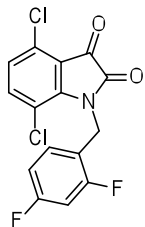
81 M C16H11F2NO2 32.56 33.81



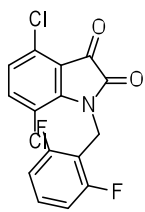
82 M C16H11F2NO2 17.28 14.40



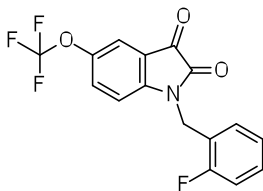
83 M C15H8Cl2FNO2 12.36 14.70



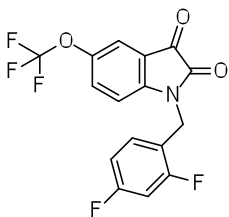
84 M C15H7Cl2F2NO2 17.23 19.10



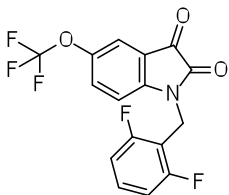
85 M C15H7Cl2F2NO2 16.40 12.19



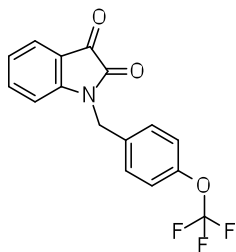
86 M C16H9F4NO3 11.30 51.77



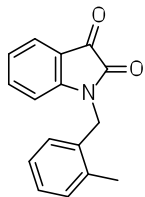
87 M C16H8F5NO3 25.85 61.90



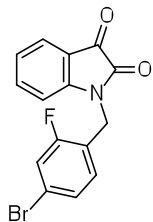
88 M C16H8F5NO3 13.57 29.82



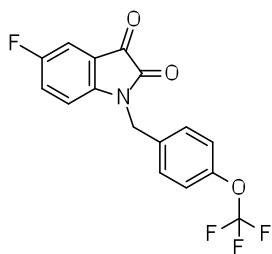
89 M C16H10F3NO3 54.72 60.47



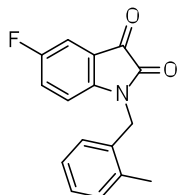
90 M C16H13NO2 43.16 36.34



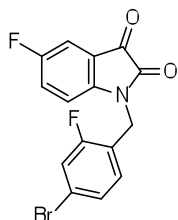
91 M C15H9BrFNO2 49.20 48.52



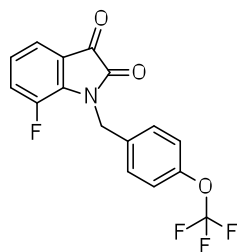
92 M C16H9F4NO3 59.81 58.39



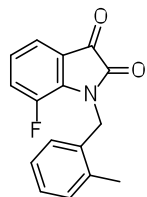
93 M C16H12FNO2 37.72 40.76



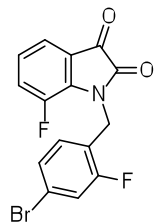
94 M C15H8BrF2NO2 70.54 63.96



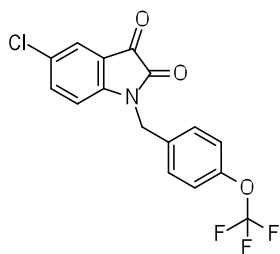
95 M C16H9F4NO3 51.78 57.70



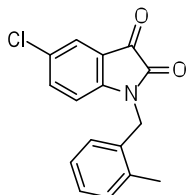
96 M C16H12FNO2 30.17 27.52



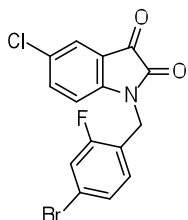
97 M C15H8BrF2NO2 39.19 46.34



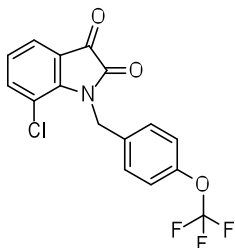
98 M C₁₆H₉ClF₃NO₃ 31.28 47.07



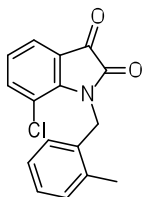
99 M C₁₆H₁₂ClNO₂ 27.65 47.26



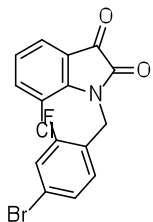
100 M C₁₅H₈BrClFNO₂ 29.89 30.39



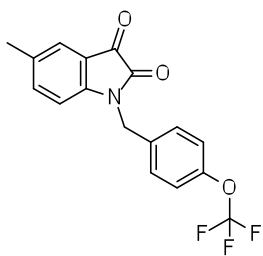
101 M C₁₆H₉ClF₃NO₃ 43.65 72.32



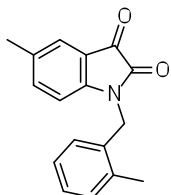
102 M C₁₆H₁₂ClNO₂ 32.83 32.56



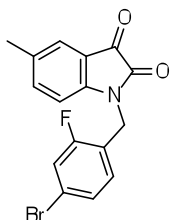
103 M C₁₅H₈BrClFNO₂ 46.52 60.75



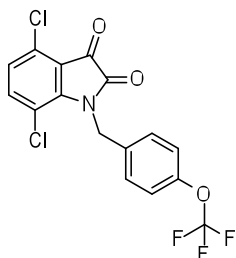
104 M C17H12F3NO3 13.83 18.92



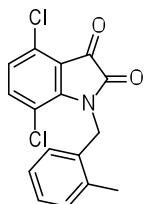
105 M C17H15NO2 20.19 29.85



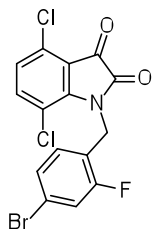
106 M C16H11BrFNO2 22.32 27.77



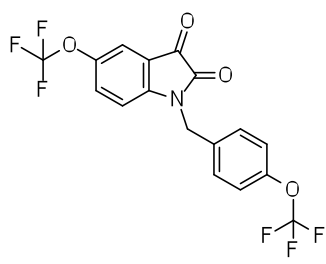
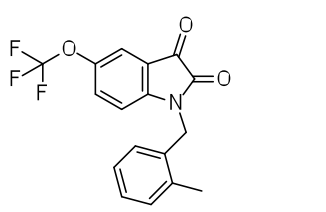
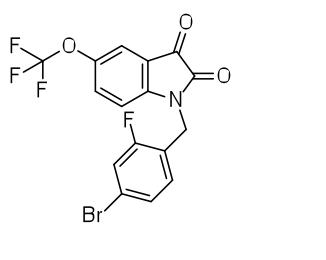
107 M C16H8Cl2F3NO3 16.03 23.24



108 M C16H11Cl2NO2 13.68 16.42



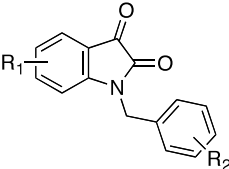
109 M C15H7BrCl2FNO2 9.93 12.38

	110	M	C17H9F6NO4	13.82	58.87
	111	M	C17H12F3NO3	26.16	59.97
	112	M	C16H8BrF4NO3	11.56	36.36

In terms of maximal potentiation efficacy, SAR from the initial 30 μM screen of the entire library suggested that 5-OCF₃ substitution of the isatin core was generally favored for greater M₅ versus M₁ activity, while halogen substitutions at the 7- position conferred a more dual M₁/M₅ activity. The % ACh max values for each compound at both M₁ and M₅ from the full singlepoint screen are show in **Table 1**. Based on the results of this screen, 18 compounds were selected for follow-up CRCs at M₁ and M₅ to determine potencies (**Table 2**). All 5-OCF₃ substituted compounds chosen from the initial screen possessed 1-5 μM potencies at M₅ and >30 μM potencies at M₁ in CRC assays, with the exception of compounds **63** and **112**, which nonetheless possessed greater M₅ versus M₁ activities (**Table 2**). Numerous benzylic substitutions were tolerated for M₁ and M₅ activity (depending also on the isatin core), methoxybenzyl was

generally favored for M₅ versus M₁ activity, and trifluoromethylbenzyl was generally favored for dual M₁/M₅ PAM activity. Most other simple congeners, including those with various methyl substitutions at R₁ or R₂ displayed weak or no potentiation activity at either receptor (**Table 2**).

Table 2. Potency SAR at M₁ and M₅ for 18 compounds selected from an initial singlepoint screen. Ca²⁺ mobilization assays with M₁ and M₅ cells were used to obtain compound CRCs in the presence of a fixed submaximal (~EC₂₀) concentration of ACh. Data represent the Mean of at least 3 independent experiments with similar results.

				
Cmpd	R ₁	R ₂	M ₁ EC ₅₀ (μM)	M ₅ EC ₅₀ (μM)
22	H	4-OMe	>10	>30
25	7-F	4-Br	3.99	1.93
33	7-Cl	4-OMe	5.38	3.96
38	4,7-Cl	3-OMe	>30	7.15
41	5-OCF ₃	3-OMe	>30	1.70
42	5-OCF₃	4-OMe	>30	1.16
44	H	4-CF ₃	5.88	3.19
46	5-F	2-CF ₃	6.21	4.09
47	5-F	4-CF ₃	8.55	7.13
49	7-F	2-CF ₃	>30	>30
50	7-F	4-CF ₃	5.18	3.26
56	7-Cl	4-CF ₃	3.20	2.11
63	5-OCF ₃	4-CF ₃	7.09	1.85
64	5-OCF ₃	2-Cl	>30	4.07
103	7-Cl	2-F, 4-Br	7.14	4.66
110	5-OCF ₃	4-OCF ₃	>30	1.86
111	5-OCF ₃	2-Me	>30	3.28
112	5-OCF ₃	2-F, 4-Br	>30	>10

Based on these findings, specifically that subtle structural changes to VU0119498 confer dramatic effects on mAChR subtype-selectivity, we also hypothesized that some of the compounds (of this 92-member library) that were inactive at M₁ and M₅ in the singlepoint screen may represent M₃ PAMs. Although identification of PAMs for M₃

was not a priority of this project, we nonetheless tested this hypothesis by evaluating 13 M_1/M_5 inactive compounds in a similar singlepoint (30 μM) screen at M_3 by Ca^{2+} mobilization assay (**Fig. 5**). Surprisingly, all were devoid of robust PAM activity at M_3 (**Fig. 5**). With the exception of only two compounds (VU0238437 and VU0238469, which bore 7-F substitution at R_1) all of these analogs contained either 5-Me or 4,7-Cl substitution at R_1 , suggesting that these modifications dial-out functional mAChR PAM activity from the VU0119498 scaffold or prevent mAChR binding altogether. The structures and VU numbers for these 13 compounds are shown in **Table 3**.

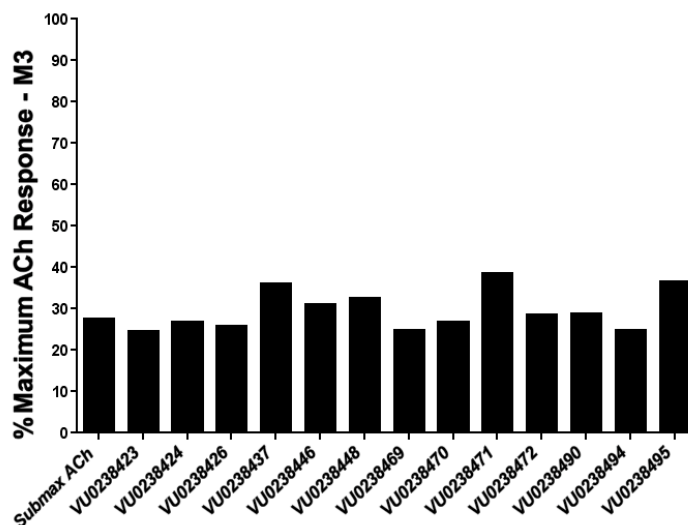


Figure 5. Singlepoint screen at M_3 of a subset of VU0119498 analogs chosen based on inactivity at M_1 and M_5 . Ca^{2+} mobilization assays with M_3 cells were used to obtain singlepoint (30 μM) potentiation responses for each analog in the presence of a submaximal ($\sim\text{EC}_{20}$) concentration of ACh. Data represent results from a single experiment.

Table 3. Structures and VU numbers for 13 VU0119498 analogs chosen for a M₃ PAM singlepoint screen based on their inactivity at M₁ and M₅ in the initial singlepoint screen of 92-member matrix library.

<u>R₁</u>	<u>R₂</u>	<u>Compound</u>
5-Me	4-OMe	VU0238423
4,7-Cl	4-Br	VU0238424
4,7-Cl	4-OMe	VU0238426
7-FI	2-Cl	VU0238437
4,7-Cl	2-CF ₃	VU0238446
4,7-Cl	2-Cl	VU0238448
7-FI	2-FI	VU0238469
4,7-Cl	2-FI	VU0238470
4,7-Cl	2,4-FI	VU0238471
4,7-Cl	2,6-FI	VU0238472
5-Me	4-OCF ₃	VU0238490
4,7-Cl	2-Me	VU0238494
4,7-Cl	2-FI,4-Br	VU0238495

***In vitro* characterization of M₅ PAM VU0238429**

In light of the high M₅ versus M₁ potentiation preference displayed by analog **42** (1.16 μM M₅ EC₅₀ and >30 μM M₁ EC₅₀) in these assays, the full subtype-selectivity profile of this compound was obtained in similar Ca²⁺ assays using M₂, M₃, and M₄ cells (**Fig. 6**). Likewise, full subtype-selectivity determination was also performed with compound **56**, which was the most potent dual M₁/M₅ potentiator in the initial evaluation at both receptors (2.11 μM M₅ EC₅₀ and 3.20 μM M₁ EC₅₀), as shown in **Figure 7**.

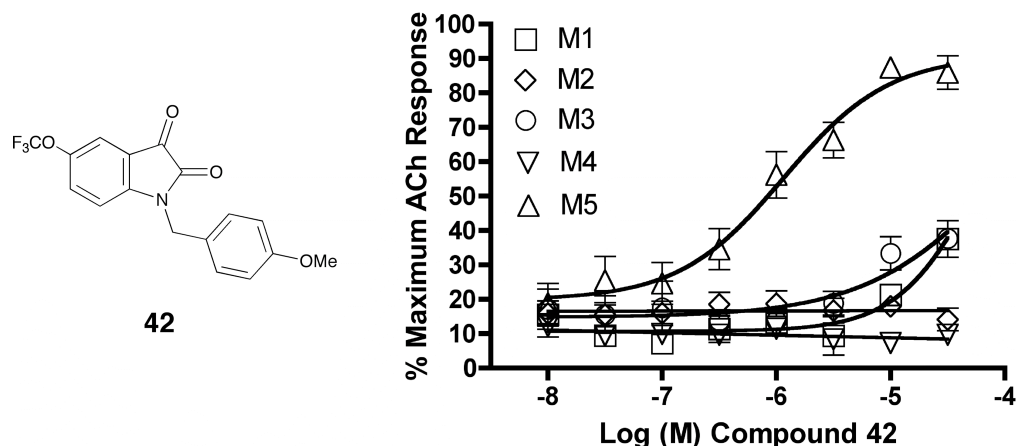


Figure 6. mAChR subtype-selectivity of compound 42 (VU0238429) displaying high M₅ PAM selectivity. Ca²⁺ mobilization assays with M₁-M₅ cells were used to obtain compound CRCs in the presence of a fixed submaximal (~EC₂₀) concentration of ACh (EC₅₀ values: M₁ = >30 μM, M₃ = >30 μM, M₅ = 1.1 μM 91% ACh max). Data represent the Mean ±S.E.M. of at least 3 independent experiments with similar results.

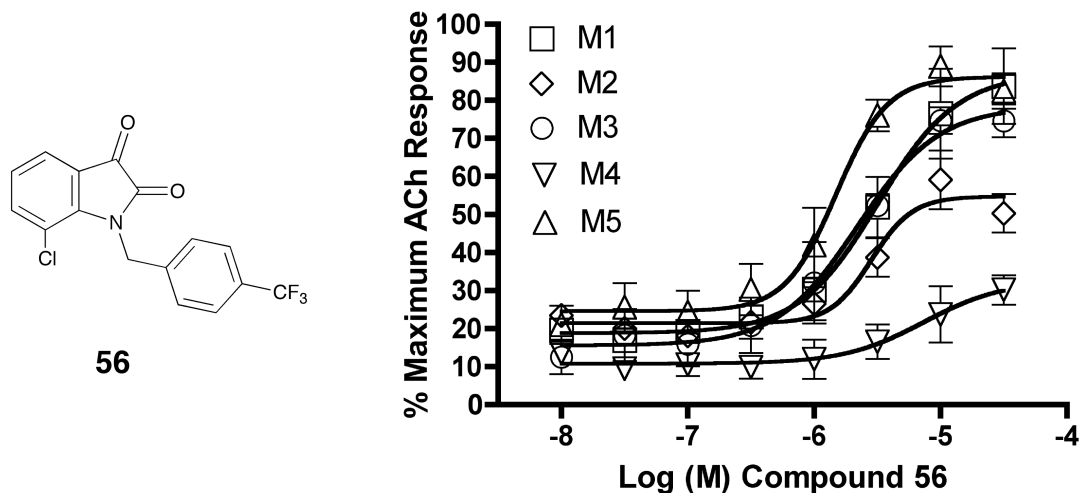


Figure 7. mAChR subtype-selectivity of compound 56 displaying pan-mAChR PAM activity. Ca²⁺ mobilization assays with M₁-M₅ cells were used to obtain compound CRCs in the presence of a fixed submaximal (~EC₂₀) concentration of ACh (EC₅₀ values: M₁ = 3.2 μM 87% ACh max, M₃ = 2.2 μM 78% ACh max, M₅ = 2.1 μM 86% ACh max, M₂ = 2.8 μM 55% ACh max, M₄ = >10 μM). Data represent the Mean ±S.E.M. of at least 3 independent experiments with similar results.

Remarkably, compound 42 (VU0238429) had similarly poor potency at M₃ as at M₁, with potentiation of the ACh ~EC₂₀ beginning to emerge only in the double-digit

micromolar range (**Fig. 6**). Gratifyingly, this compound maintained its lack of potentiation activity at M₂ and M₄ (in cells co-transfected with G_{q15}) at up to 30 μM (**Fig. 6**). Given these data, the approximately 1.16 μM M₅ potency of compound **42** provides >30x PAM selectivity for M₅ versus the other four subtypes, thus representing the first highly M₅-preferring M₅ ligand ever reported. Conversely, compound **56** (VU0238441) was found to retain the M₁/M₃/M₅ potentiation profile of the parent HTS hit **113** and also interestingly possessed modest potentiation at M₂ and M₄ at higher concentrations (**Fig. 7**). Despite the high M₅-preference of VU0238429 observed in these functional PAM assays, it is unknown if this compound (or any of the other analogs) possesses high M₅-binding specificity or if its selectivity is primarily functional with similar binding affinities for multiple subtypes. Binding experiments aimed at answering this question are hindered by an absence of radioligand(s) for the putative allosteric site at which these PAMs bind; however, functional studies may be pursued, which are discussed later in this thesis (Chapter VI).

To further evaluate the ability of compound **42** (VU0238429) to potentiate ACh-induced activation of M₅, we obtained full CRCs for ACh in M₅ cells in the presence of either vehicle or a fixed (30 μM) concentration of compound **42** (**Fig. 8**). In these assays, compound **42** induced a robust 14x left-shift of the ACh CRC, which was virtually identical to that found with the parent HTS hit VU0119498 when evaluated in the similar assay at M₁. Moreover, compound **42** lacked intrinsic agonist activity at M₅ when tested up to 30 μM in the absence of ACh (**Fig. 8**).

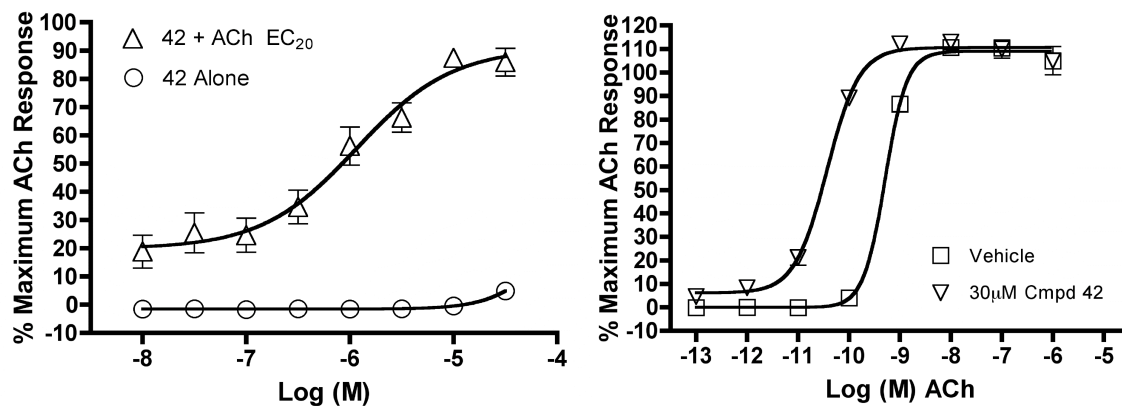


Figure 8. Compound **42** (VU0238429) requires ACh to activate M₅ and causes a robust increase in ACh potency at M₅. Ca²⁺ mobilization assays with M₅ cells were used to obtain compound CRCs in the presence and absence of a submaximal (~EC₂₀) concentration of ACh (left panel) and ACh CRCs in the presence and absence of compound (30 μM, right panel). ACh EC₅₀ was left-shifted 14x by compound **42** (VU0238429). Data represent the Mean ±S.E.M. of at least 3 independent experiments with similar results.

We also evaluated HTS hit VU0119498 and the highly M₅-preferring analog **42** (VU0238429) in competition-binding experiments with M₅-CHO membrane preparations using the orthosteric radioligand [³H]-NMS, a potent pan-mAChR antagonist. At up to 30 μM, compound **42** lacked competition with [³H]-NMS, consistent with an allosteric mode of binding to M₅ (**Fig. 9**). By contrast, VU0119498 exhibited approximately 50% inhibition of radioligand binding at 30 μM (**Fig. 9**). This inhibition by VU0119498 could be due either to direct competitive orthosteric binding or to negative cooperativity via an allosteric site; however, further experiments to investigate these possibilities were not performed due to a greater focus on VU0238429. When competition curves of ACh were obtained (**Fig. 9**) in the presence and absence of VU0238429 (30 μM) at M₅ cell membranes, this PAM caused a pronounced increase in the K_i of the low affinity binding state of the receptor (~15x) with only a modest effect on the K_i of the high affinity binding state (~1.5x), which suggests that the primary mechanism of potentiation by

VU0238429 at M_5 is by enhancement of ACh binding, possibly via stabilization of the high affinity receptor conformation (Fig. 9).

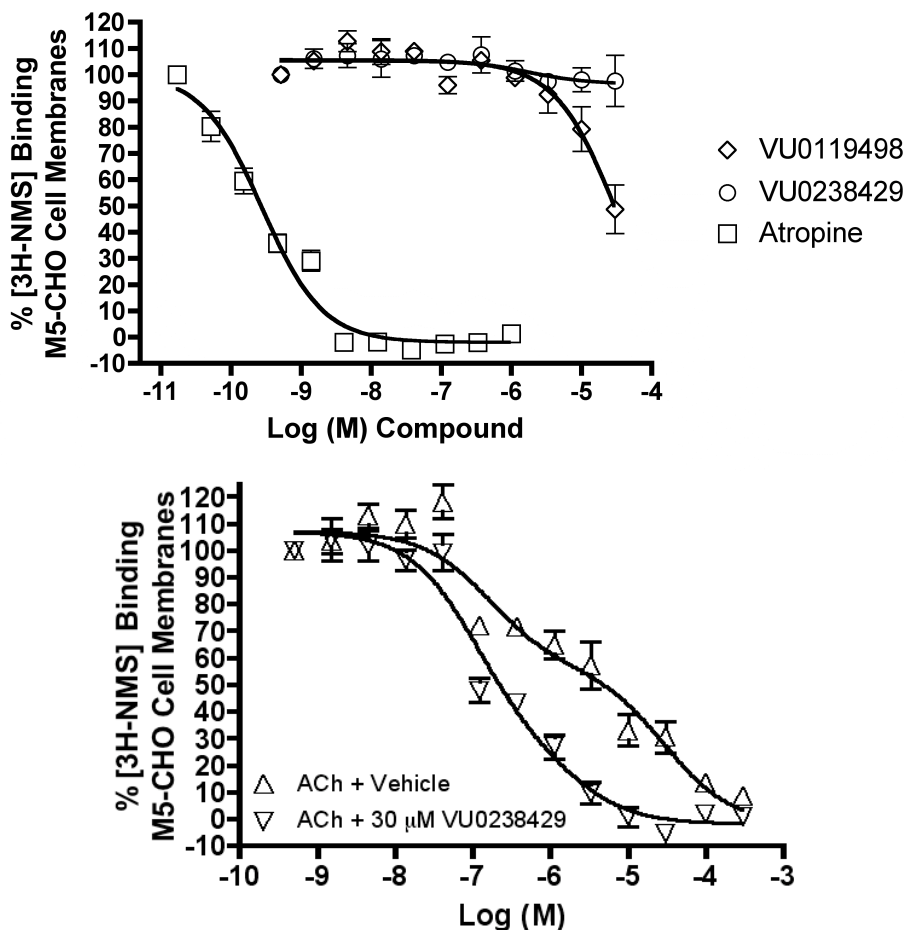
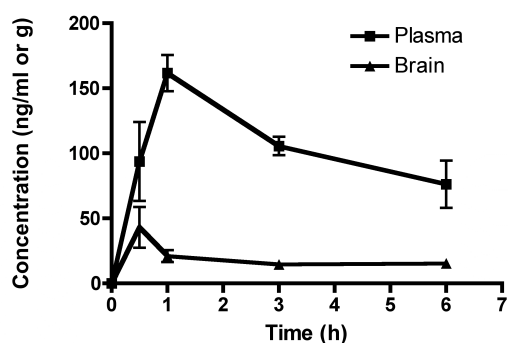


Figure 9. Competition binding experiments with VU0238429 and compound VU0119498. $[^3\text{H}]\text{-NMS}$ (0.1 nM) binding to M_5 cell membranes was measured (top panel) in the presence of increasing concentrations of test compounds or atropine control ($K_i = 0.21$ nM). $[^3\text{H}]\text{-NMS}$ (0.1 nM) binding to M_5 cell membranes was used to obtain CRCs of ACh in the presence and absence of compound 42 (30 μM , bottom panel). ACh curves exhibited two-site competition (+Vehicle: K_i high affinity = 123 nM, K_i low affinity = 22 μM ; +VU0238429: K_i high affinity = 81 nM, K_i low affinity = 1.39 μM). Data represent the Mean \pm S.E.M. of at least 3 independent experiments with similar results.

In vivo rat pharmacokinetics of M₅ PAM VU0238429

We then determined rat *in vivo* pharmacokinetics and brain penetration of the M₅ PAM to evaluate its ability to serve as an *in vivo* tool compound. Unfortunately, VU0238429 exhibited poor systemic absorption after I.P. administration with maximum concentration in plasma (161.7 ng/ml) being achieved within 1 hour (**Fig. 10**). However, it was eliminated relatively slowly from systemic circulation with an elimination half-life of 4.7 hours, which is desirable for *in vivo* studies (**Fig. 10**). Although quickly taken up in the brain, it displayed poor brain penetration with an AUC-brain/AUC-plasma value of 0.2514 (**Fig. 10**).



PK Parameter	Plasma	Brain
C_{max} (ng/ml or g) (mean \pm SD)	161.7 \pm 13.9	43.08 \pm 15.68
T_{max} (h)	1	0.5
Elimination half life (h)	4.7	3.69
AUC _(0-6h) (ng.h/ml or g) (mean \pm SD)	621.1 \pm 39.9	158.62 \pm 47.23
CL/F (ml/min)	145	
V/F (L/kg)	59.6	
AUC _{brain} /AUC _{plasma}	0.25	

Figure 10. Rat pharmacokinetic PBL study of VU0238429 and calculated PK parameters. Concentration of compound in brain and plasma over a 6-hour time course was measured by LC/MS/MS following a single 10 mg/kg (IP) dose using male Sprague-Dawley rats. Data represent the Mean \pm S.E.M. with $N=3$. Study performed by S. Jadhav.

Optimization of M₅ PAM VU0238429

Despite the relatively limited scope of the initial matrix analog library in terms of structural modification, we found clear SAR associated with this novel mAChR PAM chemotype, with 5-OCF₃ modification of the isatin core and 3- or 4- position OMe substitutions of the benzyl ring conferring strong M₅ PAM preference versus M₁-M₄. In contrast, virtually all modifications conferring increased M₁ PAM activity simultaneously increased M₅ PAM activity. As exemplified in the case of compound **56**, 7-Cl substitution of the isatin core carried comparably high M₁/M₅ potency and efficacy, but also caused degeneration into a pan muscarinic potentiator as revealed by CRC profiling at all five subtypes. Based on these initial findings from the matrix library and the identification of VU0238429 as the first M₅-preferring PAM, we began a more comprehensive optimization campaign focused on VU0238429 as the lead structure.

The rationale for further optimization included a desire to improve potency, efficacy, and subtype-selectivity, as well as to decrease potential DMPK liabilities of the lead compound. An iterative parallel analog synthesis approach was used to drive the VU0238429 optimization as this methodology provides a more focused and efficient route compared to generation of matrix libraries or singleton syntheses because global structural diversity and random SAR exploration was no longer a priority based on the results from the initial 92-member matrix library around VU0119498. As introduced previously (Chapter I), iterative libraries are well suited to optimizations aimed at improving specific pharmacological or physiochemical characteristics of a lead compound because they are hypothesis-driven and less random than matrix-based or

other medicinal chemistry optimization strategies. Based on the initial VU0119498 SAR and from consideration of chemistry/synthetic route accessibility and efficiency, we outlined a number of modifications to VU0238429 to explore (**Fig. 11**).

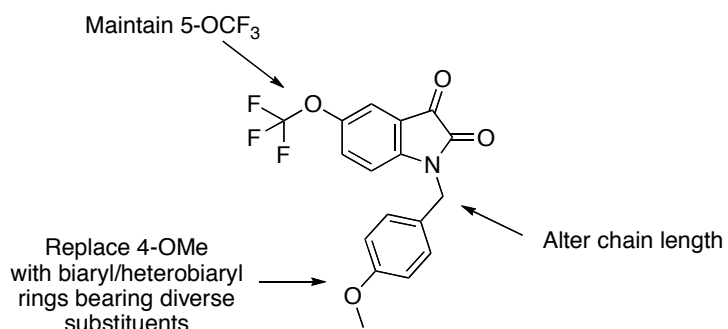


Figure 11. Initial optimization strategy for M₅ PAM VU0238429.

Given the importance of the 5-OCF₃ moiety of the isatin core to M₅ subtype-selectivity, it was held constant while the *N*-alkyl chain was lengthened and while the benzyl ring was substituted at the *para* position with different aryl/heteroaryl rings in place of the methoxy group of the lead structure. Libraries were prepared according to the scheme depicted in **Figure 12**, wherein commercial 5-(trifluoromethoxy)indoline-2,3-dione (compound **4**) was alkylated with *p*-bromobenzylbromide to deliver key intermediate (compound **5**). An 11-member Suzuki library was then prepared to explore the effect introducing the biaryl and heterobiaryl motifs into VU0238429 (compounds **6**). In parallel, compound **4** was alkylated with functionalized phenethyl bromides (compounds **7**) to probe the effect of chain homology (compounds **8**). Compound libraries were then triaged by a singlepoint (10 μM) screen for their ability to potentiate an ~EC₂₀ of ACh in M₁ and M₅ cells using Ca²⁺ mobilization assay with VU0238429 included as a positive control (**Fig 12**).

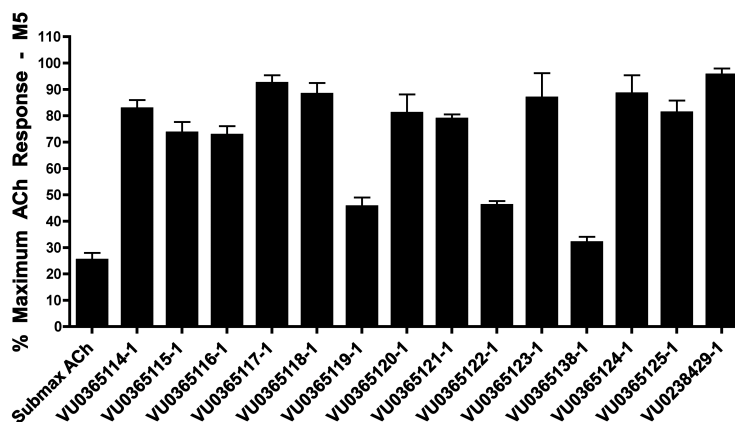
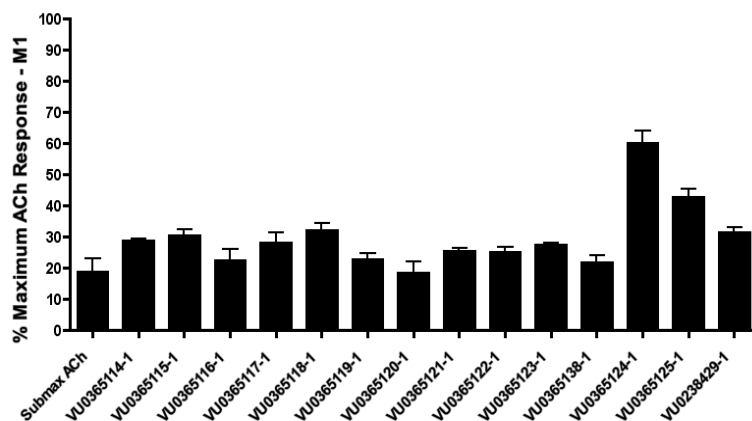
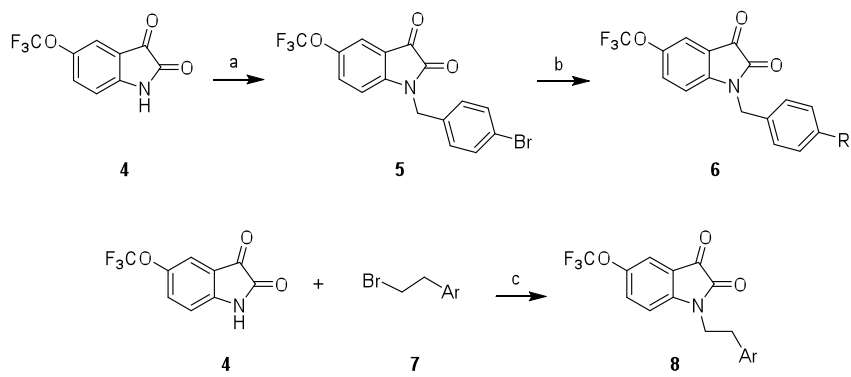
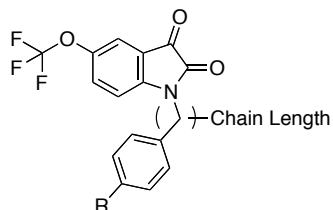


Figure 12. Synthesis and M₁/M₅ singlepoint screening of biaryl/heterobiaryl and phenethyl analogs of VU0238429. 13 compounds were synthesized (top panel) by a) p-bromobenzylbromide, K₂CO₃, KI, ACN, rt, 16 h (99%); b) R-B(OH)₂, Pd(Pt-Bu₃)₂, Cs₂CO₃, THF:H₂O, mw, 120 °C, 20 min (10-90%); c) K₂CO₃, KI, ACN, rt, 16 h (50-90%). Ca²⁺ mobilization assays with M₁ and M₅ cells were used to obtain singlepoint (10 μM) potentiation responses for each analog in the presence of a submaximal (~EC₂₀) concentration of ACh (middle and bottom panels). Data represent the Mean ±S.E.M. of at least 3 independent experiments with similar results.

From these singlepoint screens at M_1 and M_5 , select compounds were assayed using full CRCs based on the general high M_5 versus M_1 potentiation in terms of % ACh max efficacy observed with numerous members of this library. The potency SAR and associated efficacy data from the singlepoint screens at M_1 and M_5 for this library is presented in **Table 4**. In general, chain homologation (compounds **8**, i.e. VU0365124 and VU0365125) proved unsuccessful as potency and M_5 -selectivity was compromised despite retention of PAM efficacy at higher concentrations. For example, the direct phenethyl analog of VU0238429 (compound **8a**, i.e. VU0265124) possessed a M_5 EC_{50} of 4.9 μ M and 78% ACh max response and a M_1 EC_{50} >10 μ M and 90 % ACh max response (**Table 4**). Biaryl and heterobiaryl analogs (compounds **6**) proved far more productive, affording a number of M_5 PAMs with high selectivity versus M_1 (>30 μ M M_1 EC_{50} s) and low micromolar M_5 EC_{50} s (**Table 4**). All other analogs possessed M_5 EC_{50} s >10 μ M. In general, both 5- and 6-membered heterocycles were tolerated as was simple phenyl substitution (compound **6a**). Potency was very similar for most of these analogs (M_5 EC_{50} s 2.7 μ M to 4.8 μ M) as were % ACh max values (70-85%). Shallow SAR was again noted with compounds either being active in this potency range or inactive as M_5 PAMs.

Table 4. M₁ and M₅ potency SAR for biaryl/heterobiaryl and phenethyl analogs of VU0238429. Ca²⁺ mobilization assays with M₁ and M₅ cells were used to obtain compound CRCs in the presence of a fixed submaximal (~EC₂₀) concentration of ACh. n/d = potency not determined (no CRCs and the % ACh max values represent singlepoint screen data). Data represent the Means of at least 3 independent experiments.



Cmpd	VU#	Chain Length	R	M5 EC ₅₀ , ACh max	M1 EC ₅₀ , ACh max
6a	0365114	CH ₂		2.7 uM, 85%	>30 uM, n/a
6b	0365115	CH ₂		n/d, 73%	n/d, 30%
6c	0365116	CH ₂		n/d, 73%	n/d, 22%
6d	0365117	CH ₂		2.8 uM, 90%	>30 uM, n/a
6e	0365118	CH ₂		4.8 uM, 98%	>30 uM, n/a
6f	0365119	CH ₂		n/d, 46%	n/d, 23%
6g	0365120	CH ₂		n/d, 81%	n/d, 18%
6h	0365121	CH ₂		3.6 uM, 88%	>30 uM, n/a
6i	0365122	CH ₂		n/d, 46%	n/d, 25%
6j	0365123	CH ₂		3.3 uM, 85%	>30 uM, n/a
6k	0365138	CH ₂		n/d, 31%	n/d, 21%
8a	0365124	C ₂ H ₄		4.9 uM, 78%	>10 uM, 90%
8b	0365125	C ₂ H ₄		n/d, 81%	n/d, 42%

Given the relatively high potency and efficacy of compounds **6a** and **6d**, and the highest efficacy observed from compound **6e**, these three analogs were chosen for characterization in ACh CRC fold-shift (**Fig. 13**) and M₃ CRC selectivity (**Fig. 13**) via Ca²⁺ mobilization assays. M₃ selectivity was determined due to the lower likelihood that M₂ and M₄ activity would present itself in light of previous SAR for this chemical series and the fact that M₅ shares highest amino acid sequence identity with M₃, thus rendering it the most obvious of the remaining mAChR subtypes to check for selectivity first. As seen in **Figure 13**, compound **6a** (VU0365114) exhibits very high PAM selectivity for M₅ versus M₁ and M₃, which is even greater than that of the parent compound VU0238429. Interestingly, the 3-thiophene substitution of compound **6d**, which is a common and well-recognized bio-isosteric replacement for a phenyl ring, exhibited a much more narrow selectivity window versus M₃ than compound **6a** (**Fig. 13**). This serves as a clear example of the idiosyncratic and often-unpredictable SAR observed with many GPCR allosteric modulators. Likewise, the chloropyridine moiety of compound **6e** is electronically homologous (and modestly similar sterically) to the phenyl ring of compound **6a**; however, it too confers an approximately equal loss of selectivity versus M₃ as the thiophene of compound **6d** (CRC data for compound **6e** not shown).

In terms of ACh CRC fold-shift, these biaryl/heterobiaryl congeners proved far superior to VU0238429 with robust ACh potency left-shift of >50x compared to the 14x left-shift induced by VU0238429 (**Fig. 13**). As observed with other mAChR PAMs such as BQCA (discussed in more detail in Chapter V), intrinsic agonist activity was present with both compound **6a** and **6d**, which is reflected by baselines that begin at (~25-50% ACh max) for the ACh CRCs obtained in the presence of 30 μM compound (**Fig. 13**).

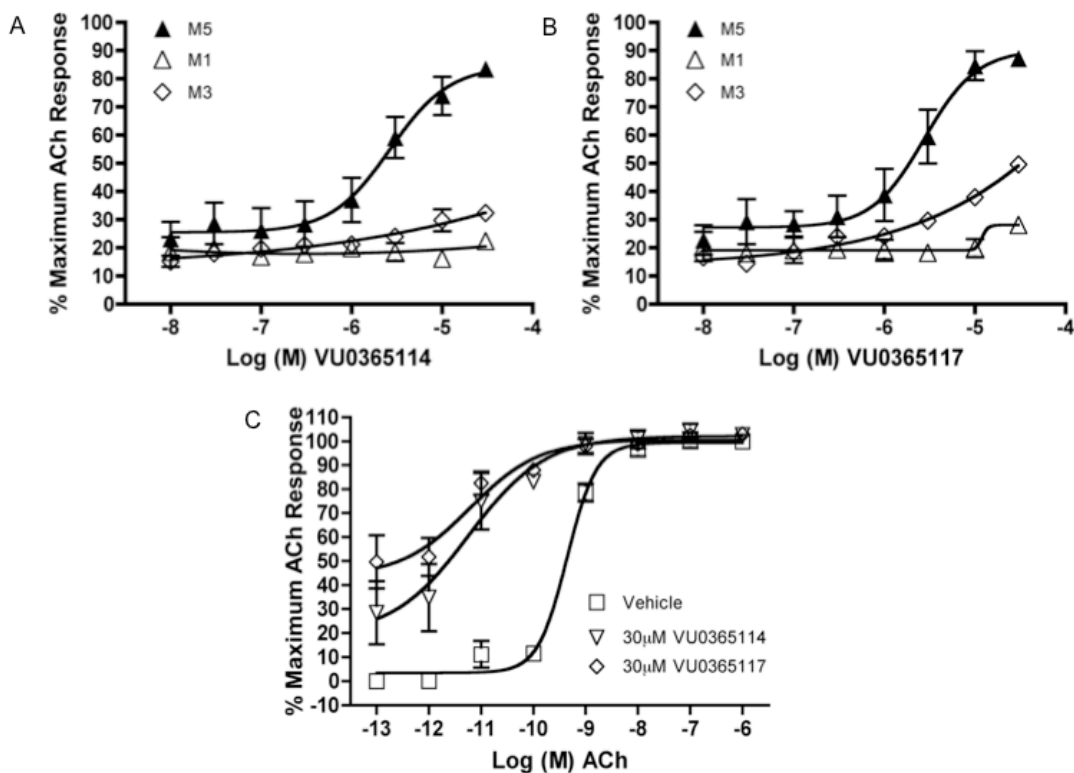


Figure 13. M₁, M₃, and M₅ subtype-selectivity and ACh CRC fold-shift of compound **6a** (VU0365114) and **6d** (VU0365117). Ca²⁺ mobilization assays with M₁, M₃, and M₅ cells were used to obtain compound CRCs in the presence of a fixed submaximal (~EC₂₀) concentration of ACh (top panels, VU0365114 EC₅₀ values: M₅ = 2.7 μM 85% ACh max, M₃ = >10 μM, M₁ = >30 μM, VU0365117 EC₅₀ values: M₅ = 2.8 μM 90% ACh max, M₃ = >10 μM, M₁ = >30 μM). Ca²⁺ mobilization assays with M₅ cells were used to obtain ACh CRCs in the presence and absence of test compounds (bottom panel). Actual fold-shift values not determined due to intrinsic agonist activity of test compounds and therefore reported as >50x left-shift for both compounds. Data represent the Mean ±S.E.M. of at least 3 independent experiments with similar results.

Encouraged by the potency, high ACh CRC fold-shift, and subtype-selectivity of VU0365114 (compound **6a**), we hypothesized that a hybrid analog of this compound and the parent VU0238429 lead in the form of a bi-aryl ether on the southern portion of the scaffold may provide to a more optimal M₅ PAM. We also sought to explore bioisosteric replacements of the ketone at the 3-position of the isatin core or possibly

deletion/replacement of the entire keto-amide moiety, which is not a common drug-like structure and may represent a DMPK liability as an efflux pump (e.g. Pgp) substrate, potentially underlying the poor *in vivo* PK profile of VU0238429. The strategy for this library iteration is presented in **Figure 14**.

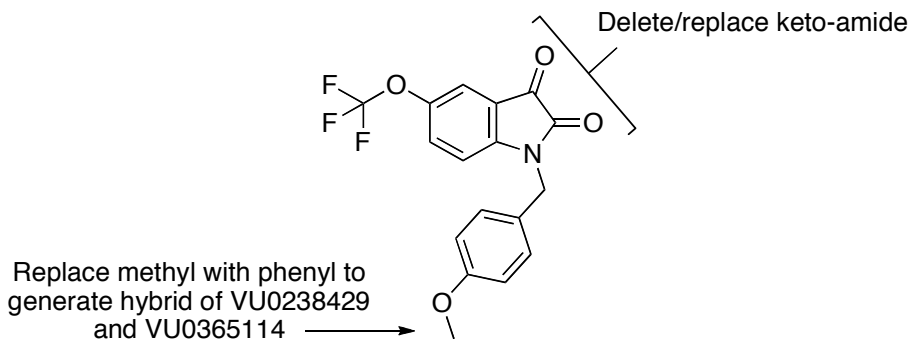
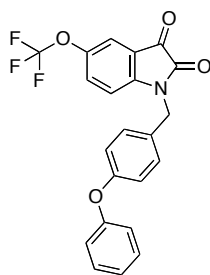


Figure 14. Strategy for second round of M₅ PAM analog library iterations.

The hybrid analog was synthesized according to the same general alkylation procedure described previously for earlier compounds (**Fig. 4** and **Fig. 12**). Briefly, commercial 5-trifluoromethoxyisatin was treated with *p*-phenoxybenzyl bromide in the presence of K₂CO₃ and subjected to microwave irradiation at 160 °C for 10 minutes to afford the desired compound as VU0400265 (68% yield). This analog was then profiled in CRCs at M₁-M₅ (in the presence of an ~EC₂₀ of ACh) using Ca²⁺ mobilization assays (**Fig. 15**). The potency of VU0400265 (1.9 μM) and % ACh max (75%) for this analog was comparable to that of VU0238429 and VU0365114; however, it exhibited complete selectivity for M₅ with no elevation of the ACh ~EC₂₀ at any other mAChR subtype at up to 30 μM (**Fig. 15**). This represented the most selective M₅ PAM to date; however, it remains unknown whether or not this compound binds M₁-M₄.



VU0400265

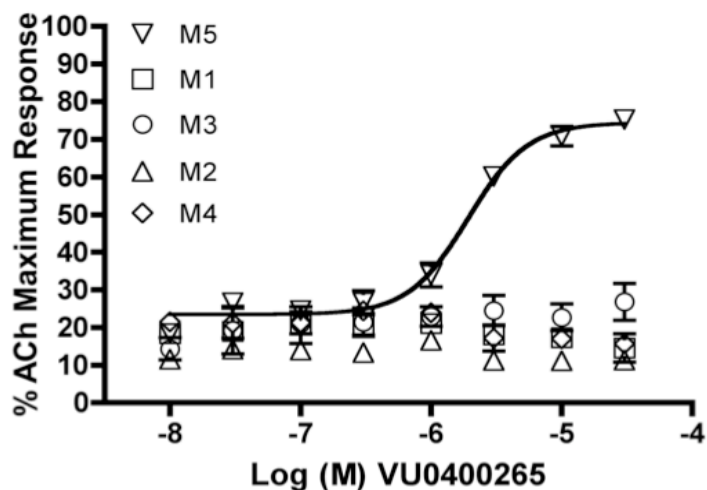


Figure 15. Structure, mAChR subtype-selectivity profile, and ACh CRC fold-shift for VU0400265, the first M₅-selective PAM representing a hybrid of VU0238429 and VU0365114. Ca²⁺ mobilization assays with M₁-M₅ cells were used to obtain compound CRCs in the presence of a fixed submaximal (~EC₂₀) concentration of ACh (EC₅₀ values: M₅ = 1.9 μM, 75% ACh max, M₁-M₄: >30 μM). Data represent the Mean ±S.E.M. of at least 3 independent experiments with similar results.

During the preparation of this phenoxybenzyl analog (VU0400265), we simultaneously generated a library of substituted indole and oxindole analogs to test the importance of the keto-amide moiety (2-,3-position carbonyls) of the isatin headpiece as part of the strategy outlined in **Figure 14**. To this end, 14 compounds were synthesized using previously described alkylation conditions (data not shown), which were then screened at 30 μM in M₁ and M₅ cells in the presence of an ACh ~EC₂₀ by Ca²⁺ mobilization assay, similar to previous singlepoint screens (**Fig. 16**). In both cell lines, VU0119498 and VU0238429 were used as positive controls.

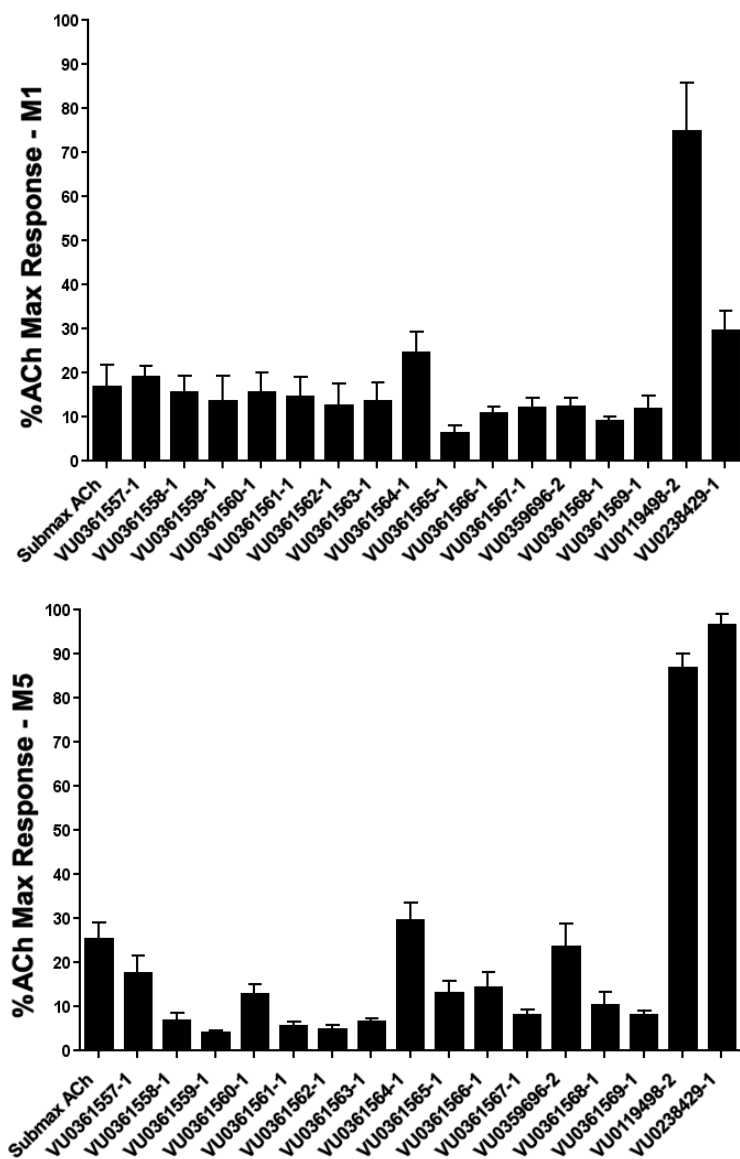


Figure 16. M₁/M₅ singlepoint screening of substituted indole and oxindole analogs. Ca²⁺ mobilization assays with M₁ and M₅ cells were used to obtain singlepoint (30 μM) potentiation responses for each analog in the presence of a submaximal (~EC₂₀) concentration of ACh. M₁/M₃/M₅ HTS hit VU0119498 and M₅ PAM lead VU0238429 were included as positive controls. Data represent the Mean ±S.E.M. of at least 3 independent experiments with similar results.

However, none of these modifications were tolerated for PAM activity at either receptor subtype (regardless of the southern benzyl substitution present), and some

appeared to induce modest inhibition of the ACh response at M₅, suggesting possible antagonism or negative allosteric modulation. Other attempts at replacing the 2-position carbonyl by introducing an eastern carboxylic acid in this position included synthesis of a small set of benzylated scaffolds (data not shown); however, these compounds were extremely unstable and degraded quickly at room temperature, thus they were not tested for mAChR PAM activity.

Having then established the importance of the keto-amide structure of the isatin core, we turned to specific bio-isoteric replacements for the 3-position ketone, which included gem di-fluoro, spirocyclopropyl, and a chiral tertiary alcohol. These structural changes are well-known mimetics for ketones as they retain the general electronic and steric characteristics of a ketone carbonyl, with the exception of the tertiary alcohol due to its hydrogen bond donation property (as compared to the hydrogen bond accepting property of a ketone). These three analogs were synthesized using the VU0238429 template (i.e. retention of *p*-methoxybenzyl on the southern portion) as shown in the scheme of **Figure 17**.

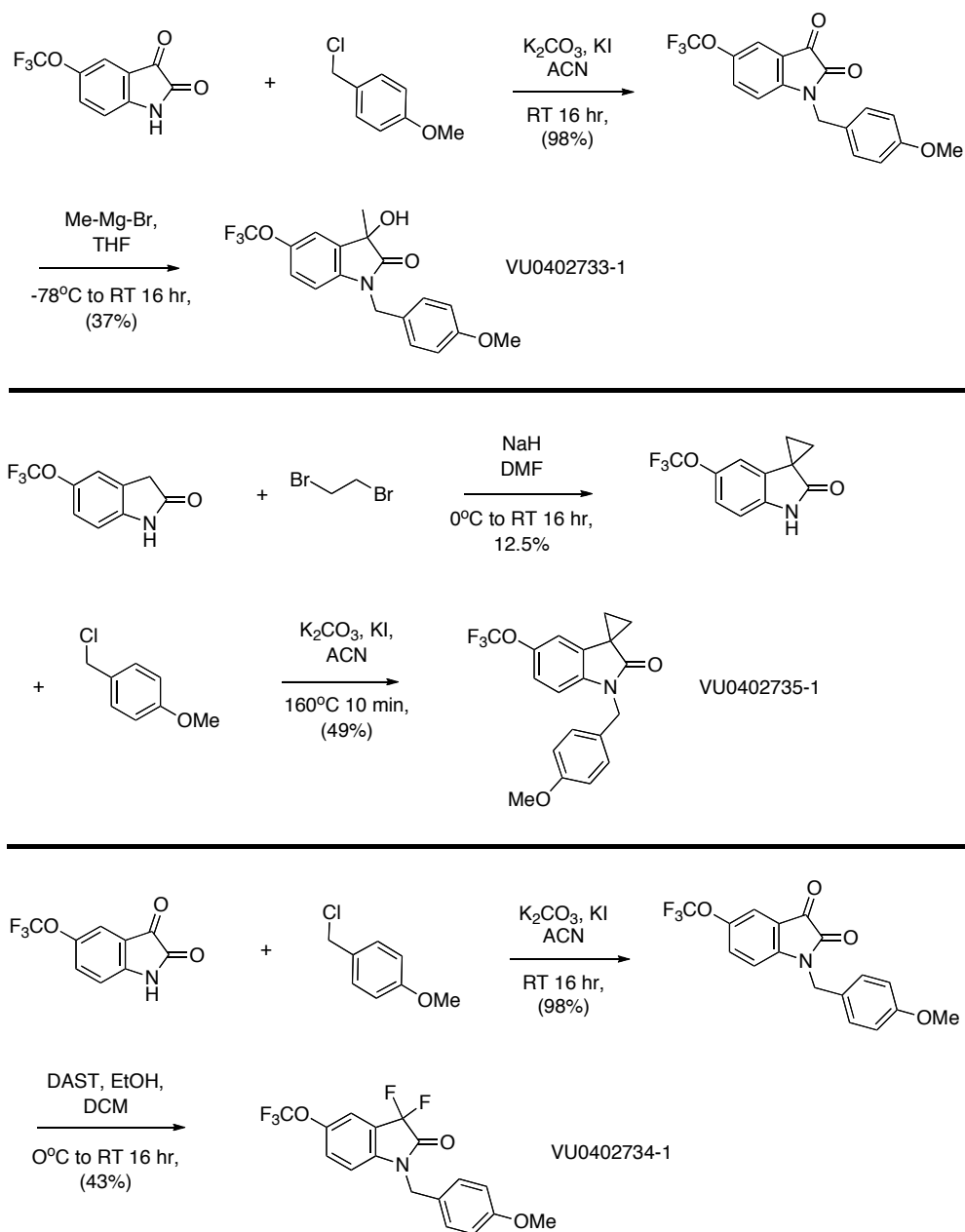


Figure 17. Synthesis of oxindole M₅ PAM analogs VU0402733, VU0402734, VU0402735.

Each compound was then tested via Ca²⁺ mobilization in CRCs at M₅ in the presence of an ACh ~EC₂₀ (**Fig. 18**). Gem-difluoro substitution (VU0402734) was extremely well tolerated and provided a modest increase in M₅ PAM potency, whereas spirocyclopropyl substitution (VU0402735) completely abolished M₅ PAM activity (**Fig.**

18). Interestingly, the chiral tertiary alcohol analog (VU0402733) exhibited an approximately ~10x right-shift in potency compared to that of the parent M₅ PAM VU0238429 (Fig. 18). These SAR data indicated that gem-difluoro would be ideal for subsequent analog generation, and it may confer an improved *in vivo* PK profile to this M₅ PAM series in contrast to retention of the isatin-based headpiece of VU0238429. Furthermore, this modification was synthetically favorable as any isatin-containing analog could be fluorinated in a simple one-step manner (Fig. 17).

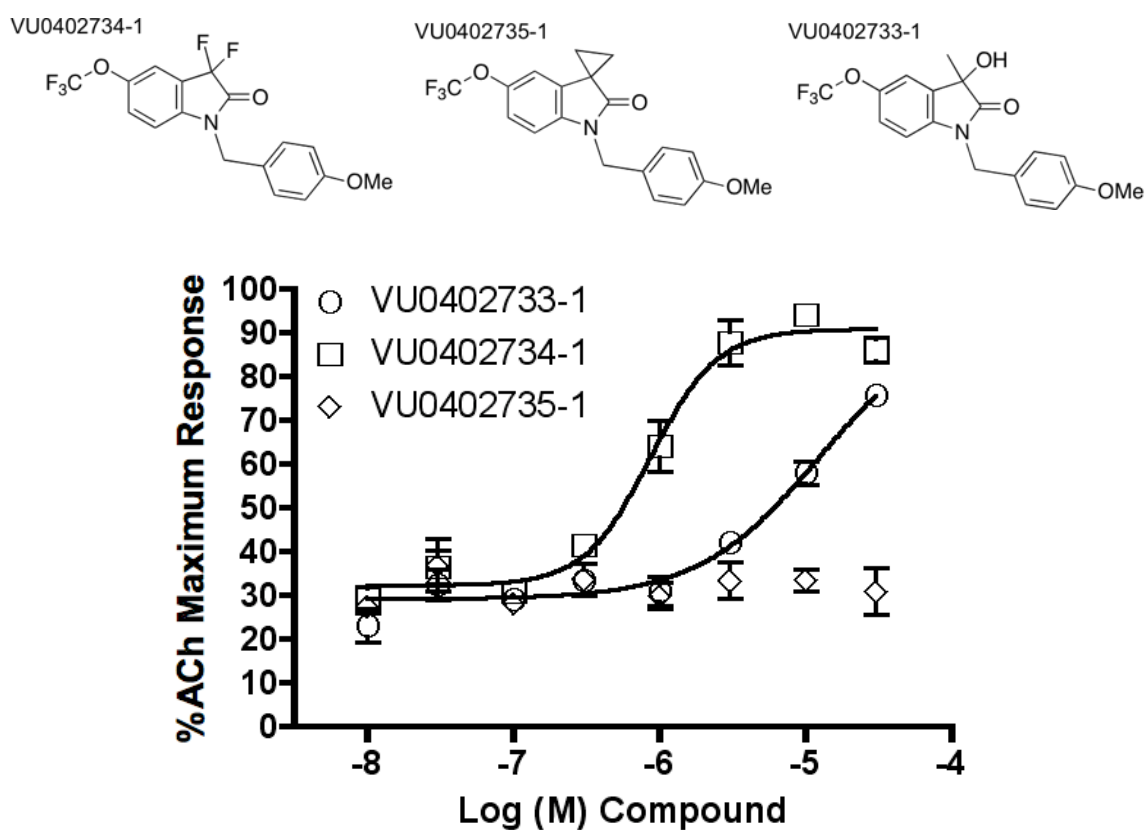


Figure 18. Structures and CRCs for M₅ PAM analogs bearing 3-position ketone replacements. Ca²⁺ mobilization assays with M₅ cells were used to obtain compound CRCs in the presence of a fixed submaximal (~EC₂₀) concentration of ACh (EC₅₀ values: VU0402734 = 870 nM, 90% ACh max, VU0402733 = >10 μM, VU0402735 = >30 μM). Data represent the Mean ±S.E.M. of at least 3 independent experiments with similar results.

Following this, VU0402734 was profiled in CRCs assays at M₁ and M₃ in the presence of an ACh ~EC₂₀ to determine if this modification altered subtype-selectivity (**Fig. 19**). Not only did gem-difluorination of the M₅ PAM scaffold result in greater potency, it also decreased PAM activity at M₁ (relative to the VU0238429 parent subtype-selectivity profile) and exhibited similarly low activity at M₃ (**Fig. 19**), which provided further confidence that this modification would be worth retaining for a final optimized scaffold.

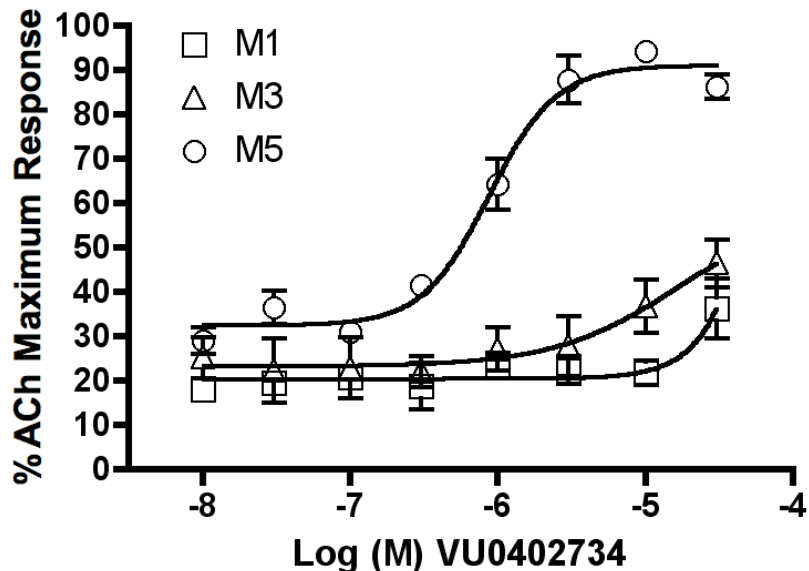


Figure 19. M₁, M₃, and M₅ subtype-selectivity profile for VU0402734, the gem-difluoro analog of M₅ PAM VU0238429. Ca²⁺ mobilization assays with M₁, M₃, and M₅ cells were used to obtain compound CRCs in the presence of a fixed submaximal (~EC₂₀) concentration of ACh (EC₅₀ values: M₅ = 870 nM, 90% ACh max, M₁ = >30 μM, M₃ = >30 μM). Data represent the Mean ±S.E.M. of at least 3 independent experiments with similar results.

Having completed the optimization strategy outlined in **Figure 14** and establishing important SAR demonstrating the favorable effect of the southern bi-aryl ether on M₅ PAM subtype-selectivity with no loss of potency as well as the northern

gem-difluoro substitution on both M₅ PAM subtype-selectivity and potency, a third iteration of parallel synthesis was planned (**Fig. 20**). At this point, movement of the 5-position OCF₃ group on the isatin core, introduction of mono or difluorines to the ortho position(s) on the southern benzyl ring, and southern 3-position biaryl/heterobiaryl extensions were planned in order to further investigate SAR around the M₅ PAM scaffold (**Fig. 20**). Rotation from the 5- to 6-position of the OCF₃ moiety was specifically investigated due to the fact that no 6-position substitutions were present in the initial 92-member matrix library around VU0119498. Impetus for fluorination of the southern benzyl ring in the *ortho* position(s) stemmed from SAR findings with M₁ PAMs derived from BQCA and from VU0119498 as part of a parallel but separate optimization project (discussed in Chapter V), which revealed an increase in PAM potency via fluorination in this position. Finally, biaryl/heterobiaryl extension at the 3-position of the southern benzyl ring was sought due to the fact that 3-methoxybenzyl (compound 41 from the 92-member matrix library) was well tolerated based on its M₅ versus M₁ PAM potency (**Table 2**) as well as the finding that a piperonyl group (VU0366628, synthesized using one-step *N*-alkylation method as previously described) in the southern region was well-tolerated for M₅ PAM activity (**Fig. 21**). Given that the gem-difluoro or ketone of the 3-position on the core both appear similar in pharmacology, the latter was maintained temporarily to increase speed of synthesis (i.e. reduce by one step).

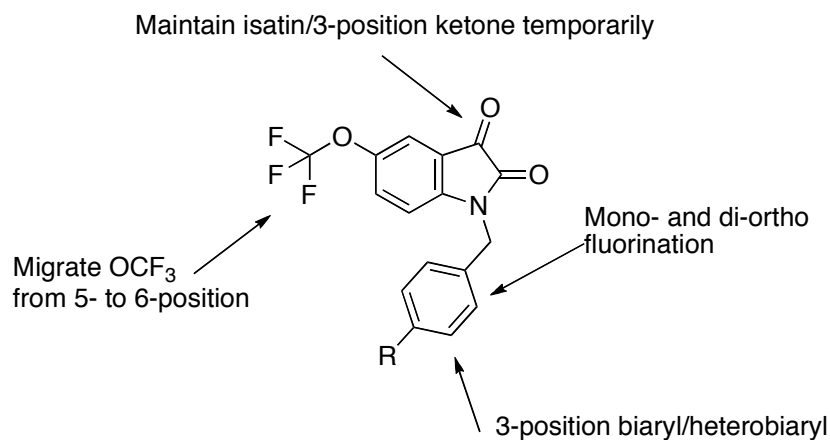


Figure 20. Optimization strategy for third round of M_5 PAM library iterations.

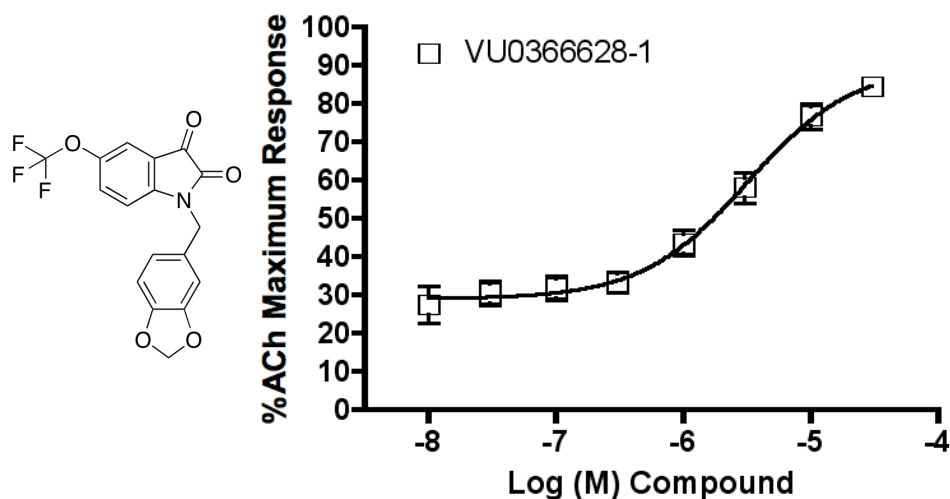


Figure 21. Structure and M_5 PAM activity of piperonyl analog VU0366628. Ca^{2+} mobilization assays with M_5 cells were used to obtain compound CRCs in the presence of a fixed submaximal ($\sim\text{EC}_{20}$) concentration of ACh (EC_{50} values: $M_5 = 3.2 \mu\text{M}$, 87% ACh max). Data represent the Mean \pm S.E.M. of at least 3 independent experiments with similar results.

Synthesis of mono and di-ortho fluorinated analogs was carried out using the same general alkylation conditions described previously with the naked 4-bromobenzyl

halide reactant(s) being replaced by the fluorine substituted congeners that were then Suzuki coupled with phenyl boronic acid (**Fig. 12**) to afford the desired products as VU0366625 and VU0366626 (**Fig. 22**). The *p*-phenylbenzyl southern moiety was used due to better commercial availability of the fluorinated bromobenzyl halide in lieu of the corresponding fluorinated methoxybenzyl and also because this moiety (based on VU0365114) is comparable if not superior to that of VU0238429. Both new fluorinated analogs were evaluated in CRCs at M₅ by Ca²⁺ mobilization assay in the presence of an ACh ~EC₂₀ (**Fig. 22**). Remarkably, di-fluorination of the benzyl ring in the *ortho* positions completely abolished M₅ PAM activity while mono-fluorination resulted in a substantial decrease in both potency and efficacy.

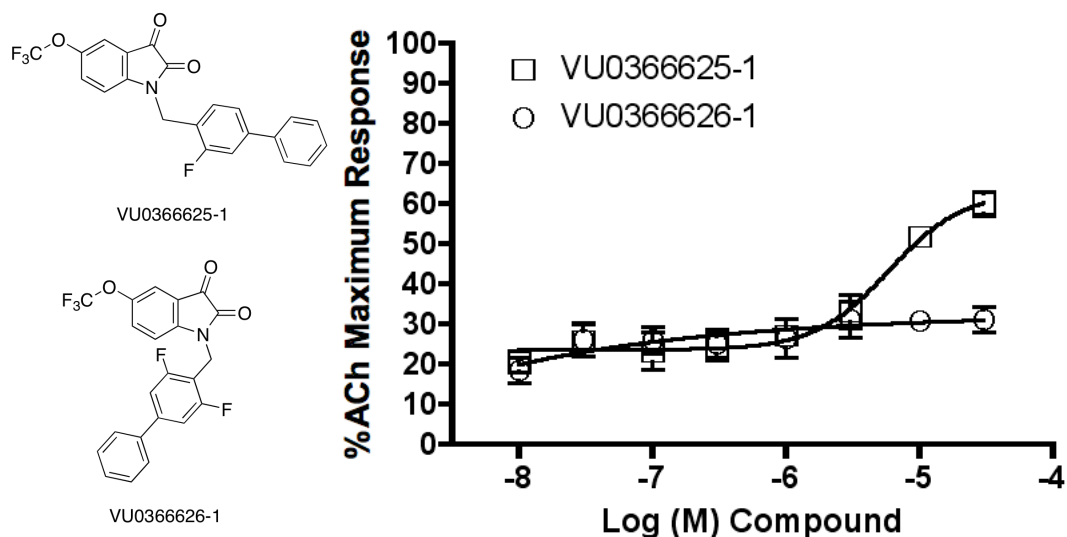


Figure 22. Structures and CRCs for *ortho*-fluorinated M₅ PAMs based on VU0365114 lead structure. Ca²⁺ mobilization assays M₅ cells were used to obtain compound CRCs in the presence of a fixed submaximal (~EC₂₀) concentration of ACh (EC₅₀ values: VU0366625 = 5.9 μM 60% ACh max, VU0366626 = >30 μM). Data represent the Mean ±S.E.M. of at least 3 independent experiments with similar results.

Fluorine atoms, which are approximately the same size in as hydrogen atoms, exhibit partial hydrogen-bond accepting properties, withdraw electron density from aromatic rings, and increase lipophilicity (i.e. calculated logP [cLogP]). One or more of these properties carried by these specific fluorinations compromises either binding to M₅ and/or functional PAM activity, although it is difficult to ascertain the exact reason(s) underlying this effect given an absence of structural knowledge for the putative allosteric site at which this M₅ PAM series binds. Given these SAR data, no subsequent libraries were generated with *ortho*-fluorine substitution(s).

Returning temporarily to the biaryl/heterobiaryl extension investigation, we simultaneously prepared analogs bearing direct phenyl, 2-thiophene, 3-thiophene, or phenoxy substitutions at the *meta* position of the southern benzyl ring, as outlined in the strategy presented in **Figure 20**. These analogs were synthesized according to the same alkylation procedure described previously using commercially available benzyl halides bearing the desired meta-substitutions, thus Suzuki couplings were not necessary. All of these analogs were devoid of M₅ PAM activity up to 10 μM and showed only a moderate elevation of an ACh ~EC₂₀ at 30 μM in Ca²⁺ mobilization assays with M₅ cells (data not shown, *N*=1). Based on these results, further derivatizations in the form of alternate heterocycles in this meta-benzyl position were not performed.

In parallel and again in accordance with the aims of the third round of SAR exploration as outlined in **Figure 20**, 6-OCF₃ analogs of VU0365114 and VU0238429 (the two lead M₅ PAMs containing the isatin headpiece) were prepared using the same synthetic route described previously, starting in this case with the commercially available 6-substituted isatin material. Both compounds were then tested in CRCs at M₅ in the

presence of an ACh \sim EC₂₀ by Ca²⁺ mobilization assays (**Fig. 23**). M₅ potency was moderately decreased in the case of VU0400267 (5.7 μ M) but unchanged in the case VU0400266 (2.7 μ M); however, efficacy was enhanced, with % ACh max values approaching 95-100% for both analogs (**Fig. 23**). Interestingly, subtype-selectivity eroded (**Fig. 23**) when these compounds were tested in similar CRC assays at M₁-M₄.

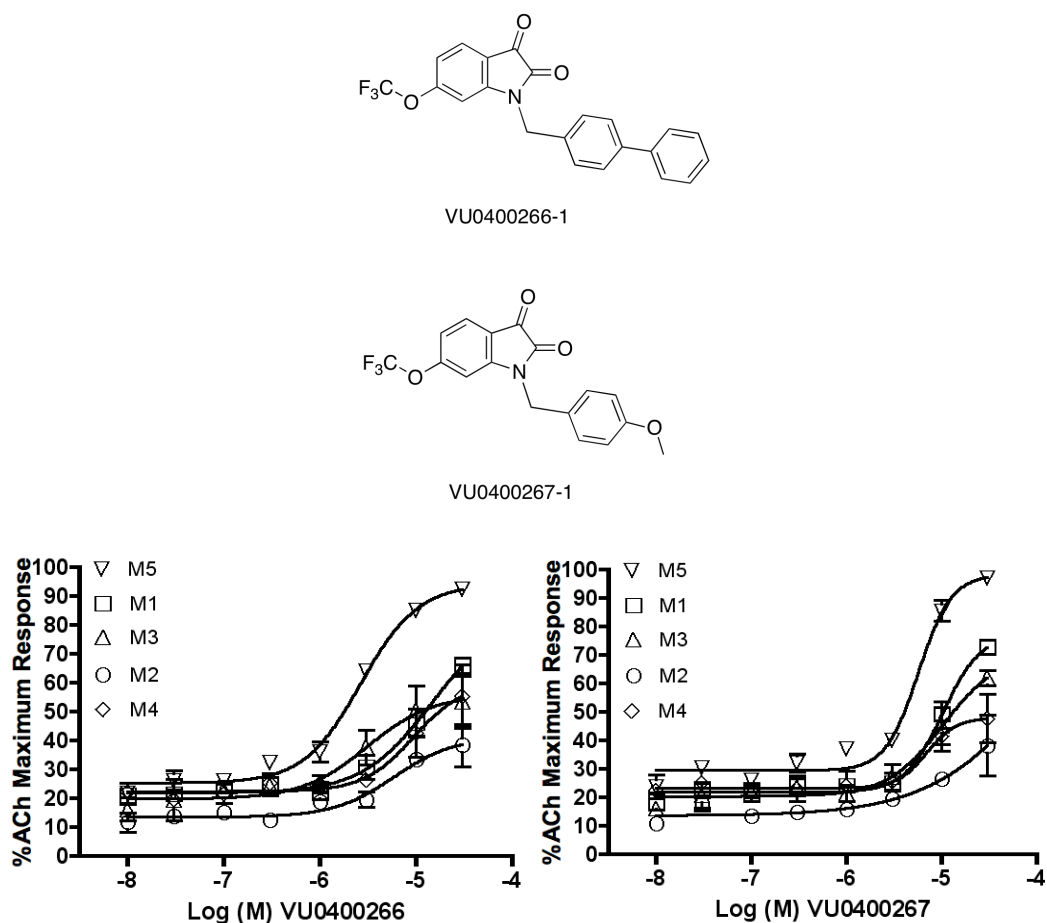


Figure 23. Subtype-selectivity profiles for VU0400266 and VU0400267. Ca²⁺ mobilization assays with M₁-M₅ cells were used to obtain compound CRCs in the presence of a fixed submaximal (\sim EC₂₀) concentration of ACh (EC₅₀ values: VU0400266 M₅ = 2.7 μ M, 95% ACh max, M₁-M₄ >10 μ M; VU0400267 M₅ = 5.7 μ M 98% ACh max, M₁-M₄ >10 μ M). Data represent the Mean \pm S.E.M. of at least 3 independent experiments with similar results.

These SAR clearly suggested that 6-position migration of the OCF₃ group was not favored going forward, yet it was unknown whether or not the phenoxybenzyl southern moiety of earlier analogs could rescue the selectivity of a 6-OCF₃ template given that it provided a completely M₅-selective PAM (VU0400265, **Fig. 15**). To test this hypothesis, we synthesized a small 2x2 matrix library containing 5-OCF₃ and 6-OCF₃ substituted headpieces with gem-difluorines at the core's 3-position and each bearing either 3- or 4-phenoxybenzyl southern moieties. The gem-difluoro versions were prepared because they too increased subtype-selectivity (although only modestly) and because the phenoxybenzyl analog VU0400265 had never been di-fluorinated. The 3-phenoxybenzyl substitutions were made due to the possibility that rotation of the OCF₃ from the 5- to 6-position may no longer be favored with southern *para*-substitution (e.g. due to rotation of the scaffold in the binding site). Again, synthesis proceeded as described previously using *N*-alkylation conditions on the respective commercially available starting materials with the substituted benzyl halides. These four analogs were tested in CRCs at M₅ in the presence of an ACh ~EC₂₀ via Ca²⁺ mobilization assays (**Fig. 24**). As expected, the gem-difluorinated 5-OCF₃ headpiece bearing a southern 4-phenoxybenzyl substitution (VU0403751) exhibited potent M₅ PAM activity with an EC₅₀ of 1.6 μM and a 69% ACh max (**Fig. 24**). Likewise, the corresponding 6-OCF₃ analog (VU0403753) exhibited an EC₅₀ of 3.6 μM and an 81% ACh max (**Fig. 24**). In contrast, both *meta*-phenoxybenzyl analogs (VU0403752 and VU0403754) were devoid of M₅ PAM activity at up to 30 μM (**Fig. 24**), further confirming that the *para*-position is more optimal for the southern benzyl substitutions.

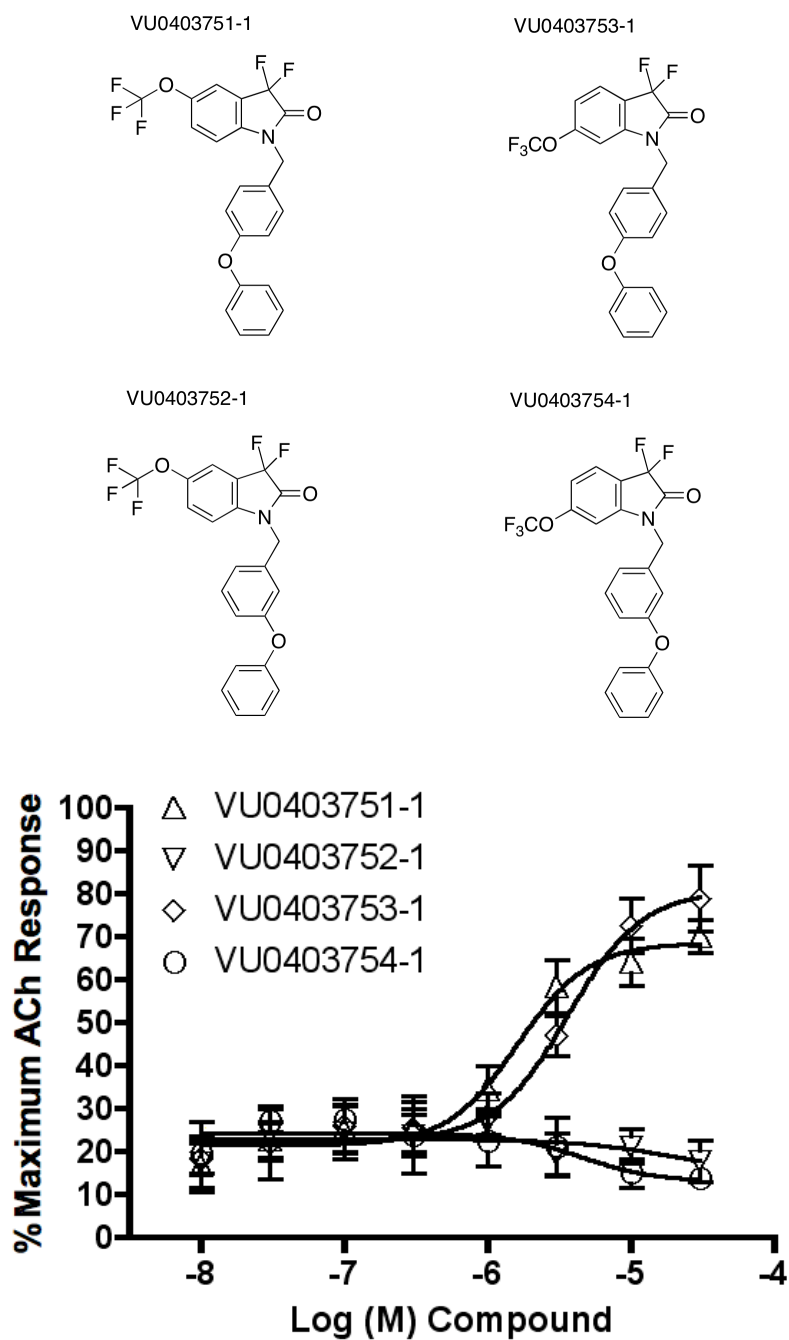


Figure 24. Structures and M_5 CRCs for 2x2 matrix library of phenoxybenzyl gem-difluoro analogs. Ca^{2+} mobilization assays with M_5 cells were used to obtain compound CRCs in the presence of a fixed submaximal ($\sim EC_{20}$) concentration of ACh (EC_{50} values: VU0403751 = 1.6 μM , 69% ACh max; VU0403753 = 3.6 μM , 81% ACh max; VU0403752 = $>30 \mu M$; VU0403754 = $>30 \mu M$). Data represent the Mean \pm S.E.M. of at least 3 independent experiments with similar results.

Next, both VU0403751 and VU0403753 were profiled for subtype-selectivity in CRCs at M₁ and M₃ (**Fig. 25**), with the former maintaining its high M₅-selectivity comparable to the parent VU0400265 isatin-based compound and the latter exhibiting an increase in M₅-selectivity engendered by the gem-difluoro and phenoxybenzyl substitutions. However, because the 6-OCF₃ group in VU0403753 still introduced M₁ and M₃ potentiation at higher concentrations despite the selectivity-engendering substitutions made to its core and southern portions, further optimization did not utilize the 6-position of the core headpiece despite its favorable effect on M₅ PAM efficacy.

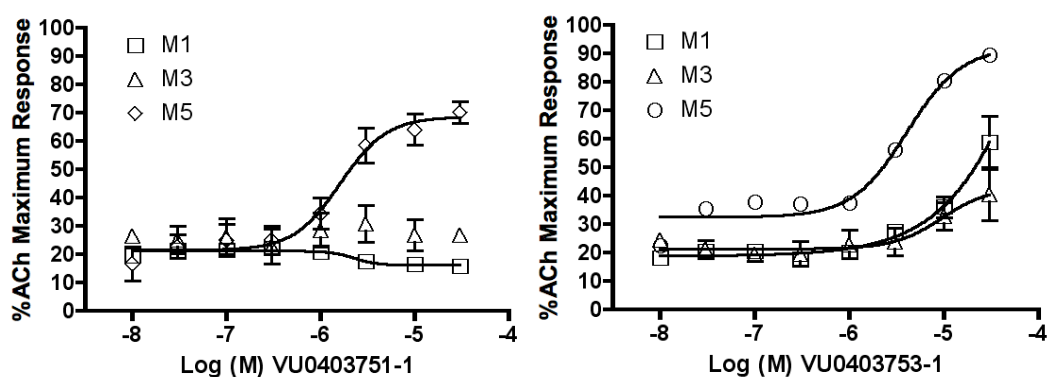


Figure 25. M₁, M₃, and M₅ CRCs for VU0403751 and VU0403753. Ca²⁺ mobilization assays with M₁, M₃, and M₅ cells were used to obtain compound CRCs in the presence of a fixed submaximal (~EC₂₀) concentration of ACh (EC₅₀ values: VU0403751 M₅ = 1.6 μM, 69% ACh max; VU0403751 M₁-M₄ >30 μM; VU0403753 M₅ = 3.6 μM, 81% ACh max; VU0403753 M₁ and M₃ = >10 μM). Data represent the Mean ±S.E.M. of at least 3 independent experiments with similar results.

Having then further established the favorable effect of gem-difluoro substitution at the 3-position of the scaffold's core on M₅ PAM potency and subtype-selectivity, the VU0403751 and earlier VU0402734 lead analogs bearing gem-difluorines were tested in ACh CRC fold-shift experiments by Ca²⁺ mobilization assays with M₅ cells (**Fig. 26**). At 30 μM, these compounds induced approximately 6x and 23x left-shifts of the ACh curve,

respectively, with the stronger potentiator VU0402734 inducing moderate intrinsic agonist activity (**Fig. 26**). These results agreed well with previous SAR from the homologous isatin sister analogs of these two compounds and added additional confirmation that gem-difluorination conferred increased PAM efficacy.

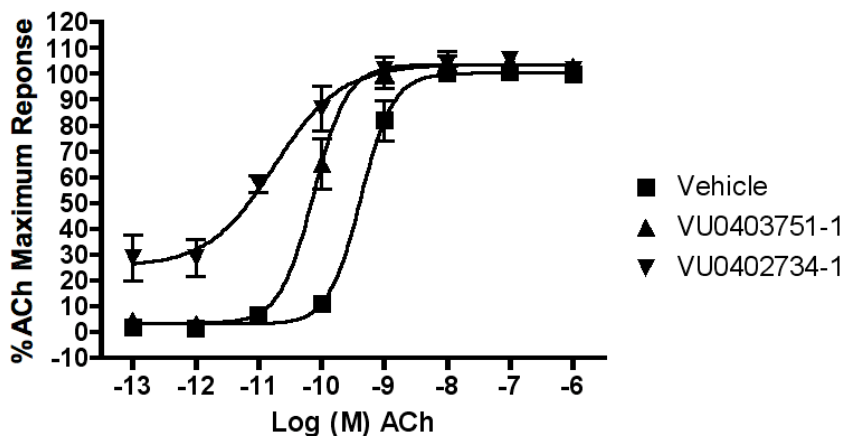


Figure 26. ACh CRC fold-shift effect of gem-difluoro lead analogs VU0403751 and VU0402734. Ca^{2+} mobilization assays with M_5 cells were used to obtain ACh CRCs in the presence and absence of test compounds. VU0403751 induced an approximately 6x left-shift and VU0402734 induced an approximately 23x left-shift with moderate intrinsic agonism at 30 μM . Data represent the Mean \pm S.E.M. of at least 3 independent experiments with similar results.

To be comprehensive and before concluding that only 5-position substitution on the core was favorable, we synthesized two tricyclic di-fluoromethyldioxyene analogs, which represented hybrids of 5- OCF_3 and 6- OCF_3 groups in terms of general electronics, lipophilicity, and to a lesser extent steric bulk. These compounds were synthesized using one-step alkylation methods utilizing commercial 2,2-difluoro[1,3]dioxolo[4,5-f]indole-6,7-dione as starting material, again with 4- and 3-phenoxybenzyl halides. The structures and M_5 CRCs for these compounds in Ca^{2+} mobilization assays in the presence of an ACh $\sim\text{EC}_{20}$ are shown in **Figure 27**. Neither compound exhibited robust PAM activity and therefore this tricyclic template was abandoned (**Fig. 27**).

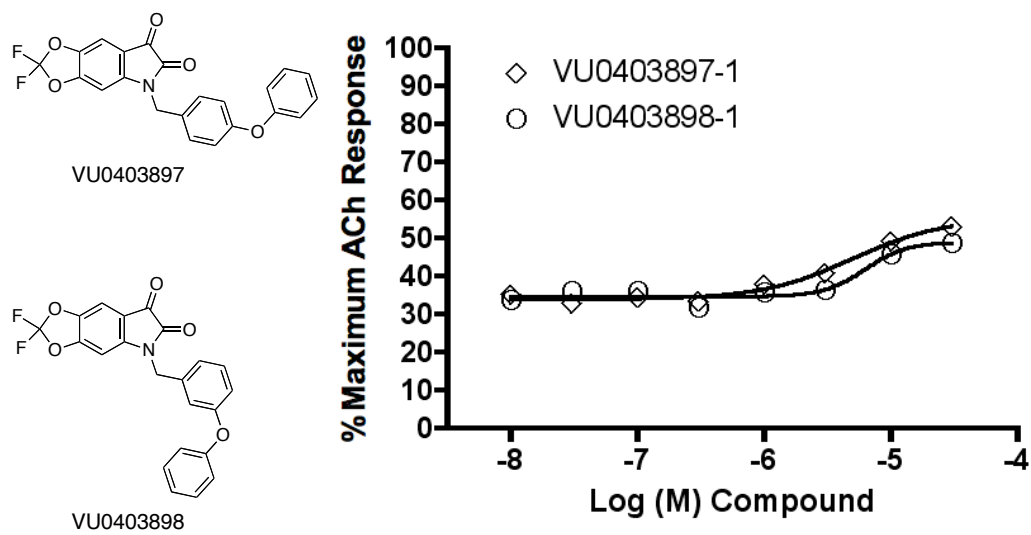
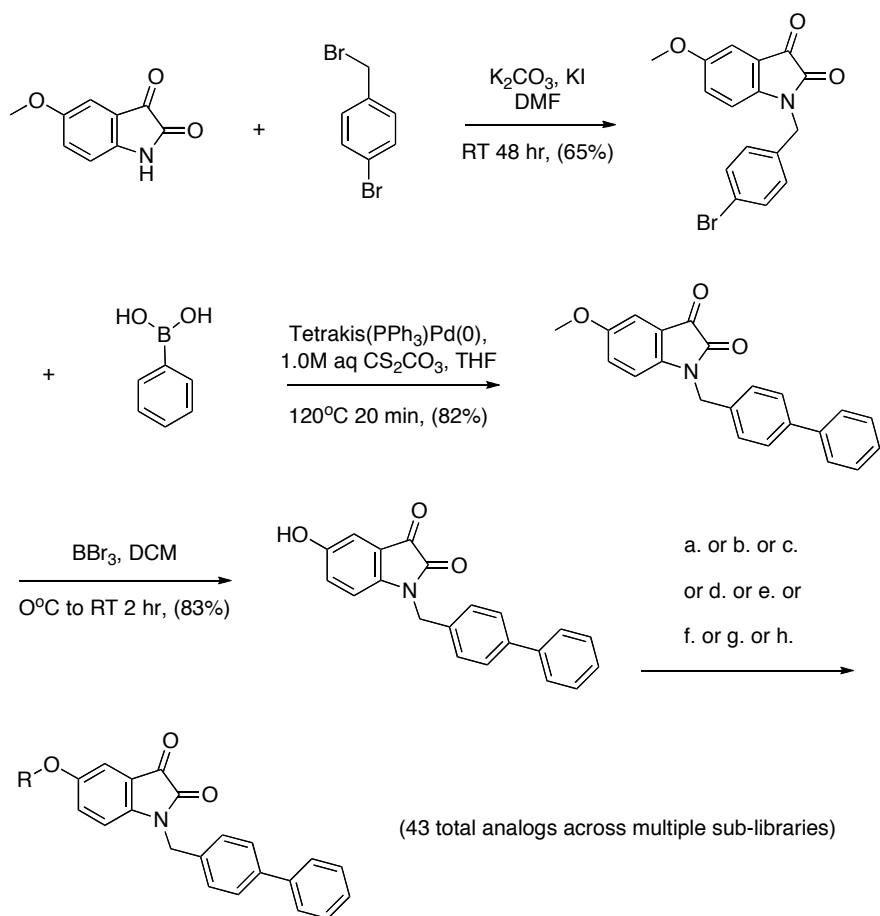


Figure 27. M_5 CRCs for tricyclic analogs VU0403897 and VU0403898. Ca^{2+} mobilization assays with M_5 cells were used to obtain compound CRCs in the presence of a fixed submaximal ($\sim EC_{20}$) concentration of ACh (EC_{50} values: VU0403897 and VU0403898 = $>10 \mu M$). Data represent the results of one experiment.

For the fourth iteration of parallel libraries, the western 5-OCF₃ group was chosen as a point of derivation (**Fig. 28**). Although movement of this moiety to the 6-position of the core was found to erode subtype-selectivity (despite enhancement of M_5 PAM efficacy), other substitutions beyond those present in the initial 92-member matrix library (5-OCF₃, 5-Cl, 5-F, 5-Me) to the 5-position had not been explored. In particular, alkyl extensions of the trifluoro group in the form of an ethoxy or propoxy ether and deletion of the trifluoro group altogether via synthesis of the 5-methoxy analog was planned. These structures would provide important insight to the significance of the OCF₃ group. Beyond these three specific changes, we also sought an extensive SAR survey through synthesis of a diverse set of benzyl, heteroaryl, alkyl, substituted alkylamine, etc... off of a 5-position ether. Most of these analogs could be accessed synthetically via generation of the 5-hydroxy starting material, which would involve methyl-deprotection of a 5-

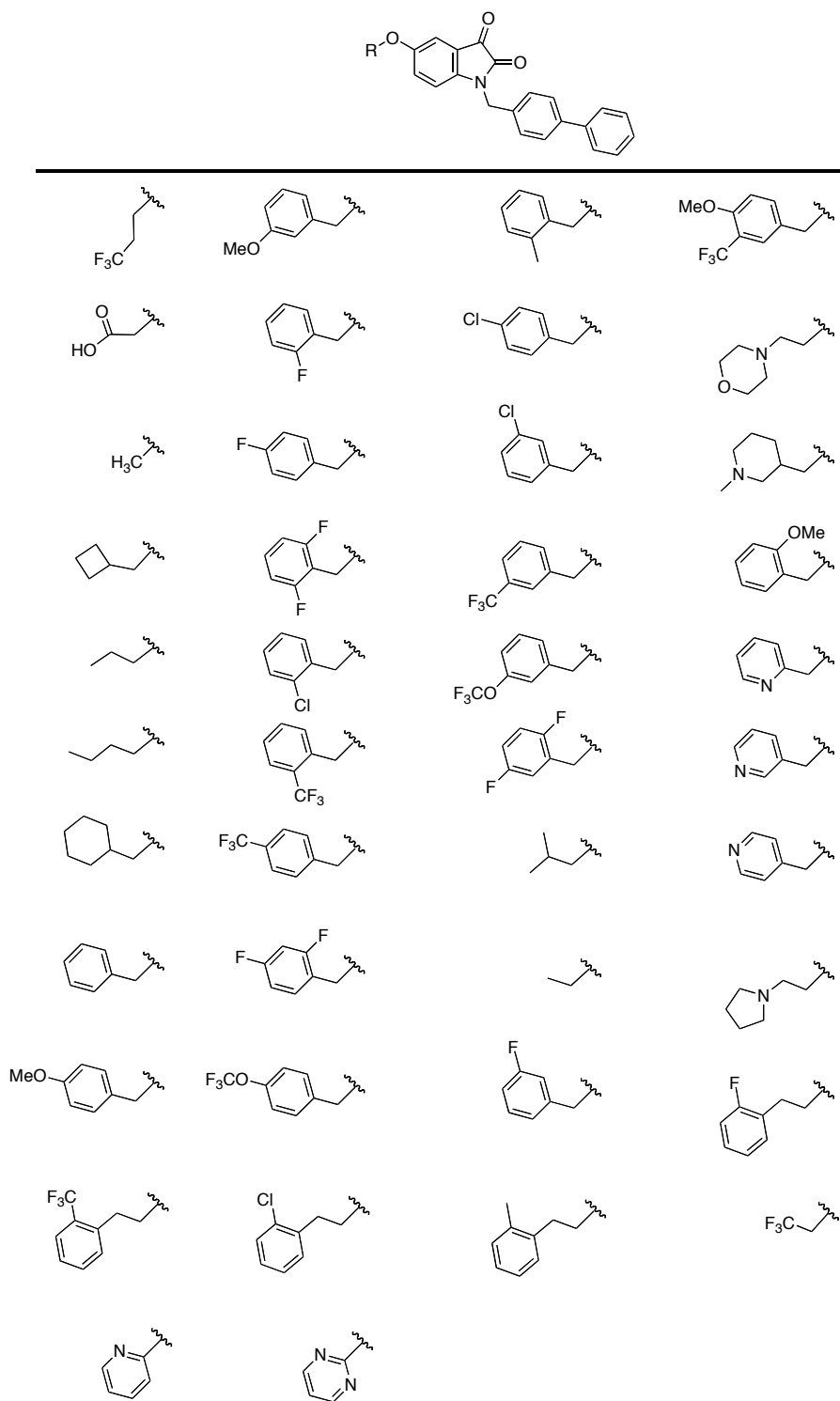
methoxy substrate. In light of this synthetic route, the *p*-phenylbenzyl moiety of VU0365114 was chosen as the southern piece to be held constant for these libraries, since its mAChR pharmacology confers it with “lead” status comparable or perhaps greater than that of the methoxybenzyl southern moiety in VU0238429, and its use would not result in problematic bis-hydroxyl production during the methyl-deprotection step, unlike VU0238429. The synthetic scheme for this set of libraries is presented in **Figure 28**, and a complete list of structures generated is shown in **Table 5**. The rationale for the broad range of substituents was simply to increase the likelihood of uncovering useful SAR since no previous analogs investigated such modification in the western region of this general M₅ PAM scaffold.



- a.: R-X, CS_2CO_3 , KI, DMF, 120°C 30 min, (avg. 20%), R = 27 analogs
- b.: (1) ethylchloroacetate, CS_2CO_3 , KI, DMF, 120°C 30 min, (16%)
 then (2) LiOH, THF, H_2O , 120°C 10 min, (43%)
- c.: R-OH, PS- PPh_3 , DIAD, THF, RT 16 hr, (avg. 4%), R = 10 analogs
- d.: 4-(2-chloroethyl)morpholine HCl, NaH, KI, DMF, 55°C 24 hr (4%)
- e.: 3-chloromethyl-1-methylpiperidine HCl, CS_2CO_3 , KI, DMF 180°C 30 min, (1%)
- f.: 1,1,1-trifluoro-2-iodoethane, K_2CO_3 , DMF, 160°C 10 min, (4%)
- g.: 2-fluoropyridine, CS_2CO_3 , DMF, 160°C 20 min, (3%)
- h.: 2-chloropyridine, K_2CO_3 , DMF, 100°C 30 min, (14%)

Figure 28. Synthetic scheme for generation of a diverse set of M_5 PAM analogs based on VU0365114 bearing western ethers. Analogs were synthesized by utilization of eight sub-library/singleton chemistry routes (a.-h.) using the 5-hydroxy(*N*-substituted)isatin starting material following methyl-deprotection.

Table 5. Structures of western ether analog library based on M₅ PAM VU0365114. All analogs were devoid of robust M₅ PAM activity in 10 μM singlepoint screen (**Fig. 29**).



Following synthesis and purification, the compounds were evaluated in a singlepoint PAM (10 μM) Ca^{2+} mobilization assay in the presence of an ACh $\sim\text{EC}_{20}$ with M_5 cells (**Fig. 29**). Remarkably, all analogs were devoid of any considerable PAM activity, suggesting in agreement with all previous SAR that the 5-OCF₃ group is absolutely required for activity at M_5 and even the subtle derivation to trifluoroethoxy in this position causes loss of the PAM effects (**Fig. 29**). Intriguingly, a subset of analogs in this screen induced partial inhibition of the submaximal ACh concentration, which may reflect either orthosteric antagonism or possible NAM activity (**Fig. 29**). Each of these analogs bore basic amines on similarly long alkyl tethers to the oxygen at the 5-position of the isatin core, with the three most basic analogs inducing the greatest inhibition (**Fig. 30**).

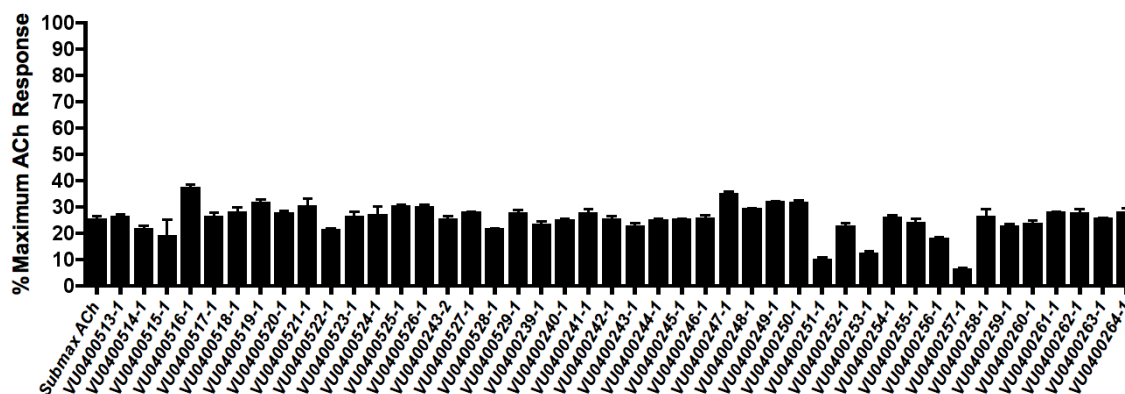


Figure 29. M_5 singlepoint screening of western ether analogs (**Table 5**). Ca^{2+} mobilization assays with M_5 cells were used to obtain singlepoint (10 μM) potentiation responses for each analog in the presence of a submaximal ($\sim\text{EC}_{20}$) concentration of ACh. Data represent the Mean \pm S.E.M. of at least 3 independent experiments with similar results.

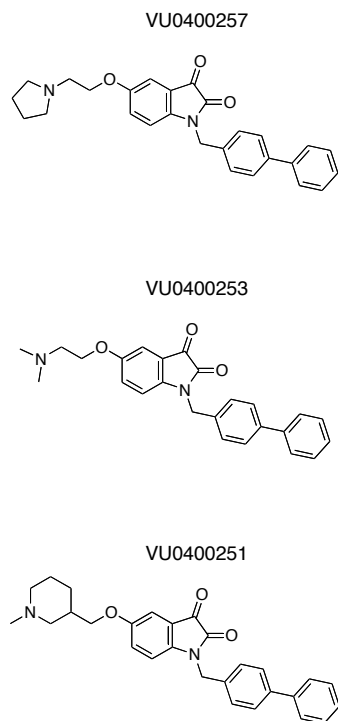


Figure 30. Basic-amine containing western ether analogs that partially inhibited an ACh \sim EC₂₀ response in M₅ PAM screen shown in **Figure 29**, suggesting potential M₅ NAM or antagonism.

Based on these data, an exploratory optimization project was launched in hopes of discovering M₅ NAMs or antagonists (of which there are none at present reported in the international scientific or patent literature), which has identified a number of additional compounds maintaining the western basic alkylamine that exhibit complete inhibition of an ACh \sim EC₈₀ with upper micromolar-level potency in CRCs using M₅ cells by Ca²⁺ mobilization. Although not a focus of this thesis, this discovery may eventually lead to M₅-preferring or selective NAMs or antagonists suitable as research tools, which would provide invaluable insight to M₅ neurobiology across a range of possible studies (discussed further in Chapter VI). However, given the structure of ACh itself, it is possible that the basic amines of these putative M₅ NAMs/antagonists may be inhibiting the ACh response via orthosteric antagonism, especially due to the comparable distance

between the nitrogen and the oxygen of the ether. If orthosteric antagonism does in fact underly these data, M₅-preference or selectivity may still be achievable due to the remainder of the scaffold. Whether or not such a mechanism for selectivity is present with these analogs is currently unknown, as no radioligand binding studies have been performed to assess allosteric versus orthosteric modes of modulation.

Returning to the M₅ PAM SAR revealed by this large library, we opted to maintain the 5-OCF₃ moiety of the scaffold's core indefinitely, as it alone appeared to provide the M₅ potentiation effect. This extremely flat SAR (around the western area of the scaffold) is common with many GPCR allosteric modulators and can be a difficult impediment to optimization projects. In the case of these western ether analogs, a number of modifications were explored and importantly the crucial 5-methoxy analog (VU0366627), which was synthesized and also tested separately in Ca²⁺ mobilization CRCs at M₅ (**Fig. 31**). This compound provided a stark example of the narrow steric and electronic tolerance(s) of the receptor-binding interaction of the scaffold as this analog lacked M₅ PAM activity at up to 10 μM with only modest potentiation occurring at 30 μM (**Fig. 31**). Whether the hydrophobic properties of the three fluorines, their electronic attenuation of the hydrogen-bond accepting potential of the neighboring oxygen, and/or their own partial hydrogen-bond accepting characteristics underlies this tight SAR remains unknown.

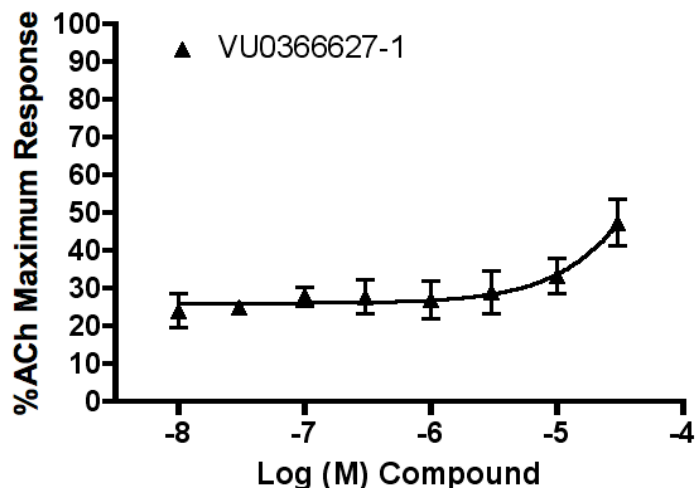
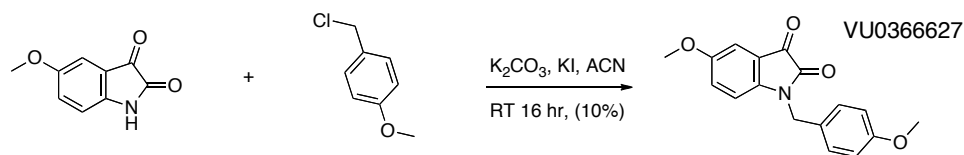


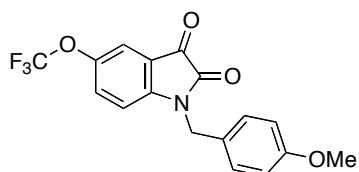
Figure 31. Synthesis and M_5 CRC for 5-methoxy analog VU0366627. Ca^{2+} mobilization assays with M_5 cells were used to obtain compound CRC in the presence of a fixed submaximal ($\sim EC_{20}$) concentration of ACh ($EC_{50} = >10 \mu M$). Data represent the Mean \pm S.E.M. of at least 3 independent experiments with similar results.

Ancillary pharmacology and physicochemical optimization of M_5 PAMs

Having investigated a large number of structural modifications to the general VU0238429 M_5 PAM scaffold across four rounds of targeted libraries and uncovering important SAR to obtain a set of optimized lead compounds, we temporarily halted the medicinal chemistry efforts and determined ancillary off-target pharmacological activity via radioligand binding screens at MDS Pharma/Ricerca. Both the isatin containing and gem-difluoro congeners of the two most potent and most subtype-selective compounds (VU0238429, VU0402734, VU0400265, VU0403751, respectively), as well as the moderately potent and highly subtype-selective intermediate lead VU0365114 were

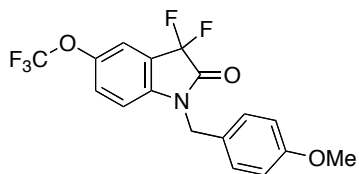
chosen for testing, which involved $N=2$ singlepoint (10 μM) screening across approximately 75 different GPCRs, ion channels, transporters, nuclear hormone receptors, enzymes, and RTKs. For any off-target binding that resulted in $>50\%$ inhibition, the protein and % inhibition is reported for each compound in **Table 6**.

Table 6. Ancillary/off-target binding screening results for five M_5 PAM leads (10 μM). Data represent the Mean of 2 independent experiments with similar results. Experiments performed by MDS Pharma/Ricerca.



VU0238429

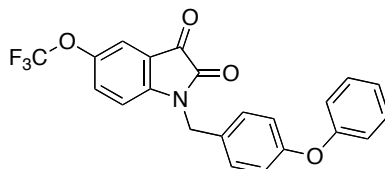
<u>Target/Protein</u>	<u>Species</u>	<u>% Inhibition</u>
Adenosine A_3	Human	65
Adrenergic α_{2A}	Human	99
NE Transporter	Human	66
Cannabinoid CB_1	Human	84
Dopamine $D_{4,2}$	Human	61
Histamine H_1	Human	62
Histamine H_2	Human	55
Opiate μ	Human	70
hERG K^+ Channel	Human	60



VU0402734

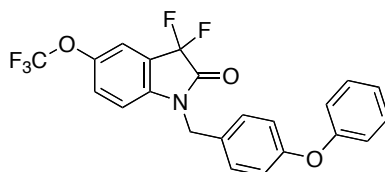
<u>Target/Protein</u>	<u>Species</u>	<u>% Inhibition</u>
Adenosine A_3	Human	68
Adrenergic α_{2A}	Human	98
NE Transporter	Human	71
Cannabinoid CB_1	Human	64
Dopamine D_3	Human	58

Dopamine D _{4,2}	Human	57
Histamine H ₁	Human	68
Histamine H ₂	Human	59
Opiate μ	Human	73
hERG K ⁺ Channel	Human	65
PDE-4/Rolipram	Rat	60
Na ⁺ Channel Site-2	Rat	60



VU0400265

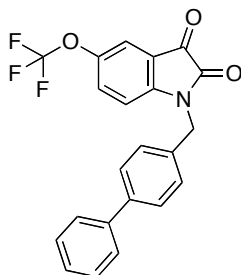
Target/Protein	Species	% Inhibition
Adenosine A ₁	Human	50
Adenosine A ₃	Human	97
Adrenergic α_{1A}	Rat	79
Adrenergic α_{1D}	Human	66
Adrenergic α_{2A}	Human	100
Adrenergic β_1	Human	89
NE Transporter	Human	93
Bradykinin B ₁	Human	52
Ca ²⁺ L-Type Channel	Rat	74
Cannabinoid CB ₁	Human	109
Dopamine D ₁	Human	99
Dopamine D _{2S}	Human	85
Dopamine D ₃	Human	79
DA Transporter	Human	90
GABA Transporter	Rat	56
Histamine H ₁	Human	99
Histamine H ₂	Human	101
Imidazoline I ₂	Rat	50



VU0403751

Target/Protein	Species	% Inhibition
-----------------------	----------------	---------------------

Adenosine A ₁	Human	55
Adenosine A _{2A}	Human	51
Adenosine A ₃	Human	97
Adrenergic α _{1A}	Rat	62
Adrenergic α _{1D}	Human	67
Adrenergic α _{2A}	Human	98
Adrenergic β ₁	Human	86
NE Transporter	Human	91
Bradykinin B ₁	Human	60
Ca ²⁺ L-Type Channel	Rat	79
Cannabinoid CB ₁	Human	106
Dopamine D ₁	Human	100
Dopamine D _{2S}	Human	86
Dopamine D ₃	Human	76
DA Transporter	Human	86
GABA Transporter	Rat	56
Histamine H ₁	Human	93
Histamine H ₂	Human	96



VU0365114

<u>Target/Protein</u>	<u>Species</u>	<u>% Inhibition</u>
Adenosine A ₃	Human	98
Adrenergic α _{1B}	Rat	51
Adrenergic α _{1D}	Human	70
Adrenergic α _{2A}	Human	99
Adrenergic β ₁	Human	86
NE Transporter	Human	86
Ca ²⁺ L-Type Channel	Rat	73
Cannabinoid CB ₁	Human	68
Dopamine D ₁	Human	104
Dopamine D _{2S}	Human	89
Dopamine D ₃	Human	75
DA Transporter	Human	74
Endothelin ET _A	Human	92
Endothelin ET _B	Human	51

Histamine H ₁	Human	102
Histamine H ₂	Human	103
Leukotriene CysLT ₁	Human	104
Muscarinic M ₁	Human	78
Muscarinic M ₂	Human	96
Muscarinic M ₃	Human	62
Opiate κ	Human	98
Opiate μ	Human	100
hERG K ⁺ Channel	Human	69
Prostanoid EP ₄	Human	72
Serotonin 5-HT _{2B}	Human	67
Serotonin Transporter	Human	64

These ancillary pharmacology data clearly indicated that the southern methoxybenzyl moiety (VU0238429 and VU0402734) was favored over the phenoxybenzyl (VU0400265 and VU0403751), as the latter introduced a large number of off-target activities, including pronounced binding to DAT and multiple DA receptors, which would pose serious difficulties in many M₅ neurobiology experiments (particularly those focused on the VTA, SNc, and/or striatum). Gem di-fluorination (VU0402734 and VU0403751) dialed in modest D₃ receptor (58% inhib.), PDE-4 (60% inhib.), and sodium channel site-2 (60% inhib.) activity, which did not raise substantial concerns for most potential M₅ studies. VU0365114, bearing the highly lipophilic linear bi-phenyl southern motif on the 5-OCF₃ isatin core, suffered from the highest number of off-target activities.

Given these results, further optimization of the southern biaryl ether moiety was performed in order to reduce/eliminate its associated off-target activities and further explore SAR. Specifically, introduction of more polar and heteroatomic moieties to the southern ether would likely reduce off-target activities that may be due to the increased lipophilicity of the distal phenyl ring in VU0400265 and VU0403751 as compared to the

methyl group of VU0238429 and VU0402734. Furthermore, a reduction in the relatively high cLogPs of these compounds would likely aid in the overall physiochemical and drug-like properties of the scaffold, particularly if introducing basic amines to allow HCl salt formation is tolerated.

To this end, we replaced the distal phenyl ring with various 5- or 6-member naked or mono-substituted heterocyclic rings while holding constant the remainder of the M₅ PAM scaffold. Due to the challenging synthesis of these analogs (**Fig. 32**), which required derivatization at the first rather than the last step as well as laborious reaction conditions and purifications, only four compounds were generated to explore this SAR (**Fig. 32**).

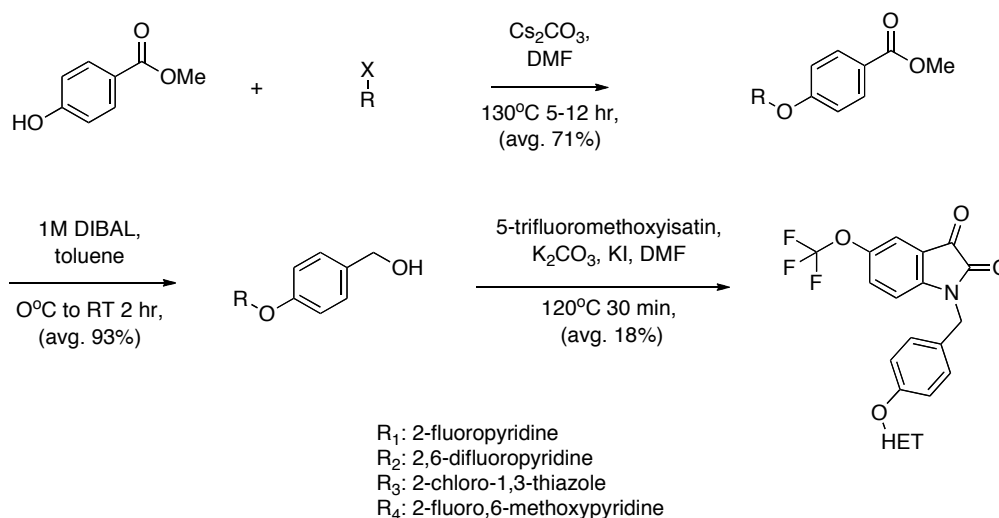


Figure 32. Synthesis of four southern heterobiaryl ether analogs based on VU0400265.

These four southern heterobiaryl ether analogs were then evaluated in CRCs at M₅ in the presence of an ACh ~EC₂₀ by Ca²⁺ mobilization assay and exhibited PAM activity with comparable potency (1.5 μM to 3.2 μM) to the phenoxybenzyl analog VU0400265

(**Fig. 33**). These compounds proved advantageous given our goal of improving the physiochemical properties of VU0400265 (cLogP = 5.8, true logP = 4.6) as lipophilicity was decreased approximately by a full order of magnitude (cLogPs = 4.1-5.1) and the presence of a basic amine afforded HCl salt formation. However, their efficacies (46-62% ACh max) were moderately lower than that of the parent VU0400265 (75% ACh max) compound (**Fig. 33**).

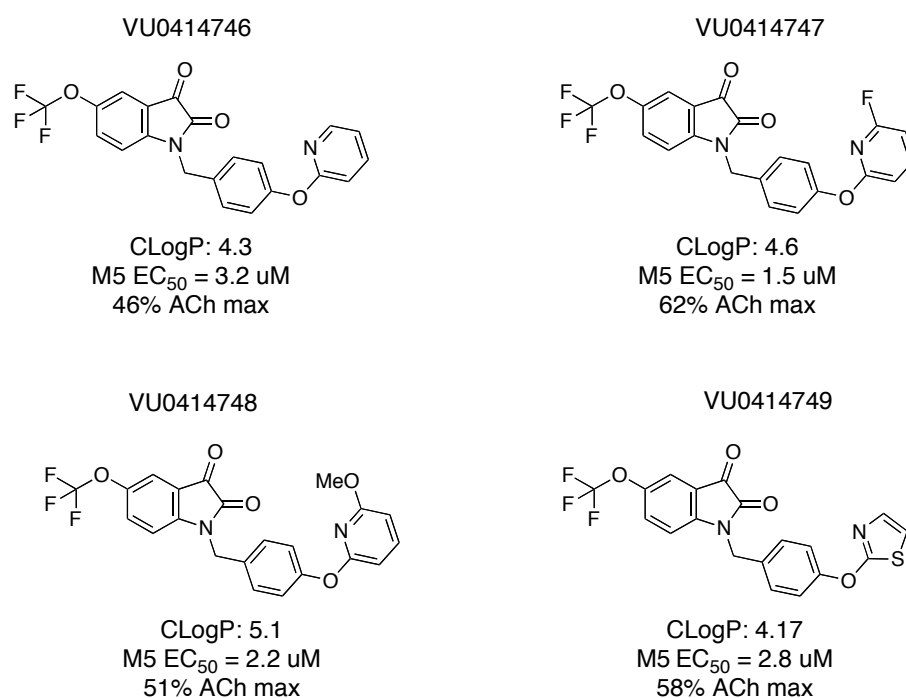


Figure 33. Structures, lipophilicities, and M₅ potency/efficacy for four heterobiaryl ether M₅ PAMs. Ca²⁺ mobilization assays with M₅ cells were used to obtain compound CRCs in the presence of a fixed submaximal (~EC₂₀) concentration of ACh. Data represent the Mean of at least 3 independent experiments with similar results.

The fluoropyridine ether analog VU0414747 was selected as the most potent and efficacious compound from this small 4-member library for evaluation in ACh CRC fold-shift assays (**Fig. 34**). At 30 μ M, VU0414747 induced a modest 6x left-shift of the ACh

CRC and was devoid of intrinsic agonism, similar to the parent VU0400265 (**Fig. 34**). Although this degree of maximal potentiation is significant, previous analogs bearing straight biaryl/heterobiaryl southern motifs (i.e. without the ether linkage, such as VU0365114) exhibited much broader fold-shift values and %ACh max responses at 30 μ M (**Fig. 13**).

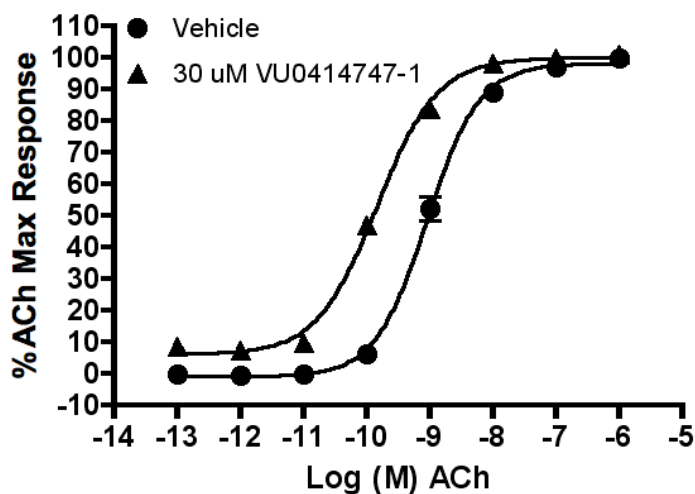
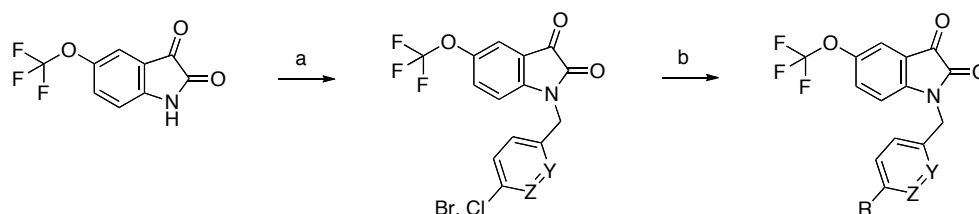


Figure 34. M_5 ACh CRC foldshift assay with analog VU0414747. Ca^{2+} mobilization assays with M_5 cells were used to obtain ACh CRCs in the presence and absence of test compound (6x left-shift). Data represent the Mean \pm S.E.M. of at least 3 independent experiments with similar results.

Therefore we returned to the straight biaryl/heterobiaryl southern scaffold and likewise explored introduction of basic amines in the form of un-substituted pyridines in the proximal and/or distal locations of the linear southern motif (**Fig. 35**). In order to survey multiple combinations of regio-isomeric pyridines, a matrix-like library approach was utilized for this synthesis (**Fig. 35**). Standard *N*-alkylation conditions provided the *para* -Cl or -Br intermediates, which were then subjected to Suzuki-couplings with the various heterocyclic boronic acids to afford the final products (**Fig. 35**). A similar route

was utilized to obtain VU0415485 as a singleton, which contained a distal 3,5-pyrimidyl *para* substitution off of a proximal benzyl ring (**Fig. 35**). The final compounds (as well as the Cl-bearing intermediate VU0414754) were then profiled in M₅ CRCs in the presence of an ACh ~EC₂₀ by Ca²⁺ mobilization assay to obtain potency and efficacy data (**Fig. 35**).



<u>Compound</u>	<u>Y, Z</u>	<u>R</u>	<u>M₅ EC₅₀, ACh max</u>
VU0415483	CH, CH	3-pyridyl	1.6 μM, 51%
VU0415484	CH, CH	4-pyridyl	2.8 μM, 60%
VU0415485	CH, CH	3,5-pyrimidyl	2.1 μM, 53%
VU0414754	CH, N	Cl	2.4 μM, 80%
VU0415478	CH, N	phenyl	3.8 μM, 76%
VU0415479	CH, N	3-pyridyl	4.0 μM, 53%
VU0415480	CH, N	4-pyridyl	4.4 μM, 50%
VU0415481	N, CH	phenyl	3.1 μM, 47%
VU0415487	N, CH	3-pyridyl	>30 μM, n/a
VU0415482	N, CH	4-pyridyl	>30 μM, n/a

Figure 35. Synthesis and SAR for southern heterobiaryl amine-containing M₅ PAM analogs. Reagents and conditions: (a) 4-bromobenzyl bromide, K₂CO₃, KI, DMF, rt, 48 h (99%), OR 5-bromo-2-(bromomethyl)pyridine OR 5-(bromomethyl)2-chloropyridine, K₂CO₃, KI, DMF, rt, 48 h (98%); (b) Het-B(OH)₂, 5 mol % Pd(PPh₃)₄, 1.0 M aq. Cs₂CO₃, THF, mw, 120 °C, 20 min (5-18%). Ca²⁺ mobilization assays with M₅ cells were used to obtain compound CRCs in the presence of a fixed submaximal (~EC₂₀) concentration of ACh. Data represent the Mean of at least 3 independent experiments with similar results.

This effort produced a number of moderately-highly potent M₅ PAM compounds with a wide range of efficacies (**Fig. 35**). Importantly, these SAR data suggested that 3-pyridyl in the proximal ring location was uniformly favored over 2-pyridyl in the same position, as the former exhibited compounds with the best balance of potency/efficacy (of this library) while the latter was virtually inactive regardless of the distal ring substitution present (**Fig. 35**). This provided success similar to that of the heterobiaryl ether analog library in that M₅ PAM potency/efficacy was generally retained while cLogP values were simultaneously reduced by 1-1.5 orders of magnitude (true logP for VU0415478 = 3.6), and likewise providing the ability to formulate HCl salts.

Furthermore, the *p*-phenyl substituted 3-pyridyl analog VU0415478 exhibited a robust 14x left-shift of an M₅ ACh CRC at 30 μM in Ca²⁺ mobilization assays and displayed modest intrinsic agonist activity, which agreed well with previous SAR suggesting that a linear biaryl/heterobiaryl southern moiety confers greater ACh CRC fold-shift (and associated % ACh max values in CRC assays) than related analogs containing a biaryl/heterobiaryl ether (**Fig. 36**).

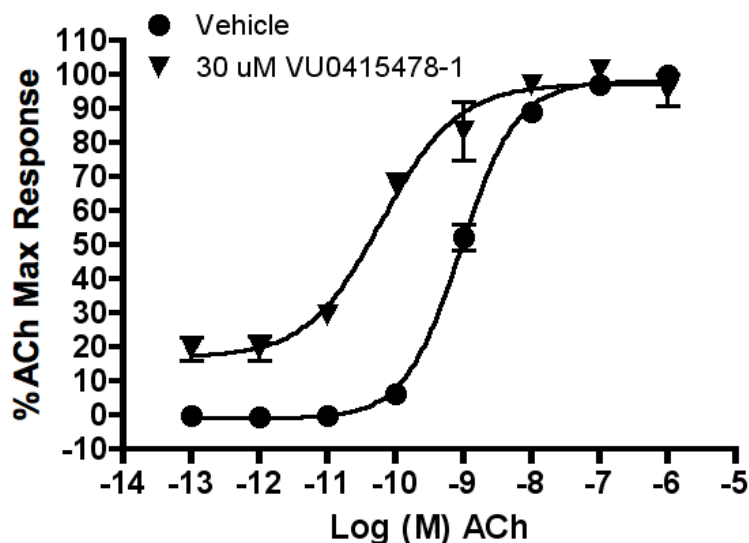


Figure 36. M_5 ACh CRC fold-shift assay with analog VU0415478. Ca^{2+} mobilization assays with M_5 cells were used to obtain ACh CRCs in the presence and absence of test compound (14x left-shift). Data represent the Mean \pm S.E.M. of at least 3 independent experiments with similar results.

In light of the well-tolerated 3-pyridyl replacement for the southern benzyl ring, which increased polarity and thereby decreased lipophilicity for the heterobiaryl sub-series of compounds, we hypothesized that this nitrogen substitution would be similarly tolerated in the original M_5 PAM lead VU0238429 structure bearing a southern *p*-methoxy moiety. Thus the 3-pyridyl congener was synthesized via one-step standard microwave alkylation conditions with the commercially available chloromethyl-methoxypyridine and with the 5-trifluoromethoxyisatin starting material as previously described, although the final yield (4%) was very low due to poor recovery from reverse-phase HPLC purification (i.e. not due to poor % conversion of starting material to product) (**Fig. 37**). This compound (VU0415486) exhibited 3.2 μ M M_5 potency and 47% ACh max efficacy in CRC assays using Ca^{2+} mobilization (**Fig. 37**). Due to the relatively low efficacy, VU0415486 was not further characterized in the form of ACh CRC fold-shift or subtype-selectivity assays was not performed.

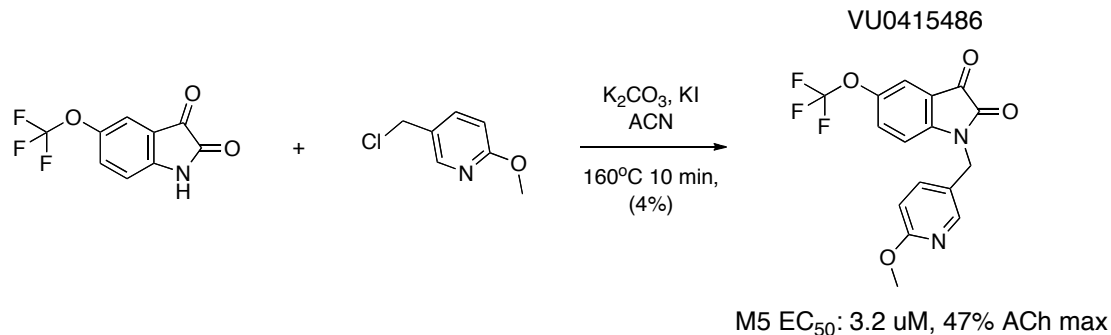


Figure 37. Synthesis and M₅ potency/efficacy of VU0415486, the 3-pyridyl congener of VU0238429. Ca²⁺ mobilization assays with M₅ cells were used to obtain compound CRCs in the presence of a fixed submaximal (~EC₂₀) concentration of ACh. Data represent the Mean of at least 3 independent experiments with similar results.

Finally, to more comprehensively explore SAR in the southern region of the M₅ PAM scaffold for the purpose of identifying additional compounds with improved physiochemical properties and reduced ancillary/off-target activities, we synthesized a small library of analogs bearing either acidic or basic moieties at R shown in **Figure 38**, as well as the de-methylated phenol congener of the original *p*-methoxybenzyl motif. For each of these analogs, the gem-difluorinated core was used for reasons of convenience related to starting material availability at the time. Starting with the methoxybenzyl-bearing VU0402734, methyl de-protection afforded the phenol (VU0414750), which was used as starting material for subsequent *O*-alkylations (detailed conditions described in Chapter II) with the corresponding alkyl halides to obtain the three compounds of **Figure 38**. Each analog was profiled in M₅ CRCs with an ACh ~EC₂₀ by Ca²⁺ mobilization assays (**Fig. 38**). However, the ethylpyrrolidine (VU0414751) exhibited a fully efficacious (~100% ACh max) agonist effect at 30 μM despite absence of any potentiation of the ACh ~EC₂₀, which suggests possible orthosteric agonism that may be

conferred by the ACh-like structure of this particular motif (i.e. basic amine with ethyl tether to oxygen). By contrast, the morpholine (VU0414752) and carboxylic acid (VU0414753) analogs lacked both agonism and PAM activity. Interestingly, the phenol (VU0414750) exhibited concentration-dependent inhibition of the ACh \sim EC₂₀, suggesting potential NAM or antagonist activity.

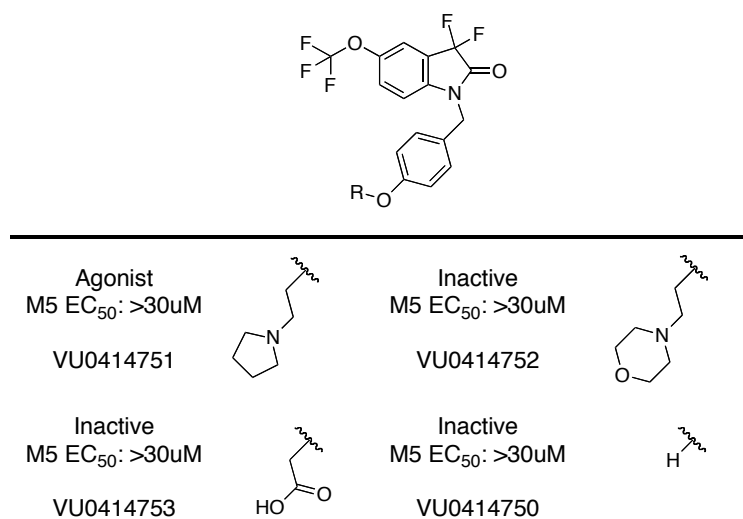


Figure 38. Structures and M₅ potency/efficacy of acidic and basic moieties in the distal southern region of the M₅ PAM scaffold. Ca²⁺ mobilization assays with M₅ cells were used to obtain compound CRCs in the presence of a fixed submaximal (\sim EC₂₀) concentration of ACh. Data represent the Mean of at least 3 independent experiments with similar results.

In order to further investigate the potential NAM activity of VU0414750, similar CRC assays were performed using Ca²⁺ mobilization with M₅ cells in the presence of an \sim EC₅₀ and \sim EC₈₀ of ACh (**Fig. 39**). These experiments revealed similar concentration-dependent inhibition of the ACh response, which is consistent but not necessarily suggestive of true NAM activity for this phenol compound. Due to the greater focus on optimizing M₅ PAMs, further examination of this compound in radioligand-binding or

other assays was not performed. However, given these present data and in light of the compound's structure, VU0414750 may represent the first M₅ NAM.

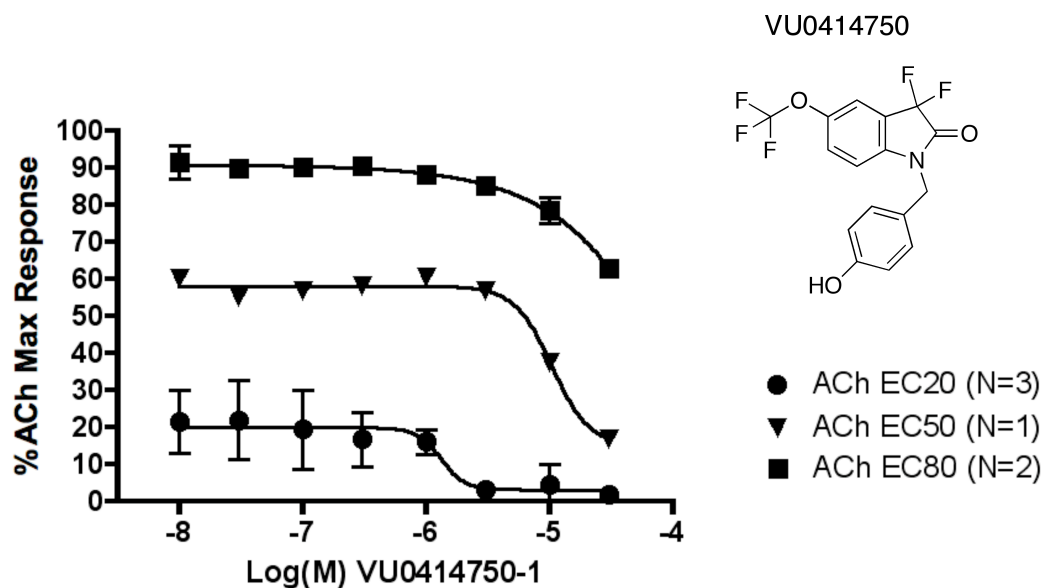
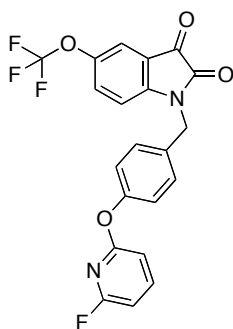


Figure 39. M₅ ACh inhibition CRCs for VU0414750, a potential M₅ NAM. Ca²⁺ mobilization assays with M₅ cells were used to obtain compound CRCs in the presence of a fixed submaximal (~EC₂₀, ~EC₅₀, and ~EC₈₀) concentrations of ACh. Data represent the Mean ±S.E.M. or results of 1-3 experiments.

The switch in VU0414750 from methoxy to hydroxy at the *para* benzylic position is relatively modest; however, a growing number of “molecular switches” that confer dramatic changes to the pharmacological mode of modulation of a given scaffold have appeared in recent GPCR allosteric modulator medicinal chemistry literature^{133,134}. Given that the methoxy moiety possesses hydrogen-bond accepting properties while the phenol is a hydrogen-bond donor, it is possible that hydrogen-bond mediated attraction or repulsion of a key residue/motif in the M₅ receptor allosteric binding site is responsible for switching this PAM scaffold into a NAM scaffold. This hypothesis will require further experimental exploration, as discussed in more detail in Chapter VI.

Having thus surveyed a wide range of modifications to the southern region of the M₅ PAM scaffold with the aim of decreasing lipophilicity/cLogP while simultaneously maintaining potency, efficacy, and subtype-selectivity, we re-assessed ancillary off-target activity for VU0414747 and VU0415478. These were chosen because they represented the most potent and efficacious compounds with reduced cLogP values from the most recently discussed heterobiaryl ether and straight heterobiaryl libraries, respectively. Unfortunately, in the same assays described previously for ancillary pharmacology screening (performed by MDS Pharma/Ricerca, **Table 6**), which used a large panel of off-targets in competition binding at 10 μM, both compounds exhibited a wide range of activities (**Table 7**).

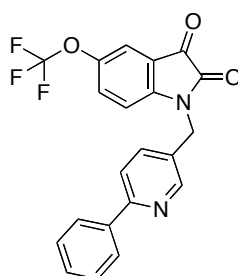
Table 7. Ancillary/off-target binding screening results for physiochemically-optimized M₅ PAMs VU0414747 and VU0415478 (10 μM). Data represent the Mean of 2 independent experiments with similar results. Experiments performed by MDS Pharma/Ricerca.



VU0414747

Target/Protein	Species	% Inhibition
Adenosine A ₃	Human	75
Adrenergic α _{1D}	Human	61
Adrenergic α _{2A}	Human	101
Adrenergic β ₁	Human	70
NE Transporter	Human	106
Ca ²⁺ L-Type Channel	Rat	68
Cannabinoid CB ₁	Human	93

Dopamine D ₁	Human	89
Dopamine D _{2S}	Human	58
Dopamine D ₃	Human	78
Dopamine D _{4,2}	Human	53
Endothelin ET _A	Human	79
Histamine H ₁	Human	100
Histamine H ₂	Human	96
Leukotriene CysLT ₁	Human	99
Muscarinic M ₁	Human	51
Muscarinic M ₂	Human	75
Tachykinin NK ₁	Human	-72
Opiate κ	Human	61
Opiate μ	Human	91
hERG K ⁺ Channel	Human	69
Serotonin 5-HT _{2B}	Human	56
Na ⁺ Channel Site-2	Rat	64



VU0415478

<u>Target/Protein</u>	<u>Species</u>	<u>% Inhibition</u>
Adenosine A ₃	Human	73
Adrenergic α _{1D}	Human	76
Adrenergic α _{2A}	Human	97
Adrenergic β ₁	Human	59
NE Transporter	Human	106
Bradykinin B ₂	Human	-53
Ca ²⁺ L-Type Channel	Rat	56
Cannabinoid CB ₁	Human	70
Dopamine D ₁	Human	88
Dopamine D _{2S}	Human	66
Dopamine D ₃	Human	87
Endothelin ET _A	Human	79
GABA Transporter	Rat	57
Histamine H ₁	Human	88
Histamine H ₂	Human	92
Leukotriene CysLT ₁	Human	86

Muscarinic M ₂	Human	78
Opiate μ	Human	90
hERG K ⁺ Channel	Human	63
Na ⁺ Channel Site-2	Rat	51

Despite the substantially reduced cLogP values for these analogs versus earlier leads within the series, broad off-target activity was observed (**Table 7**), which suggests, in light of the previous ancillary pharmacology SAR shown in **Table 6**, that the southern heterobiaryl moiety (with or without an internal ether linkage) engenders promiscuous off-target binding. These results, and the dopamine D₁ and D₂ receptor binding in particular, were surprising and present an impediment to utilization of these two advanced lead compounds in M₅-related neurobiology studies. Nonetheless, both compounds (VU0414747 and VU0415478) and their parent libraries revealed useful SAR and may serve as starting points for a more exhaustive optimization effort to survey a larger range of heterobiaryl and heterobiaryl substitutions that may be devoid of some or ideally all of these off-target liabilities (discussed in more detail in Chapter VI).

***In vitro* characterization of M₅ PAMs at rat M₅ receptor**

For all *in vitro* M₅ assays performed throughout this optimization, cell lines expressing the human receptor were used. Because species-specific differences in PAM activity have been found with other mAChR allosteric modulators (e.g. M₄ PAMs described in Chapter III)¹²⁶, and because future M₅ electrophysiology experiments and *in vivo* studies will be performed using rats, we determined the effect of early lead compound VU0238429 at the rat M₅ receptor. Increasing fixed concentrations of

VU0238429 resulted in concentration-dependent left-shifting of an ACh CRC in rM₅ cells by Ca²⁺ mobilization assay (**Fig. 40**), with a maximum fold-shift of approximately 30x at the top concentration (30 μM).

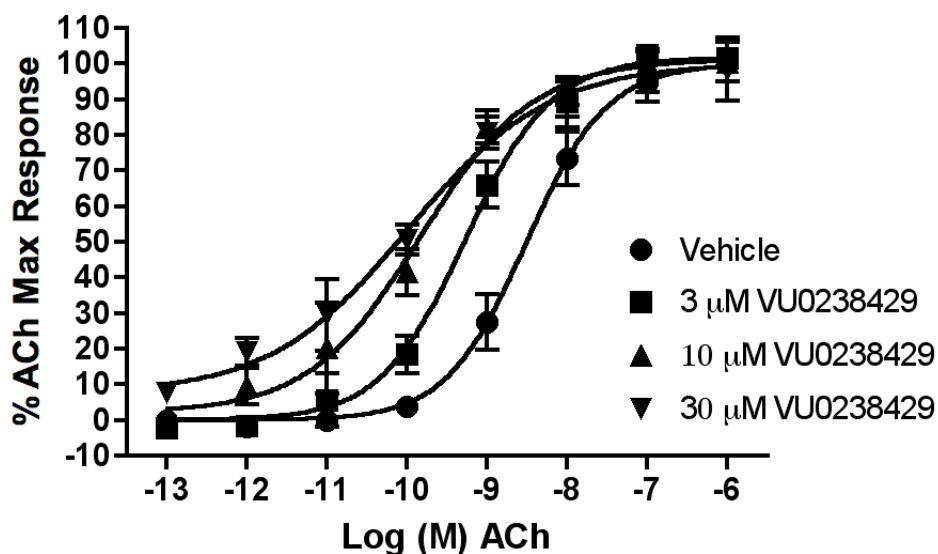


Figure 40. Rat M₅ ACh CRC fold-shift assay with early lead compound VU0238429. Ca²⁺ mobilization was used to obtain CRCs of ACh in the absence and presence of increasing fixed concentrations of test compound (30 μM maximum fold-shift = 30x). Data represent Mean +/-SEM from at least three independent determinations. Experiments performed by Dan Foster.

These data suggest that this novel series of M₅ PAMs is not only active at the rat M₅ receptor but may also be more efficacious, as the maximum fold-shift observed for VU0238429 at hM₅ was 14x. Further examination of VU0238429 and other lead compounds in rM₅ assays, including CRCs to determine potencies, will be required to confirm this possibility. Likewise, subtype-selectivity across all rat mAChRs will be important to confirm prior to initiation of neurobiology experiments. Nonetheless, it was gratifying to find that VU0238429 was active in this rM₅ PAM experiment.

It is possible that differences in receptor expression/reserve between our rat and human mAChR cell lines could influence the relative activity of a given PAM, resulting in an illusory greater or lesser activity. In the case of our findings with VU0238429 at rM₅ and hM₅, it is unlikely that differences in receptor expression/reserve between cell lines have confounded the data interpretation for several reasons. First, Ca²⁺ mobilization readouts under the assay conditions used with our mAChR CHO cells, which have been generated using identical stable transfection techniques, are typically less sensitive to such effects because receptor expression is extremely high (i.e. large reserve) across each cell line. Correspondingly, the potency of ACh in parallel CRC assays using rat versus human M₅ cells is essentially identical (0.5-3 nM ACh EC₅₀ for both), which further supports the hypothesis that the larger ACh CRC fold-shift observed at rM₅ reflects truly comparable or perhaps greater PAM efficacy at the rat versus human receptor.

Summary

In summary, this first and presently only class of highly subtype-selective M₅ positive allosteric modulators was discovered from the optimization of an M₁ PAM HTS hit (VU0119498). A large matrix-analog library was generated around VU0119498, which quickly provided SAR that conferred M₅-preference. This led to discovery of an early lead compound, VU0238429, which displayed approximately 1 μM M₅ PAM potency with >30x subtype-selectivity versus M₁-M₄ by *in vitro* Ca²⁺ mobilization assay. This compound was found to potentiate ACh activation of M₅ via allosteric enhancement of agonist affinity in radioligand binding studies using M₅ cell membranes and induced

an approximately 14x left-shift of an ACh CRC in M₅ cells by Ca²⁺ mobilization. However, VU0238429 possessed relatively poor *in vivo* PK properties and required further optimization to confer more drug-like characteristics. Ultimately, a number of subsequent lead compounds were discovered, which maintained low micromolar to sub-micromolar M₅ potency and high subtype-selectivity but with improved DMPK and physiochemical properties. However, problematic ancillary off-target binding for many of these compounds will require that future neurobiological experiments be carefully planned and controlled (such as evaluation of the M₅ PAM alone in the absence of agonist). In initial experiments using the rat M₅ receptor, this series of PAMs retained equal or possibly greater ACh CRC fold-shift efficacy than at human M₅, suggesting that these compounds are suitable for future rat neurobiology studies as they do not exhibit an undesirably loss of activity between the two species.

At present, these novel compounds represent the only tools available to the mAChR research field to pharmacologically investigate the role(s) of selective M₅ activation in native/WT neurobiological systems. Furthermore, this optimization effort represents part of the unprecedented finding that selective M₅ or M₁ (as discussed in Chapter III) PAM activity can be engendered via structural modification of the same lead compound displaying multiple mAChR PAM activities (VU0119498). Future experiments and potential optimization efforts are presented in detail in Chapter VI.

Chapter V

DISCOVERY, OPTIMIZATION, AND CHARACTERIZATION OF NOVEL SUBTYPE-SELECTIVE MACHR1 LIGANDS

M₁ PAMs derived from VU0119498

Based on the successful discovery of numerous M₅-preferring and selective PAMs from SAR exploration and optimization of the M₁/M₃/M₅ PAM HTS hit VU0119498 (Chapter IV), we hypothesized that this *N*-benzyl isatin scaffold could likewise be used as a starting point for discovery of novel M₁-preferring or selective PAMs¹³⁵. The broad SAR observed, for example in the initial 92-member matrix library, which explored the effect of various simple substitutions to the isatin core and southern benzyl moiety, as well as the structural similarity between VU0119498 and the Merck M₁ PAM series based on BQCA (discussed later in this Chapter), provided further rationale for this hypothesis.

Our initial optimization strategy is outlined in **Figure 1**, and as SAR with allosteric ligands is often shallow, we employed an iterative parallel synthesis approach. From our M₅ PAM optimization work where we often counter-screened on M₁, we quickly learned that most substitutions (with the exception of 5-OCF₃) on the isatin ring led to either loss of activity or pan-mAChR activation profiles with various degrees of potency, efficacy, and subtype-selectivity (Chapter IV). Thus, our first libraries employed a naked isatin core and surveyed diversity on the southern benzyl moiety. Modification of chain length from benzyl to phenethyl linkage as well as

biaryl/heterobiaryl extension in the para position was performed based primarily on SAR findings from the M5 PAM series (Chapter IV).

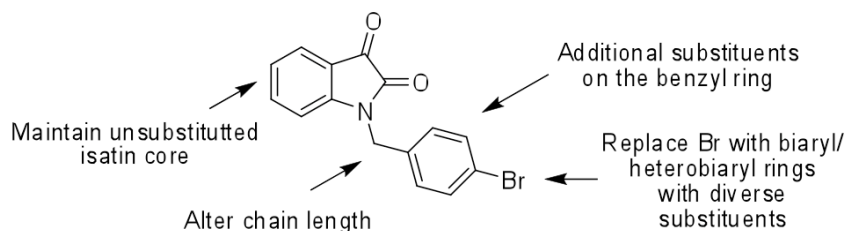


Figure 1. Initial optimization strategy for VU0119498 aimed at discovering modifications that engender increased M₁ PAM activity and subtype-selectivity.

Libraries were prepared according to the scheme shown in Figure 2, wherein commercial indoline-2,3-dione (compound **7**) was alkylated with p-bromobenzylbromide to deliver key intermediate (compound **8**). A 10-member Suzuki library was then prepared to explore the effect of introduction of biaryl and heterobiaryl motifs into VU0119498 providing analogs (compounds **9**). In parallel, the isatin starting material (compound **7**) was also alkylated with functionalized phenethyl bromides (compounds **10**) to probe the effect of chain homologation (compound **11**).

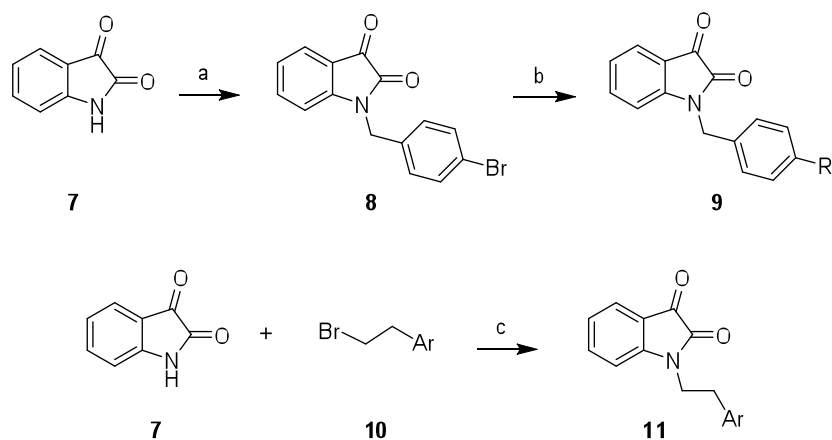


Figure 2. Synthesis of initial biaryl/heterobiaryl library based on VU0119498. Reagents and conditions: a) *p*-bromobenzylbromide, K_2CO_3 , KI, ACN, rt, 16 h (97%); b) RB(OH)_2 , $\text{Pd(P}t\text{-Bu}_3)_2$, CS_2CO_3 , THF: H_2O , mw, 120°C , 20 min (15-90%); c) K_2CO_3 , KI, ACN, rt, 16 h (50-90%). B(OH)_2 reactants used to generate 10-member parallel library in b): 2,5-difluorophenyl, 6-fluoropyridin-3-yl, 4-methoxyphenyl, pyrazole, *N*-methylpyrazole, 3,4-dichlorophenyl, 2-methoxyphenyl, 6-chloropyridin-3-yl, 4-propoxyphenyl, and 4-chlorophenyl. Br-ethyl-Ar reactants used in c): 4-methoxyphenyl and 4-bromophenyl.

This 12-member (total) library was then triaged by a singlepoint (10 μM) screen that examined the compounds' ability to potentiate an $\sim\text{EC}_{20}$ concentration of ACh by Ca^{2+} mobilization assay with M_1 and M_5 CHO cells (**Fig. 3**). Only one analog (VU0365137, compound **9a**) demonstrated robust M_1 versus M_5 potentiation. All other analogs exhibited weak M_1 potentiation and/or comparable activity at M_5 , with the exception of VU0365110 (the 2,5-difluorophenyl congener), which exhibited robust dual M_1/M_5 activity. In follow-up CRC assays at M_1 , M_3 , and M_5 , VU0365137 (compound **9a**), which possessed an *N*-methylpyrazole in the 4-position of the southern benzyl ring, displayed an M_1 EC_{50} of 2.3 μM , and high selectivity versus M_3 and M_5 (**Fig. 4**). Moreover, this analog afforded a ~ 5 -x left-shift of the M_1 ACh CRC at 10 μM , and a larger ~ 14 -x left-shift at 30 μM , with $\sim 30\%$ intrinsic allosteric agonism by Ca^{2+} mobilization assay.

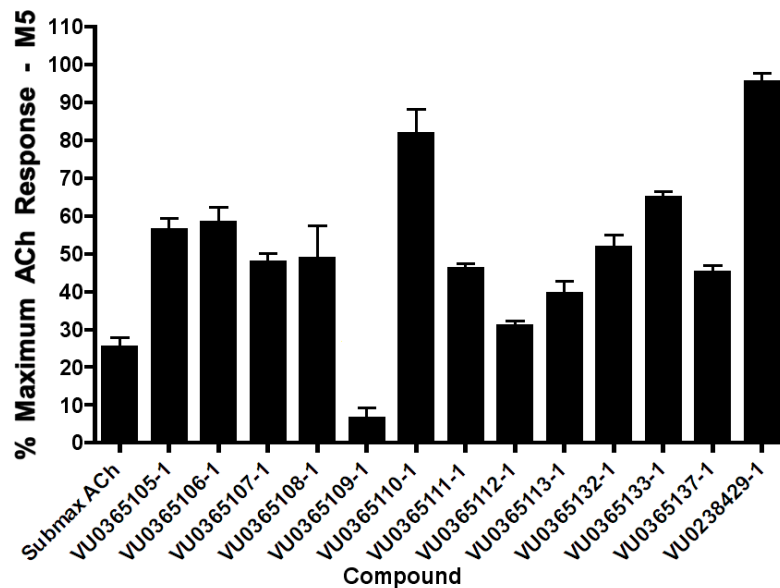
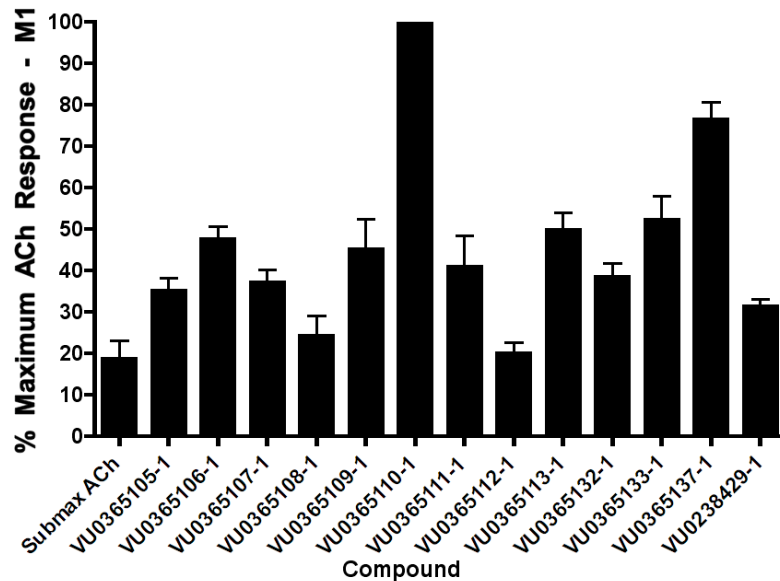


Figure 3. Singlepoint (10 μ M) M₁/M₅ screen of initial 12-member biaryl/heterobiaryl and phenethyl analog library based on VU0119498. Ca²⁺ mobilization assays were performed to obtain % ACh max values induced by each test compound in the presence of an ACh ~EC₂₀ with M₁ (top panel) and M₅ (bottom panel) CHO cells. Data represent Means +/- SEM from at least three independent determinations.

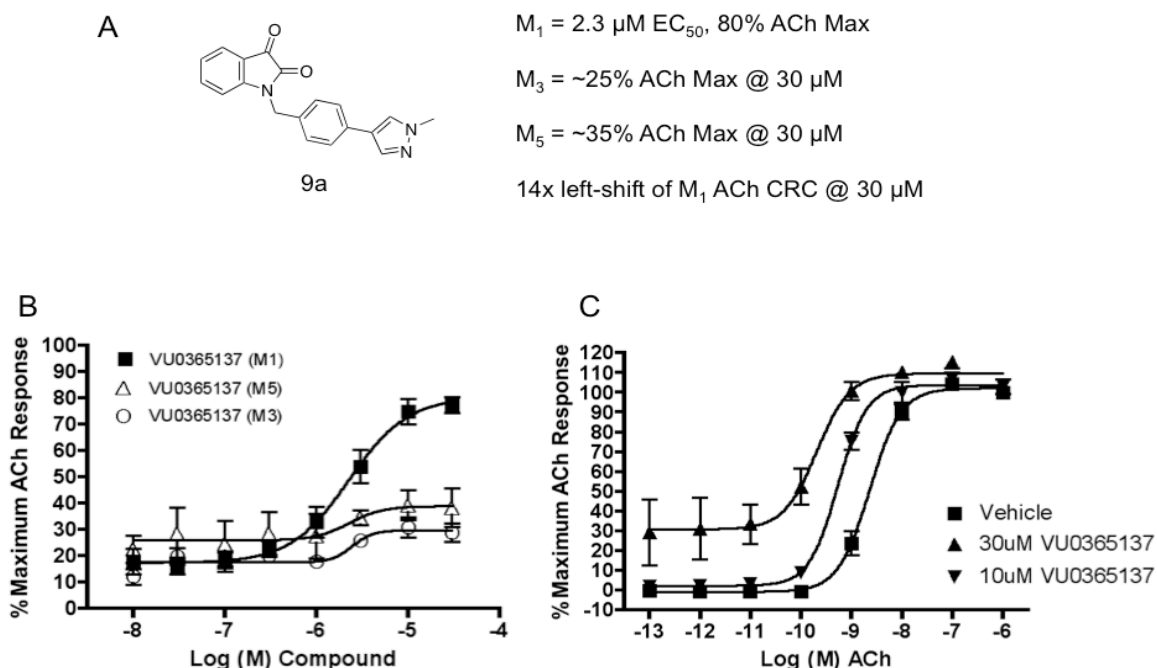


Figure 4. A) Structure and PAM activity of VU0365137; B) CRCs for VU0365137 in the presence of a ACh $\sim\text{EC}_{20}$ at M_1 , M_3 and M_5 ; C) ACh CRC fold-shift assay at M_5 with 10 μM and 30 μM VU0365137, providing an $\sim 5\text{x}$ and $\sim 14\text{x}$ left-shift, respectively. Data represent means of at least three independent determinations with similar results using mobilization of intracellular calcium in M_1 , M_3 , or M_5 CHO cells.

Intriguingly, the 5-OCF₃ congener of VU0365137 (compound **9a**) was an equipotent M_5 -preferring PAM (as reported in Chapter IV), highlighting the ‘molecular switch’ to engender M_5 preference. Despite this shallow SAR, it was exciting to see that we could rapidly obtain an M_1 -preferring PAM from our initial M_1 , M_3 , M_5 PAM lead via this small analog library.

We next incorporated subtle changes, in the form of fluorine atoms, to the lead VU0365137 scaffold. The rationale for these modifications stemmed in part from SAR around the Merck M_1 PAM BQCA series, which demonstrated that mono- or di-fluoro substitution in the *ortho* positions(s) of the southern benzyl ring and/or on the western aryl ring of the core headpiece conferred increased potency/efficacy (discussed later in

this chapter). Following the synthetic route outlined previously in **Figure 2**, analogs with fluorine on both the isatin core and the southern benzyl ring were readily prepared and evaluated for their ability to potentiate an \sim EC₂₀ of ACh at M₁ via Ca²⁺ mobilization.

This SAR revealed that fluorine substitution was well tolerated on both the isatin core (4,7-difluoro or 7-fluoro) and on the benzyl ring (2-fluoro and 2,6-difluoro), as shown in **Table 1**. The addition of a single fluorine atom to the 2-position of the benzyl ring delivered VU0366369 with an M₁ EC₅₀ of 830 nM (65% ACh max) – comparable to BQCA (M₁ EC₅₀ = 845 nM) and advantageously without the problematic carboxylic acid moiety (**Table 1**). This single change caused an approximately 3-fold increase in potency over VU0365137. A 2,6-difluorobenzyl congener (VU0366368) provided equivalent M₁ potency with a slightly diminished ACh max response (60%), as shown in **Table 1**. However, as fluorine content increased (compounds **12c-12e**; fluoro-substitutions on both the isatin core and benzyl ring) ACh max values decreased (40-55%) despite retention of comparable potencies (**Table 1**).

Table 1. SAR of fluorine-bearing analogs of lead compound VU0365137. Ca^{2+} mobilization assays were used to obtain CRCs for each analog in M_1 cells in the presence of an ACh $\sim\text{EC}_{20}$. Data represent Mean values from at least three independent determinations.

12

Cmpd	VU Number	Compound	$\text{M}_1 \text{EC}_{50}$ (μM) ^a	% ACh Max ^a
12a	0366369		0.83	65
12b	0366368		0.86	60
12c	0366370		2.3	55
12d	0366367		1.1	40
12e	0366372		1.2	50

Gratifyingly, VU0366369 was found to be a highly selective M_1 PAM, with minimal/no activation of M_2 - M_5 up to 30 μM (**Fig. 5a-b**). However, in M_1 ACh CRC fold-shift experiments, this compound as well as the di-fluoro congener (compound **12b**) displayed only a subtle effect, increasing the potency of ACh by only 3x and 2x

respectively, at 30 μ M (**Fig. 5c**). Lack of correlation between PAM potency and fold-shift is commonly observed within series of mAChR allosteric modulators and underscores the importance of determining both parameters when establishing SAR.

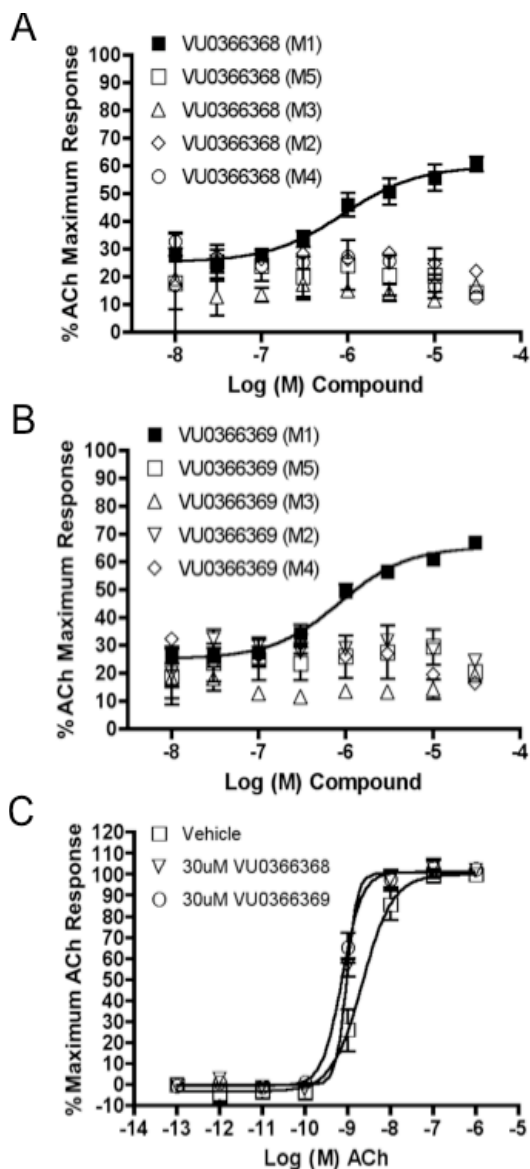


Figure 5. A) and B) CRCs for VU0366368 (compound **12b**) and VU0366369 (compound **12a**) in the presence of a ACh \sim EC₂₀ at M₁, M₂/G_qi₅, M₃, M₄/G_qi₅ and M₅; C) M₁ ACh CRC fold-shift assay with 30 μ M of VU0366369 and VU0366368, providing an approximately 3- and 2-fold-shift, respectively. Data represent Mean of at least two independent determinations with similar results using mobilization of intracellular calcium in M₁, M₂/G_qi₅, M₃, M₄/G_qi₅ and M₅ CHO cells.

Thus, optimization of the M₁, M₃, M₅ PAM HTS hit VU0119498, which previously led to the discovery of the first selective M₅ PAM (VU0400265), provided VU0366369, a highly selective and potent M₁ PAM, which represented only the second known M₁ PAM chemotype; however, it has modest efficacy. Furthermore, the ability to dial in or out M₁ and M₅ PAM activity within a single scaffold is unprecedented.

Interestingly, gem-difluorination of the 3-position on the isatin core within this series of M₁ PAMs resulted in substantially reduced potency and efficacy (data not shown), in stark contrast with the increased potency, efficacy, and subtype-selectivity conferred by this modification in the related M₅ PAM series (Chapter IV). However, replacement of the naked isatin core with a homologous cyclic carbamate ring system within the original VU0365137 M₁ PAM lead scaffold using the same alkylation conditions shown in **Figure 2** provided VU0366367. In Ca²⁺ mobilization CRC experiments at M₁ in the presence of an ACh ~EC₂₀, this analog exhibited similar potency and efficacy as the isatin-bearing parent, with an EC₅₀ of 1.4 μM and 65% ACh max response (**Fig. 6**). This is a highly desirable modification to the scaffold as the cyclic carbamate core is more drug-like and does not carry the DMPK-related liabilities of the isatin core. Further optimization of this cyclic carbamate series in the form of additional southern biaryl/heterobiaryl substitutions is currently underway; however, early data suggest that SAR around this series is relatively flat and no subtype-selectivity is known.

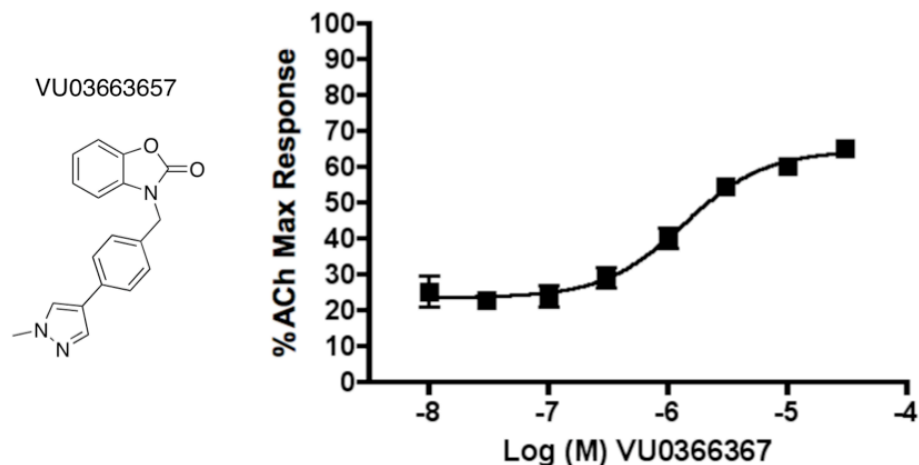


Figure 6. Structure and M₁ PAM CRC for VU03663657. Ca²⁺ mobilization assays were performed to obtain a CRC of VU03663657 in the presence of an ACh ~EC₂₀ with M₁ cells. Data represent Means +/- SEM from at least three independent determinations.

M₁ PAMs VU0028767 and VU0090157

As in Chapter IV, other novel M₁ PAMs such as VU0028767 and VU0090157 were identified by same HTS that identified VU0119498 (**Fig. 7**)²⁷. Optimization of these compounds was of lesser priority and a limited investigation into SAR around these two hits found extremely shallow SAR. Any change to the VU0028767 structure resulted in a complete loss of M₁ PAM activity (data not shown), and resynthesis of the hit itself following HTS identification produced spurious results that may have been due to chemical instability of the structure (**Fig. 7**). For these reasons, further attempts at VU0028767 optimization were not pursued. In a similar vein, SAR revealed by a series of VU0090157 analogs was quite flat; however, replacement of the nitro group on VU0090157 with bromine was tolerated for M₁ PAM activity, as was deletion of the southern *N*-methyl moiety (data not shown).

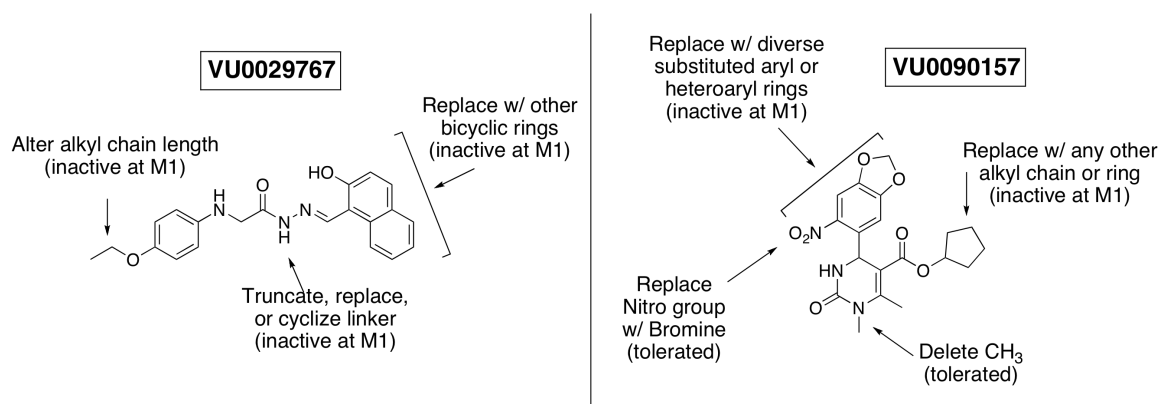


Figure 7. SAR summary for M₁ PAM HTS hits VU0029767 and VU0090157.

Any changes to the eastern ester side-chain in the form of alternative linear alkyl (e.g. ethyl, propyl, etc...) or cyclo alkyl (e.g. cyclobutyl, cyclohexyl, etc...) substituents resulted in complete loss of M₁ PAM activity (data not shown). Likewise a more exhaustive exploration of replacements for the nitro-piperonyl headpiece in the form a diverse 17-member library revealed that modification to this northern region compromises M₁ PAM activity (**Fig. 8, Fig. 9**).

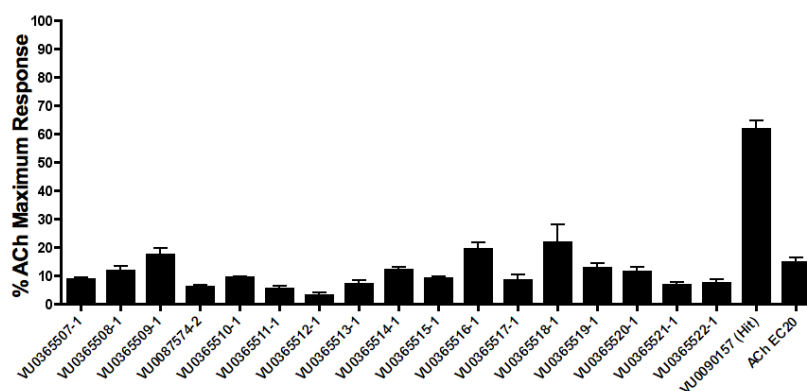


Figure 8. Singlepoint (10 μM) M₁ PAM screen of VU0090157 analogs bearing diverse northern substitutions. Ca²⁺ mobilization assays with M₁ cells were used to obtain % ACh max values for each compound in the presence of an ACh ~EC₂₀. Parent hit compound included as positive control. Data represent Mean ± SEM from at least three independent determinations.

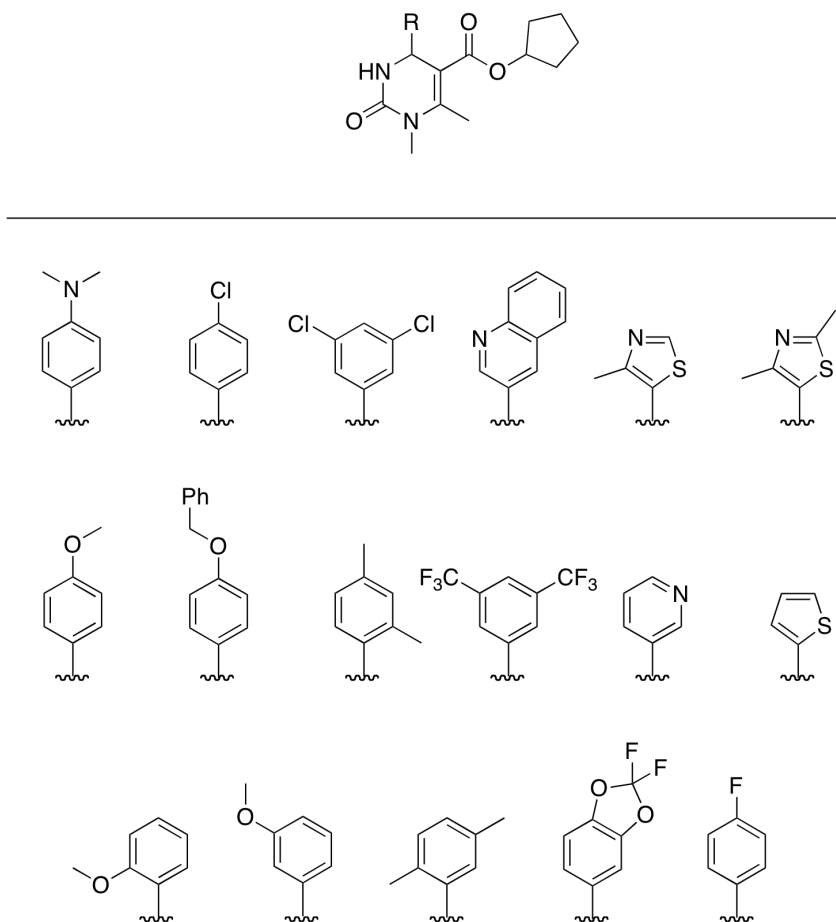


Figure 9. Structures of VU0090157 analogs generated to explore SAR at the northern headpiece.

M₁ PAM BQCA and analogs

Concomitant with discovery of the novel and diverse M₁ PAM scaffolds from the VU HTS campaign and the subsequent optimization of the VU0119898 to obtain the series of M₁ PAMs (e.g. VU0365137 and VU0366369), Merck disclosed a series of novel M₁ PAMs based on a substituted benzyl quinolone carboxylic acid template¹³⁶. The main exemplified compound bore a *p*-methoxybenzyl substitution on the naked quinolone carboxylic acid core and was subsequently termed BQCA¹³⁷. This compound was

reported to exhibit robust PAM activity at human M₁ with an EC₅₀ of 845 nM and a 50% ACh max intrinsic agonist activity at 100 μM in Ca²⁺ mobilization assays performed in the presence of a fixed ACh ~EC₂₀¹³⁷. In similar assays with human M₁ cells, BQCA was reported to induce a 130x left-shift of an ACh CRC at 100 μM¹³⁷. However, GPCR PAMs can display species specificity (as exemplified in the case of the M₄ PAM series discussed in Chapter III), and the activity of BQCA at the rat M₁ receptor were not initially reported. As discussed in the Introduction (Chapter I), a lack of truly-subtype selective M₁ activators with drug-like properties has precluded *in vivo* investigations into the role M₁ in both basic neurobiology and in the context of various CNS disorders such as Alzheimer's disease and schizophrenia. Therefore, attainment of an M₁ PAM suitable as an *in vivo* tool for use in basic and pre-clinical rodent studies would provide a major advancement to the field.

Thus, in order to determine whether BQCA and/or related compounds have properties needed for use in rodent studies, we resynthesized BQCA and a panel of 20 analogs to identify selective PAMs for the rat M₁ receptor¹³⁸. Three libraries were generated each consisting of seven compounds possessing the same *N*-benzyl substitutions on either an 8-fluorinated quinolone carboxylic acid (compounds **Ia-Ig**), a quinolone carboxylic acid (compounds **IIa-IIg**, including BQCA), or a 5,8-difluorinated quinolone carboxylic acid (compounds **IIIa-IIIg**) template, respectively (**Fig. 10**).

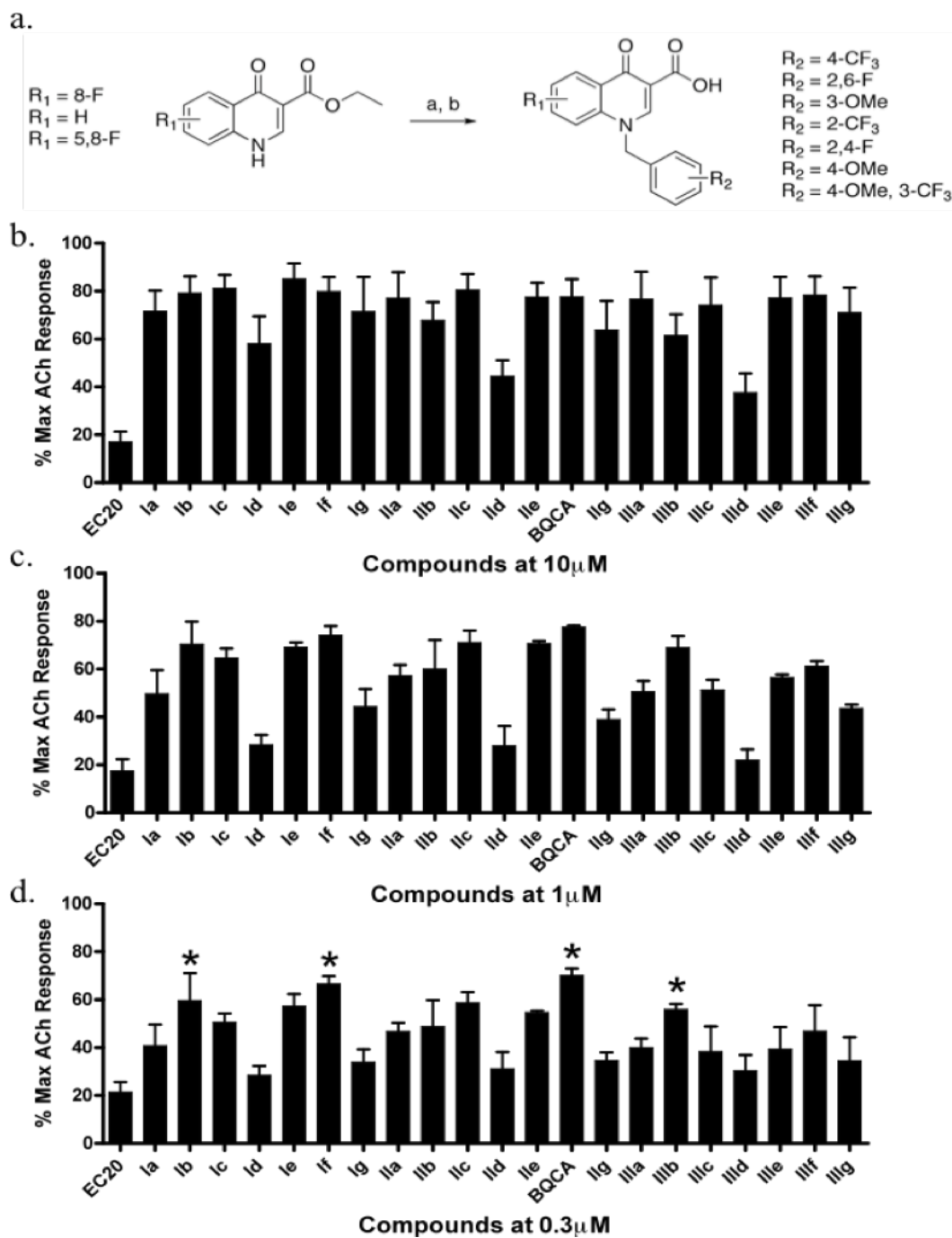


Figure 10. Synthesis and screening of BQCA and BQCA analogs at rat M₁. a.) reagents and conditions: a. K₂CO₃, KI, R-Br, DMF, 24 hr. at r.t., b. LiOH, 9:1 THF:H₂O 10 min. 120 °C μwave. Ca²⁺ mobilization assays with rat M₁ cells were used to obtain singlepoint % ACh max values for each compound at b.) 10 μM, c.) 1 μM, or d.) 0.3 μM in the presence of an ACh ~EC₂₀. Four compounds, denoted by an asterisk (*), were selected for further evaluation based on their structural diversity and efficacy at 0.3 μM. Data represent the mean ± S.E.M. of 3 independent determinations. Experiments performed by A. Brady.

The activity of BQCA and related compounds was evaluated by measuring effects on Ca^{2+} mobilization of each compound at 10, 1, or 0.3 μM (Fig. 10b-d) prior to the addition of an $\sim\text{EC}_{20}$ concentration of ACh. From the panel, four compounds (one of which was parent BQCA) that exhibited robust potentiator activity at 0.3 μM were selected for further evaluation based on their structural diversity (Fig. 10d). All four compounds had similar potencies at the rM_1 receptor, with EC_{50} values in the 200-400 nM range as determined by CRCs of each compound in the presence of an ACh $\sim\text{EC}_{20}$ by Ca^{2+} mobilization assay (Fig. 11a). Each of these four compounds elicited a robust increase in ACh potency at rat M_1 , as manifest by 10-23x left-shifts of an ACh CRC when applied at 3 μM in Ca^{2+} mobilization assays (Fig. 11b)

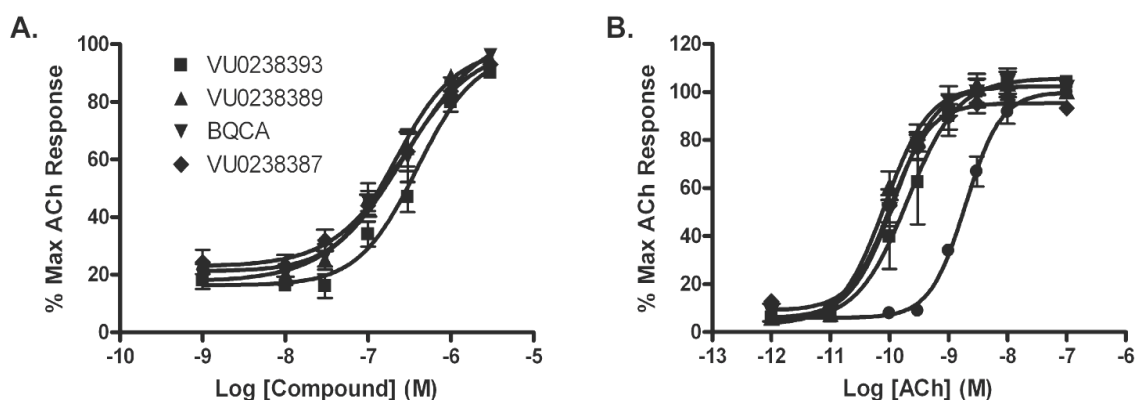


Figure 11. a) CRCs of BQCA and three analogs in the presence of an ACh $\sim\text{EC}_{20}$ at rat M_1 in Ca^{2+} mobilization assays (EC_{50} values: VU0238389 = 187 ± 39 nM; VU0238393 = 404 ± 59 nM; BQCA = 316 ± 102 nM; and VU0238387 = 284 ± 32 nM). b.) Ca^{2+} mobilization was used to obtain ACh CRCs in the absence and presence of each compound at 3 μM (fold-shifts: VU0238389 = 23x, VU0238393 = 10x, BQCA = 16x, and VU0238387 = 19x). Data represent the Mean \pm S.E.M. of 3 independent determinations. Experiments performed by A. Brady.

Following this survey of BQCA analog SAR at rat M_1 , which found a number of well tolerated southern benzylic substitutions as well as mono- and di-fluoro substitutions to the quinolone core, further *in vitro*, *ex-vivo*, and *in vivo* experiments were performed

using the parent BQCA compound due to the comparable potency/efficacy across these analogs. In radioligand binding experiments using rat M₁ cell membranes, BQCA lacked competition with the orthosteric antagonist [³H]-NMS at up to 10 μM and increased the affinity of ACh for rat M₁ by 31x at 3 μM (data not shown). These data provide strong evidence that BQCA potentiates ACh-induced M₁ activation via an allosteric enhancement of ACh affinity. Furthermore, BQCA lacked any agonist, PAM, or antagonist activity at a panel of 15 other GPCRs (including M₂-M₅) in Ca²⁺ mobilization assays performed by Millipore's GPCR Profiler Service™ (data not shown). In a single-dose (10 mg/kg IP) rat PK/PBL study, BQCA exhibited sub-optimal yet satisfactory pharmacokinetics with a brain:plasma AUC ratio of 0.09, a brain C_{max} of 1181 ng/mL at T_{max} 1 hr, and a brain T_{1/2} of 2 hr (data not shown).

Having thus determined that BQCA possessed acceptable rat M₁ potency/efficacy, selectivity, and systemic pharmacokinetics rendering it suitable for rodent electrophysiology experiments and behavioral studies, no further optimization or investigation into additional SAR for this series was performed. Nonetheless, these analogs and initial characterization experiments provided crucial evidence and rationale for the utility of BQCA as an acceptable small molecule tool for selective activation of rat M₁. A large-scale (30 g) batch of BQCA was prepared according to the scheme in **Figure 10a** as the Na⁺-salt, which was jet-milled and made available to collaborators in order to facilitate a range of M₁ neurobiology studies. Such investigations found that activation of M₁ induced a robust inward current and increased spontaneous excitatory post-synaptic currents (EPSCs) in medial pre-frontal cortical (mPFC) pyramidal cells in rodent brain slices, and that BQCA-mediated M₁ activation increased firing of mPFC

pyramidal cells and restored discrimination reversal learning in a transgenic mouse model of AD *in vivo*¹³⁸.

The BQCA M₁ PAM medicinal chemistry work was primarily focused on screening/assays with M₁ cells with the exception of subtype-selectivity confirmation at M₂-M₅ for BQCA itself. Analogs generated in the 20-member panel were not screened at any of the other mAChRs and it remained a question as to whether any structural modifications to the BQCA scaffold could confer PAM activity for subtypes other than M₁, similar to SAR findings with the VU0119498 *N*-benzyl isatin series of mAChR PAMs. Moreover, the fact that M₁-preferring/selective compounds as well as M₅-preferring/selective compounds could be obtained by subtle modification to the VU0119498 structure (Chapter IV), which is itself highly similar to the BQCA scaffold apart from the latter's carboxylic acid moiety, suggested that it may be possible to dial-in BQCA activity at other mAChRs. Specifically, we hypothesized that appending a western -OCF₃ group to the 6-position of the BQCA quinolone core would engender M₅ PAM activity in a manner analogous to its effect on the VU0119498-derived PAMs (Chapter IV).

To test this hypothesis, two singleton BQCA analogs were synthesized according to the scheme in **Figure 10a**, starting with the commercial 6-trifluoromethoxy quinolone carboxylate, which was then *N*-alkylated with *p*-methoxy and *p*-phenoxy benzyl halides to afford VU0400268 and VU0400269 (**Fig. 12**). These benzyl groups were selected because they represented two of the most favored/optimal southern moieties within the VU0238429-based M₅ PAM series. Each compound was then profiled in CRCs at M₅ in the presence of an ACh ~EC₂₀ by Ca²⁺ mobilization assay (**Fig. 12**). Surprisingly,

essentially no PAM activity was observed at up to 30 μ M for either compound, suggesting that the BQCA template is poorly compatible with M_5 binding and/or functional activity (Fig. 12).

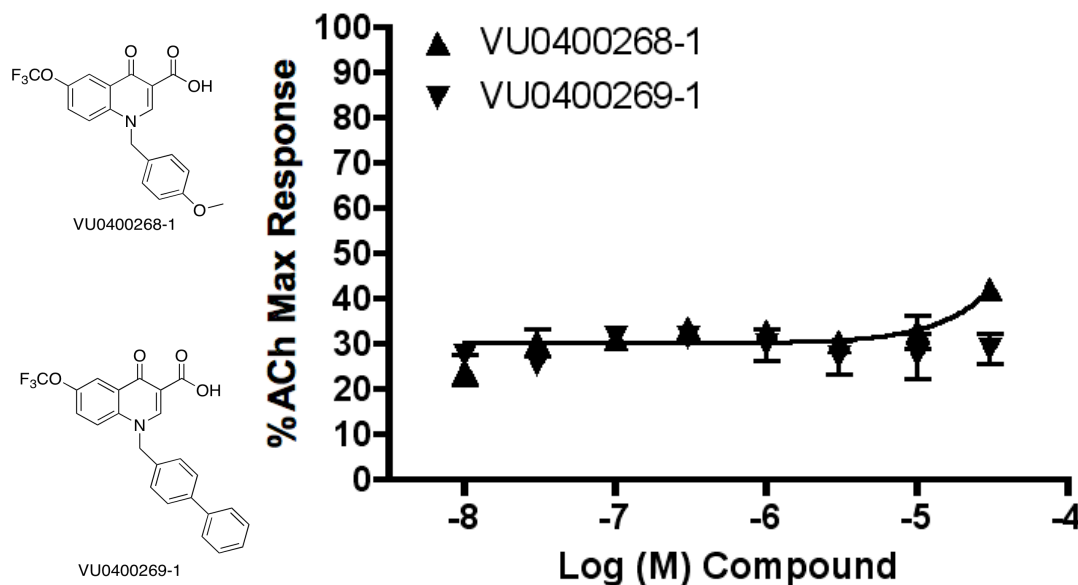


Figure 12. Structure and M_5 CRCs for BQCA-based analogs VU0400268 and VU0400269. Ca^{2+} mobilization was used to obtain CRCs of each compound in the presence of an ACh $\sim EC_{20}$ using M_5 cells. Data represent Mean \pm SEM from at least three independent determinations.

M_1 PAMs derived from MLPCN probe project

As part of the NIH Roadmap Initiative, the MLSCN/MLPCN comprises a nationwide consortium of small molecule screening and medicinal chemistry centers aimed at discovering and optimizing novel small molecules for molecular targets that lack known and/or acceptable tool compounds by which to study their role(s) in biology and disease. Given the scarcity of selective mAChR small molecules possessing drug-

like characteristics (Chapter I), an HTS of the then 65,000-member MLSCN/MLPCN compound collection was performed to identify novel M₁ ligands. This screen was performed while the mAChR PAM projects (Chapters III-V) were underway and prior to most of the associated publications/disclosures arising from our M₁ PAM discovery and optimization efforts. Utilizing a functional cell-based fluorescence assay that measured Ca²⁺ mobilization in rat M₁ CHO cells during first addition of a test compound followed by an ACh or CCh ~EC₈₀, this screen was originally designed to identify M₁ antagonist hits. Indeed, a number of novel M₁ antagonist series were obtained¹³⁹⁻¹⁴¹, which ultimately led to the discovery of the highly M₁-selective antagonist probe compound VU0255035 (discussed later in this Chapter)¹⁴⁰.

Following the HTS and subsequent M₁ antagonist medicinal chemistry work, the screening data were re-analyzed to look for compounds that elevated the ACh ~EC₈₀. Although this was not an ideal assay format for identification of PAMs, the data mining proved fruitful as approximately 200 compounds flagged as possible potentiators. These putative M₁ PAM hits were re-ordered from the commercial vendor and then screened in a singlepoint 30 μM PAM assay in the presence of an ACh ~EC₂₀ by Ca²⁺ mobilization in M₁ cells (**Fig. 13**). From this screen, only two compounds exhibited robust potentiation activity (VU0165202 and VU0108370) and were thus carried forward to further characterization (**Fig. 13**). Interestingly, both hits were based on the same benzyl-substituted indole sulfonyl amide bearing a distal methyloxazole and differed only a single halogen substitution on the southern benzyl ring (**Fig. 13**).

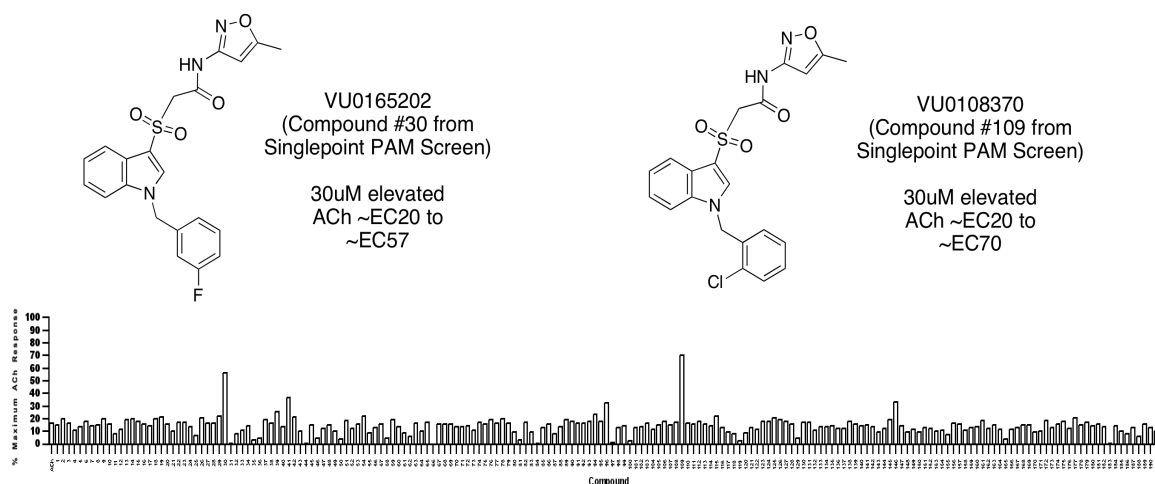


Figure 13. Structure of two M_1 PAM hits identified by 30 μM singlepoint screen of approximately 200 re-ordered putative PAMs identified from a functional M_1 antagonist HTS campaign. Ca^{2+} mobilization was used to obtain % ACh max values for each test compound at 30 μM in the presence of an ACh $\sim\text{EC}_{20}$ using M_1 cells. Data represent a single determination performed in triplicate.

In follow-up CRCs of each compound at M_1 in the presence of an ACh $\sim\text{EC}_{20}$, the 3-fluoro VU0165202 and the 2-chloro VU0108370 exhibited EC_{50} values of 5.5 μM and $>10 \mu\text{M}$, respectively (**Fig. 14**). These were exciting results as both compounds exhibited clear concentration-dependent potentiation of ACh at M_1 .

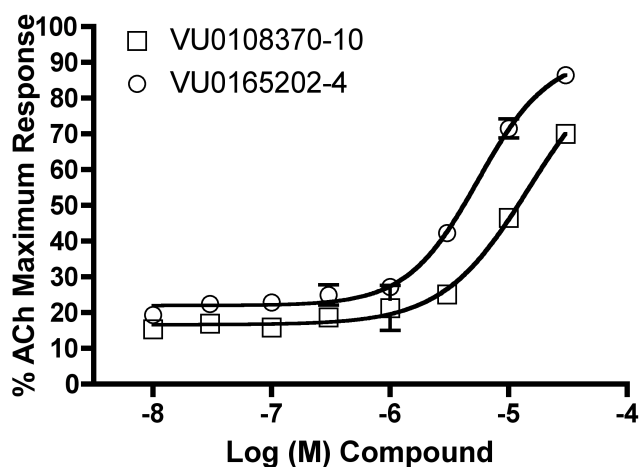


Figure 14. M_1 CRCs of PAM hits VU0108370 and VU0165202. Ca^{2+} mobilization was used to CRCs for each test compound in the presence of an ACh $\sim\text{EC}_{20}$ using M_1 cells (VU0165202 $\text{EC}_{50} = 5.5 \mu\text{M}$, VU0108370 $\text{EC}_{50} = >10 \mu\text{M}$). Data represent Mean \pm SEM from at least two independent determinations.

Initial optimization efforts focused on a wide range of modifications to the scaffold, including sequential truncation from both the southern and northern termini, as well as a number of diverse benzyl substitutions (**Fig. 15**). A total of 19 analogs as well as parent hit VU0108370 were prepared according to the scheme shown in **Figure 16**, which were then triaged for M₁ PAM activity at 10 μM in the presence of an ACh ~EC₂₀ by Ca²⁺ mobilization (data not shown).

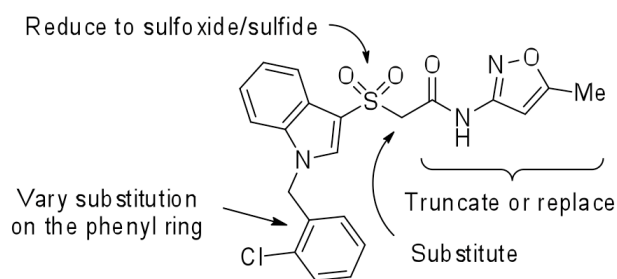


Figure 15. Initial optimization strategy for M₁ PAM hit VU0108370.

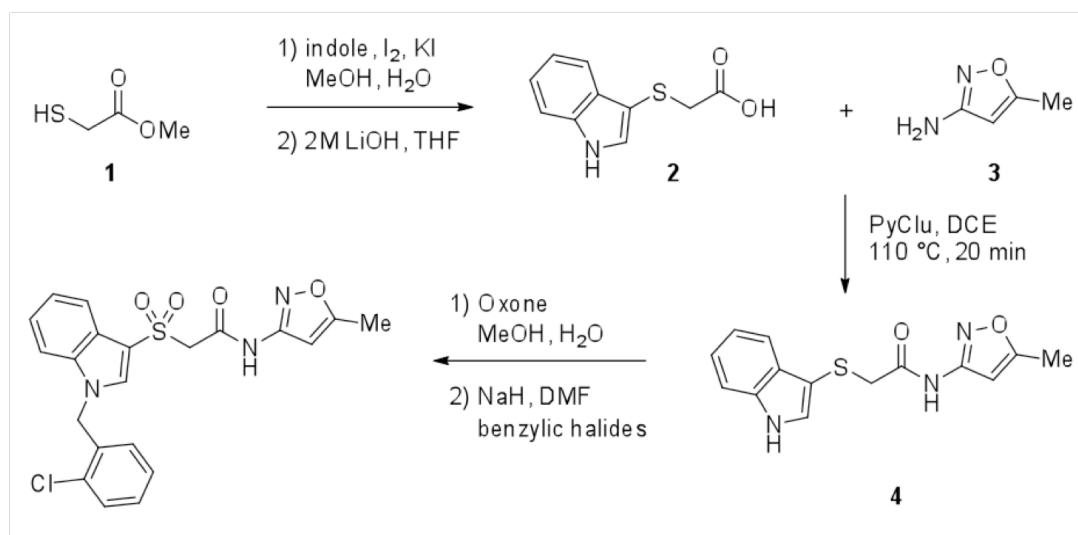


Figure 16. Synthesis of M₁ PAM hit VU0108370 used to generate southern benzyl-derivatized library. Syntheses performed by P. Reid.

Ultimately, three compounds were chosen for M₁ CRC assays to determine potencies (**Fig. 17**). These SAR data revealed that substitution of the *meta* position on the southern benzyl ring was favored, with the *m*-Cl analog specifically exhibiting the highest potency and efficacy (**Fig. 17**).

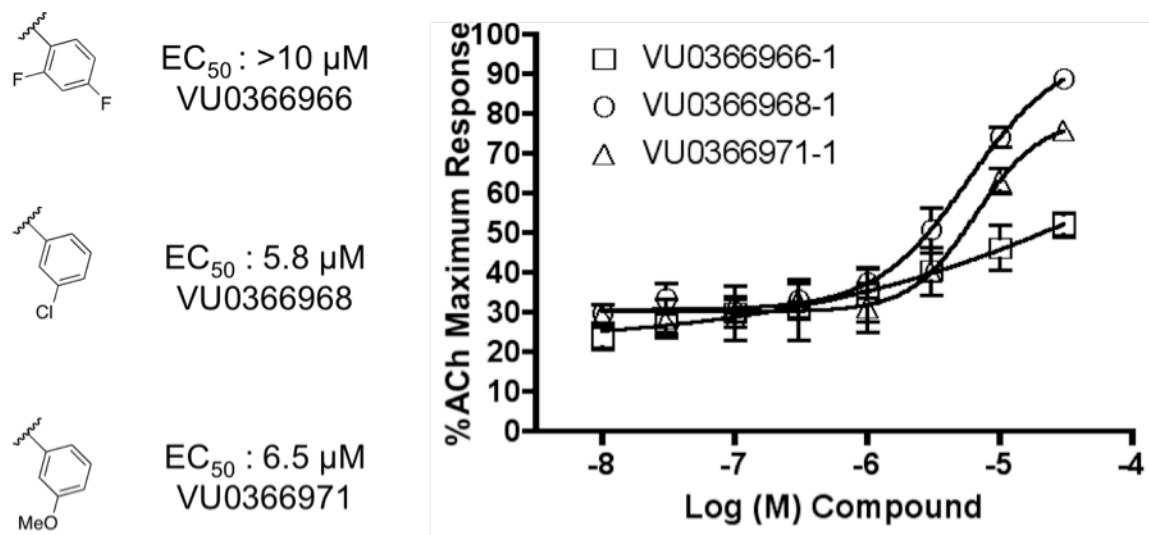


Figure 17. Structures and M₁ PAM CRCs of southern benzyl analogs based on the VU0108370 / VU0165202 scaffold identified from a larger singlepoint triage assay. Ca²⁺ mobilization was used to obtain CRCs each compound in the presence of an ACh $\sim EC_{20}$ using M₁ cells. Data represent Mean \pm SEM from at least three independent determinations.

Therefore, additional compounds containing *m*-bromine or *m*-*N*-methylpyrazine substitutions (the latter was chosen based on previous VU0119498-based M₁ PAM SAR) on the benzyl ring were synthesized as singletons using the general scheme presented in **Figure 16**. Simultaneously, sulfoxide and thioester congeners of the *m*-bromo compounds were prepared to explore the effect of sequential oxygen deletion from the central linker's sulfone (**Fig. 18**). Each of these compounds were then profiled in CRCs at M₁ in the presence of an ACh $\sim EC_{20}$ by Ca²⁺ mobilization assay (**Fig. 18**).

Gratifyingly, the *N*-methylpyrazole (VU0402606, $EC_{50} = 3.2 \mu\text{M}$) increased potency by approximately $\sim 2\times$ over the chlorine-bearing lead (VU0366368, $EC_{50} = 5.8 \mu\text{M}$) and exhibited a notable 102% maximal ACh response at M_1 (Fig. 18). The bromine-bearing analog (VU0402604, $EC_{50} = 3.8 \mu\text{M}$) was only slightly less potent, whereas the sulfoxide and thioether analogs (VU0402605 and VU040260) exhibited moderately weaker potency and inactivity, respectively (Fig. 18).

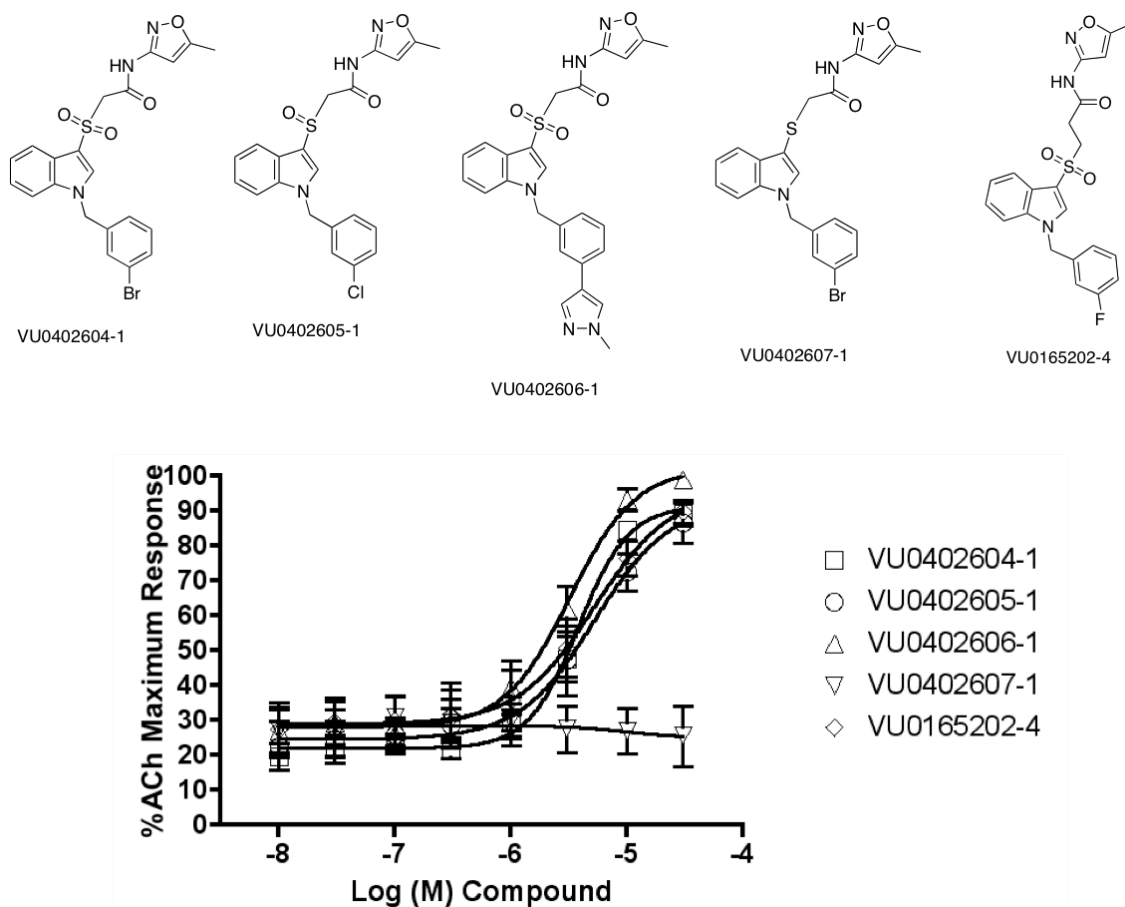
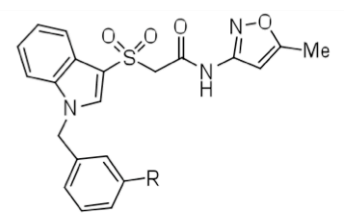
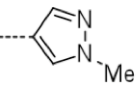
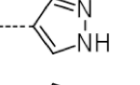
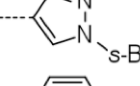
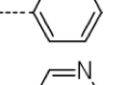
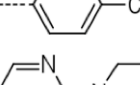
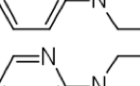
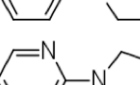
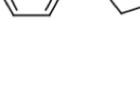


Figure 18. Structures and M_1 PAM CRCs of *meta*-substituted southern benzyl analogs based on the VU0108370 / VU0165202 scaffold. Ca^{2+} mobilization was used to obtain CRCs each compound in the presence of an ACh $\sim EC_{20}$ using M_1 cells (EC_{50} values: VU0402604 = $3.8 \mu\text{M}$, VU0402605 = $5.2 \mu\text{M}$, VU0402606 = $3.2 \mu\text{M}$, VU0402607 = $>30 \mu\text{M}$, VU0165202 included as positive control). Data represent Mean \pm SEM from at least three independent determinations.

These SAR data suggested that, like the VU0119498- and BQCA-related M₁ PAMs, biaryl/heterobiaryl southern motifs are favored for increased potency/efficacy. To further explore such substitutions, the *m*-bromo compound was used as starting material for microwave-assisted Suzuki couplings to obtain a small parallel library of biaryl/heterobiaryl analogs using standard conditions. These were then evaluated in CRCs at M₁ in the presence of an ACh ~EC₂₀ by Ca²⁺ mobilization assay (**Table 2**).

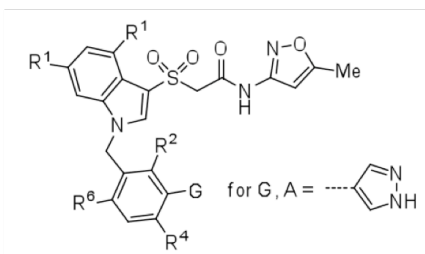
Table 2. SAR for 3-position biaryl/heterobiaryl analogs based on VU0402606. Ca²⁺ mobilization was used to obtain compound CRCs in the presence of an ACh ~EC₂₀ with M₁ cells. Data represent Mean values from at least three independent determinations. Syntheses performed by P. Reid.



R	M ₁ EC ₅₀ (μM)	%ACh Max
	3.21	102
	2.19	90
	> 10	-
	> 10	-
	> 10	-
	> 10	-
	> 10	-
	> 10	-

Of these, only the parent *N*-methylpyrazole and its desmethyl congener exhibited robust M₁ PAM activity. Interestingly, the deletion of the methyl group conferred a subtle increase in potency but simultaneously reduced efficacy (VU0404010, EC₅₀ = 2.2 μM, 90% ACh max). We concluded that the pyrazole would thus be held constant and hypothesized for our next iteration of synthesis that fluorination of the benzyl ring and/or indole core in a manner homologous to that of the VU0119498-derived and BQCA M₁ PAMs would confer a modest increase in potency. In order to test this hypothesis, a library of fluorinated analogs was prepared according to general scheme of **Figure 16**. These compounds were then profiled in CRCs at M₁ to determine potency (**Table 3**).

Table 3. SAR for fluorinated analogs based on VU0404010 lead. Ca²⁺ mobilization was used to obtain compound CRCs in the presence of an ACh ~EC₂₀ with M₁ cells. Data represent Mean values from at least three independent determinations. Syntheses performed by P. Reid.



G	R ¹	R ²	R ⁴	R ⁶	M ₁ EC ₅₀ (μM)	%ACh Max
A	H	H	F	H	> 10	-
Br	H	H	F	H	> 10	-
Cl	H	H	F	H	> 10	-
Br	F	H	H	H	5.37	103
A	F	H	H	H	1.85	102
Cl	H	F	H	H	5.10	56
Br	H	F	H	H	> 10	-
A	H	F	H	H	4.40	103
A	H	H	H	F	3.07	96
Br	H	H	H	F	1.38	84

This effort proved fruitful as the 3-bromo,6-fluorobenzyl analog exhibited the highest potency of any compound in this series (VU0405652, $EC_{50} = 1.4 \mu\text{M}$, **Table 3**). 4,6-difluorination of the indole core in combination with the des-methylpyrazole in the 3-position of the benzyl ring provided a similarly potent analog (VU0405645, $EC_{50} = 1.9 \mu\text{M}$, **Table 3**). With such potencies, these two new leads had reached the general criteria for an M_1 PAM probe compound and were therefore carried into further characterization with a concurrent halt in medicinal chemistry. At $30 \mu\text{M}$, both compounds exhibited large ($\sim >45\text{-}100\text{x}$) ACh CRC fold-shifts at rat M_1 by Ca^{2+} mobilization assay (**Fig. 19**), which is comparable to the magnitude of potentiation induced by BQCA at human M_1 .

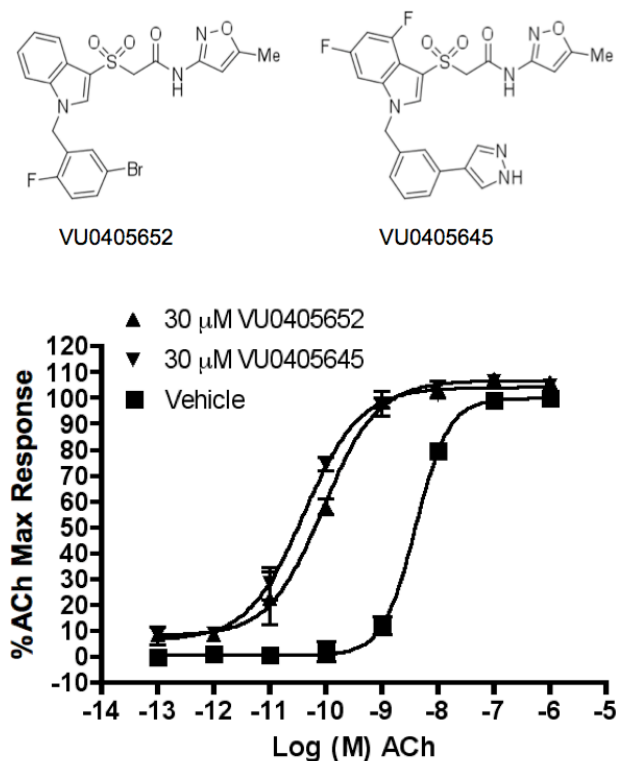


Figure 19. Structure and ACh CRC fold-shifts for M_1 PAM leads VU0405652 and VU0405645. Ca^{2+} mobilization was used to obtain CRCs for ACh in the absence and presence of $30 \mu\text{M}$ test compound using M_1 cells (VU0405652 = 45x left-shift, VU0405645 = 98x left-shift). Data represent Mean \pm SEM from at least three independent determinations.

Although we had thus obtained potent and efficacious M₁ PAMs of a novel HTS-identified drug-like chemotype from this medicinal chemistry effort, subtype-selectivity remained a question for these final lead/probe compounds. Throughout the optimization campaign, both of the parent HTS hits (VU0165202 and VU0108370) as well as various intermediate lead compounds from the project were evaluated in CRCs in the presence of an ACh ~EC₂₀ at M₃ and M₅ by Ca²⁺ mobilization assays (**Fig. 20**). This was performed due to the higher likelihood that any loss of subtype-selectivity would first manifest at one or both these two off-target mAChRs given the higher structural homology amongst M₁/M₃/M₅ and based on the SAR from the other M₁ PAM series. None of these compounds exhibited any potentiation at either subtype (**Fig. 20**).

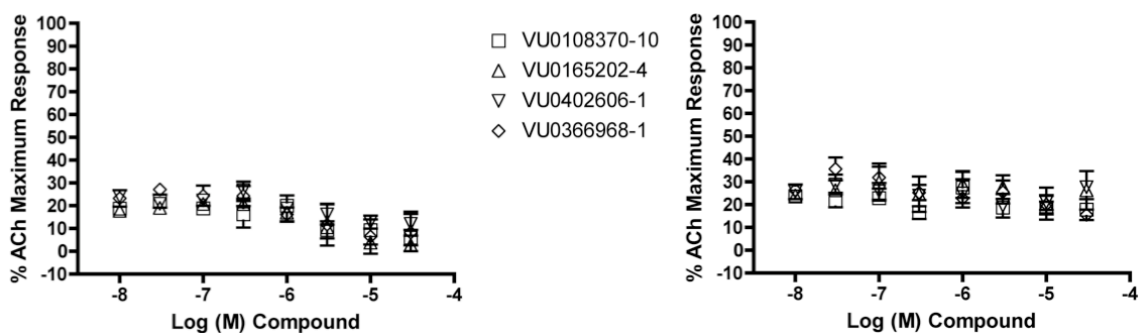


Figure 20. M₃ and M₅ subtype-selectivity CRCs for original M₁ PAM HTS hits and select intermediate lead analogs. Ca²⁺ mobilization was used to obtain CRCs for each compound in the presence of an ACh ~EC₂₀ using M₃ (left panel) or M₅ (right panel) cells. Data represent Mean +/-SEM from at least three independent determinations.

However, to definitively assess full subtype-selectivity for the final probe compound VU0405652, CRC assays at M₂-M₅ were performed in the presence of an ACh ~EC₂₀ by Ca²⁺ mobilization assay. These experiments revealed complete selectivity for M₁ at up to 30 μM, further supporting the conclusion that this chemical series represents a third known chemotype of M₁-selective PAMs in addition to the VU0119498- and

BQCA-derived series (**Fig. 21**). Furthermore, this particular probe (VU0405652) possessed favorable physiochemical and drug-like properties in the form of relatively high aqueous solubility ($c\text{LogP} = 3.9$) and a general lack of obvious DMPK liabilities. Despite their high selectivity for M_1 in functional PAM assays, it remains unknown if these novel compounds exhibit true binding specificity for M_1 or if they indeed bind to one or more of the other mAChRs but exhibit neutral or negative modulatory effects. Further experiments to address this question as well as a number of *in vitro* and *in vivo* studies aimed at studying M_1 neurobiology and therapeutic relevance have been planned and are presently underway.

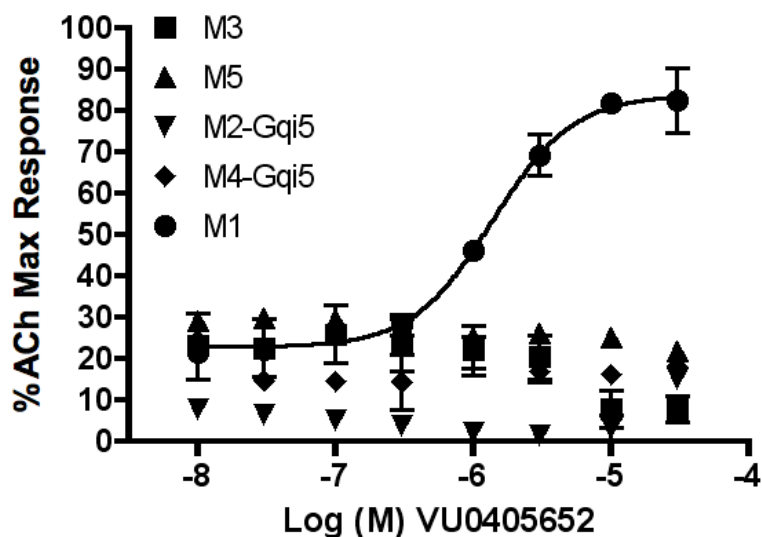


Figure 21. mAChR subtype-selectivity for probe compound VU0405652. Ca^{2+} mobilization was used to obtain CRCs in the presence of an ACh $\sim\text{EC}_{20}$ in M_2 - M_5 cells (EC_{50} values all $> 30 \mu\text{M}$). Data represent Mean \pm SEM from at least three independent determinations.

As a final effort to mine the VHTSC compound collection for additional SAR and/or identify new related scaffolds around this series of novel M_1 PAMs, a structure similarity search was performed using via a cheminformatic approach. This virtual

screen produced a large number of compounds within the VU collection, which possessed varying degrees of similarity to the basic VU0108370 scaffold. To assess M₁ PAM activity, these compounds were screened at 10 μM in singlepoint Ca²⁺ mobilization assays at M₁ in the presence of an ACh ~EC₂₀ (**Fig. 22**). Remarkably, only direct congeners of the VU0108370 scaffold appeared as active hits, which further confirmed the shallow SAR observed among this series of M₁ allosteric modulators.

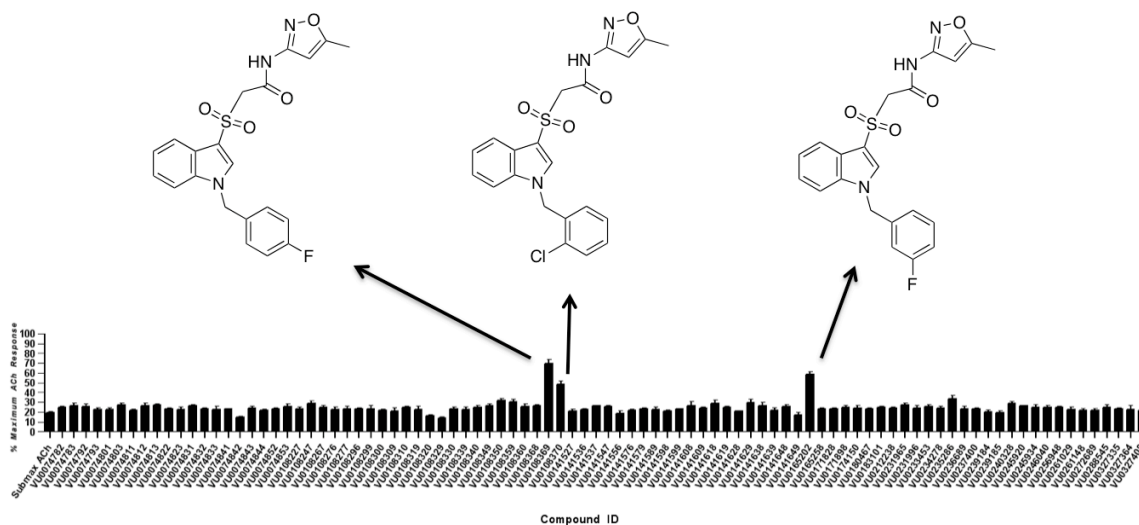


Figure 22. Singlepoint (10 μM) screen of a large panel of compounds from the VU HTS collection identified from a VU0108370-based structure similarity virtual screen. Ca²⁺ mobilization was used to obtain singlepoint (10 μM) % ACh max responses for each compound in the presence of an ACh ~EC₂₀ using M₁ cells. Data represent Mean +/-SEM from at least three independent determinations.

M₁ agonist VU0357017 and analogs

Although a number of useful M₁ PAM small molecule tools had been identified from the medicinal chemistry projects, no M₁ agonists possessing optimal potency,

selectivity, and DMPK characteristics required for use as *in vivo* tools existed. As discussed in the Introduction (Chapter I), a variety of compounds have been reported to activate the M₁ receptor in the absence of ACh with high subtype-selectivity. However, these compounds (such as AC-42, 77-LH-28-1, NDMC, and TBPB) all suffered from one or more flaws that precluded universal suitability as both *in vitro* and *in vivo* tools for studying M₁ neurobiology and the therapeutic potential of M₁ activation. Such defects include, for example, functional antagonism of one or more of the other mAChRs, significant off-target ancillary pharmacological activities, and/or poor systemic PK profiles. Therefore, it would be highly advantageous to discover novel drug-like M₁ agonist chemotype(s) that don't suffer from these and related limitations. Direct activation of M₁ in the absence of ACh is likely to reveal deeper neurobiological insight than reliance on M₁ PAMs alone, and M₁ agonists may offer therapeutic advantages over PAMs in treatment of certain CNS disorders. Furthermore, a growing body of evidence suggests that ligand-directed bias/signaling downstream of a given GPCR target may confer substantially different utilities/effects unique to each small molecule chemotype¹¹⁷. In light of these considerations, identification of a novel class of M₁ agonists became a focus of our research and of the MLSCN/MLPCN probe discovery enterprise. A comprehensive presentation and discussion of this project, which ultimately identified a number of novel allosteric M₁ agonists, including VU0357017, lies beyond the scope of this Chapter¹⁴². However, a brief overview highlighting this author's contribution is shown in the remainder of this section.

Similar to many of the mAChR allosteric ligand discovery projects, a HTS was performed of the then 65,000-member MLSCN/MLPCN compound collection aimed at

discovering novel M₁ agonists via functional cell-based fluorescent Ca²⁺ mobilization assay. This screen provided approximately 2,000 putative agonist primary hits. A subset of these compounds were tested in CRCs with M₁-CHO cells, and in parallel, counter screened against M₄/G_{q15} CHO cells using Ca²⁺ mobilization assays. Two highly structurally-similar hits, resynthesized as VU0207811 and VU0177548, were found to be initially selective (>50-fold) for M₁ vs. M₄ with M₁ EC₅₀ values of 804 nM (69% ACh max) and 1.74 μM (52% ACh max), respectively, and both later displayed high selectivity for M₁ versus all other mAChRs (**Fig. 23**). These compounds provided an excellent starting point to initiate a chemical optimization effort aimed at increasing potency and developing properties suitable for studies of selective M₁ activation *in vivo*.

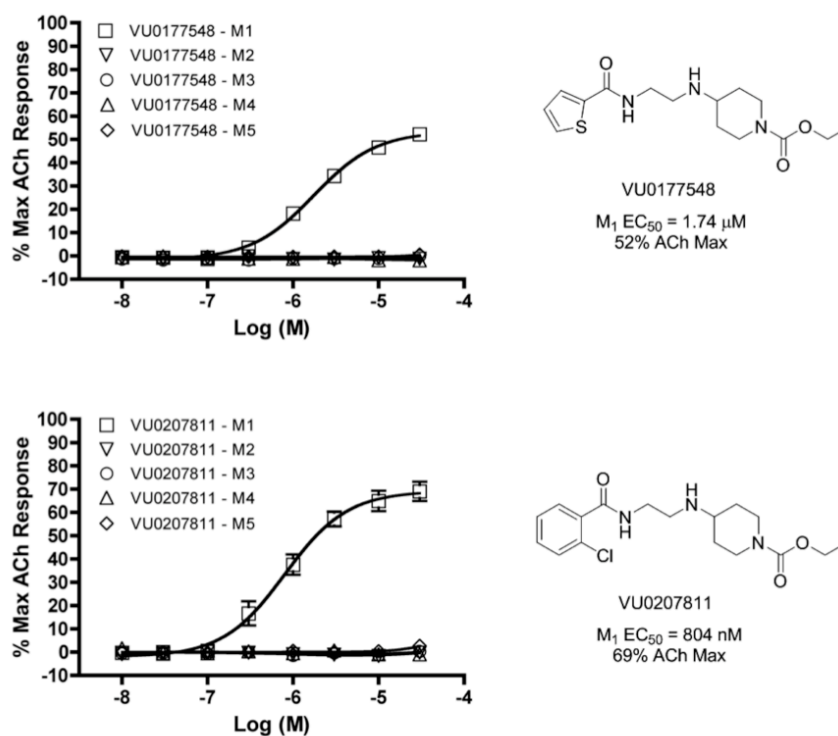


Figure 23. Structure and subtype-selectivity profiles of novel M₁ agonist HTS hits. Ca²⁺ mobilization was used to obtain CRCs of each compound in M₁-M₅ cells. Data represent Mean \pm SEM from at least three independent determinations. Syntheses performed by P. Kennedy.

Subsequently, medicinal chemistry began with synthesis of a 25-member matrix library, which simultaneously varied the western aryl, central linker, and eastern carbamate of the scaffold (data not shown). From singlepoint screening of this library using Ca^{2+} mobilization with M_1 cells (data not shown), it became clear that SAR was steepest at the western aryl region and progressively shallower throughout the remainder of the scaffold. A variety of substituted phenyl moieties were well tolerated (**Fig 24, top panel**); however, a wide range of further modifications to the central linker and eastern carbamate resulted in complete loss of M_1 activity (**Fig. 24, bottom panel**).

Cmpd	Structure	M1 EC ₅₀	%ACh _{max}
VU0184670		152 nM	85
VU0357017		198 nM	81
VU0359993		154 nM	79
VU0359995		154 nM	72
VU0360014		459 nM	80
VU0360010		>10 μM	13

Diagram illustrating SAR modifications that abolish M_1 activity:

- Basic heterocycles abolish M_1 activity
- N-Me inactive
- β -fluorination abolishes M_1 activity
- Alternate carbamates amides or amines abolish M_1 activity
- Alternate chain lengths inactive
- N-Me inactive
- Electron Donating and withdrawing moieties tolerated

Figure 24. M_1 agonist SAR revealed by initial matrix library and singleton syntheses. Ca^{2+} mobilization was used to obtain CRCs of each compound with M_1 cells. Data represent Mean \pm SEM from at least three independent determinations. Syntheses and experiments performed by E. Lebois.

Of these early analogs, the naked phenyl-bearing VU0184670 and its 2-methyl congener VU0357017 exhibited the greatest balance of M₁ potency and efficacy (**Fig. 24, top panel**). Therefore, they were selected for further *in vitro* characterization in subtype-selectivity (**Fig. 25**), M₂-M₅ functional antagonism (**Fig. 26**), and [³H]-NMS competition binding (**Fig. 27**) assays. Similar to the parent HTS hits, neither VU0184670 nor VU0357017 exhibited any activation of M₂-M₅ at up to 30 μM (**Fig. 25**). Furthermore, they possessed little to no functional antagonism of an ACh ~EC₈₀ at these other mAChRs, in contrast to the M₁ agonist TBPB control (**Fig. 26**). Consistent with an allosteric mode of binding, both compounds failed to compete with the orthosteric radioligand [³H]-NMS for binding to M₁-M₅ membranes at up to 10 μM; however, moderate inhibition was observed at 30 μM (**Fig. 27**). Whether or not this represents orthosteric competition or negative cooperativity via an allosteric site remains to be determined.

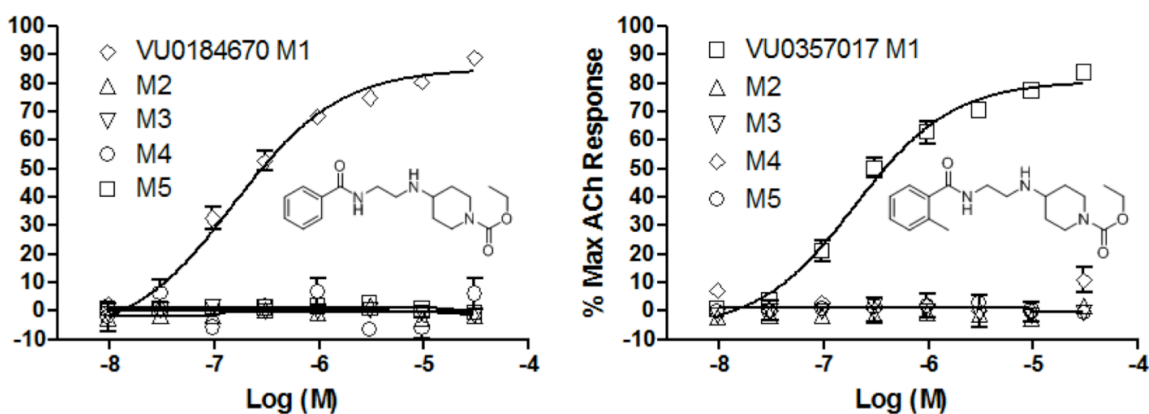


Figure 25. mAChR subtype-selectivity profiles of M₁ agonist leads VU0184670 and VU0357017. Ca²⁺ mobilization was used to obtain CRCs of each compound with M₁-M₅ cells. Data represent Mean +/-SEM from at least three independent determinations.

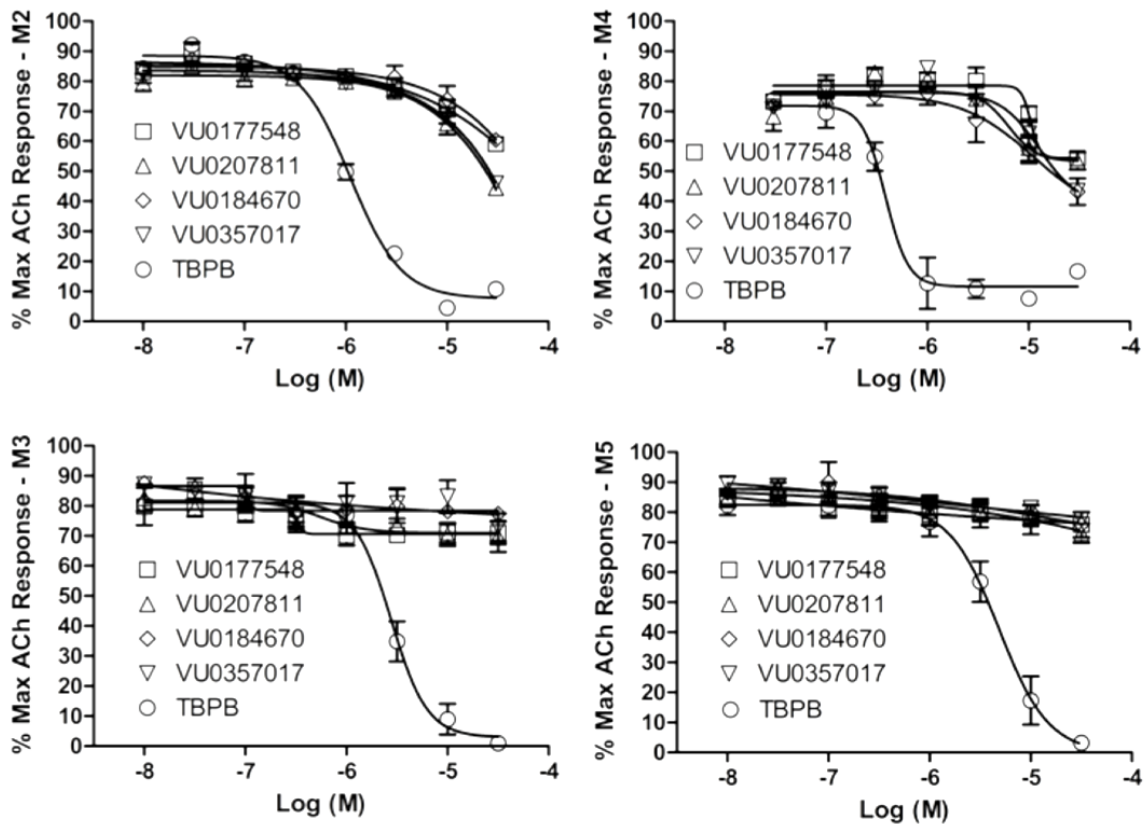


Figure 26. M₂-M₅ functional antagonism profiles of M₁ agonist leads VU0184670 and VU0357017 as well as parent hits VU0177548 and VU0207811. Ca²⁺ mobilization was used to obtain CRCs of each compound in the presence of an ACh ~EC₈₀ with M₂-M₅ cells. TBPB included as positive control. Data represent Mean +/-SEM from at least three independent determinations. Experiments performed in part by E. Lebois.

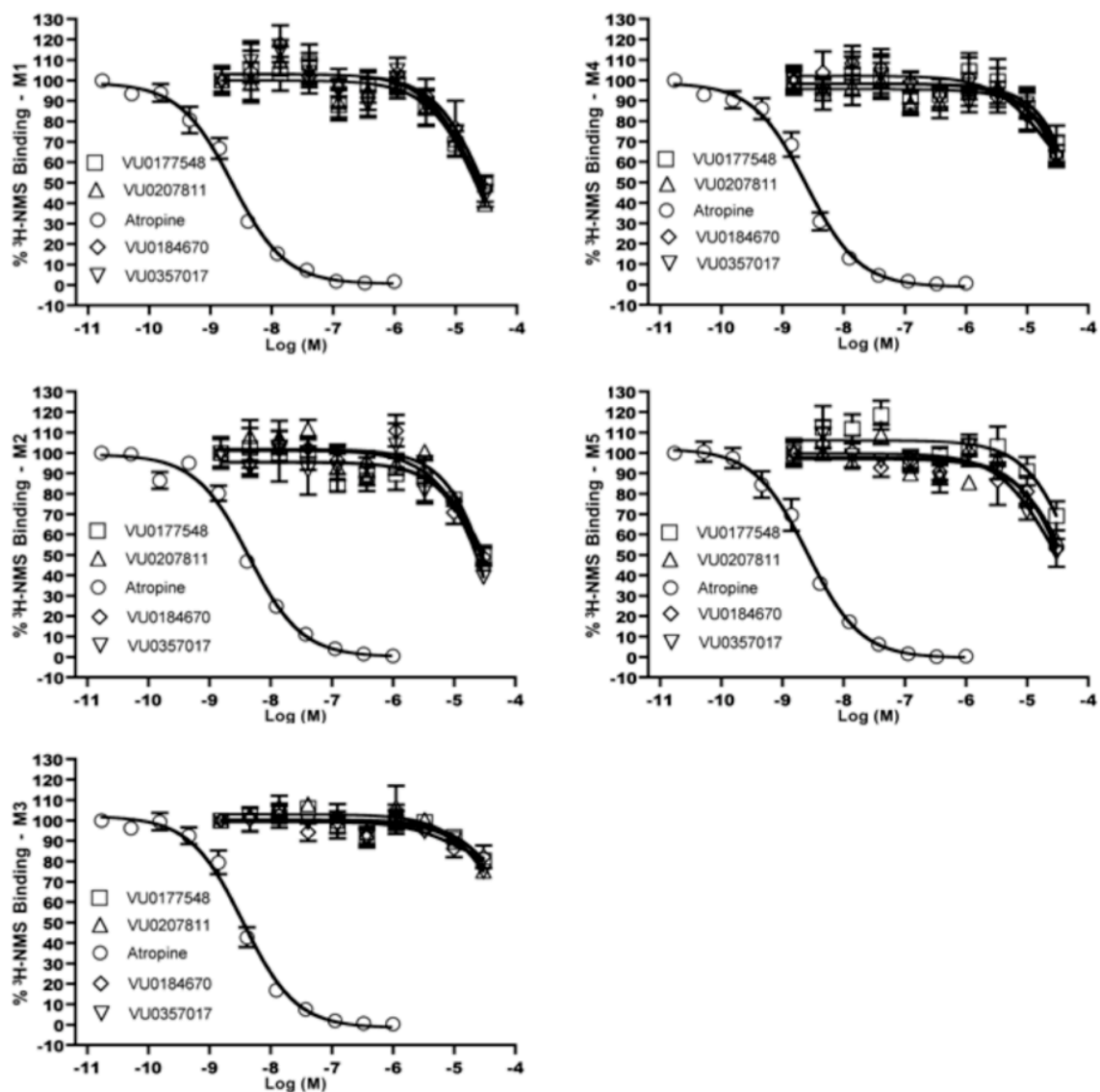


Figure 27. [³H-NMS] competition binding CRCs with parent M₁ agonist HTS hits VU0177548 and VU0207811 as well as lead compounds VU0184670 and VU0357017 (all test compound IC₅₀ values = >30 μM). Atropine used as positive control. M₁ atropine IC₅₀ = 2.22 nM ± 0.60 nM; K_i of 1.27 nM ± 0.36 nM. M₂ atropine IC₅₀ = 4.32 nM ± 1.63 nM; K_i = 3.24 nM ± 1.16 nM. M₃ atropine IC₅₀ = 4.16 nM ± 1.04 nM; K_i = 2.21 nM ± 0.53 nM. M₄ atropine IC₅₀ = 2.38 nM ± 1.07 nM; K_i = 0.77 nM ± 0.34 nM. M₅ atropine IC₅₀ = 3.39 nM ± 1.16 nM; K_i = 2.84 nM ± 0.84 nM. Results represent Mean ± SEM from at least three independent experiments.

Additional evidence that this novel series of compounds activates M₁ via an allosteric mechanism was obtained from Ca²⁺ mobilization assays at the orthosteric-site Y381A mutant M₁ receptor, which exhibits a substantial loss in ACh potency versus the

WT M₁ cell line via disruption of a crucial ACh-receptor interaction mediated by the native tyrosine residue. The M₁ allosteric agonist NDMC potently and fully activates this Y381A mutant M₁ receptor, thereby providing a means for normalization of responses to other test compounds. CRCs of both parent HTS hits as well as the two lead compounds in this cell line revealed retention of agonist potency and partial efficacy (Fig. 28), consistent with an allosteric receptor activation and in dramatic contrast to TBPB (data not shown).

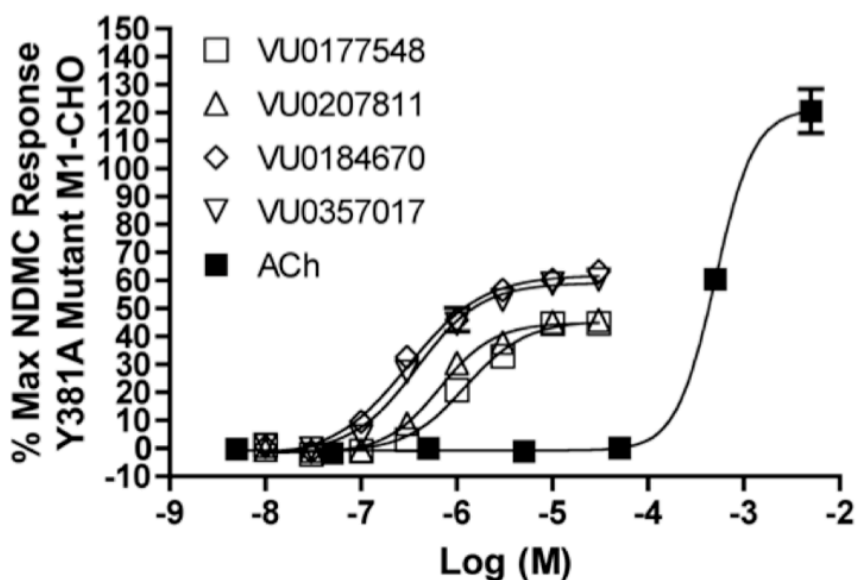


Figure 28. CRCs of M₁ agonist leads VU0184670 and VU0357017 as well as parent hits VU0177548 and VU0207811 in Y381A mutant M₁ cells. Ca²⁺ mobilization was used to obtain CRCs of each compound (and ACh itself as positive control). EC₅₀ values: VU0177548 and VU0207811 = 1.2 μM and 0.66 μM, respectively; VU0184670 and VU0357017 = 0.30 μM and 0.38 μM, respectively. Data represent Mean +/- SEM from at least three independent determinations, normalized as % max response to a high concentration of NDMC.

Together, these data provided compelling evidence that this novel class of M₁ agonists activates the receptor via an allosteric site that is topographically distinct from

the orthosteric site and with a high degree of subtype-selectivity (>100x). Further experiments, including Schild analysis of functional assays with orthosteric antagonist atropine that exhibited a non-competitive interaction (data not shown) and extensive M₁ receptor site-direct mutagenesis guided by computer GPCR homology models (data not shown), provided additional insight to the allosteric mechanism of action. In particular, specific residues of extracellular loop 3 and the first turn of transmembrane-spanning helix 7 are believed to comprise the unique allosteric site at which these M₁ agonists bind to the receptor (data not shown).

With these *in vitro* mAChR pharmacological and structural biochemical data in hand, we next evaluated the lead compounds VU0357017 and VU0184670 in ancillary/off-target pharmacology binding assays (at MDS Pharma/Ricerca) and in standard single-dose rat PK/PBL studies in order to assess their suitability as *in vivo* research tools (data not shown). Gratifyingly, both compounds possessed remarkably clean ancillary pharmacology profiles at 10 μ M across a large panel of 67 different GPCR, ion channel, enzyme, nuclear hormone receptor, and transporter off-targets (only significant activity for either compound was a modest ~65% inhibition of binding to the Sigma₁ receptor). Furthermore, they exhibited highly desirable *in vivo* rat PK, with high CNS penetration (brain/plasma ratios: both \gg 1.0). Ultimately, these novel compounds served as the basis for a large number of *ex-vivo* brain slice electrophysiology and *in vivo* behavioral studies, which have provided crucial insight to the role of M₁ activation in discrete brain regions and in various animal models of CNS function/disease. Further chemical optimization of this series has uncovered comprehensive SAR for multiple sub-

series, which possess even greater potency and efficacy as M₁ allosteric agonists and are presently serving as potential drug discovery leads.

In order to pharmacologically investigate the role of M₁ activation in hippocampal-dependent learning and memory, a series of brain slice electrophysiology and *in vivo* behavioral experiments were performed using lead compound VU0184670¹⁴². M₁-mediated regulation of NMDAR currents in CA1 hippocampal pyramidal neurons is believed to play an important role in certain aspects of learning and memory, and some of the pro-cognitive effects of traditional mAChR agonists seen in clinical trials have been attributed to this cholinergic mechanism. We utilized whole-cell patch clamp techniques with rat brain slice preparations to determine the effect of VU0357017 on CA1 hippocampal pyramidal NMDAR currents. At 30 μM (bath application), VU0357017 significantly increased the peak amplitude of NMDA-evoked inward currents to 137% of baseline after approximately 2 minutes (data not shown). In a related rat behavioral study *in vivo* systemic dosing of VU0357017 fully reversed (at highest dose of 10 mg/kg, IP) scopolamine-induced disruption of contextual fear conditioning and in a dose-dependent manner (data not shown). Under the specific test conditions used, contextual fear-conditioning represents a traditional behavioral model of hippocampal-dependent learning and memory function, which is severely disrupted by mAChR antagonists such as scopolamine. Therefore, these findings are consistent with the hypothesis that M₁ plays an essential role in ACh-mediated mechanisms of learning and memory in the hippocampus. However, based on data from other pharmacological experiments and on studies using mAChR-KO mice, it is known that other subtypes in addition to M₁ have important roles in cholinergic mechanisms of cognitive function (Chapter I).

M₁ agonist TBPB and analogs

Prior to our discovery of the novel M₁ allosteric agonist series represented by lead compound VU0357017, we reported on a structurally unrelated compound termed TBPB as a potent mAChR agonist possessing high M₁-selectivity in functional cell-based assays (Fig. 29)¹⁴³. We performed extensive *in vitro* and *in vivo* characterization of TBPB and found via M₁ mutagenesis and other molecular pharmacology studies that this ligand activates M₁ in the absence of ACh with high subtype selectivity and via an allosteric mechanism. We also found that TBPB potentiates NMDAR currents in rodent hippocampal pyramidal cells without altering excitatory or inhibitory synaptic transmission using *ex-vivo* electrophysiology techniques, and that TBPB-mediated M₁ activation drives non-amyloidogenic processing of APP and decreases amyloid- β *in vitro*. Furthermore, TBPB was efficacious in rodent behavioral models predictive of anti-psychotic activity *in vivo* without inducing M₂/M₃-related side effects.

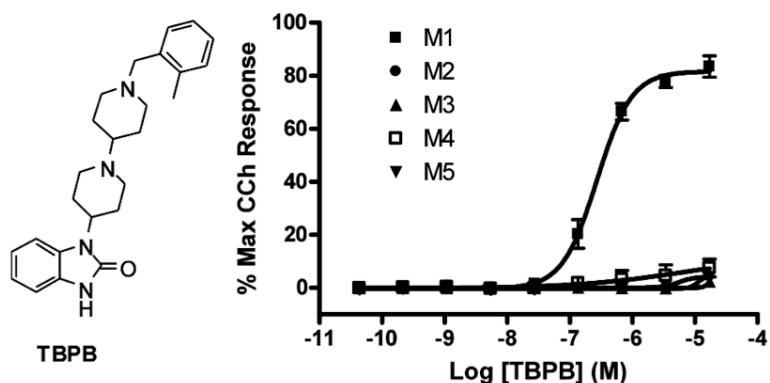


Figure 29. Structure and mAChR subtype-selectivity of M₁ agonist TBPB. Ca²⁺ mobilization was used to obtain CRCs of TBPB in M₁-M₅ cells. Data represent Mean \pm SEM from at least three independent determinations. Experiments performed by A. Brady.

However, TBPB was an unoptimized screening hit with moderate antagonist activity at dopamine D₂ receptor (D₂) (IC₅₀ = 2.6 μM). Despite an [¹⁸F]-fallypride micro-positron emission tomography (PET) study that confirmed the in vivo efficacy in rodent models of psychosis observed with TBPB was the result of selective M₁ activation and not due to D₂, we hoped to diminish D₂ activity through a lead optimization campaign using an iterative parallel synthesis approach^{144,145}. For our initial library, analogs were prepared by a reductive amination sequence employing a functionalized piperidone and 4-(2-keto-1-benzimidazoliny)piperidine or the 5-chloro congener and polymer-supported triacetoxyborohydride (**Fig. 30**).

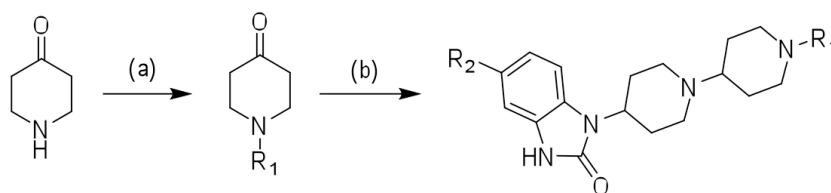


Figure 30. First round of synthesis of TBPB analogs. Reagents and conditions: (a) K₂CO₃, ArCH₂Br, DCM, 70-88%; (b) MP-B(OAc)₃H, 4-(2-keto-1-benzimidazoliny)piperidine or 5-chloro-1-(4-piperidinyl)-2-benzimidazolone, DCM, rt, 24 hr, 85-95%.

In the first round of library synthesis, efforts focused on commercially available piperidinones (wherein R₁ is either an alkyl or carbamate moiety). Subsequent rounds of library synthesis utilized the same scheme but with substituted benzylic R₁ moieties generated by standard alkylation chemistry on the piperidone starting material. These analogs were then tested in CRCs at both the M₁ and dopamine D₂ receptors in cell-based Ca²⁺ mobilization assays. Out of an initial 24-member library with simple aliphatic and carbamate derivatives of TBPB, only an ethyl carbamate analog (compound 1b, **Table 4**) retained M₁ agonist activity.

Table 4. M₁ and D₂ potency/efficacy SAR for TBPB analogs synthesized according to **Figure 30**. Ca²⁺ mobilization was used to obtain compound CRCs with M₁ and D₂ cells. Data represent Mean +/-SEM of at least three independent determinations. Experiments performed by A. Brady.

Cmpd	R ¹	R ²	M1 EC ₅₀ ^a (nM)	%CCh Max ^a	D2 IC ₅₀ ^a (μM)
1a	2-MeBn	H	289	82	2.65
1b	CO ₂ Et	H	2.1	65	>10
1c	2-MeBn	Cl	1030	84	35% at 10 μM
1d	Bn	Cl	356	74	35% at 10 μM
1e	2-CF ₃ Bn	H	410	82	30% at 10 μM
1f	2-CF ₃ Bn	Cl	1500	83	ND
1g	2-ClBn	H	260	44	2.06
1h	2-ClBn	Cl	1800	49	ND
1i	2-NO ₂ Bn	H	120	48	1.13
1j	2-NO ₂ Bn	Cl	1100	42	ND
1k	2-CNBN	H	490	23	40% at 10 μM
1l	2-CNBN	Cl	1600	27	ND

Compound **1b** displayed substantially improved M₁ potency (EC₅₀ = 2.1 nM) with moderate efficacy (65% CCh max), but lost selectivity versus M₂-M₅, thereby degenerating into a pan-mAChR partial agonist (**Fig. 31**).

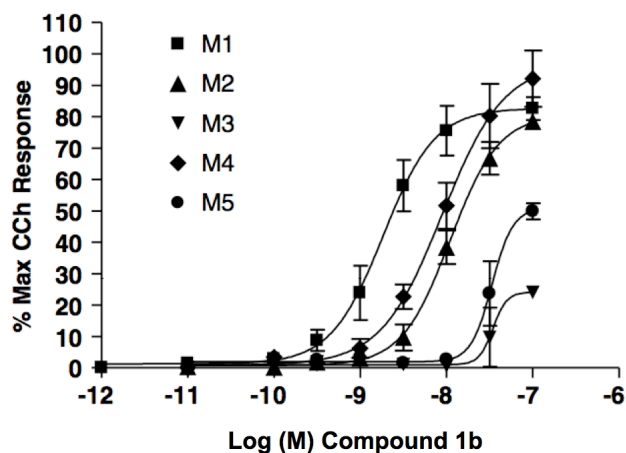


Figure 31. mAChR subtype-selectivity profile for TBPB analog **1b**. Ca²⁺ mobilization was used to obtain CRCs with M₁-M₅ cells. Data represent Mean +/-SEM from at least three independent determinations. Experiments performed by A. Brady.

The subsequent round of parallel synthesis focused on diverse distal benzylic substitutions at R₁ with the 4-(2-keto-1-benzoimidazoliny)piperidine TBPB headpiece bearing either hydrogen or a chlorine atom in the 5-position, the latter of which was introduced to block a site of oxidative metabolism we identified (data not shown). This effort generated over 60 analogs; however, the SAR proved to be rather ‘flat’. If the benzyl group possessed substituents in the 3- or 4-positions, all M₁ agonism was lost (EC₅₀ >20 μM). As shown in **Table 4**, it was possible to synthesize other analogs with selective M₁ partial agonism (M₁ EC₅₀ values of 120 nM to 1.8 μM, >50 μM vs. M₂-M₅), but the degree of efficacy varied widely (23-84%). Incorporation of a 5-Cl atom into TBPB to block metabolism resulted in compound **1c**, an analog that maintained the same efficacy as TBPB, but lost ~5-fold potency (**Table 4**). Removal of the 2-Me group resulted in an analog comparable to TBPB, compound **1d** (**Table 4**). Attempts to replace the metabolically labile 2-methyl group with alternative chemical moieties (compounds **1e-1i**) generally led to a significant diminution in M₁ efficacy (<50%), M₁ potency, or both (**Table 4**). However, the 2-nitrobenzyl analogue (compound **1i**) proved more potent than TBPB (M₁ EC₅₀ = 120 nM), but efficacy fell to 42% CCh max response (**Table 4**). One exception to this was the 2-CF₃ group, which provided an analog with an M₁ EC₅₀ of 410 nM and 82% max efficacy (**Table 4**).

With respect to D₂ inhibition, compound **1e** maintained a mAChR profile comparable to TBPB, but D₂ inhibition was greatly diminished (~30% @ 10 μM), indicating that this compound might prove to be a more useful biological tool to probe M₁ than TBPB. The moderately more potent than TBPB compound **1i**, also displayed increased D₂ inhibition (IC₅₀ = 1.13 μM); however, a dual M₁ agonist/D₂ antagonist may

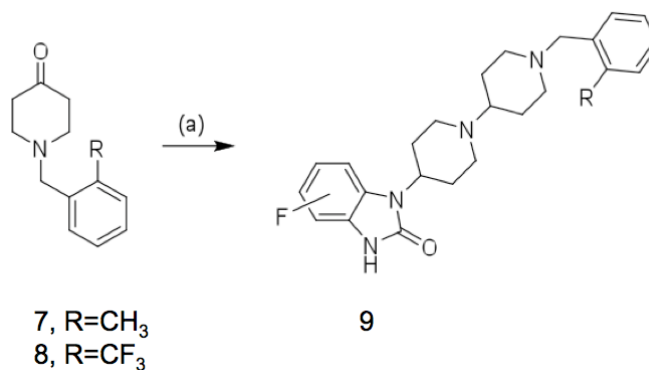
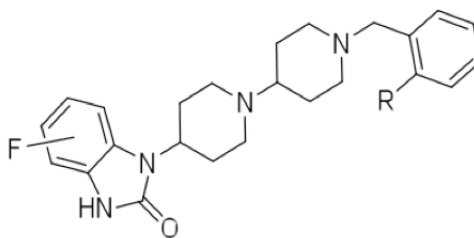


Figure 33. Synthesis of additional fluorinated TBPB analogs. Reagents and conditions: (a) MP-B(OAc)₃H, 4-, 5- and 6-fluoro-1-(piperidin-4-yl)-1-*H*-benzo[*d*]imidazol-2(3*H*)-ones **17**, 50-90%.

The final fluorine-substituted analogs were prepared by a reductive amination sequence employing either 2-methyl benzyl piperidone (compounds **7**) or 2-trifluoromethyl benzyl piperidone (compounds **8**) and the 4-, 5- or 6-fluoro-1-(piperidin-4-yl)-1-*H*-benzo[*d*]imidazol-2(3*H*)-ones (compounds **9**) (**Fig. 33**). As shown in **Table 5**, TBPB analog compounds **9** containing a fluorine atom were uniformly less active than the un-substituted parents, TBPB and compound **1e**. However, analogs such as **9b** and **9c** possessed sub-micromolar EC₅₀s and were equally efficacious (850 nM, 85% CCh max and 760 nM, 84% CCh max, respectively); moreover, they carried no significant D₂ antagonism. Based on these SAR data, we prepared additional 4-(2-(keto-1-benzoimidazolyl)piperidines and TBPB analogues with alternative substitutions (Br, CN, CF₃), as shown in **Table 5**.

Table 5. SAR for fluorine-substituted TBPB analogs. Ca^{2+} mobilization was used to obtain compound CRCs with M_1 and D_2 cells. Data represent Mean \pm SEM of at least three independent determinations. Experiments performed by A. Brady.



Cmpd	R	F	$\text{M}_1 \text{ EC}_{50}$ (μM) ^a	%CCh Max ^a	$\text{D}_2 \text{ IC}_{50}$ (μM) ^a
9a	CH_3	4-F	1.06	73	>10
9b	CH_3	5-F	0.85	85	40%@10 μM
9c	CH_3	6-F	0.76	84	>10
9d	CF_3	4-F	1.71	75	>10
9e	CF_3	5-F	1.04	80	2.69
9f	CF_3	6-F	>10	ND	>10

Most fluoro-TBPB analogs were found to be either inactive or partial agonists with <20% maximum efficacy, or they were no longer selective for M_1 . Ultimately, after numerous sets of analogs had been synthesized and evaluated, we found that this was a rare instance, from our experience, where the original screening hit, TBPB, could not be significantly improved upon using these types of structural modifications. Further SAR was later explored by examining the effect of capping the TBPB scaffold's distal basic piperidine nitrogen with amides, sulfonamides, and ureas (data not shown)¹⁴⁴. These efforts revealed similarly flat SAR; however, a number of such analogs retained moderate M_1 potency, efficacy, and subtype-selectivity (data not shown).

In summary, we identified a novel series of allosteric partial agonists with high selectivity for M_1 versus M_2 - M_5 and with various degrees of D_2 antagonism based on the

general TBPB scaffold. SAR was essentially ‘flat’ within this series, with subtle changes resulting in pan-mAChR agonism, loss of M₁ potency, significantly decreased efficacy, and/or ancillary D₂ antagonism. This was a rare example in which the screening lead proved very difficult to optimize, yet still possessed a profile that enabled both *in vitro* and *in vivo* studies to be conducted. Moreover, this work further exemplifies the numerous challenges inherent to optimization of most allosteric GPCR ligands.

M₁ antagonist VU0255035 and analogs

In addition to the discovery and optimization of numerous new M₁-targeted small molecule agonists and PAMs, we hoped to obtain novel M₁-selective antagonists for use as research tools and to investigate the therapeutic potential of selective M₁ blockade in movement-related and other CNS disorders. Small molecule agonists and potentiators selective for a specific mAChR subtype have clear utility in neurobiology research and in therapeutic target validation contexts wherein activation of the receptor is required; for example, M₁ activation in Alzheimer’s disease or schizophrenia. Conversely, subtype-selective mAChR antagonism provides a complementary but distinct utility in contexts that require diminution of receptor signaling, such as in the treatment of dystonia and in basic research on the role of M₁ signaling under normal disease-free physiological conditions. Furthermore, discovery of a truly selective M₁ antagonist small molecule could provide a highly useful control in experiments with mAChR agonists or PAMs.

Therefore, our MLSCN/MLPCN center initiated an effort to identify a potent small molecule antagonist with high specificity for M₁ versus M₄ for use as a chemical

probe and lead for further optimization towards a novel therapeutic^{140,141}. Our functional HTS (performed as described previously in this Chapter for the MLSCN/MLPCN M₁ PAM project) identified a number of hits, and a limited optimization effort produced the M₁ versus M₄ selective antagonist VU0359517 (M₁ IC₅₀ = 440 nM, M₄ IC₅₀ >150 μM); however, this orthosteric mAChR antagonist displayed only 2- to 9-fold selectivity versus M₂, M₃ and M₅ (data not shown). This early effort also produced a series of weak (M₁ IC₅₀ >3.5 μM) but selective (M₂-M₅ IC₅₀ >50 μM) antagonists based on a 3,6-disubstituted-[1,2,4]-triazolo[4,3-*b*]pyridazine scaffold (data not shown)¹³⁹.

While the vast majority of our HTS hits displayed no selectivity for M₁ versus M₄, compound **1**, based on a *N*-(3-piperazin-1-yl)-3-oxopropyl)benzo[*c*][1,2,5]thiadiazole-4-sulfonamide scaffold, demonstrated a surprising >58-fold selectivity for rat M₁ (IC₅₀ = 2.55 μM) over rat M₄ (IC₅₀ >100 μM) with a similar IC₅₀ (2.72 μM) for human M₁ in Ca²⁺ mobilization assays examining the functional antagonism of an ACh ~EC₈₀. Encouraged by this result, we explored the selectivity of compound **1** versus M₂-M₅. Gratifyingly, it was >58-fold selective for M₁ versus M₂-M₅ (Fig. 34).

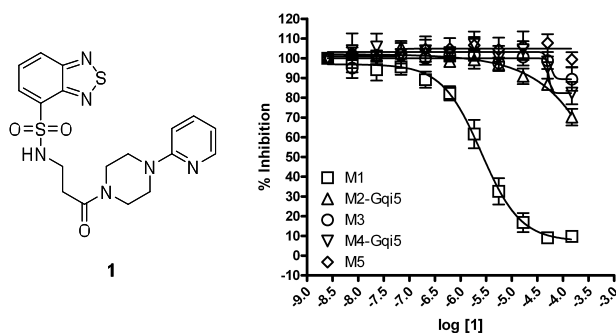


Figure 34. M₁-M₅ CRCs for compound **1**. Ca²⁺ mobilization was used to obtain CRCs of test compound in M₁-M₅ cells in the presence of an ACh ~EC₈₀. M₁ IC₅₀ = 2.6 μM. Data represent Mean +/- SEM from at least three independent determinations. Experiments performed by D. Sheffler.

While this level of selectivity was unprecedented for a small molecule M_1 antagonist, **1** did not meet the potency criteria for an MLSCN small molecule probe ($IC_{50} < 500$ nM). Therefore, we launched a chemical lead optimization campaign to improve potency for M_1 while maintaining high selectivity versus M_2 - M_5 . Analogs of compound **1** were synthesized in a library format according to the scheme presented in **Figure 35**. For the first round of library synthesis, our strategy was to explore alternative amides in place of the 2-pyridylpiperazine moiety. Commercially available benzo[*c*]thiadiazole-4-sulfonyl chloride (compound **2**) was treated with β -alanine methyl ester to afford, after saponification, acid (compound **3**). Subsequent coupling with a diverse collection of 24 primary and secondary amines under standard solution phase parallel synthesis conditions employing polymer-supported reagents and scavengers provided analogs **4**. All compounds were purified by mass-guided HPLC to analytical purity.

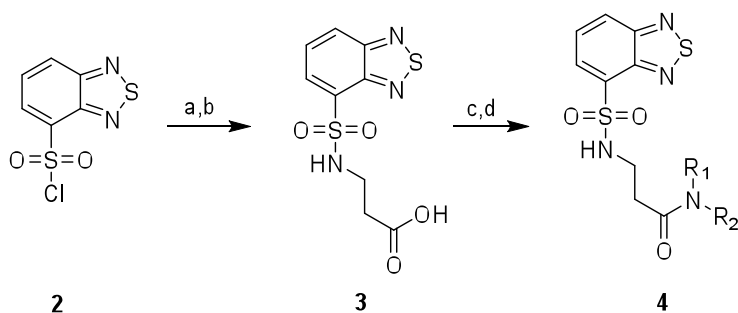
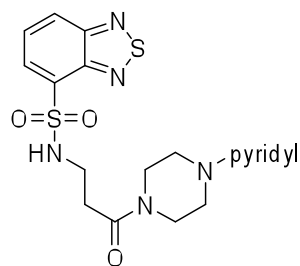


Figure 35. Synthesis of compound **1** analogs. Reagents and conditions: (a) β -alanine methyl ester, DCM, DIEA, rt; (b) LiOH, THF/ H_2O /MeOH, rt; (c) R_1R_2NH , PS-DCC, HOBT, DCM, DIEA; (d) $MP-CO_3^{2-}$. Syntheses performed by C. Lindsley.

Evaluation of this library against M₁-M₅ cells by Ca²⁺ mobilization assay in the presence of an ACh ~EC₈₀ demonstrated that SAR for this series was relatively flat, with regioisomeric pyridylpiperazine amides **5** being the only active analogs of **4** (**Table 6**). The activity of the HTS lead compound **1** was confirmed by re-synthesis (M₁ IC₅₀ = 2.37 μM, M₂-M₅ IC₅₀ >10 μM). With respect to SAR for this series, functionalized phenyl piperazine analogs, aliphatic piperazines, and other heterocyclic analogs were all devoid of M₁ antagonist activity. Relative to the 2-pyridyl analog (compound **1**), the 3-pyridyl congener (compound **5a**) possessed roughly equivalent activity at M₁ (IC₅₀ = 3.19 μM), while also maintaining selectivity versus M₂-M₅. The 4-pyridyl variant (compound **5b**) provided a ~17-fold increase in M₁ activity (IC₅₀ = 133 nM) relative to the HTS hit.

Table 6. M₁-M₅ SAR for active M₁ antagonist analogs **5**. Ca²⁺ mobilization was used to obtain compound CRCs in M₁-M₅ cells in the presence of an ACh ~EC₈₀. Data represent Mean +/-SEM of at least three independent determinations. Experiments performed by D. Sheffler.



5

	R	M1 IC ₅₀ (μM) ^a	M2 IC ₅₀ (μM) ^a	M3 IC ₅₀ (μM) ^a	M4 IC ₅₀ (μM) ^a	M5 IC ₅₀ (μM) ^a
1	2-pyridyl	2.37±1.6	>10	>10	>10	>10
5a	3-pyridyl	3.19±1.5	>10	>10	>10	>10
5b	4-pyridyl	0.13±0.03	>10	>10	>10	>10

A high degree of subtype-selectivity ($>75\times$ for M_1 versus M_2-M_5) was also maintained (M_2-M_5 IC_{50} s >10 μ M) for compound **5b** as shown in **Figure 36**. Compound concentrations were solubility limited, but little inhibition of an ACh $\sim EC_{80}$ at M_2-M_5 was observed for compound **5b** at up to 100 μ M in some experiments. Thus, this analog represented the most functionally subtype-selective small molecule M_1 antagonist ever reported; however, its binding subtype-selectivity remained a question. Due to this unprecedented mAChR subtype-selectivity in functional cell-based assays (**Fig. 36**), we hypothesized that this compound binds to an allosteric site on the M_1 receptor.

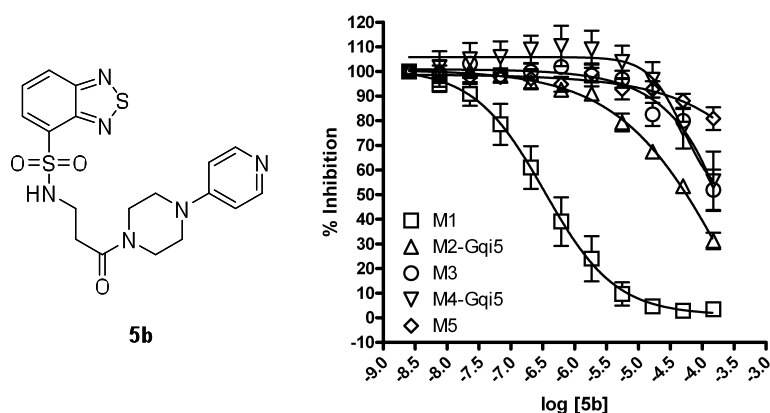
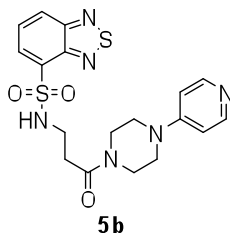


Figure 36. M_1 - M_5 CRCs for lead compound **5b**. Ca^{2+} mobilization was used to obtain CRCs of test compound in M_1 - M_5 cells in the presence of an ACh $\sim EC_{80}$. M_1 IC_{50} = 133 ± 28 nM. Data represent Mean \pm SEM from at least three independent determinations. Experiments performed by D. Sheffler.

To test this hypothesis, [3H]-NMS competition binding experiments were conducted under equilibrium conditions to obtain K_i values for compound **5b** as well as atropine controls at M_1 - M_5 cell membranes. As shown in **Table 7**, compound **5b** exhibited potent inhibition of orthosteric radioligand binding with an M_1 K_i of 14.9 nM with 45- to 159-fold K_i selectivity versus M_2-M_5 .

Table 7. Summary of functional and binding mAChR subtype-selectivity for M₁ antagonist (compound **5b**). Ca²⁺ mobilization was used to obtain CRCs of test compound in M₁-M₅ cells in the presence of an ACh ~EC₈₀. [³H]-NMS competition binding was used to obtain CRCs of test compound and atropine positive control under equilibrium with M₁-M₅ cell membranes. Atropine K_i values: M₁ = 0.8 nM, M₂ = 2.6 nM, M₃ = 1.1 nM, M₄ = 0.6 nM, M₅ = 1.6 nM. Data represent Mean +/-SEM from at least three independent determinations. Experiments performed by D. Sheffler.



mAChR	IC ₅₀ (nM) ^a	Fold selectivity	K _i (nM) ^a	Fold selectivity
M1	133		14.9	
M2	>10,000	>75	661.3	45
M3	>10,000	>75	876.9	59
M4	>10,000	>75	1177.6	79
M5	>10,000	>75	2362.3	159

These results were surprising and led us to further explore the mechanism of antagonism via Schild analysis of PI hydrolysis experiments. In these experiments, compound **5b** caused parallel concentration-dependent rightward shifts of an ACh CRC, which translated in a Schild analysis to a K_d of 16 nM (slope = 0.90±0.08, data not shown). These data support the previous results from the [³H]-NMS binding experiments in suggesting that compound **5b** is an orthosteric M₁ antagonist. Therefore, we rejected our original allosteric binding hypothesis pending further testing in the form of kinetic binding experiments.

Prior to conducting *in vivo* experiments, the selectivity of compound **5b** was evaluated against larger panels of molecular targets. In binding assays at both the UNC Psychoactive Drug Screen and against a large panel of GPCRs, ion channels,

transporters, nuclear hormone receptors, and kinases (MDS Pharma/Ricerca), compound **5b** was devoid of significant ancillary pharmacology (data not shown). Next, we performed a rat single-dose (10 mg/kg) PK/PBL study that revealed a brainAUC/plasmaAUC ratio of 0.48 and other similarly acceptable PK parameters for use of this compound *in vivo* following systemic dosing (data not shown).

In a subsequent acute rodent behavioral study, our M₁ antagonist (compound **5b**) exhibited *in vivo* efficacy following systemic (I.P.) administration in a pilocarpine-induced mouse seizure model by reducing M₁-mediated seizure activity and increasing survival at doses that did not disrupt acquisition of contextual fear conditioning (data not shown). These results suggested that M₁ antagonism in a therapeutic context may not result in learning and memory related side effects, although further investigation is certainly required. Based on these exciting data, we chose to further explore SAR around this chemical series by evaluating the six parameters shown in **Figure 37**. However, SAR was again ‘flat’ with no active analogs arising from these modifications.

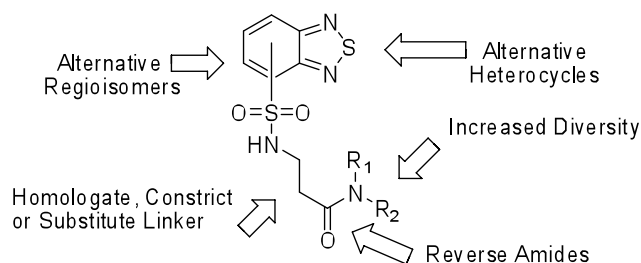


Figure 37. Additional SAR exploration around the M₁ antagonist scaffold resulting in inactive analogs.

In summary, an MLSCN M₁ antagonist chemical probe discovery project provided a selective M₁ antagonist lead (compound **1**) after a functional HTS campaign. One round of parallel synthesis afforded compound **5b**, a highly functionally selective

(>75-fold vs M₂-M₅), potent (IC₅₀ = 133 nM), and high-affinity (K_i = 14.9 nM) M₁ antagonist. Moreover, this compound possessed no significant ancillary pharmacology and exhibited a pharmacokinetic profile acceptable for *in vivo* systemic dosing in behavioral and neurochemical studies. Based on these and the preliminary *in vivo* efficacy data, compound **5b** was declared an MLSCN/MLPCN small molecule *in vitro/in vivo* probe and assigned the identifier VU0255035¹⁴⁰. Further experiments utilizing this novel compound and aimed at investigating the therapeutic potential of selective M₁ antagonism as well as the role of M₁ in basic neurobiology are currently underway.

Summary

In summary, numerous novel small molecule ligands selectively-targeting the M₁ receptor and suitable for *in vitro* and *in vivo* use have been discovered, including three classes of PAMs, two classes of agonists, and a single class of antagonists. Prior to this work, the mAChR field was largely devoid of truly M₁-selective ligands that possessed the drug-like pharmacological characteristics necessary for use in rodent *in vivo* neurobehavioral and neurochemical studies. Utilizing functional cell-based screening and hypothesis-driven medicinal chemistry techniques, highly-selective M₁ tools have successfully been discovered, which have provided crucial insight to the role of M₁ in basic neurobiology and within the context of therapeutic target validation. Specifically, studies with these compounds have revealed and confirmed the role of M₁ activation in mediating ACh-induced potentiation of NMDAR currents in CA1 hippocampal pyramidal neurons, in regulation of APP processing, and in a variety of anti-psychotic

and pro-cognitive behavioral effects. Furthermore, the diversity of chemotypes across the different series of M₁ PAMs (e.g. BQCA, VU0366369, and VU0405652) and M₁ agonists (e.g. VU0357017 and TBPB) provides a rich set of tools for studying ligand-directed/biased signaling downstream of M₁, which represents a growing area of research important to both basic and translational neurobiology.

Chapter VI

SUMMARY AND FUTURE DIRECTIONS

Muscarinic acetylcholine receptors are important to numerous physiological processes in both the CNS and periphery^{16,18}. In light of their distinct localizations and putative functional roles as suggested by genetic KO mice studies, multiple mAChR subtypes may represent attractive drug targets for treatment of a variety of CNS diseases and disorders^{44,111}. However, since the initial cloning of the genes encoding the individual rodent and human mAChR subtypes more than two decades ago, relatively little pharmacological progress has been made towards obtaining a deep understanding of the role(s) of each subtype in mammalian neurobiology. This has been due largely to a failure of efforts aimed at discovering highly subtype-selective mAChR ligands. Indeed, few drug-like muscarinic compounds exist that are suitable for use as research tools or as drug discovery leads. Like other GPCR subfamilies, the orthosteric binding site is highly conserved across the mAChRs, which has contributed heavily to this longstanding paucity of highly subtype-selective ligands. This is especially apparent in the case of M₅, as no small molecules possessing even moderate selectivity for M₅ have been reported in the international scientific or patent literature. Similarly, until recently no ligands existed for studying the effects of selective M₄ modulation. A number of chemotypes have been discovered to possess high functional and/or binding selectivity for M₁, yet many of these compounds suffer from sub-optimal pharmacological properties and off-target activities that limit their utility in basic and clinical research (Chapter I).

Here we described a variety of medicinal chemistry and neuropharmacology research projects aimed at discovering, optimizing, and characterizing novel highly subtype-selective mAChR ligands for M₁, M₄, and M₅^{27,124,126,131,132,135,138-146}. Using functional HTS and cheminformatic techniques, screening hits were identified that, through subsequent chemical optimization, lead to discovery of novel series of M₄ PAMs and M₅ PAMs as well as multiple series of M₁ PAMs, allosteric M₁ partial agonists, and M₁ antagonists, each possessing high subtype-selectivity (>30-100x) in functional cell-based assays. Lead compounds from the M₄ PAM project and multiple M₁-related projects were then used in a variety of electrophysiological and neurobehavioral experiments to investigate the precise role(s) of these subtypes in the CNS. In the case of M₅, the first and currently only series of highly subtype-selective ligands, M₅ PAMs derived from an initial pan-M₁, -M₃, -M₅ PAM screening hit, were obtained and characterized. Abbreviated summaries for the M₄ PAM and M₅ PAM projects, associated potential further optimization efforts, as well as future *in vitro* and *in vivo* studies are presented below.

M₄ PAMs based on VU010010

The first series of small molecule mAChR PAMs possessing high potency and subtype-selectivity for rat M₄ were obtained using a virtual cheminformatic database mining approach based on the structure of LY2033298, the first potent and selective human M₄ PAM (**Fig. 1**)^{124,125,127}. This involved the initial discovery of VU010010, which possessed an approximately 400 nM rM₄ potency and induced a robust 47x left-

shift of an rM₄ ACh CRC at 30 μM in Ca²⁺ mobilization assays (**Fig. 1**). This compound, although useful in limited electrophysiological studies, suffered from poor physiochemical properties (logP ~ 4.5) and lacked CNS penetration *in vivo* following systemic dosing in a rat PK/PBL study. Subsequent optimization efforts employing a DOS strategy revealed flat SAR around most regions of the VU010010 scaffold; however, multiple benzamide substitutions on the eastern side were well tolerated. This initial optimization campaign identified VU0152099 and VU0152100 as analogs of VU010010 possessing similar rM₄ PAM potency and efficacy but with improved solubility and ultimately acceptable *in vivo* rat PK profiles (**Fig. 1**). After a series of *in vitro* characterization experiments, which revealed that these compounds potentiated both ACh binding affinity and efficiency of G-protein coupling through an allosteric mechanism, these lead M₄ PAMs were used in rat behavioral studies to investigate the antipsychotic potential of selective M₄ activation *in vivo*. Both VU0152099 and VU0152100 exhibited robust and dose-dependent reversal of amphetamine-induced hyperlocomotion after I.P. injection with an absence of sedative effects, which provided the first reported behavioral evidence suggesting M₄ activation (or PAM) may be efficacious in the treatment of psychosis.

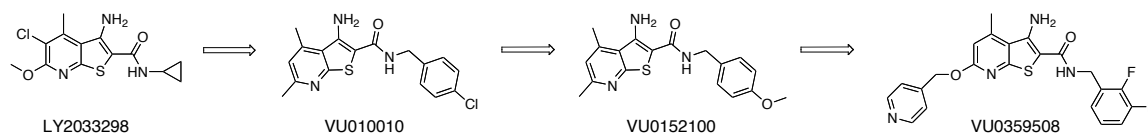


Figure 1. Optimization progression summary for M₄ PAMs based on a substituted thienopyridine scaffold.

A more comprehensive optimization campaign was then executed in order to further explore SAR and improve the metabolic stability of the VU010010-based M₄ PAM scaffold through an iterative analog library approach¹²⁶. This involved introduction of diverse western amino or ether substitutions at the 6-position of the thienopyridine core, although only ether-linked basic amine moieties were well tolerated. Subsequent matrix-like derivatization of the eastern amide side chain led to the discovery of multiple lead compounds possessing high ACh CRC fold-shift (>40-60x at 30 μM) but relatively modest EC₅₀ values (~2 μM) at rM₄. Importantly, these newer analogs, exemplified by VU0359508 (**Fig. 1**), maintained complete subtype-selectivity, possessed improved metabolic stability *in vitro* (>90% parent remaining after 90 min incubation with rat liver microsomes), and displayed superior vehicle solubility in *in vivo* formulation studies (>10 mg/mL across multiple non-toxic carriers). However, these compounds exhibited poor/absent efficacy in reversal of amphetamine-induced hyperlocomotion following 56.6 mg/kg (I.P.) dosing in rat behavioral studies, which may have been due to their relatively lower potency compared to VU0152099 and VU0152100. Upon *in vitro* testing at the human M₄ receptor, these analogs exhibited more than 10x greater potency (~100-200 nM range), contributing to evidence that they could serve as future drug leads. Additionally, alignment with the refined H₃ antagonist pharmacophore model and subsequent competition binding experiments at H₃ suggest that this latest generation M₄ PAM series may also be used as a starting point for discovery and optimization of dual M₄ PAM/H₃ antagonist compounds, which could potentially confer more comprehensive antipsychotic utility in addressing both positive and cognitive system clusters of schizophrenia.

Although not discussed in Chapter III, preliminary *in vitro* data from experiments with a compound we discovered that is structurally related to the M₄ PAM scaffold suggests that certain modifications to the thienopyridine core confer a switch in mode of pharmacology from PAM to NAM/antagonist for this series. However, subtype-selectivity, mode of binding, and tractability in further optimization has not yet been determined. Discovery of a potent and selective M₄ NAM from our series of M₄ PAMs would provide a highly useful research tool that could be used to probe the effects of decreasing M₄ signaling within numerous neurobiology and therapeutic discovery contexts. Additional medicinal chemistry and *in vitro* characterization for such putative M₄ NAMs is required.

Beyond these chemical optimization possibilities, a number of *in vitro* and *in vivo* pharmacological studies may be pursued with the highly-selective M₄ PAMs described in Chapter III. Each of the lead compounds from this series lacked any detectable PAM activity at M₁, M₂, M₃, or M₅ in Ca²⁺ mobilization assays; however, it is not known if this high selectivity is due to binding specificity for M₄ or if these compounds in fact bind to one or more of the other mAChRs but exhibit neutral cooperativity (i.e. pharmacological silence) with ACh. To address this question and to assess the potential for probe-dependent PAM activity at other mAChRs, a series of *in vitro* experiments may be performed. These could involve measurement of radioligand binding kinetics and/or functional activity of multiple orthosteric ligands in the absence and presence of a high concentration of M₄ PAM test compound at each of the other mAChR subtypes. If differences are seen in the presence of the test compound, such data would provide evidence that the compound does bind to other mAChR subtypes in addition to M₄.

Similar assays could be performed using lead compounds from many of the mAChR projects described in Chapter V as well, as the question of binding versus functional selectivity remains unanswered for most mAChR allosteric chemotypes.

In electrophysiology experiments using rodent hippocampal slices, the early M₄ PAM lead VU010010 was found to increase CCh-mediated depression of synaptic transmission at excitatory but not inhibitory synapses. Given the high expression of M₄ in the striatum and other components of the basal ganglia, additional electrophysiological investigation into the precise role(s) of M₄ in these brain regions would advance the understanding of M₄ basic neurobiology. Furthermore, more comprehensive evaluation of the effects of selective M₄ modulation within the therapeutic context of psychosis would shed additional light on the validity of this target. Although reversal of amphetamine-induced hyperlocomotion is a highly useful acute model for predicting DA-related positive symptom antipsychotic efficacy, additional behavioral studies including conditioned avoidance responding (CAR), reversal of PCP-induced disruption of PPI, and various models of cognition could be performed with our M₄ PAMs. For studies with the more recent lead compounds (e.g. VU0359508), which possess improved physiochemical properties and metabolic stability but only modest M₄ potency, co-administration of a low dose of mAChR agonist may provide a solution to the lack of *in vivo* effect observed with these compounds. This strategy was used in the case of the original hM₄ PAM LY2033298, which lacked efficacy in a rodent CAR behavioral study when dosed alone but exhibited robust effects in the presence of a low dose of oxotremorine (that itself had no effect either)¹²⁷. Alternatively, the intermediate lead compounds VU0152099 or VU0152100 could be used. Such experiments would provide valuable insight to the

question(s) about which mAChR(s) likely mediated the antipsychotic effects observed in clinical trials of the M₁/M₄-preferring agonist xanomeline.

M₅ PAMs based on VU0238429

Following discovery of VU0119498 as a small molecule mAChR PAM with similar *in vitro* potency, efficacy, and selectivity for M₁, M₃, and M₅, SAR from a large matrix-analog library synthesis revealed that –OCF₃ substitution at the 5-position of the isatin headpiece conferred preference for M₅ activity. This was exemplified by the early lead VU0238429, the first reported M₅-preferring PAM, which possessed approximately 1 μM potency, induced a 14x left-shift of an M₅ ACh CRC at 30 μM, and exhibited >30x selectivity versus M₁-M₄ in functional Ca²⁺ mobilization assays. Subsequent radioligand binding experiments indicated that VU0238429 modulates M₅ by enhancement of ACh affinity through an allosteric mechanism. This compound was then used as the lead structure for an exhaustive chemical optimization campaign aimed at further exploring SAR and obtaining analogs with superior drug-like pharmacological properties. Guided by specific hypothesis-driven strategies, dozens of iterative parallel libraries were generated to systematically probe the effect of various structural modifications to the M₅ PAM scaffold on potency, efficacy, and subtype-selectivity. These efforts led to the discovery of intermediate leads such as VU0365114, which possessed modestly lower potency (2.7 μM) but induced a pronounced >50x left-shift of the ACh CRC at 30 μM with even greater subtype-selectivity than VU0238429. Other SAR revealed even more M₅ subtype-selectivity could be engendered by introduction of biaryl/heterobiaryl ethers

to the southern region of the scaffold, as exemplified by VU0400265, which possessed a 1.9 μM PAM EC_{50} at M_5 and lacked any detectable activity at M_1 - M_5 at up to 30 μM .

Comprehensive survey of SAR around the isatin headpiece confirmed the vital importance of the 5- OCF_3 group for M_5 PAM activity, as more than 40 different ether substitutions (including trifluoroethyl and trifluoropropyl) were inactive. However, migration of this moiety to the 6-position was tolerated and actually improved efficacy, but simultaneously compromised subtype-selectivity. Efforts to replace the 3-keto component of the isatin core successfully identified the gem-difluoro but not the spirocyclopropyl or tertiary alcohol isosteres as an optimal replacement, which conferred a moderate increase in potency, efficacy, and subtype-selectivity while removing the DMPK-related liabilities of the isatin structure. In libraries containing *ortho*-fluoro, *meta* biaryl/heterobiaryl, or *meta* biaryl/heterobiaryl ether substitutions on the southern benzyl ring, SAR was flat and M_5 PAM activity was essentially lost. These and other SAR findings from this optimization campaign are summarized in **Figure 2**.

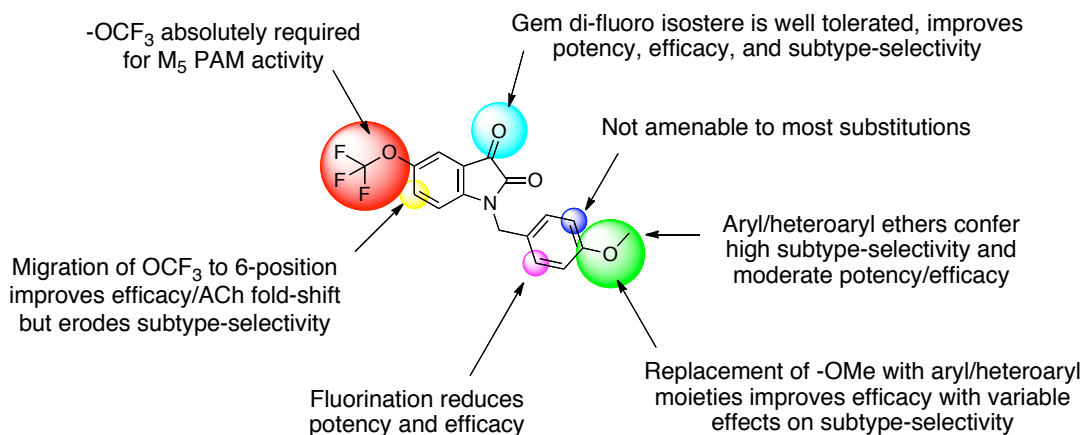


Figure 2. Abbreviated SAR summary for M_5 PAM optimization based on early lead VU0238429.

In general, the *para* position on the southern benzyl ring proved most amenable to derivatization, and therefore efforts to improve the physiochemical properties and reduce identified ancillary/off-target pharmacology liabilities focused on this region. Analogs bearing linear heterobiaryl southern motifs containing one or more nitrogens in the proximal and/or distal aromatic ring(s), such as the *p*-phenyl substituted 3-picoyl compound VU0415478, were synthesized and found to possess improved aqueous solubility and also maintained M₅ PAM activity with moderate potency and subtype-selectivity, but with slightly diminished efficacy. Similar analogs containing heterobiaryl ethers, such as the fluoro-pyridine analog VU0414747, were found to possess solubility, potency, and subtype-selectivity comparable to or greater than that of the straight non-ether heterobiaryl analogs, but with generally lower PAM efficacy.

However, despite their improved physiochemical properties, both of these later sub-series still suffered from numerous ancillary pharmacological activities revealed by a 10 μ M competition binding screen across a large panel of off-targets. Ultimately, after hundreds of compounds were synthesized and evaluated, it proved difficult to obtain analogs with the ideal combination of each important parameter such as potency, efficacy, subtype-selectivity, physiochemical properties (i.e. logP), lack of ancillary pharmacology, and drug-like structural aspects favorable for DMPK. The best analogs for each of these attributes were often from different libraries and chemical sub-series; however, a number of lead compounds containing relatively balanced pharmacological profiles, such as VU0402734, represent highly suitable M₅ PAM research tools. An overview of the optimization progression for this project, which highlights key early, intermediate, and advanced lead compounds, is presented in **Figure 3**.

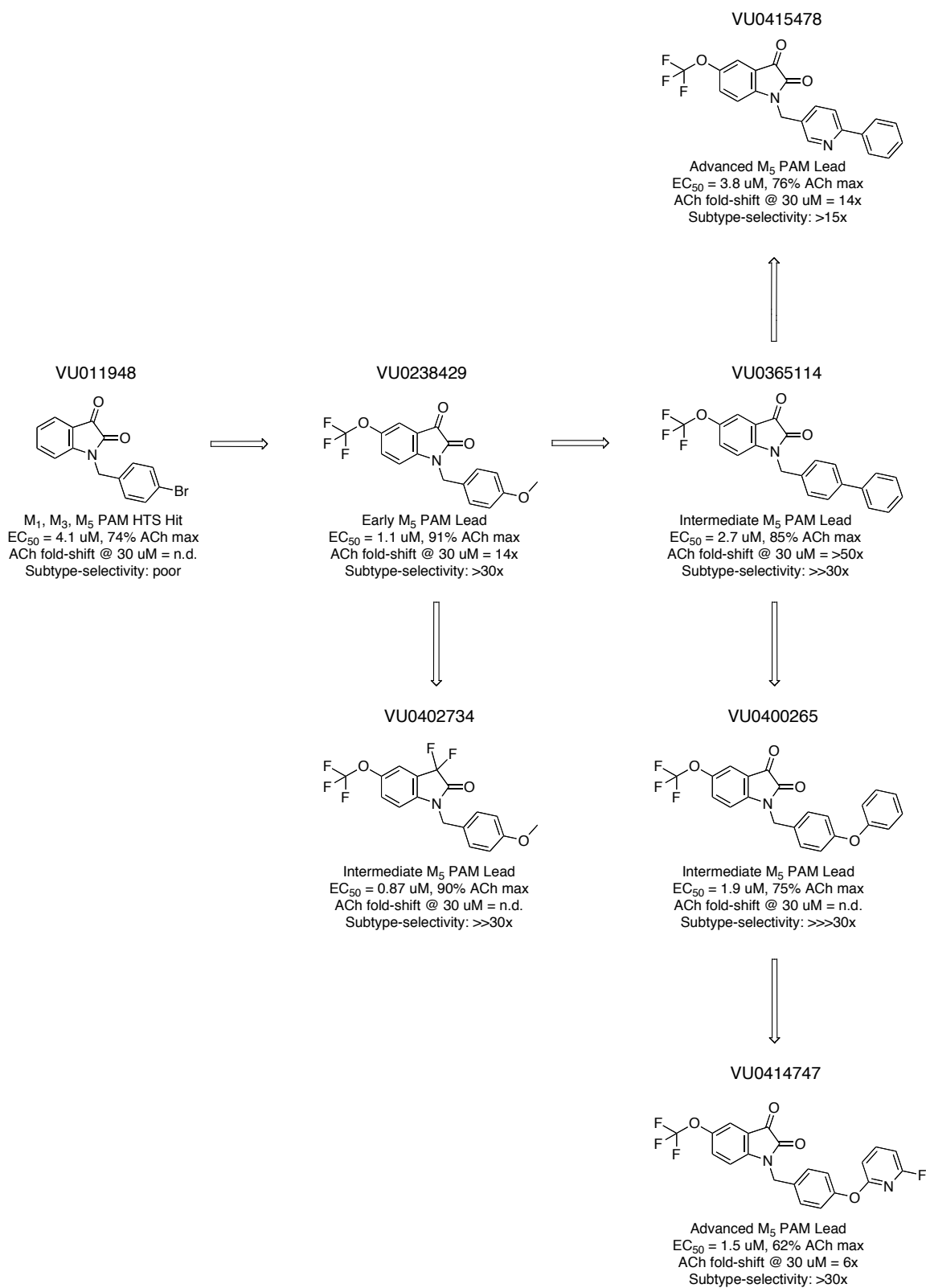


Figure 3. Overview of key lead compounds identified during M₅ PAM optimization project.

Prior to *in vivo* use, additional PK/PBL studies will be necessary to determine which compound(s) may be suitable for systemic dosing in rodent neurobehavioral and neurochemical investigations. The careful use of experimental controls and thoughtful data interpretation will be required for future studies utilizing these novel compounds given the off-target activities exhibited by many of the lead analogs. However, further optimization could be directed at this scaffold to address these activities, prior to initiation of neurobiology studies. Such efforts could be focused on heterocyclic replacement of the southern benzyl ring with isosteres such as thiophene or *m*-fluoropyridines. Likewise, introduction of one or more heteroatom(s) to the western benzo ring of the isatin core has yet to be performed. These modifications are likely to prove tolerable for M₅ PAM activity and may reveal highly useful SAR.

Due to the discrete neuronal localization of M₅, which is essentially limited to expression on mesolimbic and nigrostriatal DA projection neurons of the VTA and SNc, respectively, pharmacological investigation into the effects of selective M₅ activation will likely focus on these midbrain DA pathways and on their neurobehavioral correlates^{34,37}. As discussed in Chapter I, murine experiments measuring stimulation of forebrain DA efflux in the NAc following administration of a muscarinic agonist directly into the VTA or after electrical stimulation of hindbrain cholinergic neurons of the pons that project to the VTA (i.e. Ch.V-VI) found that genetic deletion of M₅ abolished the increase in forebrain DA efflux that was observed in WT mice⁶³. Thus, under the hypothesis that post-synaptic M₅ receptors in the VTA located on DA cell bodies and/or dendrites mediates ACh-induced neuronal excitation leading to increased DA neurotransmission in the NAc, pharmacological M₅ activation with a selective PAM would likely potentiate

DA efflux in the NAc under either of the conditions used in the two M₅-KO mice experiments. However, it is important to note that *in vivo* microdialysis studies have determined that extracellular/synaptic ACh levels in the VTA are near or below detection thresholds under resting conditions when no pharmacological or electrical stimulus of mesolimbic signaling is present, and often the measurement of changes in extracellular ACh in this region requires infusion of a low dose of an AChE inhibitor through the dialysis probe^{147,148}. It is therefore unlikely that administration of an M₅ PAM by itself would increase forebrain DA levels, unless it is co-administered with a submaximal dose of muscarinic agonist or following electrical stimulation of hindbrain cholinergic neurons to increase ACh concentration in the VTA. Analogous experiments focused on the parallel nigrostriatal DA pathway could also be performed. These would provide useful evidence for or against the putative functional role of M₅ on midbrain DA neurons that has been hypothesized from results of M₅-KO mice studies.

In animal models of drug reward, M₅ PAM administration (be it directly to the VTA or SNc, or via systemic dosing with a suitable compound) would provide behavioral insight complementary to the neurochemical studies. For instance, an M₅ PAM would be hypothesized to exacerbate drug reward behavior in cocaine self-administration and CPP models as well as worsen withdrawal-induced anxiety behaviors. Similarly, amphetamine-induced hyperlocomotion would presumably be increased by dosing of an M₅ PAM; though, ideally a dose of amphetamine low enough to cause only a subtle elevation in locomotor activity would be used to provide a window for the M₅ PAM effect. Additional behavioral paradigms (e.g. CAR) traditionally used to predict antipsychotic efficacy could be used to further characterize an M₅ PAM *in vivo*.

Beyond these experiments focused primarily on the functions of neuronal M₅, additional studies could be performed to assess the putative role of M₅ in mediating ACh-induced cerebrovasodilation. M₅-KO mice lack ACh-induced dilation of multiple cerebral blood vessels including capillary beds, arterioles, and larger arteries of the brain⁶². Furthermore, absence of M₅ but not M₁ or M₃ results in a constitutive constriction of the cerebrovasculature with a corresponding decrease in CBF⁶⁶. Thus, measurement of cerebral blood vessel diameter using cranial window techniques, *in vivo* magnetic resonance angiography, and/or *ex-vivo* tissue preparations following administration of an M₅ PAM could provide pharmacological evidence to support the hypothesized vasodilatory role of M₅ in the brain. Control experiments examining the effect of an M₅ PAM on ACh-induced vasodilation of peripheral blood vessels (where M₃ is highly-likely the mediating receptor subtype) could be used to indicate whether the M₅ PAM compound maintains subtype-selectivity in native tissues. Hemodynamic measures of CBF following M₅ PAM dosing could be obtained using laser doppler flowometry methods *in vivo* as well.

The question of whether or not the neuroanatomical and behavioral cognitive defects observed in M₅-KO mice are due to absence of neuronal or cerebrovascular M₅ (or perhaps both) could be potentially addressed by use of an M₅ PAM lacking BBB penetration and thereby acting primarily on non-neuronal M₅ receptors of the brain's blood vessels. If the neuronal atrophy and cognitive defects arising from genetic M₅ deletion are due solely to decreased CBF arising from cerebrovasoconstriction, use of a non CNS-penetrant compound would be hypothesized to exert pro-cognitive effects, presumably by enhancement of CBF alone. Conversely, if such effects were absent with

a non CNS-penetrant compound but were then found following dosing of a compound that provides high brain exposure, such results would provide evidence that lack of neuronal M₅ in the M₅-KO mice studies contributes to the cellular and behavioral defects in cognitive function. However, each of these potential studies would require important controls, such as the use of muscarinic antagonists (e.g. atropine) to reverse or compete with any observed positive M₅ PAM effects on cerebral hemodynamics or on pro-cognitive behavioral efficacy, as well as the use of M₅-KO mice. Unfortunately, these latter studies aimed at exploring the possible role of M₅ in learning and memory may be confounded by a lack of ‘window’ for which to observe such effects. Put differently, enhancement of cognition beyond a normal physiological state in WT animals is generally more challenging to detect. Conversely, neuroanatomical, electrophysiological, and behavioral measures of learning and memory are generally more sensitive to detection of impairments induced by experimental or pharmacological agents. Therefore, discovery of subtype-selective and drug-like M₅ NAMs or antagonists could potentially provide more useful and straightforward insight to this particular question.

As presented in Chapter IV, preliminary data suggests that incorporation of basic alkylamine moieties tethered by an ether at the 5-position of the isatin headpiece on the M₅ PAM scaffold may engender M₅ NAM activity. SAR for this sub-series has revealed additional modifications that improve inhibitory potency of these putative M₅ NAMs in functional assays. However, the subtype-selectivity and mode of binding for these compounds has yet to be determined. Indeed, the first series of M₅ NAMs may arise from our novel series of M₅ PAMs, which would provide a richer set of available pharmacological tools for use in obtaining a thorough understanding M₅ neurobiology.

REFERENCES

1. Csillik, B. Synaptochemistry of acetylcholine metabolism in a cholinergic neuron. *Int Rev Neurobiol* **18**, 69-140 (1975).
2. Bonner, T.I., Buckley, N.J., Young, A.C. & Brann, M.R. Identification of a family of muscarinic acetylcholine receptor genes. *Science* **237**, 527-32 (1987).
3. Woolf, N.J. & Butcher, L.L. Cholinergic systems mediate action from movement to higher consciousness. *Behav Brain Res* (2010).
4. Tansey, E.M. Henry Dale and the discovery of acetylcholine. *C R Biol* **329**, 419-25 (2006).
5. Bonner, T.I., Young, A.C., Brann, M.R. & Buckley, N.J. Cloning and expression of the human and rat m5 muscarinic acetylcholine receptor genes. *Neuron* **1**, 403-10 (1988).
6. Schafer, M.K., Weihe, E., Varoqui, H., Eiden, L.E. & Erickson, J.D. Distribution of the vesicular acetylcholine transporter (VACHT) in the central and peripheral nervous systems of the rat. *J Mol Neurosci* **5**, 1-26 (1994).
7. Varoqui, H. & Erickson, J.D. Active transport of acetylcholine by the human vesicular acetylcholine transporter. *J Biol Chem* **271**, 27229-32 (1996).
8. Taylor, P. The cholinesterases. *J Biol Chem* **266**, 4025-8 (1991).
9. Okuda, T. et al. Identification and characterization of the high-affinity choline transporter. *Nat Neurosci* **3**, 120-5 (2000).
10. Li, Y., Camp, S., Rachinsky, T.L., Getman, D. & Taylor, P. Gene structure of mammalian acetylcholinesterase. Alternative exons dictate tissue-specific expression. *J Biol Chem* **266**, 23083-90 (1991).
11. Lockridge, O. Structure of human serum cholinesterase. *Bioessays* **9**, 125-8 (1988).
12. Chatonnet, A. & Lockridge, O. Comparison of butyrylcholinesterase and acetylcholinesterase. *Biochem J* **260**, 625-34 (1989).
13. Woolf, N.J. Cholinergic systems in mammalian brain and spinal cord. *Prog Neurobiol* **37**, 475-524 (1991).
14. Mesulam, M.M., Mufson, E.J., Wainer, B.H. & Levey, A.I. Central cholinergic pathways in the rat: an overview based on an alternative nomenclature (Ch1-Ch6). *Neuroscience* **10**, 1185-201 (1983).
15. Albuquerque, E.X., Pereira, E.F., Alkondon, M. & Rogers, S.W. Mammalian nicotinic acetylcholine receptors: from structure to function. *Physiol Rev* **89**, 73-120 (2009).

16. Eglén, R.M. Muscarinic receptor subtype pharmacology and physiology. *Prog Med Chem* **43**, 105-36 (2005).
17. Wess, J. Molecular biology of muscarinic acetylcholine receptors. *Crit Rev Neurobiol* **10**, 69-99 (1996).
18. Caulfield, M.P. Muscarinic receptors--characterization, coupling and function. *Pharmacol Ther* **58**, 319-79 (1993).
19. Peleg, S., Varon, D., Ivanina, T., Dessauer, C.W. & Dascal, N. G(α)(i) controls the gating of the G protein-activated K(+) channel, GIRK. *Neuron* **33**, 87-99 (2002).
20. Zhang, Q., Pacheco, M.A. & Doupnik, C.A. Gating properties of GIRK channels activated by G α (o)- and G α (i)-coupled muscarinic m2 receptors in *Xenopus* oocytes: the role of receptor precoupling in RGS modulation. *J Physiol* **545**, 355-73 (2002).
21. Bunemann, M. & Hosey, M.M. Novel signalling events mediated by muscarinic receptor subtypes. *Life Sci* **68**, 2525-33 (2001).
22. Fernandez-Fernandez, J.M., Wanaverbecq, N., Halley, P., Caulfield, M.P. & Brown, D.A. Selective activation of heterologously expressed G protein-gated K⁺ channels by M2 muscarinic receptors in rat sympathetic neurones. *J Physiol* **515** (Pt 3), 631-7 (1999).
23. Fernandez-Fernandez, J.M., Abogadie, F.C., Milligan, G., Delmas, P. & Brown, D.A. Multiple pertussis toxin-sensitive G-proteins can couple receptors to GIRK channels in rat sympathetic neurons when expressed heterologously, but only native G(i)-proteins do so in situ. *Eur J Neurosci* **14**, 283-92 (2001).
24. Hosey, M.M. Diversity of structure, signaling and regulation within the family of muscarinic cholinergic receptors. *FASEB J* **6**, 845-52 (1992).
25. Hulme, E.C., Birdsall, N.J. & Buckley, N.J. Muscarinic receptor subtypes. *Annu Rev Pharmacol Toxicol* **30**, 633-73 (1990).
26. Gurevich, V.V. & Gurevich, E.V. Rich tapestry of G protein-coupled receptor signaling and regulatory mechanisms. *Mol Pharmacol* **74**, 312-6 (2008).
27. Marlo, J.E. et al. Discovery and characterization of novel allosteric potentiators of M1 muscarinic receptors reveals multiple modes of activity. *Mol Pharmacol* (2008).
28. Kenakin, T. & Miller, L.J. Seven transmembrane receptors as shapeshifting proteins: the impact of allosteric modulation and functional selectivity on new drug discovery. *Pharmacol Rev* **62**, 265-304 (2010).
29. Wess, J., Blin, N., Mutschler, E. & Bluml, K. Muscarinic acetylcholine receptors: structural basis of ligand binding and G protein coupling. *Life Sci* **56**, 915-22 (1995).
30. Ward, S.D., Curtis, C.A. & Hulme, E.C. Alanine-scanning mutagenesis of transmembrane domain 6 of the M(1) muscarinic acetylcholine receptor suggests

- that Tyr381 plays key roles in receptor function. *Mol Pharmacol* **56**, 1031-41 (1999).
31. Sur, C. et al. N-desmethylclozapine, an allosteric agonist at muscarinic 1 receptor, potentiates N-methyl-D-aspartate receptor activity. *Proc Natl Acad Sci U S A* **100**, 13674-9 (2003).
 32. Ferrari-Dileo, G., Waelbroeck, M., Mash, D.C. & Flynn, D.D. Selective labeling and localization of the M4 (m4) muscarinic receptor subtype. *Mol Pharmacol* **46**, 1028-35 (1994).
 33. Levey, A.I. Immunological localization of m1-m5 muscarinic acetylcholine receptors in peripheral tissues and brain. *Life Sci* **52**, 441-8 (1993).
 34. Vilaro, M.T., Palacios, J.M. & Mengod, G. Localization of m5 muscarinic receptor mRNA in rat brain examined by in situ hybridization histochemistry. *Neurosci Lett* **114**, 154-9 (1990).
 35. Wei, J., Walton, E.A., Milici, A. & Buccafusco, J.J. m1-m5 muscarinic receptor distribution in rat CNS by RT-PCR and HPLC. *J Neurochem* **63**, 815-21 (1994).
 36. Tayebati, S.K., Di Tullio, M.A., Tomassoni, D. & Amenta, F. Localization of the m5 muscarinic cholinergic receptor in rat circle of Willis and pial arteries. *Neuroscience* **122**, 205-11 (2003).
 37. Weiner, D.M., Levey, A.I. & Brann, M.R. Expression of muscarinic acetylcholine and dopamine receptor mRNAs in rat basal ganglia. *Proc Natl Acad Sci U S A* **87**, 7050-4 (1990).
 38. Yasuda, R.P. et al. Development of antisera selective for m4 and m5 muscarinic cholinergic receptors: distribution of m4 and m5 receptors in rat brain. *Mol Pharmacol* **43**, 149-57 (1993).
 39. Palacios, J.M. et al. Cholinergic receptors in the rat and human brain: microscopic visualization. *Prog Brain Res* **84**, 243-53 (1990).
 40. Levey, A.I., Kitt, C.A., Simonds, W.F., Price, D.L. & Brann, M.R. Identification and localization of muscarinic acetylcholine receptor proteins in brain with subtype-specific antibodies. *J Neurosci* **11**, 3218-26 (1991).
 41. Volpicelli, L.A. & Levey, A.I. Muscarinic acetylcholine receptor subtypes in cerebral cortex and hippocampus. *Prog Brain Res* **145**, 59-66 (2004).
 42. Elhousseiny, A., Cohen, Z., Olivier, A., Stanimirovic, D.B. & Hamel, E. Functional acetylcholine muscarinic receptor subtypes in human brain microcirculation: identification and cellular localization. *J Cereb Blood Flow Metab* **19**, 794-802 (1999).
 43. Vilaro, M.T., Wiederhold, K.H., Palacios, J.M. & Mengod, G. Muscarinic cholinergic receptors in the rat caudate-putamen and olfactory tubercle belong predominantly to the m4 class: in situ hybridization and receptor autoradiography evidence. *Neuroscience* **40**, 159-67 (1991).

44. Langmead, C.J., Watson, J. & Reavill, C. Muscarinic acetylcholine receptors as CNS drug targets. *Pharmacol Ther* **117**, 232-43 (2008).
45. Wess, J. Muscarinic acetylcholine receptor knockout mice: novel phenotypes and clinical implications. *Annu Rev Pharmacol Toxicol* **44**, 423-50 (2004).
46. Anagnostaras, S.G. et al. Selective cognitive dysfunction in acetylcholine M1 muscarinic receptor mutant mice. *Nat Neurosci* **6**, 51-8 (2003).
47. Miyakawa, T., Yamada, M., Duttaroy, A. & Wess, J. Hyperactivity and intact hippocampus-dependent learning in mice lacking the M1 muscarinic acetylcholine receptor. *J Neurosci* **21**, 5239-50 (2001).
48. Marino, M.J., Rouse, S.T., Levey, A.I., Potter, L.T. & Conn, P.J. Activation of the genetically defined m1 muscarinic receptor potentiates N-methyl-D-aspartate (NMDA) receptor currents in hippocampal pyramidal cells. *Proc Natl Acad Sci U S A* **95**, 11465-70 (1998).
49. Hamilton, S.E. et al. Disruption of the m1 receptor gene ablates muscarinic receptor-dependent M current regulation and seizure activity in mice. *Proc Natl Acad Sci U S A* **94**, 13311-6 (1997).
50. Fisahn, A. et al. Muscarinic induction of hippocampal gamma oscillations requires coupling of the M1 receptor to two mixed cation currents. *Neuron* **33**, 615-24 (2002).
51. Hamilton, S.E. & Nathanson, N.M. The M1 receptor is required for muscarinic activation of mitogen-activated protein (MAP) kinase in murine cerebral cortical neurons. *J Biol Chem* **276**, 15850-3 (2001).
52. Berkeley, J.L. et al. M1 muscarinic acetylcholine receptors activate extracellular signal-regulated kinase in CA1 pyramidal neurons in mouse hippocampal slices. *Mol Cell Neurosci* **18**, 512-24 (2001).
53. Fibiger, H.C. Cholinergic mechanisms in learning, memory and dementia: a review of recent evidence. *Trends Neurosci* **14**, 220-3 (1991).
54. Anagnostaras, S.G., Maren, S. & Fanselow, M.S. Scopolamine selectively disrupts the acquisition of contextual fear conditioning in rats. *Neurobiol Learn Mem* **64**, 191-4 (1995).
55. Gerber, D.J. et al. Hyperactivity, elevated dopaminergic transmission, and response to amphetamine in M1 muscarinic acetylcholine receptor-deficient mice. *Proc Natl Acad Sci U S A* **98**, 15312-7 (2001).
56. Yamada, M. et al. Mice lacking the M3 muscarinic acetylcholine receptor are hypophagic and lean. *Nature* **410**, 207-12 (2001).
57. Poulin, B. et al. The M3-muscarinic receptor regulates learning and memory in a receptor phosphorylation/arrestin-dependent manner. *Proc Natl Acad Sci U S A* **107**, 9440-5 (2010).

58. Matsui, M. et al. Mice lacking M2 and M3 muscarinic acetylcholine receptors are devoid of cholinergic smooth muscle contractions but still viable. *J Neurosci* **22**, 10627-32 (2002).
59. Matsui, M. et al. Multiple functional defects in peripheral autonomic organs in mice lacking muscarinic acetylcholine receptor gene for the M3 subtype. *Proc Natl Acad Sci U S A* **97**, 9579-84 (2000).
60. Stengel, P.W., Yamada, M., Wess, J. & Cohen, M.L. M(3)-receptor knockout mice: muscarinic receptor function in atria, stomach fundus, urinary bladder, and trachea. *Am J Physiol Regul Integr Comp Physiol* **282**, R1443-9 (2002).
61. Bymaster, F.P. et al. Role of specific muscarinic receptor subtypes in cholinergic parasympathomimetic responses, in vivo phosphoinositide hydrolysis, and pilocarpine-induced seizure activity. *Eur J Neurosci* **17**, 1403-10 (2003).
62. Yamada, M. et al. Cholinergic dilation of cerebral blood vessels is abolished in M(5) muscarinic acetylcholine receptor knockout mice. *Proc Natl Acad Sci U S A* **98**, 14096-101 (2001).
63. Forster, G.L., Yeomans, J.S., Takeuchi, J. & Blaha, C.D. M5 muscarinic receptors are required for prolonged accumbal dopamine release after electrical stimulation of the pons in mice. *J Neurosci* **22**, RC190 (2002).
64. Basile, A.S. et al. Deletion of the M5 muscarinic acetylcholine receptor attenuates morphine reinforcement and withdrawal but not morphine analgesia. *Proc Natl Acad Sci U S A* **99**, 11452-7 (2002).
65. Fink-Jensen, A. et al. Role for M5 muscarinic acetylcholine receptors in cocaine addiction. *J Neurosci Res* **74**, 91-6 (2003).
66. Araya, R. et al. Loss of M5 muscarinic acetylcholine receptors leads to cerebrovascular and neuronal abnormalities and cognitive deficits in mice. *Neurobiol Dis* **24**, 334-44 (2006).
67. Iadecola, C. Neurovascular regulation in the normal brain and in Alzheimer's disease. *Nat Rev Neurosci* **5**, 347-60 (2004).
68. Mies, G., Ishimaru, S., Xie, Y., Seo, K. & Hossmann, K.A. Ischemic thresholds of cerebral protein synthesis and energy state following middle cerebral artery occlusion in rat. *J Cereb Blood Flow Metab* **11**, 753-61 (1991).
69. Elhusseiny, A. & Hamel, E. Muscarinic--but not nicotinic--acetylcholine receptors mediate a nitric oxide-dependent dilation in brain cortical arterioles: a possible role for the M5 receptor subtype. *J Cereb Blood Flow Metab* **20**, 298-305 (2000).
70. Sato, A., Sato, Y. & Uchida, S. Regulation of regional cerebral blood flow by cholinergic fibers originating in the basal forebrain. *Int J Dev Neurosci* **19**, 327-37 (2001).
71. Sato, A. & Sato, Y. Cholinergic neural regulation of regional cerebral blood flow. *Alzheimer Dis Assoc Disord* **9**, 28-38 (1995).

72. Sato, A. & Sato, Y. Cerebral cortical vasodilatation in response to stimulation of cholinergic fibres originating in the nucleus basalis of Meynert. *J Auton Nerv Syst* **30 Suppl**, S137-40 (1990).
73. Gomeza, J. et al. Pronounced pharmacologic deficits in M2 muscarinic acetylcholine receptor knockout mice. *Proc Natl Acad Sci U S A* **96**, 1692-7 (1999).
74. Duttaroy, A. et al. Evaluation of muscarinic agonist-induced analgesia in muscarinic acetylcholine receptor knockout mice. *Mol Pharmacol* **62**, 1084-93 (2002).
75. Stengel, P.W., Gomeza, J., Wess, J. & Cohen, M.L. M(2) and M(4) receptor knockout mice: muscarinic receptor function in cardiac and smooth muscle in vitro. *J Pharmacol Exp Ther* **292**, 877-85 (2000).
76. Zhang, W. et al. Characterization of central inhibitory muscarinic autoreceptors by the use of muscarinic acetylcholine receptor knock-out mice. *J Neurosci* **22**, 1709-17 (2002).
77. Tzavara, E.T. et al. Dysregulated hippocampal acetylcholine neurotransmission and impaired cognition in M2, M4 and M2/M4 muscarinic receptor knockout mice. *Mol Psychiatry* **8**, 673-9 (2003).
78. Zhang, W., Yamada, M., Gomeza, J., Basile, A.S. & Wess, J. Multiple muscarinic acetylcholine receptor subtypes modulate striatal dopamine release, as studied with M1-M5 muscarinic receptor knock-out mice. *J Neurosci* **22**, 6347-52 (2002).
79. Felder, C.C. et al. Elucidating the role of muscarinic receptors in psychosis. *Life Sci* **68**, 2605-13 (2001).
80. Gomeza, J. et al. Enhancement of D1 dopamine receptor-mediated locomotor stimulation in M(4) muscarinic acetylcholine receptor knockout mice. *Proc Natl Acad Sci U S A* **96**, 10483-8 (1999).
81. Tzavara, E.T. et al. M4 muscarinic receptors regulate the dynamics of cholinergic and dopaminergic neurotransmission: relevance to the pathophysiology and treatment of related CNS pathologies. *FASEB J* **18**, 1410-2 (2004).
82. Selkoe, D.J. Alzheimer's disease: genes, proteins, and therapy. *Physiol Rev* **81**, 741-66 (2001).
83. Terry, A.V., Jr. & Buccafusco, J.J. The cholinergic hypothesis of age and Alzheimer's disease-related cognitive deficits: recent challenges and their implications for novel drug development. *J Pharmacol Exp Ther* **306**, 821-7 (2003).
84. Ibach, B. & Haen, E. Acetylcholinesterase inhibition in Alzheimer's Disease. *Curr Pharm Des* **10**, 231-51 (2004).
85. Coyle, J.T., Price, D.L. & DeLong, M.R. Alzheimer's disease: a disorder of cortical cholinergic innervation. *Science* **219**, 1184-90 (1983).

86. Francis, P.T., Palmer, A.M., Snape, M. & Wilcock, G.K. The cholinergic hypothesis of Alzheimer's disease: a review of progress. *J Neurol Neurosurg Psychiatry* **66**, 137-47 (1999).
87. Mohapel, P., Leanza, G., Kokaia, M. & Lindvall, O. Forebrain acetylcholine regulates adult hippocampal neurogenesis and learning. *Neurobiol Aging* **26**, 939-46 (2005).
88. Canet-Aviles, R.M., Anderton, M., Hooper, N.M., Turner, A.J. & Vaughan, P.F. Muscarine enhances soluble amyloid precursor protein secretion in human neuroblastoma SH-SY5Y by a pathway dependent on protein kinase C(alpha), src-tyrosine kinase and extracellular signal-regulated kinase but not phospholipase C. *Brain Res Mol Brain Res* **102**, 62-72 (2002).
89. Caccamo, A. et al. M1 receptors play a central role in modulating AD-like pathology in transgenic mice. *Neuron* **49**, 671-82 (2006).
90. Forlenza, O.V. et al. Muscarinic agonists reduce tau phosphorylation in non-neuronal cells via GSK-3beta inhibition and in neurons. *J Neural Transm* **107**, 1201-12 (2000).
91. Zuchner, T., Perez-Polo, J.R. & Schliebs, R. Beta-secretase BACE1 is differentially controlled through muscarinic acetylcholine receptor signaling. *J Neurosci Res* **77**, 250-7 (2004).
92. Jacobsen, J.S., Reinhart, P. & Pangalos, M.N. Current concepts in therapeutic strategies targeting cognitive decline and disease modification in Alzheimer's disease. *NeuroRx* **2**, 612-26 (2005).
93. Whitehouse, P.J. et al. Alzheimer's disease and senile dementia: loss of neurons in the basal forebrain. *Science* **215**, 1237-9 (1982).
94. Bierer, L.M. et al. Neurochemical correlates of dementia severity in Alzheimer's disease: relative importance of the cholinergic deficits. *J Neurochem* **64**, 749-60 (1995).
95. Procter, A.W. Neurochemical correlates of dementia. *Neurodegeneration* **5**, 403-7 (1996).
96. Wiley R.G., L.D.A. *Molecular Neurosurgery with Targeted Toxins*, (Humana Press, 2005).
97. Nitsch, R.M., Slack, B.E., Wurtman, R.J. & Growdon, J.H. Release of Alzheimer amyloid precursor derivatives stimulated by activation of muscarinic acetylcholine receptors. *Science* **258**, 304-7 (1992).
98. Lin, L., LeBlanc, C.J., Deacon, T.W. & Isacson, O. Chronic cognitive deficits and amyloid precursor protein elevation after selective immunotoxin lesions of the basal forebrain cholinergic system. *Neuroreport* **9**, 547-52 (1998).
99. Lin, L., Georgievska, B., Mattsson, A. & Isacson, O. Cognitive changes and modified processing of amyloid precursor protein in the cortical and hippocampal system after cholinergic synapse loss and muscarinic receptor activation. *Proc Natl Acad Sci U S A* **96**, 12108-13 (1999).

100. Bodick, N.C. et al. Effects of xanomeline, a selective muscarinic receptor agonist, on cognitive function and behavioral symptoms in Alzheimer disease. *Arch Neurol* **54**, 465-73 (1997).
101. Ferrari-DiLeo, G., Mash, D.C. & Flynn, D.D. Attenuation of muscarinic receptor-G-protein interaction in Alzheimer disease. *Mol Chem Neuropathol* **24**, 69-91 (1995).
102. Mash, D.C., Flynn, D.D. & Potter, L.T. Loss of M2 muscarine receptors in the cerebral cortex in Alzheimer's disease and experimental cholinergic denervation. *Science* **228**, 1115-7 (1985).
103. Tsang, S.W. et al. Impaired coupling of muscarinic M1 receptors to G-proteins in the neocortex is associated with severity of dementia in Alzheimer's disease. *Neurobiol Aging* **27**, 1216-23 (2006).
104. Kapur, S., Mizrahi, R. & Li, M. From dopamine to salience to psychosis--linking biology, pharmacology and phenomenology of psychosis. *Schizophr Res* **79**, 59-68 (2005).
105. Javitt, D.C. & Zukin, S.R. Recent advances in the phencyclidine model of schizophrenia. *Am J Psychiatry* **148**, 1301-8 (1991).
106. Olney, J.W., Newcomer, J.W. & Farber, N.B. NMDA receptor hypofunction model of schizophrenia. *J Psychiatr Res* **33**, 523-33 (1999).
107. Newcomer, J.W. et al. Ketamine-induced NMDA receptor hypofunction as a model of memory impairment and psychosis. *Neuropsychopharmacology* **20**, 106-18 (1999).
108. Millan, M.J. N-methyl-D-aspartate receptor-coupled glycineB receptors in the pathogenesis and treatment of schizophrenia: a critical review. *Curr Drug Targets CNS Neurol Disord* **1**, 191-213 (2002).
109. Bridges, T.M., Williams, R. & Lindsley, C.W. Design of potent GlyT1 inhibitors: in vitro and in vivo profiles. *Curr Opin Mol Ther* **10**, 591-601 (2008).
110. Breier, A. Developing drugs for cognitive impairment in schizophrenia. *Schizophr Bull* **31**, 816-22 (2005).
111. Wess, J., Eglen, R.M. & Gautam, D. Muscarinic acetylcholine receptors: mutant mice provide new insights for drug development. *Nat Rev Drug Discov* **6**, 721-33 (2007).
112. Christopoulos, A. Allosteric binding sites on cell-surface receptors: novel targets for drug discovery. *Nat Rev Drug Discov* **1**, 198-210 (2002).
113. Rudolph, U. et al. Benzodiazepine actions mediated by specific gamma-aminobutyric acid(A) receptor subtypes. *Nature* **401**, 796-800 (1999).
114. Christopoulos, A. & Kenakin, T. G protein-coupled receptor allosterism and complexing. *Pharmacol Rev* **54**, 323-74 (2002).

115. Conn, P.J., Christopoulos, A. & Lindsley, C.W. Allosteric modulators of GPCRs: a novel approach for the treatment of CNS disorders. *Nat Rev Drug Discov* **8**, 41-54 (2009).
116. Bridges, T.M. & Lindsley, C.W. G-protein-coupled receptors: from classical modes of modulation to allosteric mechanisms. *ACS Chem Biol* **3**, 530-41 (2008).
117. Thomas, R.L., Mistry, R., Langmead, C.J., Wood, M.D. & Challiss, R.A. G protein coupling and signaling pathway activation by m1 muscarinic acetylcholine receptor orthosteric and allosteric agonists. *J Pharmacol Exp Ther* **327**, 365-74 (2008).
118. Wess, J. Allosteric binding sites on muscarinic acetylcholine receptors. *Mol Pharmacol* **68**, 1506-9 (2005).
119. Birdsall, N.J. & Lazareno, S. Allosterism at muscarinic receptors: ligands and mechanisms. *Mini Rev Med Chem* **5**, 523-43 (2005).
120. Heinrich, J.N. et al. Pharmacological comparison of muscarinic ligands: historical versus more recent muscarinic M1-preferring receptor agonists. *Eur J Pharmacol* **605**, 53-6 (2009).
121. Lebon, G., Langmead, C.J., Tehan, B.G. & Hulme, E.C. Mutagenic mapping suggests a novel binding mode for selective agonists of M1 muscarinic acetylcholine receptors. *Mol Pharmacol* (2008).
122. Langmead, C.J. et al. Characterization of a CNS penetrant, selective M1 muscarinic receptor agonist, 77-LH-28-1. *Br J Pharmacol* **154**, 1104-15 (2008).
123. Esteban, A. & Hilliard, D. Thienopyridines as allosteric potentiators of the M4 muscarinic receptor. Vol. US 2009/0105244 A1 (Eli Lilly and Company, 2005).
124. Brady, A.E. et al. Centrally active allosteric potentiators of the M4 muscarinic acetylcholine receptor reverse amphetamine-induced hyperlocomotor activity in rats. *J Pharmacol Exp Ther* **327**, 941-53 (2008).
125. Shirey, J.K. et al. An allosteric potentiator of M4 mAChR modulates hippocampal synaptic transmission. *Nat Chem Biol* **4**, 42-50 (2008).
126. Kennedy, J.P. et al. Synthesis and structure-activity relationships of allosteric potentiators of the m(4) muscarinic acetylcholine receptor. *ChemMedChem* **4**, 1600-7 (2009).
127. Chan, W.Y. et al. Allosteric modulation of the muscarinic M4 receptor as an approach to treating schizophrenia. *Proc Natl Acad Sci U S A* **105**, 10978-83 (2008).
128. Esbenshade, T.A. et al. The histamine H3 receptor: an attractive target for the treatment of cognitive disorders. *Br J Pharmacol* **154**, 1166-81 (2008).
129. Tiligada, E., Zampeli, E., Sander, K. & Stark, H. Histamine H3 and H4 receptors as novel drug targets. *Expert Opin Investig Drugs* **18**, 1519-31 (2009).

130. Chazot, P.L. Therapeutic potential of histamine H3 receptor antagonists in dementias. *Drug News Perspect* **23**, 99-103 (2010).
131. Bridges, T.M. et al. Discovery of the first highly M5-preferring muscarinic acetylcholine receptor ligand, an M5 positive allosteric modulator derived from a series of 5-trifluoromethoxy N-benzyl isatins. *J Med Chem* **52**, 3445-8 (2009).
132. Bridges, T.M. et al. Chemical lead optimization of a pan G(q) mAChR M(1), M(3), M(5) positive allosteric modulator (PAM) lead. Part I: Development of the first highly selective M(5) PAM. *Bioorg Med Chem Lett* **20**, 558-62 (2010).
133. Sharma, S. et al. Discovery of molecular switches that modulate modes of metabotropic glutamate receptor subtype 5 (mGlu5) pharmacology in vitro and in vivo within a series of functionalized, regioisomeric 2- and 5-(phenylethynyl)pyrimidines. *J Med Chem* **52**, 4103-6 (2009).
134. Sharma, S., Rodriguez, A.L., Conn, P.J. & Lindsley, C.W. Synthesis and SAR of a mGluR5 allosteric partial antagonist lead: unexpected modulation of pharmacology with slight structural modifications to a 5-(phenylethynyl)pyrimidine scaffold. *Bioorg Med Chem Lett* **18**, 4098-101 (2008).
135. Bridges, T.M. et al. Chemical lead optimization of a pan Gq mAChR M1, M3, M5 positive allosteric modulator (PAM) lead. Part II: development of a potent and highly selective M1 PAM. *Bioorg Med Chem Lett* **20**, 1972-5 (2010).
136. Lindsley, C., Shipe, W., Yang, F. & Bunda, J. Benzyl-substituted quinolone m1 receptor positive allosteric modulators. Vol. US 2010/0009962 A1 (Merck, 2007).
137. Ma, L. et al. Selective activation of the M1 muscarinic acetylcholine receptor achieved by allosteric potentiation. *Proc Natl Acad Sci U S A* **106**, 15950-5 (2009).
138. Shirey, J.K. et al. A selective allosteric potentiator of the M1 muscarinic acetylcholine receptor increases activity of medial prefrontal cortical neurons and restores impairments in reversal learning. *J Neurosci* **29**, 14271-86 (2009).
139. Lewis, L.M. et al. Synthesis and SAR of selective muscarinic acetylcholine receptor subtype 1 (M1 mAChR) antagonists. *Bioorg Med Chem Lett* **18**, 885-90 (2008).
140. Weaver, C.D. et al. Discovery and development of a potent and highly selective small molecule muscarinic acetylcholine receptor subtype I (mAChR 1 or M1) antagonist in vitro and in vivo probe. *Curr Top Med Chem* **9**, 1217-26 (2009).
141. Sheffler, D.J. et al. A novel selective muscarinic acetylcholine receptor subtype 1 antagonist reduces seizures without impairing hippocampus-dependent learning. *Mol Pharmacol* **76**, 356-68 (2009).
142. LeBois, E.P. et al. Discovery and Characterization of Novel Subtype-Selective Allosteric Agonists for the Investigation of M1 Receptor Function in the Central Nervous System. *ACS Chemical Neuroscience* **1**, 104-1221 (2010).

143. Jones, C.K. et al. Novel selective allosteric activator of the M1 muscarinic acetylcholine receptor regulates amyloid processing and produces antipsychotic-like activity in rats. *J Neurosci* **28**, 10422-33 (2008).
144. Miller, N.R. et al. Synthesis and SAR of analogs of the M1 allosteric agonist TBPB. Part II: Amides, sulfonamides and ureas--the effect of capping the distal basic piperidine nitrogen. *Bioorg Med Chem Lett* **18**, 5443-7 (2008).
145. Bridges, T.M. et al. Synthesis and SAR of analogues of the M1 allosteric agonist TBPB. Part I: Exploration of alternative benzyl and privileged structure moieties. *Bioorg Med Chem Lett* **18**, 5439-42 (2008).
146. Marlo, J.E. et al. Discovery and characterization of novel allosteric potentiators of M1 muscarinic receptors reveals multiple modes of activity. *Mol Pharmacol* **75**, 577-88 (2009).
147. Dobbs, L.K. & Mark, G.P. Comparison of systemic and local methamphetamine treatment on acetylcholine and dopamine levels in the ventral tegmental area in the mouse. *Neuroscience* **156**, 700-11 (2008).
148. You, Z.B., Wang, B., Zitzman, D. & Wise, R.A. Acetylcholine release in the mesocorticolimbic dopamine system during cocaine seeking: conditioned and unconditioned contributions to reward and motivation. *J Neurosci* **28**, 9021-9 (2008).